

Voltage control in MV distribution networks with a large share of distributed renewable generation

Nikolaos Papazacharopoulos

DELFTE UNIVERSITY OF TECHNOLOGY
FACULTY OF ELECTRICAL ENGINEERING MATHEMATICS AND COMPUTER SCIENCE (EEMCS)

The undersigned hereby certify that they have read and recommend to the
Faculty of Applied Sciences (TNW) for acceptance the thesis entitled

VOLTAGE CONTROL IN MV DISTRIBUTION NETWORKS
WITH A LARGE SHARE OF DISTRIBUTED RENEWABLE GENERATION

by

NIKOLAOS PAPAZACHAROPOULOS

in partial fulfilment of the requirements for the degree of

MASTER OF SCIENCE IN SUSTAINABLE ENERGY TECHNOLOGY

Dated:

June 20, 2014

Responsible instructor:

Dr. M. Gibescu (TU Eindhoven, TU Delft)

First reviewer:

Prof.ir. W.L. Kling (TU Eindhoven)

Second reviewer:

Dr. J.L. Rueda Torres (TU Delft)

Advisor:

Ir. P. Vaessen (DNV GL)

ABSTRACT

Traditionally, voltage control in MV distribution networks has been focused on dealing with voltage drop along radially operated feeders. The actual implemented controllers use local voltage measurements and have been designed and calibrated for a passive and radial use of the MV system. The presence of distributed renewable generation (DRG) makes these assumptions no longer valid. The power generated by DRG units will increase the voltage at adjacent nodes and even cause it to be higher than the voltage at the primary substation. Consequently, the presence of DRG will affect voltage control in distribution systems and it needs to be reconsidered whether methods like local voltage control and reactive power injection can still enable the network operator to cope with the newly introduced voltage rise issues.

The aim of this study is to create a new voltage control strategy, which will not only successfully limit voltage variations, but also allow for an increased penetration of DRG. The proposed coordinated voltage control strategy deploys control of HV/MV transformers On-Load Tap Changers in combination with active power control provided by Intelligent Nodes, that allows network reconfiguration. The Cigré MV distribution network benchmark is used as a basis for the test system, while appropriate models for the PV Power Plants, the Wind Power Plants and the Intelligent Nodes were developed. In order to draw realistic simulation results, a summer / winter seasonal variation is featured. The proposed voltage control algorithm is incrementally developed, allowing for the identification of factors hindering the controller performance and the development of a control algorithm which is more targeted towards dealing with specific issues. The commercial power system simulation software DlgSILENT PowerFactory 15.0 is used for carrying out these simulations.

The analysis of simulation results shows that the proposed voltage control strategy is capable of facilitating the transition towards active MV distribution networks, by offering considerably higher DRG penetration levels and strictly bound network voltages. The modelled controller is particularly applicable to MV distribution networks across North Europe. Among others, the limiting factors for an increased DRG penetration are identified, along with the effects that the reactive power control and the choice of voltage limits have. Finally, recommendations for future research are provided.

Keywords

voltage control, MV distribution network, distributed renewable generation, On-Load Tap Changer, Intelligent Node

CONTENTS

Abstract	v
Contents	vii
List of Figures.....	xi
List of Tables.....	xiii
1 Introduction.....	1
1.1 Introduction.....	1
1.2 Study of power systems	1
1.2.1 General approach	1
1.2.2 Modelling	2
1.2.3 Software tools.....	3
1.3 Distributed generation	4
1.3.1 Overview	4
1.3.2 Drivers for DG growth.....	4
1.3.3 Controllability and grid connection type	4
1.3.4 Challenges to increased penetration of DG	4
1.4 Thesis objective and approach	5
1.4.1 Problem formulation	5
1.4.2 Objective	5
1.4.3 Research questions.....	5
1.4.4 Approach.....	6
1.4.5 Limitations	6
1.5 Research framework	7
1.6 Thesis outline	7
2 MV distribution systems.....	9
2.1 Introduction.....	9
2.2 Basic aspects of MV distribution networks	9
2.2.1 Overview	9
2.2.2 Topology	9
2.2.3 Operation and control	10
2.2.4 Organisation and communication	11
2.3 Grid codes	11
2.3.1 Requirements for voltage	11
2.3.2 Requirements for DG	13
2.4 Voltage drop in a distribution system.....	13
2.4.1 Traditional distribution system	13
2.4.2 DG impact on voltage drop	13
2.4.3 Sensitivity analysis	14
2.5 Voltage regulation	15
2.5.1 Overview	15
2.5.2 On-Load Tap Changer	15
2.5.3 DRG	17

2.5.4	Intelligent Node	19
2.6	Conclusions	21
3	System modelling.....	23
3.1	Introduction.....	23
3.2	Modelling approach	23
3.3	Cigré European MV distribution network benchmark model.....	24
3.4	Load models.....	25
3.4.1	Consumption data	25
3.4.2	Mathematical representation.....	28
3.5	Distributed renewable generation models	30
3.5.1	Photovoltaic Power Plant model	30
3.5.2	Wind Power Plant model	35
3.6	Intelligent Node model	40
3.6.1	Overview	40
3.6.2	'BESS' block	41
3.6.3	'PWM Converters' block	41
3.6.4	'PQ Controller' block.....	42
3.6.5	'Charge / Current Limiter' block	42
3.7	Conclusions	44
4	Voltage control concept	45
4.1	Introduction.....	45
4.2	Coordinated voltage control concept	45
4.2.1	Previous work and basic description	45
4.2.2	Control objective and boundary conditions	46
4.2.3	Coordination and communication aspects	46
4.2.4	Advanced OLTC Controller	47
4.2.5	Philosophy of the Intelligent Node controller	50
4.3	System conditions.....	54
4.3.1	Overview of the test system	54
4.3.2	Simulation scenarios	56
4.4	Proof of concept.....	57
4.4.1	Followed approach	57
4.4.2	Evaluation criteria	57
4.4.3	Base case control scenario.....	58
4.4.4	Advanced OLTC control scenario	70
4.4.5	Coordinated voltage control scenario	77
4.4.6	Comparison of control scenarios	89
4.5	Conclusions	93
5	Conclusions and future work	95
5.1	Conclusions	95
5.1.1	Proposed voltage control strategy.....	95
5.1.2	Factors limiting the DRG penetration	96
5.1.3	Tap changing frequency and voltage quality	96
5.1.4	Effect of reactive power.....	97
5.1.5	Choice of voltage limits.....	97
5.2	Future work	98
APPENDIX A :	Cigré European MV distribution network.....	99
A.1	HV-MV subtransmission equivalent network	99

<u>Contents</u>	ix
A.2 HV/MV transformers	99
A.3 Lines.....	99
A.4 Overhead line conductor rating	101
A.5 Loads.....	101
APPENDIX B : Photovoltaic Power Plant model.....	103
B.1 Step-up transformer	103
B.2 'Voltage Controller' block	103
APPENDIX C : Wind Power Plant model.....	105
C.1 Step-up transformer	105
C.2 'Mechanical System' block	105
C.3 Calculation of λ_{design} and cp, max	105
C.4 'Voltage Controller' block	106
APPENDIX D : Intelligent Node model	107
D.1 Step-up transformer	107
D.2 'BESS' and 'PWM converters' blocks	107
D.3 'PQ Controller' block.....	108
APPENDIX E : Coordinated Voltage Controller	109
E.1 'AVC Relay' and 'Primary Controller' blocks	109
E.2 'Voltage Controller' block	109
APPENDIX F : Detailed simulation results	111
F.1 Base case control scenario	111
F.2 Advanced OLTC control scenario	111
Nomenclature.....	113
Bibliography	117

LIST OF FIGURES

Figure 1.1: "Vertical-to-Horizontal" transformation of the power system [2]	1
Figure 1.2: The interactive demonstration table of the Watt Connects project	7
Figure 2.1: Basic topologies of distribution networks [43]	9
Figure 2.2: Typical structure of a Dutch MV distribution grid [41]	10
Figure 2.3: Typical voltage variations in a radially operated MV/LV distribution network [41]	12
Figure 2.4: Single line diagram and corresponding phasor diagram illustrating the voltage drop in a distribution system [26]	13
Figure 2.5: Single line diagram illustrating the voltage drop in a distribution system with DG	14
Figure 2.6: OLTC representation and its equivalent circuit diagram [26]	16
Figure 2.7: Basic OLTC transformer: (a) controller arrangement [26], (b) illustration of tap changing [54]	16
Figure 2.8: Example of a <i>PFfix</i> characteristic curve [56]	17
Figure 2.9: Example of a <i>PFP</i> characteristic curve [39]	18
Figure 2.10: Example of a <i>QU</i> characteristic curve [56]	18
Figure 2.11: Example of a <i>PU</i> characteristic curve	19
Figure 2.12: MV distribution network section [43]: (a) single line diagram along with IN optimal placement, (b) problematic voltage profiles prior to the IN connection, (c) improved voltage profiles after the IN connection	20
Figure 2.13: Example of Intelligent Node configuration [61]	20
Figure 3.1: Frequency bands and time scales of various dynamic phenomena in power systems [62]	23
Figure 3.2: Cigré European MV distribution network benchmark	24
Figure 3.3: Residential weekly load profiles	25
Figure 3.4: Commercial / Industrial weekly load profiles	26
Figure 3.5: Resulting weekly load profiles for different network sections: (a) summer period, (b) winter period	27
Figure 3.6: Resulting weekly load profiles for the network section that is modelled in detail: (a) summer period, (b) winter period	28
Figure 3.7: Single line diagram of a Photovoltaic Power Plant (PVPP) connected to the MV distribution grid	30
Figure 3.8: Block diagram of the Photovoltaic Power Plant (PVPP) model	31
Figure 3.9: Solar irradiance weekly time series	33
Figure 3.10: Active power output of a PVPP model with $P_{nom} = 0.7 \text{ MW}$	33
Figure 3.11: Block diagram of the Voltage Controller model	34
Figure 3.12: Single line diagram of a Wind Power Plant (WPP) connected to the MV distribution grid	35
Figure 3.13: Block diagram of the Wind Power Plant (WPP) model	35
Figure 3.14: Wind speed weekly time series	36
Figure 3.15: Active power output of a WPP model with $P_{nom} = 4 \text{ MW}$	37
Figure 3.16: Block diagram of the Mechanical System model	37
Figure 3.17: Normal rotor speed versus power control characteristic (dashed) and its first-order approximation (solid)	39
Figure 3.18: Single-line diagram of a 2-port Intelligent Node (IN) connected to the MV distribution grid	40
Figure 3.19: Block diagram of the Intelligent Node (IN) model	40
Figure 3.20: Block diagram of the PQ Controller model	42
Figure 3.21: Flow chart of the Charge / Discharge Limiter control algorithm	43
Figure 4.2: Block diagram of the Advanced OLTC Controller model (the shown model is for HV/MV transformer 0-1)	47
Figure 4.3: Flow chart of the AVC Relay control algorithm	49
Figure 4.4: Block diagram of the Intelligent Node Controller model (the shown model is for Intelligent Node 8)	50
Figure 4.5: Block diagram of the Voltage Controller model	52

Figure 4.6: Single line diagram of the test system (communication links are denoted with dashed lines)	55
Figure 4.7: Critical nodes voltage for base case control scenario: (a) F1 - summer, (b) F2 – summer, (c) F1 – winter, (d) F2 - winter.....	61
Figure 4.8: Voltage as a function of time and distance from substation, for base case control scenario during summer: (a) branch '1-2-3-4-5-6', (b) branch '1-2-3-8-9-10-11', (c) branch '1-2-3-8-7', (d) branch '12-13-14'	62
Figure 4.9: Voltage as a function of time and distance from substation, for base case control scenario during winter: (a) branch '1-2-3-4-5-6', (b) branch '1-2-3-8-9-10-11', (c) branch '1-2-3-8-7', (d) branch '12-13-14'	63
Figure 4.10: Transformer 0-1 results for base case control scenario during summer: (a) secondary bus voltage, (b) tap position, (c) power.....	66
Figure 4.11: Transformer 0-12 results for base case control scenario during summer: (a) secondary bus voltage, (b) tap position, (c) power.....	67
Figure 4.12: Transformer 0-1 results for base case control scenario during winter: (a) secondary bus voltage, (b) tap position, (c) power.....	68
Figure 4.13: Transformer 0-12 results for base case control scenario during winter: (a) secondary bus voltage, (b) tap position, (c) power.....	69
Figure 4.14: Transformer 0-1 results, for advanced OLTC control scenario during summer: (a) critical nodes voltage, (b) tap position, (c) power.....	73
Figure 4.15: Transformer 0-12 results, for advanced OLTC control scenario during summer: (a) critical nodes voltage, (b) tap position, (c) power.....	74
Figure 4.16: Transformer 0-1 results, for advanced OLTC control scenario during winter: (a) critical nodes voltage, (b) tap position, (c) power.....	75
Figure 4.17: Transformer 0-12 results, for advanced OLTC control scenario during winter: (a) critical nodes voltage, (b) tap position, (c) power.....	76
Figure 4.18: Results for coordinated voltage control scenario (IN 6 only) during summer: (a) voltage at nodes controlled by IN 6, (b) tap position of OLTC 0-1, (c) OLTC 0-1 error signals	80
Figure 4.19: Detailed view of action cases for coordinated voltage control scenario (IN 6 only) during summer: (a) action mode 1 (#1), (b) action mode 1 (#2), (c) action mode 4 (#1), (d) action mode 4 (#2)	81
Figure 4.20: Results for coordinated voltage control scenario (IN 6 only) during summer: (a) active power exchange of IN 6, (b) SOC level of IN 6	82
Figure 4.21: Results for coordinated voltage control scenario (IN 6 only) during winter: (a) initial and corrected active power set-points for side 6, (b) initial and corrected active power set-points for side 6_tie, (c) SOC level of IN6	83
Figure 4.22: Results for coordinated voltage control scenario (INs 6 & 8) during summer: (a) voltage at nodes of Feeder 2, (b) tap position of OLTC 0-12, (c) OLTC 0-12 error signals.....	86
Figure 4.23: Detailed view of action cases for coordinated voltage control scenario (INs 6 & 8) during summer: (a) action mode 1 (#1), (b) action mode 1 (#2), (c) action mode 1 (#3).....	87
Figure 4.24: Results for coordinated voltage control scenario (INs 6 & 8) during summer: (a) active power exchange of IN 8, (b) SOC level of IN 8	88
Figure 4.25: Results for coordinated voltage control scenario (INs 6 & 8) during winter: (a) active power exchange of IN 8, (b) SOC level of IN 8	89
Figure 4.26: Maximum installed DRG capacity for different voltage controller types	91
Figure 4.27: Number of tap changes performed in one week as a function of voltage controller type and season: (a) OLTC 0-1, (b) OLTC 0-12, (c) OLTC 0-1 & OLTC 0-12	92
Figure 4.28: Voltage Quality Index as a function of voltage controller type and season	93
Figure A.1: Geometry of overhead and underground lines of European MV distribution network benchmark.....	99

LIST OF TABLES

Table 2.1: Typical line parameters [49] [50]	14
Table 3.1: Load demand in the MV distribution network.....	26
Table 3.2: Exponential load parameters	30
Table 4.1: List of variables that appear in Figure 4.3	49
Table 4.2: Responsibility share of each device participating in the coordinated voltage control scheme.....	50
Table 4.3: Offered IN operation modes	51
Table 4.4: Base case control scenario – maximum hosted DRG capacity	58
Table 4.5: Base case control scenario – Basic OLTC Controller parameters and simulation results	58
Table 4.6: Advanced OLTC control scenario (unchanged hosted DRG capacity) – simulation results.....	70
Table 4.7: Advanced OLTC control scenario – maximum hosted DRG capacity	70
Table 4.8: Advanced OLTC control scenario – simulation results.....	70
Table 4.9: Coordinated voltage control scenario (IN 6) – maximum hosted DRG capacity.....	77
Table 4.10: Coordinated voltage control scenario (IN 6) – simulation results	77
Table 4.11: Coordinated voltage control scenario (INs 6 & 8) – maximum hosted DRG capacity.....	84
Table 4.12: Coordinated voltage control scenario (IN 6 & 8) – simulation results	84
Table 4.13: Simulation results for different voltage control schemes.....	90
Table 4.14: Necessary remote communication infrastructure for different voltage control schemes	90
Table A.1: HV-MV subtransmission equivalent network parameters of European MV distribution network benchmark [42]	99
Table A.2: HV/MV transformer parameters of European MV distribution network benchmark [42].....	99
Table A.3: Geometry of overhead and underground lines of European MV distribution network benchmark.....	100
Table A.4: Conductor parameters of overhead lines of European MV distribution network benchmark [42]	100
(coloured cells contain calculation results)	100
Table A.5: Conductor parameters of underground lines of European MV distribution network benchmark [42]	100
(coloured cells contain calculation results)	100
Table A.6: Connections and line parameters of European MV distribution network benchmark [42]	100
(coloured cells contain calculation results)	100
Table A.7: Used parameters for overhead line conductor current rating calculation	101
Table A.8: Load parameters of European MV distribution network benchmark [42]	101
Table B.1: Step-up transformer parameters of the PVPP model.....	103
Table B.2: Voltage controller parameters of the PVPP model.....	103
Table C.1: Step-up transformer parameters of the WPP model.....	105
Table C.2: Mechanical system parameters of the WPP model.....	105
Table C.3: Voltage controller parameters of the WPP model	106
Table D.1: Step-up transformer parameters of the IN models.....	107
Table D.2: BESS and PWM converters parameters of the IN models	107
Table D.3: Detailed battery specifications	107
Table D.4: PQ Controller parameters of the IN models	108
Table E.1: AVC Relay and Primary Controller parameters	109
Table E.2: Voltage Controller parameters	109
Table F.1: Base case control scenario – maximum & minimum voltage of selected nodes	111
Table F.2: Advanced OLTC control scenario (maximum DRG penetration) – maximum & minimum voltage of selected nodes	111

1 INTRODUCTION

1.1 INTRODUCTION

An electric power system is a set of interacting devices that convert primary energy sources (e.g. heat) into electricity and then transport and distribute the electrical energy to consumers, where it is used in this form or converted to other forms of energy (e.g. mechanical energy). Electric power systems have been, for more than half a century, based on large centralised generating stations at a relatively small number of locations. In these stations, the voltage is stepped up to high voltage (HV, more than 110 kV) and extra high voltage (EHV, up to 400 kV) levels, before it can be transmitted over long distances –with relatively low losses– through interconnected transmission systems. Afterwards, the voltage from the HV transmission systems is stepped down to radially operated medium voltage (MV) distribution systems and then to radial low voltage (LV) distribution systems, where the electric power is distributed to the loads [1] [2]. The above described power system structure represents a traditional, “vertically” operated and controlled structure, which is now in the process of transformation to a “horizontal” structure due to the increasing penetration of renewable and distributed resources. The transition from “vertically” operated power systems towards “horizontally” operated power systems is illustrated in Figure 1.1.

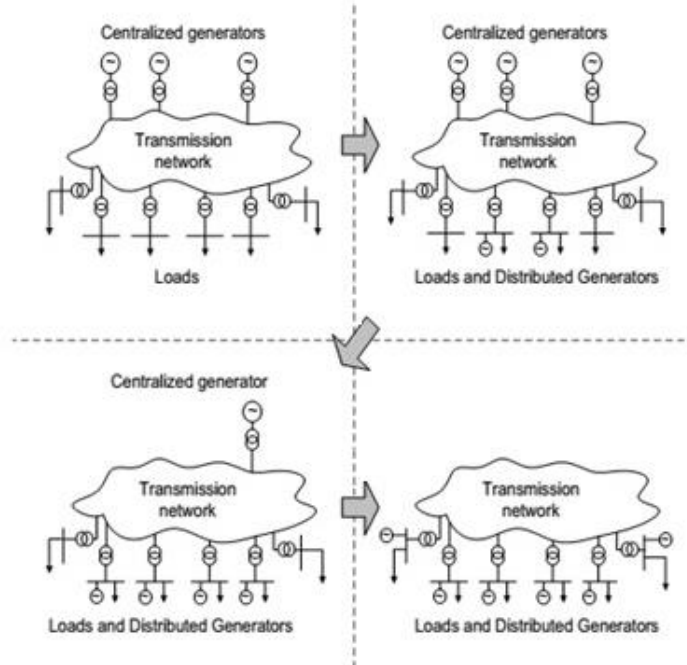


Figure 1.1: “Vertical-to-Horizontal” transformation of the power system [2]

1.2 STUDY OF POWER SYSTEMS

1.2.1 GENERAL APPROACH

Interconnected power systems have been characterised as the largest and most complex systems ever built by man [3]. Due to the size and the complexity of such systems, a theoretical study based on reference handbooks is necessary [4] [1] [5] [6], though it is not enough by itself. Computer-aided simulations offer enhanced analysis possibilities and a more in-depth knowledge of power systems. Nowadays, digital simulation studies reflect the standard procedure for power system operation, planning and testing.

1.2.2 MODELLING

A systematic study of power systems is based on the methodological approach of modelling. After the physical system has been modelled, simulations can be run using computer analysis tools. The scope of a study determines the way that a physical system is mathematically represented, as well as the extent of simplifications made. In general, the collective dynamics of the various elements constituting the system may be written mathematically as a set of ordinary differential equations (ODEs). For most dynamic studies, except from fast electromagnetic transient studies, the dynamics of transmission lines and loads are neglected and replaced by a set of algebraic constraints. This substitution replaces the ODE description of the system with one consisting of differential-algebraic equations (DAEs), thus reducing the order of the system [7]. Since the set equations describing a power system is highly non-linear, computer-aided iterative techniques of numerical analysis are used.

The three-phase ABC model representation with lumped parameters is the basis for model representations. All electrical quantities of the network and all model equations are then given in the three-phase ABC reference frame. Such models are commonly used in EMTP-like detailed time domain simulations. Power electronic based equipment, such as Flexible Alternating Current Transmission System (FACTS) controls and HVDC, can easily be modelled. On the other hand, in large power systems the representation of network voltages and currents in the three-phase ABC reference frame would increase the computational burden, since the electrical quantities vary with the power frequency or system frequency, even during steady-state conditions [8].

Another commonly used variable representation in power systems area is the DQ0 representation. The DQ0 or Park's transformation is mainly deployed in the derivation of model equations of electric machines. The DQ0 reference frame is a reference frame rotating with the system frequency. Under balanced steady-state operation the electrical quantities have constant values, while during electromechanical oscillations these quantities vary slowly with time (2-3 Hz). This leads to faster simulation times under balanced conditions, although under unbalanced conditions the efficiency can drastically decrease [8]. Following to the above stated, if all time derivatives of basic power system quantities (voltage and current magnitudes along with their respective phase angles) are set to zero, then the defining equations of power flow in a strictly stationary system are obtained. These are the classical phasors as originally defined around the early 19th century for analysing stationary conditions and have been used until today as the defining equations in computing steady-state three-phase balanced power flow (or load flow) solutions, the most frequently used computation in power system operation and planning [9]. Additionally, when the system response to a change needs to be studied, standard load flow usually provides the initial conditions for a dynamic analysis [10].

Stationary phasor representation can also be used as a quasi-stationary approximation which allows voltages, currents or power to "slowly" vary. This approximation has been used for long-term frequency or voltage stability studies. Here, the long-term time scale refers to transients that typically last for several minutes [11]. It is also claimed that a quasi-stationary environment offers quite satisfactory accuracy for transient stability studies or, equivalently, synchronous generator rotor angle stability studies [9]. In this case, the relevant transients take place in a short-term time scale, meaning a time frame of a few seconds. Similarly, the quasi-stationary time domain simulation relies on time-scale decomposition technique, meaning that faster phenomena are represented by their equilibrium conditions instead of their full dynamics. This greatly reduces the complexity of the resulting model. As far as long-term voltage stability phenomena are concerned, the aforementioned method has been validated with respect to detailed time simulation, while offering better accuracy and richer interpretations than simple load flow based methods. Furthermore, it reproduces the long-term dynamics (see Figure 3.1 in page 23) of on-load tap changing devices (OLTCs), automatically switched shunt compensation and protection devices [12].

More recently, the application of dynamic phasor based technique allowed for accelerated power system simulations under both normal and unbalanced conditions. All dynamic phasor models are derived from their corresponding three-phase ABC and DQ0 frame based time domain models. Recent technological advances, such as FACTS controls, can also be successfully modelled. Dynamic phasor approach provides a middle ground between sinusoidal quasi-stationary representation and time-domain representation for electric power system modelling. Hence, a wider bandwidth in the frequency domain is provided, compared to the traditional slow quasi-stationary assumptions used in transient stability studies, where the electromagnetic transients are totally neglected [8]. Literature shows that, not only under unbalanced conditions the dynamic phasors based models are much more efficient than the time domain ones, but also control actions are more easily realised [13].

Another important aspect is the modelling consistency throughout the whole system. For example, in cases that it is convenient to include the transmission line dynamics for simulations, it is necessary to include dynamics of the loads as well; the combination of static load models with line dynamics often leads to erroneous conclusions. Most conventional load models, such the ZIP model, do not adequately model fast dynamics in power systems [7] [14].

1.2.3 SOFTWARE TOOLS

1.2.3.1 OVERVIEW

Over the years, various large-scale simulation software packages have played an important role in providing users a better understanding of power engineering and power system operation. The power industry is currently a noteworthy user of power system analysis and design software, on which power engineering control and operation is mainly based. Moreover, from an educational point of view, the availability of such software has enhanced the learning and research process, thus extending classroom capabilities [15]. Software packages for power system analysis can basically be divided into two classes of tools: commercial software and educational / research-aimed software. Each class covers different user profiles and needs.

1.2.3.2 COMMERCIAL SOFTWARE

Commercial software packages which are available on the market (e.g. PSS/E, PowerFactory, Simpow and PSCAD) follow an “*all-in-one*” philosophy and are typically well-tested and computationally efficient. Nevertheless, commercial software can be less user-friendly and thus less appropriate for educational purposes. In addition, commercial software is “*closed*”, in a sense that user is not allowed to change the source code or add new algorithms.

PSS/E has been developed by Siemens Power Technologies International (Siemens PTI) and its presence in the market goes back to more than 30 years [16]. It has various modules like power flow, optimal power flow, short circuit analysis, dynamic simulation, small signal analysis and reliability assessment, all combined in a graphical environment. It is a power transmission oriented software, whose model library includes emerging technologies, such as advanced FACTS devices and wind turbines. In addition, user-defined models and control scripting are supported. PSS/E software is a benchmark against which other newly developed software is tested [17].

PowerFactory was developed by DIgSILENT more than 25 years ago [18]. This software not only supports modules similar to the above described for PSS/E, but also supports power distribution studies and distributed generation (i.e. PV-cells, wind turbines, fuel cells and micro-turbines). A large model database (e.g. parts of European electricity grid, RES generation) have made it rather widespread in the power industry sector. It should be stated that v15.0 of PowerFactory has been used for the needs of this thesis.

PSCAD has been developed by Manitoba HVDC Research Centre and was first introduced as a commercial product in 1994 [19]. It is an EMTP (Electromagnetic Transients Program) used in planning, operation, design and commissioning of power systems, but also in the preparation of tender specifications. Although PSCAD was initially focused on DC phenomena, several types of studies that can be currently conducted using PSCAD include contingency study of AC networks, magnetic saturation study, control system design (coordination of FACTS and HVDC is supported), harmonic analysis, pulsing effects and lightning strike study. On the contrary, load flow is not supported, meaning that the initial conditions of an EMT simulation have to be provided by an external program. It is worth noting that due to the small integration step size, EMTP data is at the highest level and can be extracted and used in other types of applications, such as PSS/E (stability type) and real-time simulators [20].

Reference should be made to commercial digital real-time simulators such as eMEGAsim and Hypersim, which address real-time and Hardware-In-the-Loop (HIL) simulation. The term real-time has been traditionally used to describe interactive systems where the computer response is fast enough to satisfy human users. Regarding power systems and according to [21], a digital real-time simulation may be defined as “*a faithful reproduction of output waveforms, by combining systems of hardware and software, which would be identical to the waveforms or effects produced by the real power system being modelled*”. In a HIL simulation, parts of the fully digital real-time simulation, such as control or protection systems, are made with actual physical components. Consequently, power engineers can use HIL simulation to verify the safe operation of new control device before actually installing it in the electricity grid.

1.2.3.3 EDUCATIONAL / RESEARCH-AIMED SOFTWARE

For educational purposes, flexibility and ease of use are often more crucial aspects than computational efficiency. Given that specific criteria are met, non-commercial software packages can be effective educational / research tools [15]. In the last decade, high-level scientific languages, such as Matlab and Mathematica, have become popular for both research and educational purposes. For instance, Matlab is a matrix-oriented programming tool offering large plotting capabilities and a graphical environment (Simulink) which favours the control scheme design. For these reasons, a number of Matlab-based research and educational power system tools have been proposed [22]. Among these, SimPowerSystems (SPS), Power System Analysis Toolbox (PSAT) and MatPower are of greater interest.

SimPowerSystems is an application that integrates an extensive library of electrical machines, power electronics and many other power system components, along with the advanced analysis and design tools already existing in Matlab-Simulink [23]. More specifically, features offered by SPS encompass power flow, small-signal stability analysis, time domain

simulation, EMT analysis, along with a graphical user interface (GUI) and a graphical network editor (GNE). Although PSAT has many similarities with SPS, these two packages differ in that PSAT supports optimal power flow and continuity power flow (relevant to voltage stability analysis), whilst EMT analysis is not an option any more. Finally, MatPower is a simple package with non-graphical user interface, suitable for solving power flow and optimal power flow problems [24]. On the other hand, MatPower is open source and freely downloadable.

1.3 DISTRIBUTED GENERATION

1.3.1 OVERVIEW

In the last two decades, technological innovations and a changing economic and regulatory environment have resulted in a renewed interest for the use of small-scale generation, connected to local distribution systems. This type of generation is commonly called Distributed Generation (DG). Although it may be a fairly new concept in the economics literature about electricity markets, the idea of DG is not new at all, as in the early days of electricity generation this kind of generation was the rule, not the exception.

Definition

According to the definition from IEEE, “*Distributed Generation is the generation of electricity by facilities that are sufficiently smaller than central generating plants, so as to allow interconnection at nearly any point in a power system*” [25]. DG can come from renewable or non-renewable energy resources, using both modern and conventional technologies. Non-renewable DG technologies include internal combustion engines, small gas turbines, small co-generation units (CHP) and micro-turbines. Renewable DG technologies include wind turbines, photovoltaics (PV), fuel cells, small hydro-power plants, biomass and geothermal generating plants; the latter type of DG can be characterised as Distributed Renewable Generation (DRG) [26].

1.3.2 DRIVERS FOR DG GROWTH

According to the International Energy Agency (IEA) [27], five major factors have contributed to the evolution of DG, namely:

- i. Developments in distributed generation technologies,
- ii. constraints on the construction of new transmission lines,
- iii. increased customer demand for highly reliable electricity,
- iv. the electricity market liberalisation and
- v. concerns about climate change.

1.3.3 CONTROLLABILITY AND GRID CONNECTION TYPE

DG can be classified in terms of controllability and grid connection type. Below, a description of controllable and non-controllable DG, as well as a description of direct grid-connected and indirect grid-connected DG, follows [2].

Controllable DG is characterized by its ability to control the fuel (or the primary energy source) supply to the generator. Consequently, the output power is dispatchable and can be predetermined. Among the DG technologies that can be classified as controllable DG are conventional fossil fuel based generators, micro-turbines, fuel cells, geothermal power plants and biomass driven power plants. On the other hand, non-controllable DG technologies are characterised by the fact that the DG operator cannot determine the power output of the DG units. Among the DG technologies that can be classified as non-controllable DG are small hydro-power plants, wind turbines, PV and CHP plants.

Direct Grid-Connected DG includes DG units connected directly to the AC grid. In general, this generation (or conversion) can be done by means of either a synchronous or an induction generator. A synchronous generator is usually applied to steam plants, gas turbines and co-generation plants, while small hydro-power plants and older design or small wind turbines are equipped with an induction generator. On the contrary, several DG types generate DC electricity (e.g. photovoltaic panels and fuel cells), high-frequency AC (e.g. micro-turbines) or variable frequency AC (e.g. certain types of wind turbines). Therefore, a power electronics interface is necessary in order to connect these devices to the constant-frequency AC grid; these are cases of indirect grid-connected DG.

1.3.4 CHALLENGES TO INCREASED PENETRATION OF DG

The installation and connection of DG units to the distribution networks is likely to give rise to power quality issues. Imbalances between active power demand and supply can cause the system frequency to deviate from the rated value of 50 Hz. In particular, a large penetration of DRG can negatively affect frequency regulation, since DRG is mostly based on intermittent primary energy sources –such as wind speed and solar radiation– and is difficult to be centrally dispatched and

controlled. Respectively, this can have an impact on the efficiency of conventional power plants and on their emissions [25].

Furthermore, a rise in the voltage level in radial distribution systems is mentioned as probably the most important issue caused by high DG penetration [26] [28] [29] [30]. Voltage rise occurs when the customer load is at the minimum level and power injection of DG flows back to the public grid; this limits DG penetration, especially in rural areas. In addition, units connected to the grid via a power electronics interface may contribute to the harmonic distortion of the network voltage, by injecting higher harmonic current [31].

An increased share of DG can also raise protection issues. Power flow can be bidirectional within a certain voltage level, but power usually flows from higher to lower voltage levels (i.e. from the transmission to the distribution grid). An increased share of DG units may induce power flows from the medium voltage grid to the high voltage grid. Hence, different protection schemes may be required [32] [33]. What is more, unwanted “*islanded*” operation of a network section during an outage or scheduled maintenance works can create safety concerns.

Finally, it is rather debatable whether DG can be favourable for energy security. For example, it is claimed by IEA that DG can contribute to reduce the risks and costs of blackouts [27]. DG units with a power electronic interface are sometimes capable of delivering a certain amount of reactive power, thus providing ancillary service to the grid [34]. Others like CIREN, claim that DG does not contribute to system security [35].

1.4 THESIS OBJECTIVE AND APPROACH

1.4.1 PROBLEM FORMULATION

In distribution systems, the voltage magnitude at each load connection point is one of the most important parameters for the quality of power supply. Technical regulations or specific contracts define the allowed voltage range that bounds the maximum permitted variation of every bus voltage. Therefore, voltage has to be appropriately regulated, allowing variations within the permissible limits.

Traditionally, voltage control in MV distribution networks has been mainly focused on dealing with voltage drop along radially operated feeders. Direct voltage control has been carried out by On-Load Tap Changers (OLTC) installed in HV/MV substations and, less often, by on-load tap changing performed by Step Voltage Regulators (SVRs) [29]; the latter device is an autotransformer installed at a point along the feeder, so as to regulate the voltage downwards of this point and towards the feeder end. Indirect voltage control has been mainly carried out by reactive power injection, using shunt capacitor banks deployed at substation level, or Static VAR Compensators (SVCs) installed at specific points along a feeder [6]. The actual implemented controllers are provided with local voltage measurements and have been designed and calibrated for a passive and radial use of the MV system. These assumptions involve unidirectional power flows from the primary substation towards the feeders’ ends. Consequently, voltage profiles fall along the feeder with a slope directly determined both by line characteristics and power flow related to the supplied load requirements.

The presence of DRG makes these assumptions no longer valid, since the power generated by DRG units will increase the voltage at the adjacent nodes. In addition, when the generated power is high, the resulting reverse power flow (active power flow from the distribution system to the transmission system) causes the voltage at the MV nodes to be higher than the voltage at the primary substation [26]. Consequently, the presence of DRG will affect voltage control in distribution systems and it needs to be reconsidered whether methods like local voltage control and reactive power injection can still enable the network operator to cope with the newly introduced voltage rise issues. In addition, due to the relatively high R/X ratio of MV and LV grids, controlling the voltage in such grids may be more efficiently achieved by controlling active power flow.

1.4.2 OBJECTIVE

The objective of this thesis is to create a new voltage control strategy for the active management of MV distribution networks, which will not only successfully limit voltage variations within a specified range, but also allow for an increased penetration of DRG. The proposed coordinated voltage control strategy will deploy control of HV/MV transformers On-Load Tap Changers in combination with active power control provided by Intelligent Nodes, that allows network reconfiguration.

1.4.3 RESEARCH QUESTIONS

First, in order to conceptualise, design and implement the proposed Coordinated Voltage Controller, a crucial question needs to be answered:

- i. Which are the factors that limit the ability of a voltage controller to increase the installed DRG capacity in MV distribution networks, while keeping voltage variations bound within a specified range?

Following to the initial identification of the limiting factors, the second research question demands for an answer:

- ii. Which features should the proposed voltage control algorithm accommodate, in order to effectively deal with the previously identified limiting factors?

After the implementation of the proposed voltage control algorithm, its performance must be evaluated. The third research question stems directly from objective of the proposed control strategy and is formulated accordingly:

- iii. What is the maximum level of installed DRG capacity that can be reached in a given MV distribution network by applying the proposed coordinated control strategy and how is this compared against other control strategies?

The evaluation procedure would not be thorough enough if the above primary evaluation criterion was the only one used. Thus, the final research question refers to the secondary effects that the application of the proposed voltage controller can potentially have on other network components and quantities. More precisely:

- iv. What are the effects of the proposed coordinated voltage control strategy on the OLTCs operation and on the network voltage quality? In addition, what is the impact that this coordinated scheme has on the communication infrastructure of a MV distribution network?

1.4.4 APPROACH

With the penetration of DRG in MV distribution systems showing an increasing trend, a study of voltage rise and voltage drop effects in MV distribution networks will first be made. Distribution-Flexible AC Transmission Systems (D-FACTS) devices, OLTC, as well as grid reconfiguration, will be investigated as means of dealing with voltage variation problems. Afterwards, a coordinated voltage control strategy will be proposed and demonstrated. The development and implementation of the proposed control strategy will be based on modelling and simulations. More specifically, using commercial power system simulation software (DiGILENT PowerFactory), a model of a typical North-European MV distribution network will serve as a basis. The benchmark network model will be combined with power electronics-interfaced DRG models. PV Power Plants and Wind Power Plants will represent the generation part, while aggregated MV loads (in the form of MV/LV distribution transformers) will represent the consumption part. Choosing to use models of uncontrollable DRG is expected to create a more challenging regime (in terms of voltage variations) for the implemented voltage control strategy. In addition, the following modelled components will provide the basic voltage control capabilities:

- i. On-Load Tap Changer (OLTC) of the HV/MV transformer. This component provides direct voltage control.
- ii. Multi back-to-back converter, known as Intelligent Node (IN). The latter is a Voltage Source Converter-based device, able to adjust the active and reactive power flow at its terminals; an energy storage capability will also be dimensioned, based on the needs of the MV grid. This component provides indirect voltage control.

The MV network voltage control schemes will be tested on several benchmark scenarios, involving various generation and load levels (i.e. normal and reverse power flow situations), with a view to assess the consequences of the control on branch flows and nodal voltages. A coordinated regime of the above mentioned control schemes should allow for the system to adequately operate under the conditions defined by each test scenario. Assessment of the simulation results will serve as a positive feedback for the modelling and control optimisation. Finally, voltage control performance indicators will be computed and the optimal control strategy (in terms of optimal combination of OLTC and IN devices) will be chosen.

1.4.5 LIMITATIONS

Voltage control in MV distribution grids with a large share of DRG encompasses a large variety of topics related to real-time monitoring and control functions provided by DNOs, such as Power Matching, Power Routing, Demand Side Management (DSM) and Demand Response (DR) [36]. These functions, amongst others, give the possibility of local area networks to self-support their demand by DRG and to deal with transmission bottlenecks related to the actual load and generation schedules of the market parties [37].

Another topic currently of interest is the reactive power support (injection or absorption) and active power curtailment of DRG units [29] [38]. This scheme has already been implemented in many countries of North Europe (e.g. Germany), as a way to solve unwanted voltage problems associated with high penetration of PV systems in distribution networks [34]. On the other hand, as the rating of the DRG unit is fixed, injecting large amounts of reactive power necessitates a reduction in the active power injection and thus –if relying on a generation-based premium– a reduction in the net revenue of the DRG. In this thesis, the voltage support function provided by the DRG units is taken into account. The operating power factor of a power plant is variable and cannot be lower than 0.95 (inductive or capacitive). Such a choice fully complies with the German standards presented in [39] and is expected to provide realistic results, applicable to the majority of the countries situated in the North-European region. It should be noted that the converters of the DRG units are assumed to be slightly oversized in order to allow for exchanging small amounts of reactive power without curtailing active power.

Finally, bearing in mind that a thesis project is normally characterised by finite study and time limits, the aforementioned DNO control functions will not be considered within the context of this thesis. What is more, by not taking into account those schemes, it is made possible to test the feasibility of a control system that relies entirely on assets owned by the grid operator. Finally, short-term stability studies, as well as fault studies, are not within the scope of this study; only long-term dynamics due to smooth fluctuations in the production of DRG units are going to be considered.

1.5 RESEARCH FRAMEWORK

This thesis work is part of the Watt Connects project. This is a joint project of initially three partners: DNV GL (formerly DNV KEMA), Liander and Tennet. Watt Connects aims at further developing the smart grid technology, by offering involved stakeholders insight and a conceivable way to familiarise themselves with the operation and the benefits of Smart Grids. It consists of a demonstration table and appropriate simulation tools that allow for new equipment and services to be tested in conjunction with other existing technologies, in an interactive way that includes human behaviour. The fact that a system can be tested at a smaller scale significantly minimises investment risks and gives a clear view of its expected real-life performance [40].

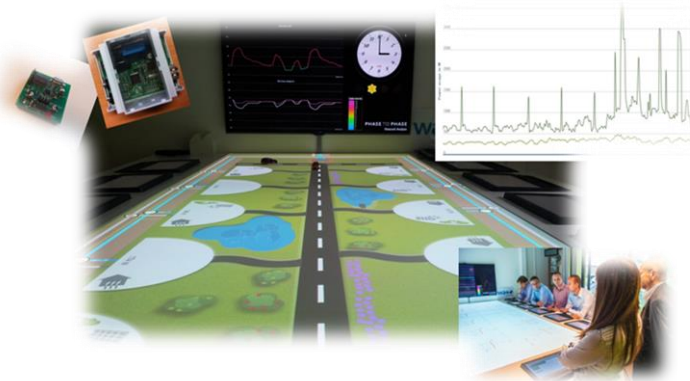


Figure 1.2: The interactive demonstration table of the Watt Connects project

Up to now, the demonstration table (see Figure 1.2) has been used for performing power flow simulations in low voltage distribution networks in the presence of DRG units. One of the future goals of DNV GL is to extend the concept of Watt Connects to the medium voltage distribution level, by enabling the system to perform similar simulations and demonstrate results to the stakeholders. Furthermore, developing novel voltage control strategies that can minimise voltage variations in the grid is also within the R&D scope of the company. With these in mind, the objective of this study is in line with the future development of the Watt Connects project and also an active research field at the university.

1.6 THESIS OUTLINE

To guide the reader through the thesis, the outline of the chapters will be given in this section.

Chapter 1 offers an introduction to the study topic. Initially, a general insight to the methods of power system study is given. Next, the basic aspects of distributed renewable generation are presented, along with the thesis objective and research questions.

In Chapter 2, the basic aspects of MV distribution systems are described, while particular importance is given to voltage related aspects. After presenting the relevant grid code requirements, the mechanism responsible for the creation of voltage drops / rises is analysed. A number of D-FACTS devices are also presented and discussed.

In Chapter 3, the modelling approach of the study is explained and a detailed review of all components of the test system is given. The MV distribution network model is initially presented, followed by a description of the load model. The DRG modelling part describes the Photovoltaic Power Plant (PVPP) and the Wind Power Plant (WPP) models, followed by the description of the Intelligent Node model.

In Chapter 4, the proposed voltage control algorithm is initially described and analysed. Then, before proceeding to the simulations part, the test system is presented. In order to prove the value and the usefulness of the proposed controller, the test system is simulated under various control schemes. The main simulation results are presented and analysed with respect to specific criteria, while the most important findings and phenomena arising from these results are discussed.

Finally, the main conclusions of the thesis work are given in Chapter 5. This chapter also gives recommendations for future work.

2 MV DISTRIBUTION SYSTEMS

2.1 INTRODUCTION

In this chapter, the basic identifying aspects of MV distribution systems are described. As the title and the scope of this thesis indicate, particular importance is given to voltage related aspects. At first, with a view to the relevant grid code requirements, an effort is made to define at which extent is a voltage variation problem acceptable or not. In addition, the mechanism responsible for the creation of voltage drops / rises is analysed. Finally, a number of devices capable of mitigating voltage variations in MV distribution networks are presented and discussed. However, this number is limited only to the devices that are going to be used in this study.

2.2 BASIC ASPECTS OF MV DISTRIBUTION NETWORKS

2.2.1 OVERVIEW

Distribution networks distribute the electrical power from the HV/MV substations to the final customers. After various transformation steps, the voltage is converted to the level that is ultimately required. The final transformation between medium and low voltage occurs in the MV/LV transformers, from which the low voltage connections leave.

Medium voltage distribution networks are designed for voltage levels between 1 kV and 25 kV [40]. Throughout Europe, MV networks are mainly operated at 10 kV or 20 kV, but also other voltage levels exist (i.e. 6, 12 and 25 kV). The advantage of operating at 20 kV is that the price of the commercially available network components is not very different from those at 10 kV, while the power transfer capability doubles.

Medium voltage connections may consist of underground cables or overhead lines. For instance, in the Netherlands MV lines entirely consist of underground cables [41]. In Germany, MV voltage lines that serve urban and suburban areas are also using underground cables, whereas rural areas are supplied by overhead lines [42].

For a long time, MV distribution networks were used to distribute electrical power unidirectionally, from HV transmission level towards LV distribution networks and large MV clients. Nowadays, the connection of distributed renewable generation (such as wind turbines, CHP, micro-CHP and solar panels) can possibly result in bidirectional power flow. Large decentralised generators and large industrial customers with capacities from 0.3 to 10 MVA can be connected to MV distribution networks, whilst the total power of a single network is in the order of 100 MVA [40].

2.2.2 TOPOLOGY

Three basic distribution network topologies exist: (a) radial, (b) ring and (c) meshed, as shown in Figure 2.1 [43].

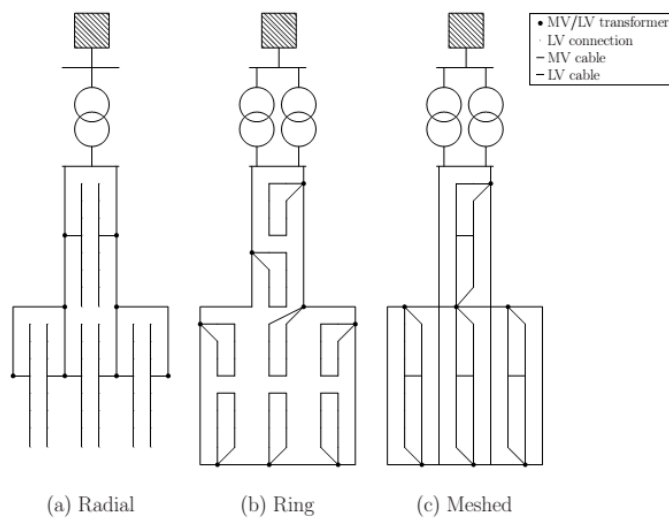


Figure 2.1: Basic topologies of distribution networks [43]

Currently, MV distribution networks have a meshed structure but are radially operated. The radial topology is characterised by only one possible supply path for each load, leading to relatively low reliability. However, an advantage of radially operated networks is that the simple and cheap maximum current-time protection scheme can be applied. The low degree of reliability obtainable with radial network is generally improved by adding emergency ties, which provide alternative routes for power supply in case of outages or scheduled interruptions. These emergency ties end with an open switch, a so called normally open point (NOP), so that a radial structure is maintained during normal conditions. This can be better understood with the help of Figure 2.2, where an example of a typical structure of a Dutch MV distribution grid is shown.

In the Netherlands, MV distribution networks mostly have ring structures and are fed either directly from an HV/MV substation (connected to the HV transmission network), or by a MV substation (connected to the MV transmission network) [41]. To the main ring a sub-ring and some stub-ends may be connected, while LV networks are connected to the MV grid by means of MV/LV transformer substations. When the distribution networks are operated radially, there is a NOP somewhere about half way of every ring and sub-ring. In the NOP, the phases are interrupted by means of a load break switch. In case of maintenance or a fault on a cable section, the load of the feeder beyond that cable section and towards the NOP will be supplied by the other feeder connected to that NOP. In case of maintenance or disturbance in a stub-end, the load can only be taken over by a mobile generator.

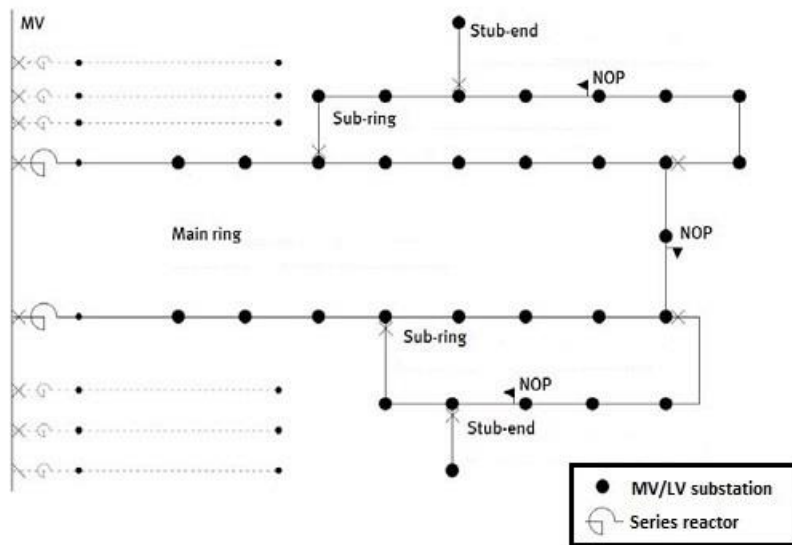


Figure 2.2: Typical structure of a Dutch MV distribution grid [41]

In the ring and meshed topologies at least two supply paths exist, which leads to higher reliability compared to the radial topology. Other advantages of meshed networks versus radial schemes are: a reduction of power losses, a better voltage profile, greater flexibility, the ability to cope with the load growth and an improvement of power quality due to the fault level increase at each bus. Moreover, as shown in [44], the meshed arrangement seems to be more suitable to accommodate a large penetration of DRG.

On the other hand, operating a network as a ring or meshed requires distance or zone protection and more switchgear, so as to ensure that only the faulted section is switched off. Thus, the network operation becomes more complicated [43]. In addition, the rising of short circuit current in each node could imply the substitution of the existing circuit breakers, due to the overcoming of their interrupting capacity.

2.2.3 OPERATION AND CONTROL

The increasing penetration of DRG has several technical implications and raises important questions as to whether the traditional approaches to operation, control and development of power systems are still adequate. This is particularly true at the distribution level, where the main portion of DRG is connected [31].

The implementation of DRG turns the “passive” distribution network into an “active” one. Under this newly introduced scheme, customers not only consume electricity, but also generate. If generation surpasses their demand, they supply the network, something that will alter the power flow in the distribution system. MV and LV distribution networks can no longer be considered as networks with unidirectional power flow. This contradicts with the concept that distribution systems have, for many years, been designed based on the assumption unidirectional power flow [5] [26].

Based on the above, the power can flow both “vertically” (i.e. from higher to lower voltage levels), as well as “horizontally” (i.e. from a MV or LV network to another, or from a generator to a load within the same MV or LV network). Such a pattern

characterises a “*horizontally*” operated power system [2]. The transition from “*vertically*” operated power systems towards “*horizontally*” operated power systems is illustrated in Figure 1.1 (see section 1.1 on page 1). Historically, “*passive*” distribution networks have been designed with a view to operate with a minimum number of control actions, since their role has been limited to just supplying electrical power from the transmission system (higher voltages) to consumers (lower voltages). Unfortunately, the practice of passive operation can limit the capacity of DRG that can be connected to an existing system. In contrast, Active Management (AM) techniques enable the distribution network operator to fully benefit from the use of the existing circuits by means of generator dispatch, control of transformer taps, control of voltage regulators, reactive power management and system reconfiguration, all in an integrated manner [31]. Active Management of MV and LV distribution networks can contribute to voltage control, balancing of generation with load and ancillary services.

In the future, distribution management systems could provide real-time network monitoring and control at key network nodes, by establishing communications between distributed generators, loads and controllable network devices (e.g. reactive compensators, voltage regulators and on-load tap changing transformers). Furthermore, active voltage control in MV level will be well coordinated with possible LV network active voltage control schemes in a hierarchical way, so that voltage deviations are first tried to be locally corrected [32].

2.2.4 ORGANISATION AND COMMUNICATION

In the past, the generation, transmission and distribution of electrical energy were centrally coordinated. For example, the planning of a new power plant was developed in close cooperation with the network planners. In addition, the active and reactive power output of power plants was coordinated with the network operator, so that overloading and network instability were prevented, while achieving an operation state with minimum losses [43]. In the course of the unbundling process, which is being implemented across Europe, the various tasks and responsibilities are split amongst different entities. A short description of several relevant entities is given below [37].

The Independent System Operator (ISO) is designated as the operator of the transmission system, who is responsible for maintaining the balance between generation and consumption. Similarly, the Transmission Network Operator (TNO) is considered as the owner of the transmission network. The unification of the TNO and the ISO, which is quite common in Europe, forms an entity called the Transmission System Operator (TSO).

The Distribution System Operator (DSO) is responsible for the real-time monitoring and control of the distribution system. Amongst others, the DSO may be responsible for emergency capacity and may be required to give priority to specific generating installations (e.g. using renewable energy sources, waste, or producing combined heat and power). Since a Distribution Network Operator (DNO) owns and operates a distribution network, DNOs and the DSO constitute together the distribution system.

Supervisory Control and Data Acquisition (SCADA), Energy Management System (EMS) and Distribution Management System (DMS) are used by the ISO, TNO, TSO, DSO and DNOs in order to be capable of real-time monitoring and control. The Information and Communication Technology (ICT) infrastructure can be enhanced to manage the operation of a very large number of small-scale generation units connected to the distribution network, by monitoring a range of variables and ensuring efficiency of generation. In this way, the introduction of DRG will be more efficient, while maintaining high standards of power quality and reliability of services. Nevertheless, related cyber-security issues must be extensively investigated [45].

In particular, ICT applications are developing rapidly in several directions, such as broadband wired and wireless internet services, satellite communication and power line communication. The standardisation of communication protocols is also developing rapidly, with the IEC 61850 family of standards as a result [46]. In the future, information about distribution network status will be increasingly obtained from sensors across the network, through high-speed wireless 4G networks and optical fibres integrated in power cables [32].

2.3 GRID CODES

2.3.1 REQUIREMENTS FOR VOLTAGE

To ensure the proper functioning of network components and devices connected to the network, the supplied voltage must comply with standards. Under normal operating conditions, the voltage limits are derived from power quality requirements; power quality requirements in Europe are based on the EN 50160 standard [47]. Regarding the derived steady-state voltage limits, it holds that: “*under normal operating conditions excluding voltage interruptions, during each period of one week, 95 % of the 10 min mean RMS values of the supply voltage shall be within the range of $U_{nom} \pm 10 \%$* ”. Here, U_{nom} stands for the declared (or nominal) voltage magnitude.

Sometimes, regulators set extra requirements at a national level. For instance, the Dutch regulations demand that voltage variations in MV distribution networks must not only be limited according to [47], but also all 10 min mean RMS values of the supply voltage shall be within the range of $U_{nom} + 10\% / - 15\%$ [48].

In Germany, special attention is given to the effects of DRG on voltage variations, since “*the magnitude of the voltage changes caused by all generating plants with a point of connection to a medium-voltage network, must at no junction point within this network exceed a value of 2 % as compared to the voltage without generating plants*” [39]. This regulation, despite being very specific and precise, seems rather impractical in its implementation; i.e., the system behaviour, both with and without DRG units installed, must first be known and then the corresponding node voltages must be compared throughout the whole examined time period.

At this point, the issue of coordination of voltages should be taken into account. In general, the voltage in a distribution network varies due to active and reactive power flow. These variations depend on the amount of power, the network components (e.g. transformers, lines) and on the network topology (radial or meshed). Assuming no DRG units connected at the MV and the LV levels, the regular voltage variations at different nodes in a typical radial distribution network can be seen in Figure 2.3 [41].

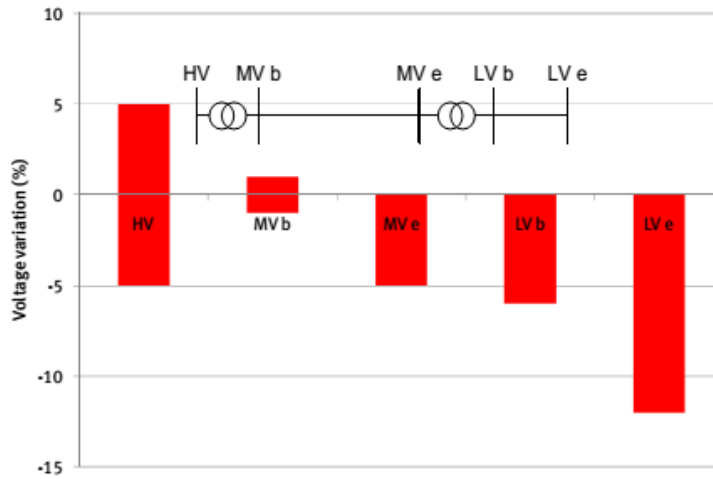


Figure 2.3: Typical voltage variations in a radially operated MV/LV distribution network [41]

Due to the continuous operation of the OLTC of the HV/MV transformer, large voltage variations that typically exist in the HV network are not present in the beginning of the MV network (MVb). Towards the end of the MV network (MVe), voltage variations increase due to the variation of power flow in the MV network. In general, a MV/LV transformer does not have any voltage control, since the tap position is fixed. Therefore, voltage variations noticed on the LV side of the transformer (LVb) will almost be the same as on the MV side (plus the voltage drop across the MV/LV transformer impedance). Additionally, any variations of power flow in the LV network will result in an increase of the voltage variation noticed at the end of the LV network (LVe). Finally, all the above voltage variations must be coordinated in a way that voltage limits are not exceeded at any node of the whole distribution network.

To the author's opinion, the approach described in [41] is built on a more realistic basis, compared to what is specified in [48] and [39]. More specifically, given that the geographical span of a distribution network is not particularly large, the prevailing weather conditions are not expected to significantly vary throughout the network; this can lead to broad similarities in the demand time series of the served loads, meaning that voltage drops in different parts of the network coincide. Consequently, according to Figure 2.3, an already significant voltage drop at the MVe level can lead to an extreme voltage drop at the LVe level. Thus, compliance with the voltage limits at the LV customers level, presupposes the enforcement of a stricter lower voltage boundary at the MV level.

Similarly, the weather conditions invariance can lead to broad similarities in the power production time series of the connected DRG units, meaning that voltage rises in different parts of the network coincide. In this case, an already significant voltage rise at the MVe level can lead to an extreme voltage rise at the LVe level. Thus, compliance with the voltage limits at the LV customers level, presupposes the enforcement of a stricter upper voltage boundary at the MV level.

Based on the above described approach, in this study the voltage variation at any node of the MV network must be bound within the range of $U_n + 3\% / - 3\%$.

2.3.2 REQUIREMENTS FOR DG

With a view to achieving high power quality and increased network reliability, distributed generators (renewable or not) connected to the MV distribution network are subject to operating requirements. Such requirements are set by regulators at a national level, meaning that differences may exist among European countries.

In the Netherlands, regulations demand that all production units connected to networks with a voltage lower than 50 kV must operate at a power factor between 1.0 and 0.85 lagging, measured at the generator terminals [48]. Furthermore, when the voltage at the PCC is below nominal, the generator must supply its maximum available amount of reactive power.

In Germany, a generating plant must operate with a reactive power output corresponding to a power factor between 0.95 lagging and 0.95 leading, measured at the PCC [39]. In the consumer reference arrow system, this means operation in the second (lagging) or in the third (leading) quadrant.

2.4 VOLTAGE DROP IN A DISTRIBUTION SYSTEM

2.4.1 TRADITIONAL DISTRIBUTION SYSTEM

A traditional distribution system is considered to be a passive distribution system, where no distributed generation exists. A basic overview of voltage drop in such a distribution system is shown with the help of the single line diagram in Figure 2.4 [26].

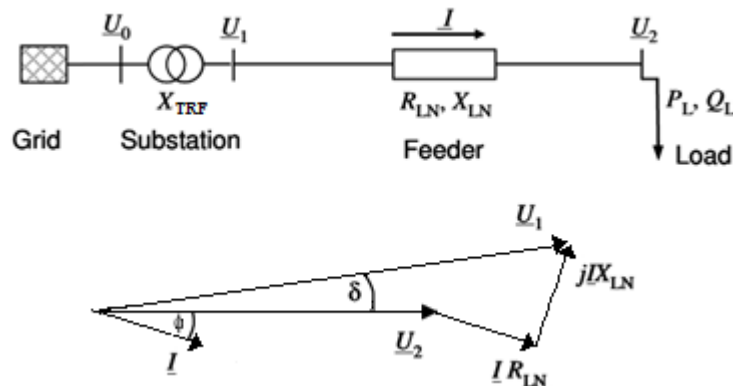


Figure 2.4: Single line diagram and corresponding phasor diagram illustrating the voltage drop in a distribution system [26]

The current \underline{I} as a function of the load complex apparent power \underline{S} and the load voltage \underline{U}_2 , is given by:

$$\underline{I} = \frac{\underline{S}^*}{\underline{U}_2^*} = \frac{\underline{P}_L - j\underline{Q}_L}{\underline{U}_2^*} \quad (2.1)$$

where P_L and Q_L are the load active and reactive power consumption, respectively. The voltage drop ΔU on the feeder is given by:

$$\Delta U = |\underline{U}_1 - \underline{U}_2| = |\underline{I} \cdot (R_{LN} + jX_{LN})| = \left| \frac{(R_{LN} \cdot P_L + X_{LN} \cdot Q_L) - j(X_{LN} \cdot P_L - R_{LN} \cdot Q_L)}{\underline{U}_2} \right| \quad (2.2)$$

where R_{LN} and X_{LN} are the feeding line resistance and reactance, respectively. For a small power flow, the voltage angle between \underline{U}_2 and \underline{U}_1 in equation (2.2) is small and the imaginary part can be neglected. Hence, the voltage drop can be approximated by the following equation:

$$\Delta U \cong \frac{R_{LN} \cdot P_L + X_{LN} \cdot Q_L}{U_2} \quad (2.3)$$

where U_2 is the load voltage magnitude.

2.4.2 DG IMPACT ON VOLTAGE DROP

When connected to a MV distribution network, a DG unit either generates or absorbs reactive power, or does not exchange any reactive power at all ($PF = 1$). Power electronics-interfaced distributed generators can also be involved in the

distribution system voltage control, i.e., when the unit operates at a constant voltage by varying its reactive power output. For a system with load and DG, as shown in Figure 2.5, the voltage drop (or rise) ΔU across the feeder can be approximated by:

$$\Delta U \cong \frac{R_{LN} \cdot (P_L - (\pm P_{DG})) + X_{LN} \cdot (Q_L - (\pm Q_{DG}))}{U_2} \quad (2.4)$$

where P_{DG} and Q_{DG} are the DG active and reactive power production, respectively. The observations that follow take into account the combined effect of active and reactive power exchange of a DG unit. Equation (2.4) indicates that if the DG unit generates reactive power or the DG unit does not exchange any reactive power with the grid, the voltage drop along the feeder is decreased. Moreover, if the generated active power is larger than the feeder load, power will flow from the DG unit towards the substation; this will cause a voltage rise. On the other hand, it is further indicated that if the DG unit absorbs reactive power, the voltage drop along the feeder can either be increased or decreased. This depends on the DG unit active and reactive power relative to the load active and reactive power and the R/X ratio of the line [26]. Storage is also included in this equation, by allowing P_{DG} to be either positive or negative, depending on whether the storage is discharging or charging.

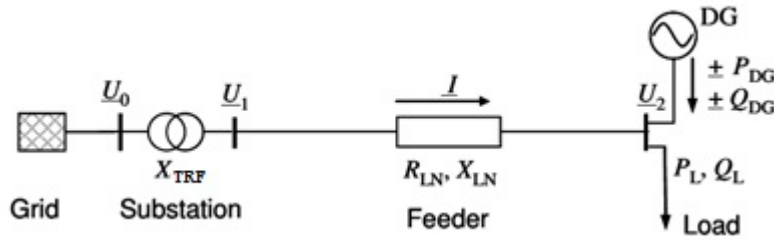


Figure 2.5: Single line diagram illustrating the voltage drop in a distribution system with DG

2.4.3 SENSITIVITY ANALYSIS

As it can be seen in subsection 2.4.1, equation (2.3) describes the voltage drop (or rise) along a line via an approximation. This relation will prove very useful in drawing several qualitative conclusions regarding the cause of voltage drop (or rise). In order to assess the influence of active and reactive power flow through a line on voltage changes, the values of R_{LN} and X_{LN} in (2.3) must be examined. Table 2.1 shows the typical normalised line parameters R'_{LN} , X'_{LN} and the typical rated current I_{rat} for high, medium and low voltage lines [49] [50].

Table 2.1: Typical line parameters [49] [50]

Type of line	R'_{LN}	X'_{LN}	I_{rat}	$\frac{R'_{LN}}{X'_{LN}}$
	[Ω/km]	[Ω/km]	[A]	[-]
HV	0.033	0.252	645	0.13
MV	0.161	0.190	396	0.85
LV	0.642	0.083	142	7.74

A more extensive search in the relevant literature confirms the data presented in Table 2.1 and allows for reaching certain conclusions. In the case of high voltage overhead transmission lines, the resistance R'_{LN} is small in comparison to the reactance X'_{LN} (ratio $R'_{LN}/X'_{LN} \ll 1$) [30]. Hence, in equation (2.3) the term $(R_{LN} \cdot P_L)$ can be neglected, meaning that the voltage change is mainly caused by reactive power flow.

In contrast, with decreasing voltage level, the reactance X'_{LN} of lines within distribution systems becomes smaller in comparison to the resistance R'_{LN} . Both medium voltage overhead lines and lines consisting of thick medium voltage cables are characterised by a ratio $R'_{LN}/X'_{LN} \cong 1$ [28] [43]. Hence, in equation (2.3) neither of the terms $(R_{LN} \cdot P_L)$ or $(X_{LN} \cdot Q_L)$ can be neglected, meaning that both active and reactive power flow influence the voltage value. Respectively, since a low voltage line is predominantly resistive (ratio $R'_{LN}/X'_{LN} \gg 1$) [30], voltage changes within a LV distribution system are mainly caused by active power flow. Overall, it can be easily deducted that:

- For a line with $R'_{LN}/X'_{LN} \ll 1$, the voltage drop (or rise) is mainly determined by reactive power flow.
- For a line with $R'_{LN}/X'_{LN} \gg 1$, the voltage drop (or rise) is mainly determined by active power flow.
- For a line with $R'_{LN}/X'_{LN} \cong 1$, the voltage drop (or rise) is determined by both active and reactive power flows.

More precisely, in the case of a MV line with DG (see the above shown third case), the term $(X_{LN} \cdot Q_L)$ may be positive or negative, depending on whether the generator produces or consumes reactive power. However, as the magnitude of the reactive power will be small compared to that of the active power, the $(R_{LN} \cdot P_L + X_{LN} \cdot Q_L)$ term will tend to be positive even in the case that reactive power is absorbed. Thus, the voltage at the PCC of the DG unit will rise above that of the HV/MV substation.

2.5 VOLTAGE REGULATION

2.5.1 OVERVIEW

There exist several means of regulating voltage in medium voltage distribution networks. To begin with, a voltage regulating device of fundamental importance is the On-Load Tap Changer (OLTC). Such devices are installed on HV/MV substation transformers and have been operating for many decades. Control and operation of the OLTC is discussed in subsection 2.5.2.

Power electronic converters used to interface DRG units with the grid can also be considered as devices with voltage regulation capabilities. Through reactive power control and / or active power curtailment of DRG, the PCC voltage can be controlled. An overview of the voltage regulation methods using the converter of a DRG unit, is given in 2.5.3

Furthermore, regarding the power control, Flexible AC Transmission Systems (FACTS) devices are becoming increasingly important [51]. Such devices combine conventional systems, power electronics and microelectronics, together with modern telecommunication systems. When applied to distribution networks, these devices are specifically characterised as distribution FACTS (D-FACTS). Additionally, the combined application of battery storage in distribution systems enables D-FACTS devices to perform not only reactive power control, but also active power control [52].

The Intelligent Node (IN) is a D-FACTS device which is of particular interest in this study. More specifically, in combination with a Battery Energy Storage System (BESS), the IN will play a major role within the scope of the proposed voltage control strategy in Chapter 4. The concept of the Intelligent Node is treated with in subsection 2.5.4. At this point, it is important to state that the list of existing D-FACTS devices is quite large [51]. In this thesis, the description of the rest D-FACTS devices has been deliberately left out of consideration; the reader who wishes to familiarise himself with this topic, should refer to the relevant bibliography [53] [6] [43].

Last but not least, the installation of shunt capacitor banks is also a means of solving voltage drop issues in the network [6]. From a practical point of view though, two aspects should be pointed out. First, capacitors are not very common in distribution systems; and second, capacitors are –almost always– disconnected at low load periods [33]. It is also known that DRG units affect the voltage profile most prominently at low load. However, in this study, both high and low load conditions will be investigated. Neglecting the shunt capacitors under maximum load could create a more stressful and challenging environment for the voltage control strategy to cope with. As a result, without loss of generality, in the rest of this thesis we will assume that there are no capacitors connected in the MV distribution system.

2.5.2 ON-LOAD TAP CHANGER

One of the key voltage regulation mechanisms available in MV distribution networks is performed by On-Load Tap Changers (OLTCs) of HV/MV power transformers. By using an OLTC, the turn ratio of a HV/MV transformer can be changed by adding turns to or subtracting turns from either the primary, or the secondary winding. As indicated by its name, changing the tap position is possible when the power transformer is carrying load. On the contrary, MV/LV transformers are usually equipped with a no-load tap changer, where the transformer ratio can only be changed when the transformer is de-energised.

The OLTC can be located at the primary or the secondary side of the transformer. In most cases, the variable tap is on the HV side [11]. One reason for this is that the current on this side is lower, making commutation easier. Another reason is that more turns are available on the HV side, thus making voltage regulation more precise.

The representation of a transformer equipped with an OLTC and its equivalent circuit diagram are shown in Figure 2.6 [26]. Notations I , U , n and y in the figure indicate current, voltage, normalisation of the transformer turn ratio and transformer admittance, respectively. Subscripts p and s indicate primary and secondary sides of the transformer, respectively.

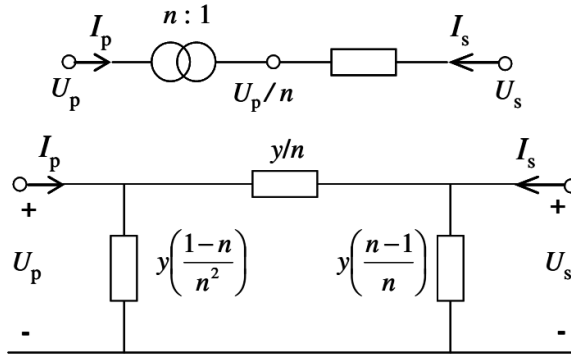


Figure 2.6: OLTC representation and its equivalent circuit diagram [26]

An OLTC basic controller is shown in Figure 2.7 (a). The OLTC controller objective is to keep the substation secondary bus voltage U_0 constant and equal to the set-point voltage U_{SET} . However, U_0 is allowed to vary around U_{SET} within a deadband range U_{DB} . This can be expressed by the following relation:

$$U_{SET} - 0.5 \cdot U_{DB} \leq U_0 \leq U_{SET} + 0.5 \cdot U_{DB} \quad (2.5)$$

OLTCs are slowly acting, discrete devices, which change the tap by one step at a time if equation (2.5) is not valid for a time period larger than the specified intentional time delay T_i (ranging from several seconds to a couple of minutes). Consequently, frequent or unnecessary tap movements, which are a cause of wear to the equipment, can be avoided. Moreover, the effect of transient voltage variation can be reduced [54]. The minimum time required for the tap changer to complete one tap movement is usually close to 5 seconds and corresponds to the mechanical time delay T_m .

However, the discrete OLTC models assume that when the OLTC is activated, it will raise or lower the transformer ratio by one tap step instantaneously [11]. Hence, this assumption necessitates that the intentional time delay is added to the mechanical time delay, forming the overall time delay T_{ov} :

$$T_{ov} = T_i + T_m \quad (2.6)$$

A tap change is thus performed if equation (2.5) is not valid for a time period larger than the overall time delay T_{ov} . This approach is also followed in this study. Furthermore, the non-sequential OLTC operation scheme is considered, where the same time delay T_{ov} is applied not only to the first tap change, but also to the subsequent tap changes; on the other hand, the sequential operation scheme (not considered here) uses different time delays for the first and the subsequent tap changes. According to the above stated, the role of the applied deadband (2.5) and of the overall time delay T_{ov} (2.6) is better understood with the help of Figure 2.7 (b).

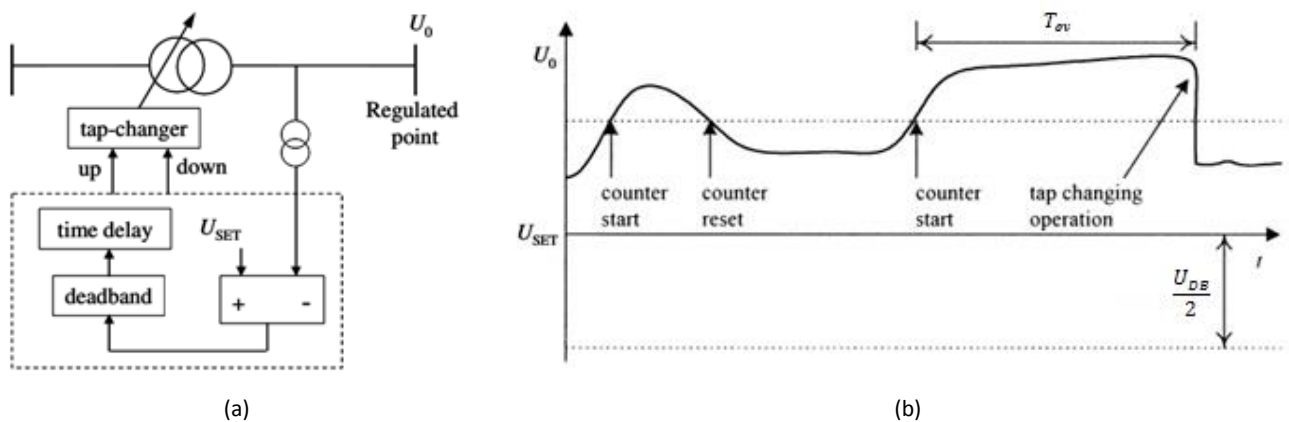


Figure 2.7: Basic OLTC transformer: (a) controller arrangement [26], (b) illustration of tap changing [54]

One important constraint is that a finite number of tap positions exists (symmetric around zero position). Consequently, the voltage regulation is restricted to a range defined by the lower and the upper voltage limit; typical values of the lower limit are from 0.85 - 0.90 pu and for the upper limit 1.10 – 1.15 pu. The size of a tap step (U_{STEP}) is usually in the range of 0.5 % - 1.5 %, with a typical value of 0.0625 %.

Instead of just controlling the substation secondary bus voltage, an OLTC is normally provided with a Line Drop Compensation (LDC) function in order to keep the voltage at a remote bus constant, without using any communication link. In practice, many OLTCs are operated with the LDC function disabled, which results in a simpler control scheme and

prevents unnecessary error [26]. What is more, since the LDC estimates the voltage drop at the remote point based on local measurements and without considering any power injection from any point at the feeder, when a DG unit (conventional or renewable) is installed at a certain feeder the LDC will not function properly [33]. From this point forward, this thesis will only discuss OLTC with the LDC function disabled.

Another category of transformer equipped with OLTC is the Step Voltage Regulator (SVR) [55]. A SVR is simply an autotransformer with a voltage ratio of 1:1 and can be installed at a point along a relatively long feeder, with the sole purpose of controlling the voltage. More specifically, the voltage at the feeder section between the HV/MV substation and the SVR is controlled by the OLTC in the substation, while the voltage at the line section between the SVR and feeder end is controlled by the OLTC in the SVR. The use of SVRs is considered by DNOs as a costly way of regulating voltage in MV distribution networks; as a result, they are seldom used. In this study, the use of SVRs for voltage control has been left out of consideration.

2.5.3 DRG

2.5.3.1 OVERVIEW

At the moment, DRG units usually operate at constant power factor ($\cos\varphi = 1$) and do not provide any ancillary services to the MV distribution network [38]. Voltage control is carried out only by the OLTCs, meaning that the last measured point in the system is at the secondary side of the OLTC transformer in the HV/MV substation. Furthermore, with a large number of DRG units connected to the MV network, local voltage increase cannot be detected. Classical voltage control thus becomes inefficient and allows only for a limited number of DRG units to be connected.

The advantage of DRG units is that they can, by reactive power dispatching, help to minimise the voltage rise they are causing and thus allow to connect a larger amount of DRG. Another method of minimising the voltage rise is by active power curtailment. With respect to power electronics-interfaced generation units, such as those presented in section 3.5, the aforementioned methods are presented and discussed in the following paragraphs.

2.5.3.2 REACTIVE POWER CONTROL

With focus on current German guidelines [39], three concepts for reactive power control are introduced, namely: constant power factor, active power dependent power factor and voltage dependent power factor. It is important to note that, according to the aforementioned technical guidelines, the power factor is measured at the PCC between the DRG unit and the MV distribution network. A description of the above stated concepts follows.

Constant power factor, PF_{fix}

Feeding in with a fixed PF , as shown in Figure 2.8 [56], is an easy and straightforward way of providing reactive power. This concept can contribute to limiting the voltage rise, since all generating units provide reactive power while feeding in. On the other hand, the main disadvantage of this method is the independency between the reactive power feed-in and the voltage. Thus, there may be a high load of reactive power even if there is no relevant voltage rise due to DRG.

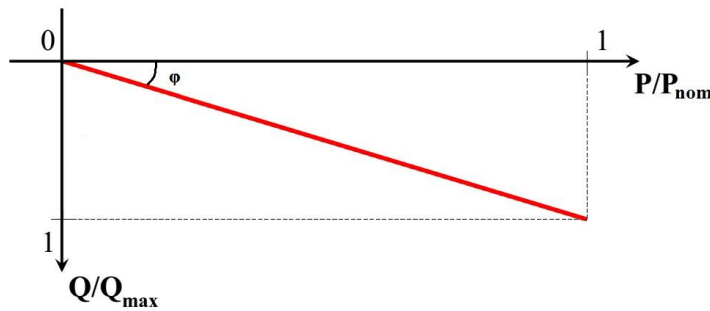
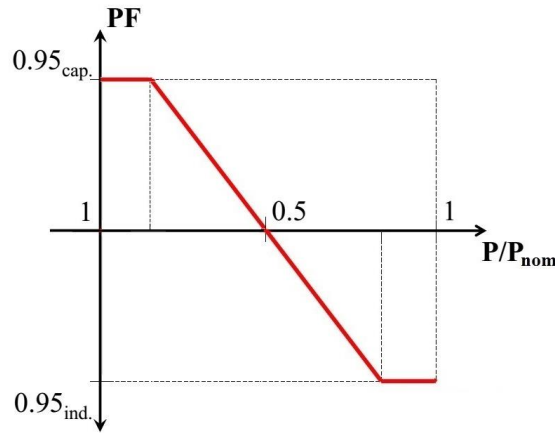


Figure 2.8: Example of a PF_{fix} characteristic curve [56]

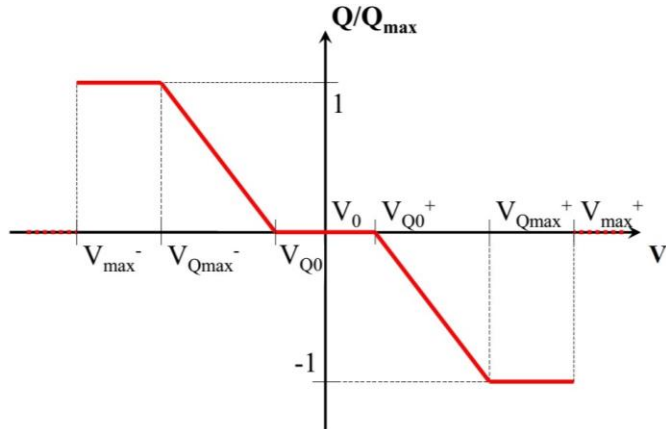
Active power dependent power factor, $PF(P)$

This concept addresses the problem of high reactive power load without lowering the positive effect on the grid voltage during maximum feed-in. The idea is to provide reactive power depending on the actual active power feed-in. An example characteristic, as given in [39], is shown in Figure 2.9. Nevertheless, in networks without severe voltage rises the reactive power provision results in an undesired additional line load.

Figure 2.9: Example of a $PF(P)$ characteristic curve [39]

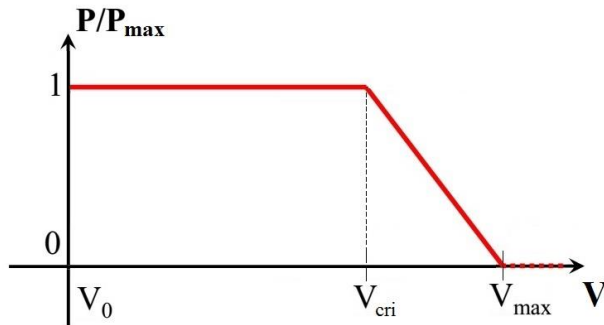
Voltage dependent reactive power, $Q(U)$

The last characteristic curve relates the reactive power exchange of a generating unit to the PCC voltage. Reactive power is injected or consumed, only when the predefined voltage thresholds are exceeded. Consequently, the unnecessary loading of the network is avoided. However, this method does not cater for a fair contribution of reactive power dispatch among DRG units in the network. For instance, generators connected towards the feeder end usually deal with larger overvoltages, meaning that they must consume larger amounts of reactive power (possibly at the cost of active power yield). An example characteristic curve is shown in Figure 2.10. The optionally applied dead band allows for a delay of reactive power injection in favour of active power yield.

Figure 2.10: Example of a $Q(U)$ characteristic curve [56]

2.5.3.3 ACTIVE POWER CURTAILMENT

Power curtailment of DRG can be applied so as to prevent overvoltages in the network. Nevertheless, it is not desirable because of the loss of renewable energy. This strategy can be combined with other mitigation methods and can thus be seen as a last resort. To prevent overvoltages at the PCC of a DRG unit, the DNO decreases the delivered active power of that unit by 50 or 100 %, regardless of the PCC voltage magnitude (this is a common practice in Belgium) [57]. However, curtailing the active power by only the necessary amount to remain within the voltage limits would lead to less rejected renewable energy. Active power is thus decreased –with respect to the maximum power that the DRG unit could deliver at that moment– and it is fully curtailed only when the PCC voltage exceeds the maximum voltage limit. An example characteristic of droop-based active power curtailment scheme, as proposed in [57], is shown in Figure 2.11.

Figure 2.11: Example of a $P(U)$ characteristic curve

2.5.4 INTELLIGENT NODE

2.5.4.1 OVERVIEW

According to literature, the Intelligent Node (IN) concept was first introduced in [41], as a means of managing the active power flow in distribution networks. Further elaboration of this concept takes place in [43], where both technical and operational aspects are analysed. The IN may be seen as a black box with on the outside a number of AC ports, and, for now, an undefined internal topology. The preliminary functional requirements of this black box are [43]:

- i. inject or consume an adjustable amount of active and / or reactive power through each of its AC ports,
- ii. supply a radial network part from any of its AC ports,
- iii. improve the power quality of the connected network parts and
- iv. store energy (optionally).

In this study, all these functions are going to be taken advantage of, except from the second one. In the following paragraphs, the possible applications of an IN, as well as its topological aspects, are discussed. It should be stated that although the IN has been used by a number of studies at a theoretical level, it has never been actually implemented and applied in a real network. A reason for this could be that a cost-benefit analysis has not yet been carried out. Regarding the actual implementation of similar devices, the Central Research Institute of Electric Power Industry in Japan has developed a medium voltage back-to-back converter application, whose basic functions are the control of voltage and power flow in a distribution system [58].

2.5.4.2 APPLICATIONS

According to the author of [43], facilitating increased network loading by controlled sharing of redundancy or by controlled power exchange between grid areas, is considered as the most important IN application. However, since no short circuit events are within the scope of this study and the line loading limit is defined by the rated line current, this application will not be further elaborated on. Additionally, voltage dip mitigation, as well as flexible coupling and decoupling of (asynchronous) grids, are also possible IN applications.

On the other hand, using the IN in order to control voltage profiles and to facilitate integration of distributed generation is very interesting application, which lies within the scope of this thesis. Here, the IN can control voltage profiles by controlling both active and reactive power flows. As explained in section 2.4, the voltage amplitude can be influenced by the injection of active and / or reactive power depending on the line R/X ratio.

In general, the connection of DRG units in a distribution network can result in reverse power flow and voltage rise –instead of voltage drop– along a feeder. If this occurs in only some of the feeders that are fed from the same HV/MV substation, then the voltage profiles of the connected feeders can possibly no longer be kept within a certain band by the transformers OLTCs. Such a network section is illustrated in Figure 2.12 (a), where the proposed location of the IN for this application is also shown. On the one hand, the inability of the transformers OLTCs to effectively control the voltage profiles is clearly shown in Figure 2.12 (b). On the other hand, an illustration of the effect which can be achieved on the voltage profiles is given in Figure 2.12 (c).

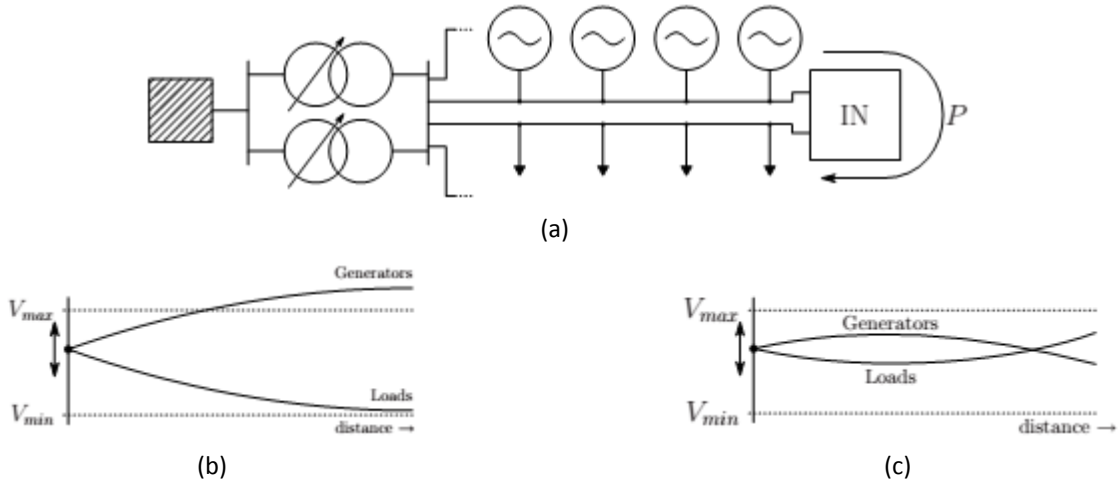


Figure 2.12: MV distribution network section [43]: (a) single line diagram along with IN optimal placement, (b) problematic voltage profiles prior to the IN connection, (c) improved voltage profiles after the IN connection

More precisely, in the case of a feeder with mainly generation, a certain amount of the generated power is absorbed by the IN. The amount of power towards the beginning of the feeder is decreased, resulting in an overall decrease of the voltage level. From a certain point in the feeder and downwards, power is transported towards the storage device. So, from this point, the voltage decreases towards the end of the feeder. In the case of a feeder with mainly load, the IN feeds the loads at the end of the feeder, resulting in an opposite effect. Subsequently, the overall voltage variations decrease, with the highest variations occurring somewhere in the middle of the network [59].

Besides active power, also reactive power can be injected or consumed, resulting in a similar effect on the voltage profile; this approach is applicable to MV distribution networks, where the lines, according to subsection 2.4.3, generally have an impedance ratio $R/X \approx 1$.

2.5.4.3 TOPOLOGY

In order to combine all the functions mentioned in paragraph 2.5.4.1 in one device, a versatile topology is required. The proposed topology consists of N voltage source converters, back-to-back connected. Their DC ports are connected to a common DC-bus, while each one of the AC ports supplies a certain feeder [60]. Practical applications will not likely involve more than four converters ($N \leq 4$), since in practice the number of feeders ending in one geographical location is limited. An example of IN configuration is illustrated in Figure 2.13 [61].

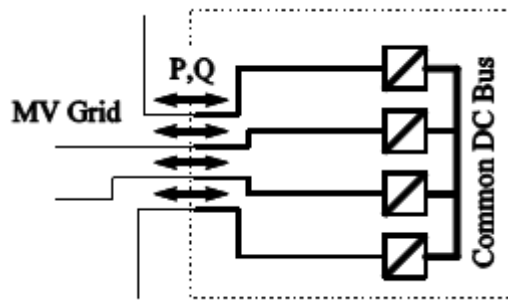


Figure 2.13: Example of Intelligent Node configuration [61]

This topology allows full control of active and reactive power flow among the feeders. Besides the STATCOM capabilities (reactive power injection or absorption), the IN has the additional capability of active power exchange thanks to its DC bus interconnection. The DC bus allows asynchronous operation of all the inverters, meaning that each AC port can have different phase angle and order, different voltage amplitude and even different frequency. If no storage is connected to the DC-bus, the active power of all converters has to add up to zero (internal losses are neglected). For reactive power such a limitation does not exist and the IN can supply to or consume reactive power from each feeder independently. Furthermore, the advantage of using power electronics as the main technology in the IN is the speed at which it can respond to system changes.

Finally, other possible topologies for the IN are based either on multiple power electronics controlled auto transformers, or multiple power electronics controlled series impedances [43]. Nevertheless, these topologies are less versatile and will not be considered in this study.

2.6 CONCLUSIONS

Concluding the chapter about the MV distribution networks, initially a description of topological, operational and organisational aspects was given. The transition already taking place in distribution networks, along with its implications, was also discussed. Moreover, a necessary insight to the Dutch and German grid codes for power quality was given. The mechanism responsible for the voltage variation problem was explained, while the influence of network line impedance characteristics was analysed. At last, several means of regulating voltage in MV distribution networks were described, namely: On Load Tap Changers, power electronics converters of DRG units and a D-FACTS device, named Intelligent Node. Despite the fact that the list of the available voltage regulating devices is large, a deliberate decision was made so as to present only the devices that are used in the following chapters of this thesis. With respect to voltage regulation offered by the DRG interfacing converters abd since a comparison of different voltage control schemes offered by DRG units is not within the scope of this study, only the concept $Q(U)$ –as suggested in [62]– is implemented in Chapter 3. Nevertheless, a brief overview of all the main concepts can be found in subsection 2.5.3.

3 SYSTEM MODELLING

3.1 INTRODUCTION

In this chapter, the modelling approach of this study is explained and a detailed review of all components of the test system is given. The chosen modelling approach greatly influences both the structure and the contents of the created models, while allowing for specific simplifying assumptions. Regarding the system components, the MV distribution network model is initially presented, followed by a description of the load model. The DRG modelling part describes the Photovoltaic Power Plant (PVPP) and the Wind Power Plant (WPP) models. Choosing these two types of uncontrollable DRG is expected to worsen the voltage variation problem and further stress out the implemented voltage control strategy. Finally, the Intelligent Node model is presented.

3.2 MODELLING APPROACH

A serious difficulty in the analysis of power systems is posed by the vast differences in time scales or frequency bands in which the various phenomena of interest occur. On one side of the time spectrum, there are phenomena that last from micro to milliseconds, while on the other side, several phenomena last from minutes to hours. Figure 3.1 gives an overview of the various areas of consideration and their characteristic time scales or frequency bands [62].

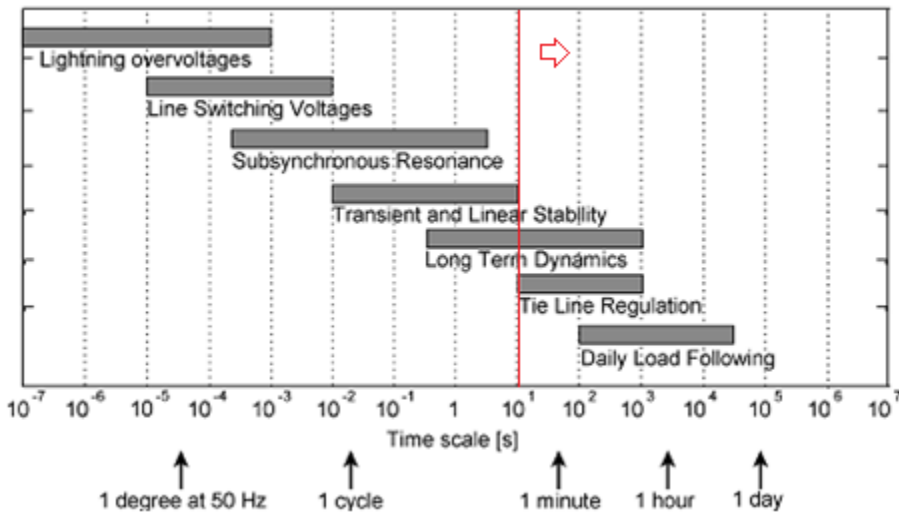


Figure 3.1: Frequency bands and time scales of various dynamic phenomena in power systems [62]

Using a complete model of the power system for studying each of the areas depicted in Figure 3.1 would result in excessive data requirements, since too many parameters need to be specified. More importantly, when high frequency phenomena are included in the model, the corresponding simulation run would be very time consuming, necessitating a small time step. To avoid these drawbacks, normally a model of the power system and its components that is tailored to the phenomena under study is used. Such a model is based on the following assumptions:

- Phenomena with a frequency above the bandwidth of interest can be neglected since they are considered to have died out before having any effect to the phenomenon under investigation
- Phenomena with a frequency below the bandwidth of interest can be neglected since they are considered to be so slow, that the values of the associated state variables do not change during the simulation run.

In this study, which focuses on voltage control, transient stability phenomena are of no interest. On the contrary, phenomena like transformer tap changing and the charge / discharge cycle of a battery are important; hence, long term dynamics are of interest. As it can be seen in Figure 3.1, the corresponding time scale ranges from several tens of seconds or minutes, up to several hours or days. With the above stated assumptions in mind, short term phenomena, which lie on

the left side of the vertical red line, can be ignored. In general, the followed modelling approach has led to the development of models which are “tailored” for the needs of the current study; they are not simplified more than they should (as this could lead to erroneous results), while at the same time they are not too complicated (this could lead to time consuming simulation runs). Finally, it should be stated that v15.0 of the power system analysis software PowerFactory from DIgSILENT has been used for the needs of this study. A time domain simulation method has been used, which –unlike quasi-steady-state load flow methods– offers great flexibility in control design and allows for accurate energy calculations imposed by the use of storage devices.

3.3 CIGRÉ EUROPEAN MV DISTRIBUTION NETWORK BENCHMARK MODEL

The Cigré medium voltage (MV) distribution network benchmark is derived from a physical MV network in southern Germany, which supplies a town and its surrounding rural area. This makes it ideal for studies on MV distribution networks of North Europe, especially when the focus is on DRG integration. Figure 3.2 depicts the network, as originally presented in [42].

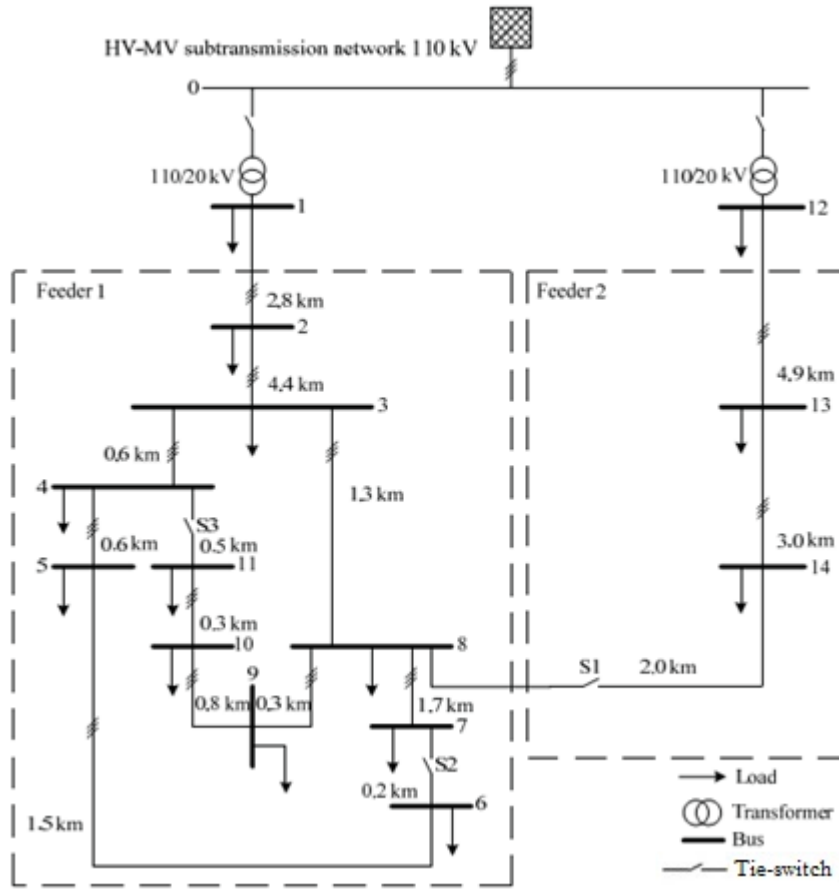


Figure 3.2: Cigré European MV distribution network benchmark

The network consists of 14 nodes with a rated voltage level of 20 kV. It is connected to the high voltage (HV) subtransmission network through two 110/20 kV transformers. Node 0 represents the slack bus of the system, characterised by constant nominal voltage magnitude and zero voltage angle. The network is ungrounded, something typical for Europe. The 110 kV subtransmission network is modelled as an external stiff network, maintaining a constant frequency of 50 Hz throughout the MV distribution network.

Feeders 1 and 2 are framed by dashed lines and can be either of meshed or radial structure, by using configuration switches S1, S2, and S3. If these switches are open, then both feeders are radial. Closing S2 and S3 in Feeder 1 creates a loop or mesh. Furthermore, both feeders are symmetrical, allowing for balanced three-phase operation. Feeder 1 is supposed to serve an urban / suburban area and consists of underground XLPE cables, with round, stranded aluminum conductors. Underground cables are buried in back-filled trenches with a protective plate. Feeder 2 is supposed to serve a rural area and consists of overhead lines with bare conductors, made of aluminum. Overhead lines are mounted on towers without neutral wires.

The transformers at the HV/MV substations have a capacity of 25 MVA each and are provided with OLTCs. The OLTCs allow for the secondary winding voltage adjustment of $\pm 10\%$, in 0.625 % increment load changing taps. In Table A.2 of APPENDIX A the complete specifications of the used HV/MV transformers are given.

Parameter values for the HV-MV subtransmission equivalent network are based on [42]. Regarding the MV distribution network, line geometries and lengths, conductor types and parameters, as well as electrical parameters of HV/MV transformers are also based on [42]. The necessary current rating calculations for the overhead lines were made according to IEC 61597 standard [63]. Detailed data related to all the above stated networks components, is given in APPENDIX A.

3.4 LOAD MODELS

3.4.1 CONSUMPTION DATA

Each one of the nodes of the MV distribution network depicted in Figure 3.2 has a load attached to it. For nodes 2-11 and 13-14, these symmetric loads represent a number of LV customers and are aggregated at MV/LV substation level. On the contrast, loads at nodes 1 and 12 represent additional MV feeders served by the HV/MV substation transformer and are not actually part of the feeder that is modelled in detail. Each load is composed of two consumption classes:

- i. Residential consumption and
- ii. Commercial / Industrial consumption.

For each load component the coincident peak apparent power S_{max} and the power factor $\cos\varphi$ are specified [42]. Detailed data can be found in section A.5 of APPENDIX A. For the needs of this study, weekly load power time series with daily and seasonal variation for both consumption classes are necessary. For consistency reasons, these time series should, not only originate from sites located in North Europe, but also be aggregated at MV/LV substation level. Although loads at nodes 1 and 12 should be aggregated at MV feeder level, choosing the same level of aggregation (and thus allowing the use of the same demand curve) for all nodes is considered to be a safe choice. The same procedure is followed in [42] and is not expected to negatively influence the validity of calculations conducted during this study.

The above stated specifications required an in-depth literature study [29] [64] [65] [66] [67]. The chosen residential demand curves for both winter and summer periods are found in [66]. These aggregated demand curves, composed by linearly interpolated 15 min. average values, are shown in Figure 3.3 and represent the patterns at the substation level of a typical MV network in The Netherlands, feeding about 200 LV customers.

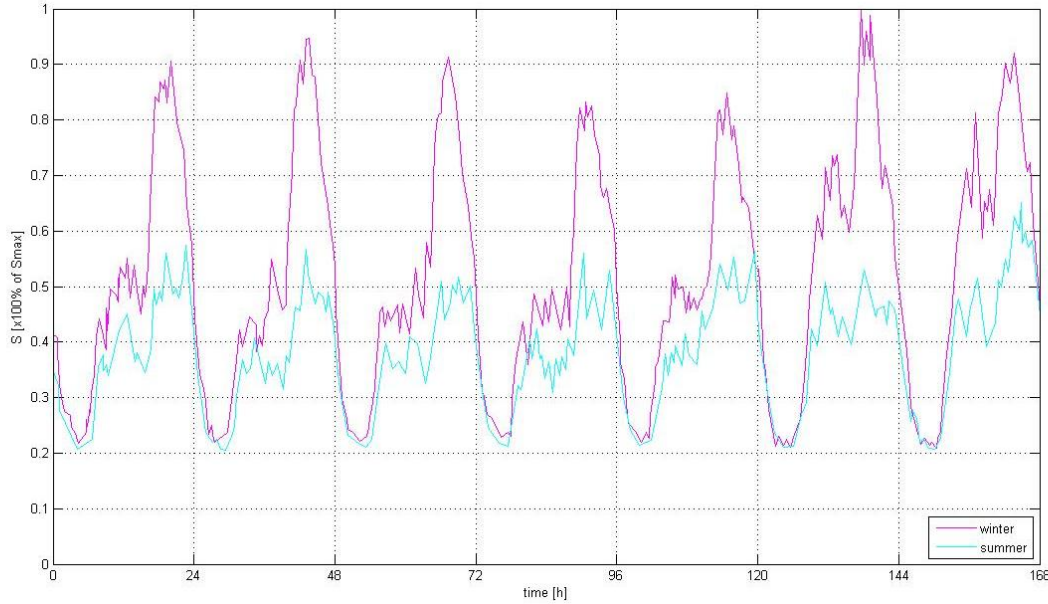


Figure 3.3: Residential weekly load profiles

In the absence of satisfactory data regarding the commercial / industrial consumption class, the daily load curve already bundled with [42] is used. Since no daily or seasonal variation is provided for this curve, it is considered acceptable that the composite load at each node varies daily and seasonally only due to its domestic component. Figure 3.4 presents the commercial / industrial weekly load profile used.

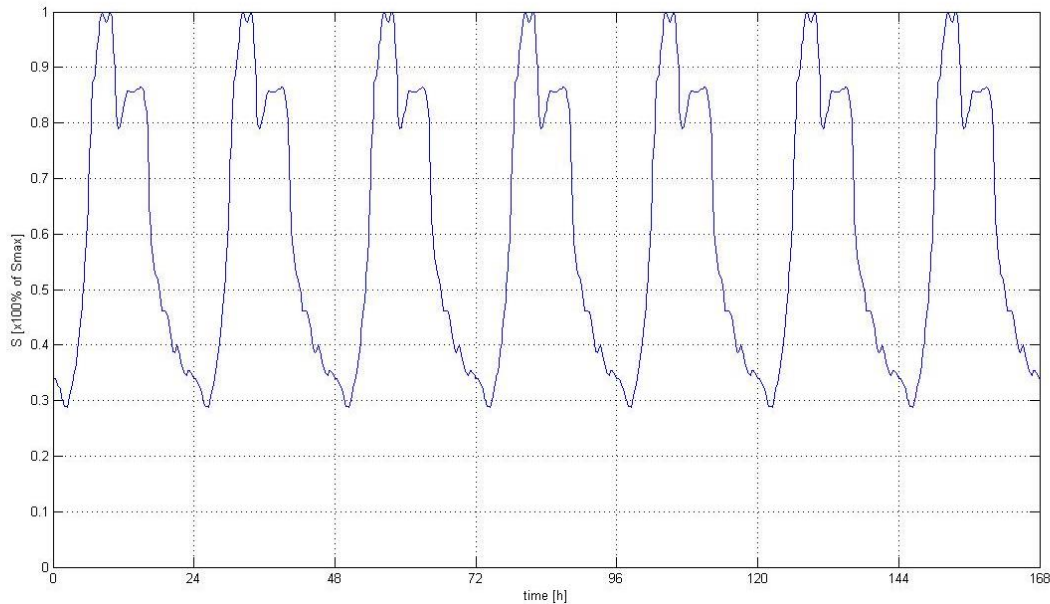


Figure 3.4: Commercial / Industrial weekly load profiles

Regarding the commercial / industrial consumption, the fact that Figure 3.4 shows no variation between weekdays and weekend, can be justified by the data presented in [65]. In this report about electricity demand in Great Britain, both the commercial and the industrial load classes show a broadly similar consumption pattern for weekdays and weekends. It is important to note that this consumption data is not aggregated at MV/LV substation level; nevertheless, the above described qualitative feature is considered to be valid for this study too, where the –aggregated at MV/LV substation level– load demand in North-European countries is of interest.

Based on Figure 3.3, Figure 3.4 and Table A.8, the resulting load demand in the system is calculated. Table 3.1 shows the results for different parts of the MV network during both summer and winter periods.

Table 3.1: Load demand in the MV distribution network

Season	Network section	Peak apparent power
		[MVA]
Summer	Feeder 1	2.73
	Feeder 2	0.53
	Feeders 1 & 2	3.25
	Section supplied by HV/MV transformer 0-1	14.93
	Section supplied by HV/MV transformer 0-12	12.91
	MV network	27.84
Winter	Feeder 1	4.03
	Feeder 2	0.56
	Feeders 1 & 2	4.47
	Section supplied by HV/MV transformer 0-1	21.88
	Section supplied by HV/MV transformer 0-12	18.38
	MV network	40.26

According to the above presented data, the following conclusions can be drawn regarding the load demand in the system:

- Feeder 1 (urban / suburban area) is significantly more loaded than Feeder 2 (rural area). During summer, the load demand in Feeder 1 is about 5 times larger than in Feeder 2. During winter, this ratio climbs up to around 7.
- The largest portion of the MV network load is supplied through HV/MV transformer 0-1. During summer, the peak apparent power demand through transformer 0-1 is about 15 % larger than through transformer 0-12. During winter, this percentage slightly grows to 20 %.
- During both summer and winter periods, the load served by Feeders 1 and 2 is roughly 9 times less than the whole MV network load.

Following to the peak values presented in Table 3.1, a visual representation of the resulting weekly load profiles is in order. In Figure 3.5, the presented load profiles presuppose that the load demand of the additional MV feeders at nodes 1 and 12 (see Figure 3.2) has been taken into account. On the contrary, the load profiles illustrated in Figure 3.6 refer only to the feeders which are modelled in detail.

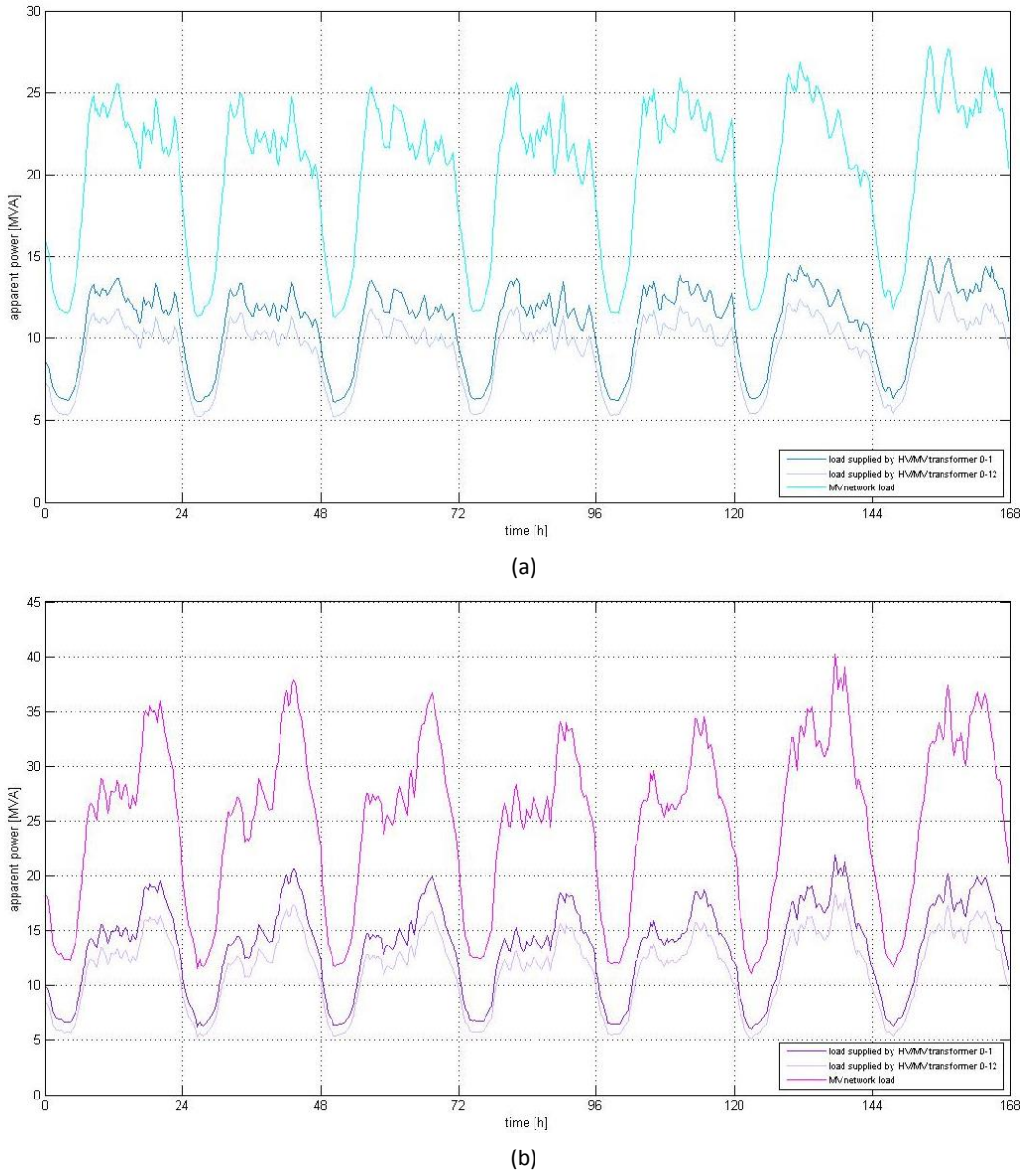


Figure 3.5: Resulting weekly load profiles for different network sections: (a) summer period, (b) winter period

A closer look at Figure 3.5 (b) and Figure 3.6 (b) reveals that during winter, the load demand profiles of all the relevant network sections follow the pattern introduced by the residential load profile (see Figure 3.3). This is natural, since, according to Table A.8, the load demand in the system is mainly due to residential loads. However, this remark does not hold for Feeder 2. In this feeder, the largest share of load demand is due to commercial / industrial loads, which follow a different pattern (see Figure 3.4).

On the other hand, although the load demand in the system is mainly due to residential loads, a closer look at Figure 3.5 (a) and Figure 3.6 (a) indicates that the above described pattern is not present during summer. This behaviour originates from the fact that the residential load demand is lower in the summer season and, therefore, the commercial / industrial load demand has now a larger influence on the resulting load demand profiles.

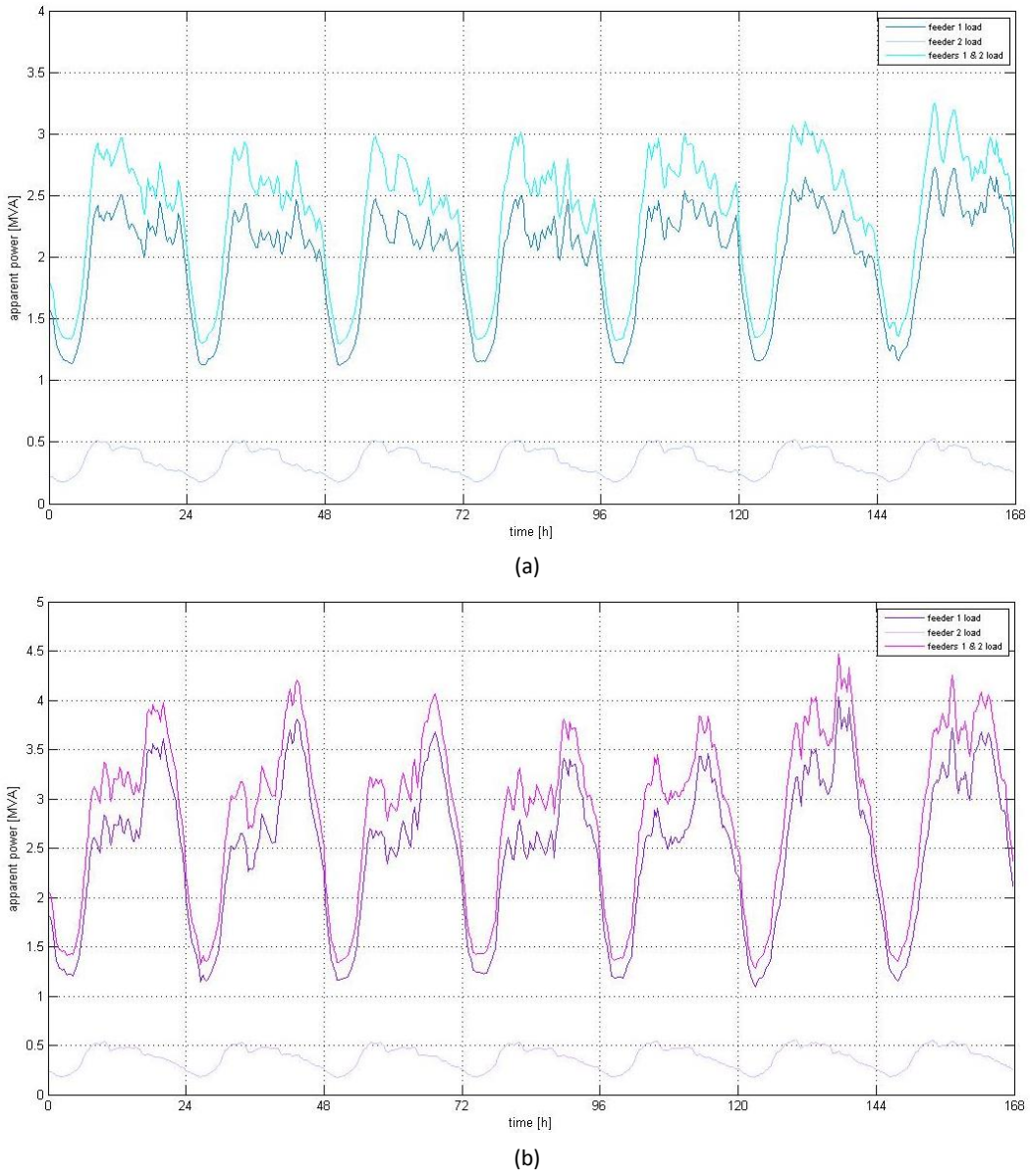


Figure 3.6: Resulting weekly load profiles for the network section that is modelled in detail: (a) summer period, (b) winter period

3.4.2 MATHEMATICAL REPRESENTATION

3.4.2.1 OVERVIEW

A load model is a mathematical representation of the relationship between a bus voltage and the power (active and reactive) or current flowing into the bus [14]. Due to the high diversity of power system loads, several standard load models have been proposed throughout time. According to [67], the main classification is in static and dynamic models. A combination of static and dynamic loads also exists, where one must first define the percentage of each participating part. The choice of load model and its accompanying parameters can significantly affect the results of a power system study [68]. What is more, such a choice should be made with a view to the type of phenomenon studied, the resulting complexity of the system and, of course, the availability of data. For example, voltage stability studies are greatly influenced by the dynamic load model used [69]. Below, more detailed descriptions for static and dynamic load models can be found.

3.4.2.2 STATIC LOAD MODELS

A static load model is not dependent on time, as it describes the relation of power (active and reactive) at a time instant with voltage and / or frequency at the same exact instant. Static load models have been used for a long time in order to represent static load components, such as resistive and lighting loads, but also to approximate dynamic load components [67]. Common static load models express active and reactive power in a polynomial or an exponential form, and can include, if necessary, a frequency dependence term [14]. A brief description of some of these models follows.

Polynomial model or ZIP model

The static characteristics of the load can be classified into constant impedance (Z), constant current (I) and constant power (P) load, depending on the power relation to the voltage. For a constant impedance load, the power dependence on voltage is quadratic, for a constant current is linear, and for a constant power, the power is independent of changes in voltage. The ZIP model is a polynomial model that represents the sum of these three categories:

$$P = P_0 \left[aP \cdot \left(\frac{V}{V_0} \right)^2 + bP \cdot \left(\frac{V}{V_0} \right) + cP \right] \quad (3.1)$$

$$Q = Q_0 \left[aQ \cdot \left(\frac{V}{V_0} \right)^2 + bQ \cdot \left(\frac{V}{V_0} \right) + cQ \right] \quad (3.2)$$

$$\alpha P + bP + cP = \alpha Q + bQ + cQ = 1 \quad (3.3)$$

where V_0 , P_0 and Q_0 refer to the pre-disturbance conditions of the system and coefficients aP , bP , cP , aQ , bQ , cQ are the weighting factors of each load category.

Exponential model

In the exponential model the power dependence is expressed as a function with a non-integer exponent:

$$P = P_0 \cdot \left(\frac{V}{V_0} \right)^{n_p} \quad (3.4)$$

$$Q = Q_0 \cdot \left(\frac{V}{V_0} \right)^{n_q} \quad (3.5)$$

where V_0 , P_0 and Q_0 are the pre-disturbance conditions of the system and the exponents n_p to n_q obtain values which depend on the load category. Values of the exponents for common load categories can be found in [67]; values for special load categories can be found in [64] [70]. Also here, in the case of n_p , n_q being equal to 0, 1 or 2, the model will represent a constant power, constant current or constant impedance load, respectively.

3.4.2.3 DYNAMIC LOAD MODELS

A dynamic load model expresses the relation of power (active and reactive) with voltage and / or frequency as a function of the voltage and / or frequency time history, usually including the present moment. Such expressions can be linear or non-linear, first or second order differential equations [69]. In addition, the use of an induction motor can also be a representation of dynamic load [71]. The parameters of these load models are normally determined by using a measurement-based approach; first by carrying out field measurements and then by observing the load response as a result of alterations caused in the system [67].

3.4.2.4 CHOSEN MODEL

DIGSILENT PowerFactory provides adequate flexibility in load modelling. As expected, a load can be modelled as static, dynamic or a combination. In the absence of appropriate dynamic load parameters, only static loads are modelled for this study. For static load modelling, equations (3.6) - (3.9) hold [71]:

$$P = P_0 \left[aP \cdot \left(\frac{V}{V_0} \right)^{e_{-aP}} + bP \cdot \left(\frac{V}{V_0} \right)^{e_{-bP}} + cP \cdot \left(\frac{V}{V_0} \right)^{e_{-cP}} \right] \quad (3.6)$$

$$Q = Q_0 \left[aQ \cdot \left(\frac{V}{V_0} \right)^{e_{-aQ}} + bQ \cdot \left(\frac{V}{V_0} \right)^{e_{-bQ}} + cQ \cdot \left(\frac{V}{V_0} \right)^{e_{-cQ}} \right] \quad (3.7)$$

$$cP = 1 - aP - bP \quad (3.8)$$

$$cQ = 1 - aQ - bQ \quad (3.9)$$

One could characterise this representation as a '*hybrid*' one, since the polynomial structure of (3.1) and (3.3) is combined with the versatility of non-integer exponents of (3.4) and (3.5). In this study equations (3.6) - (3.9) are used, with the choice of exponents made with respect to [72]. The choice of weighting factors was made according to the author's judgement and with a view to creating a realistic combination of load components for each load class. The relevant data used is provided in Table 3.2. It should be pointed out that the percentage of constant power load component in the residential

load class is the dominant one. This has been done so as to account for an increasing trend of installing home appliances equipped with switching power supply units.

Table 3.2: Exponential load parameters

Load class	Load component	Percentage of component	Parameters			
Residential	Constant power	50%	$aP = 0.50$	$aQ = 0.50$	$e_aP = 0$	$e_aQ = 0$
	Constant current	25%	$bP = 0.25$	$bQ = 0.25$	$e_bP = 1.00$	$e_bQ = 1.00$
	Constant impedance	25%	$cP = 0.25$	$cQ = 0.25$	$e_cP = 2.00$	$e_cQ = 2.00$
Commercial/Industrial	Fluorescent lighting	25%	$aP = 0.25$	$aQ = 0.25$	$e_aP = 1.00$	$e_aQ = 3.00$
	Small induction motors	50%	$bP = 0.50$	$bQ = 0.50$	$e_bP = 0.10$	$e_bQ = 0.60$
	Large induction motors	25%	$cP = 0.25$	$cQ = 0.25$	$e_cP = 0.05$	$e_cQ = 0.50$

3.5 DISTRIBUTED RENEWABLE GENERATION MODELS

3.5.1 PHOTOVOLTAIC POWER PLANT MODEL

3.5.1.1 OVERVIEW

In this subsection the Photovoltaic Power Plant (PVPP) model is described. With respect to the time scale that is of interest in this study (see Figure 3.1) and the time scales of phenomena related to the PVPP operation, several simplifications that lead to the development of a long-term dynamic model can be allowed. In the following paragraphs an effort is made to provide detailed information regarding, not only the structure and the operation of the developed model, but also the simplifying assumptions made at each part.

Figure 3.7 illustrates the single-line diagram of a three-phase PVPP with 400 V nominal AC output voltage, connected – through a 20/0.4 kV transformer and a 0.8 km line – to the Point of Common Coupling, located at the MV distribution grid. The line specifications can be found in Table A.4 and Table A.5 of APPENDIX A, depending on whether the PVPP is connected to a node of Feeder 2 or Feeder 1, respectively. The transformer caters for making an isolated ground for the PV system, as well as boosting the PVPP output voltage to the grid voltage level. The specifications of the transformer can be found in Table B.1 of APPENDIX B. Finally, the connection lines within the PVPP have been ignored.

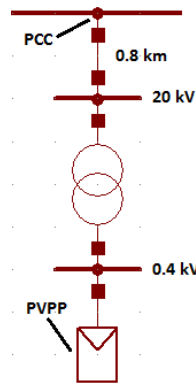


Figure 3.7: Single line diagram of a Photovoltaic Power Plant (PVPP) connected to the MV distribution grid

The PVPP consists of a PV array, a Pulse Width Modulation Voltage Source Converter (PWM-VSC) and peripheral control systems. The DC output power of the PV array feeds the PWM-VSC. There it is first transformed to AC power and then injected to the grid. In general, control is performed in the DQ0 reference frame. Choosing the d-axis voltage vector \underline{u}_d to

coincide with the terminal positive sequence voltage vector \underline{u} , makes the following equations valid for balanced three-phase operation:

$$u_d = |\underline{u}_d| = |\underline{u}| = u \quad (3.10)$$

$$u_q = |\underline{u}_q| = 0 \quad (3.11)$$

where u_d , u_q and u are the d-axis, q-axis and terminal voltage magnitudes [pu], respectively and \underline{u}_q is the q-axis voltage vector. The block diagram of the PVPP model is depicted in Figure 3.8.

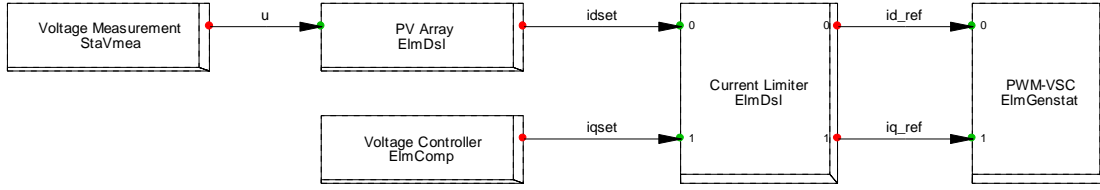


Figure 3.8: Block diagram of the Photovoltaic Power Plant (PVPP) model

A brief description of the system would start from the ‘PV Array’ block, where the incident solar irradiance is converted to electrical power (DC). Given that this power accounts for the converter output active power (AC), measuring the terminal voltage allows for a preliminary calculation of the converter d-axis output current set-point $i_{d,set}$. In the ‘Voltage Controller’ block, the PCC voltage is regulated to a reference value, resulting in a preliminary calculation of the q-axis converter output current set-point $i_{q,set}$. The preliminary current set-points are then fed to the ‘Current Limiter’ block, where restrictions regarding the PVPP operating power factor and the maximum apparent current limit of the PWM converter are applied. Finally, the output currents reference set-points are fed to the ‘PWM-VSC’ block, resulting in the grid current injection.

In the following paragraphs, a detailed description of PVPP model blocks is given. It is important to clarify that specifications and values of parameters used in the PVPP model can be found in APPENDIX B; only when it is absolutely necessary are such values given in the text.

3.5.1.2 ‘PWM-VSC’ BLOCK

In this study the PWM-VSC is considered to be lossless, meaning that the electrical power at the DC side can be fully converted to AC power at the grid side. The converter is modelled as a current source that supplies a sinusoidal current at the fundamental grid frequency [62]. This assumption is only true if the current control loops of the PWM-VSC are able to quickly reach a new set point for the current. With modern power electronic converters, featuring high switching frequencies and advanced controllers this is generally the case, provided that the converter operates within the design limits. Typically, active and reactive power at the grid side of the converter are described by the following equations:

$$P = u_d \cdot i_d + u_q \cdot i_q \quad (3.12)$$

$$Q = u_q \cdot i_d - u_d \cdot i_q \quad (3.13)$$

where i_d and i_q are the converter d-axis and q-axis output currents [pu], respectively. By applying (3.10) and (3.11), equations (3.12) and (3.13) can be simplified to:

$$P = u \cdot i_d \quad (3.14)$$

$$Q = -u \cdot i_q \quad (3.15)$$

Consequently, by controlling the d and q components of the current injected into the power network (i_d and i_q), active and reactive power (P and Q) can be independently controlled.

The converter rating S_{nom} is not set to the same value as the nominal active power output of the DRG plant, since at an operating power factor $PF \neq 1$ such a choice would lead to active power curtailment during periods of high active power output. Instead, the converter has been oversized so as to be able to provide nominal active power at a power factor $PF = 0.95$ and under nominal terminal voltage. The converter nominal apparent power is also set to be equal to the VA_{base} . Consequently, the following equations hold:

$$S_{nom} = VA_{base} \quad (3.16)$$

$$S_{nom} = \frac{P_{nom}}{0.95} = 1 \text{ p.u.} \quad (3.17)$$

$$Q_{max} = \sqrt{S_{nom}^2 - P_{nom}^2} \quad (3.18)$$

where P_{nom} is the nominal active power of the DRG plant to which the converter belongs [pu] and Q_{max} is the maximum reactive power capability of the converter [pu]. The reasoning behind this decision is the need for being in accordance with the German grid code for generating units connected to the medium voltage network [39]. To the author's opinion, this guideline is considered to be representative for MV networks located in North Europe and will thus be respected throughout this study. More specifically, although the operating power factor is variable (owing to the voltage controller), it is limited to the range:

$$PF_{min}(\text{cap.}) \dots PF \dots PF_{min}(\text{ind.}) \quad (3.19)$$

where the minimum power factor is a parameter that can potentially be changed depending on the needs of the different operating scenarios that are to be simulated. The chosen value should lie within the range of:

$$0.95 \leq PF_{min} \leq 1 \quad (3.20)$$

For completeness, it should be noted that the corresponding Dutch code specifies that a generator must operate at a power factor between 0.85 (inductive) and 1 [48]. However, if the voltage drops below its nominal value, the generator must supply its maximum available amount of reactive power.

3.5.1.3 'PV ARRAY' BLOCK

Solar cells are connected in series to form PV modules and PV modules are, in turn, connected in series or in parallel to form PV panels. PV panels are connected in series and in parallel to form PV arrays. By not taking into account the semi-conductive character of a solar cell, a PV panel can be assumed to behave as a current generator of value [73]:

$$I_{panel} = I_{sc} \cdot G \quad (3.21)$$

where I_{sc} is the PV panel short circuit-current and G is the incident solar irradiance level [kW/m^2]. The power generated by PV panels is:

$$P_{panel} = P_{max} \cdot \frac{I_{sol}}{I_{sc}} \xrightarrow{(3.21)} P_{panel} = P_{max} \cdot G \quad (3.22)$$

where P_{max} is the maximum PV panel power in STC ($G = 1 \text{ kW/m}^2$, $T_{cell} = 25^\circ\text{C}$ and AM1.5 spectrum). If the PV array consists of a number N_{panel} PV panels, all receiving the same amount of solar radiation, then the following equations hold:

$$P_{sol} = N_{panel} \cdot P_{panel} \quad (3.23)$$

$$P_{nom} = N_{panel} \cdot P_{max} \quad (3.24)$$

where P_{sol} is the output power of the PV array [pu] and P_{nom} is the nominal power of the PVPP [pu]. Combining equations (3.22) - (3.24) yields:

$$P_{sol} = P_{nom} \cdot G \quad (3.25)$$

By combining (3.17), (3.25) and by agreeing that the incident irradiance cannot be above the one specified in STC, a final expression for the PV array output power is:

$$P_{sol} = 0.95 \cdot G, \quad 0 \leq G \leq 1 \quad (3.26)$$

Equation (3.26) implies maximum extraction of solar power, something that premises Maximum Power Point Tracking (MPPT) operation of the VSC. MPPT appropriately regulates the voltage at the DC side of the converter so as to extract the highest possible energy content from the PV array. According to [34], a MPPT system normally operates at the frequency range of 20 or 30 Hz, while simulation results show that even after a 0.5 pu step change in the incident solar irradiance, the converter output power reaches its steady-state value within less than 0.5 seconds. Such time scales are much smaller than the time scale of interest in this study and therefore, the MPPT system is not modelled.

Solar irradiance weekly time series (linearly interpolated 1 min. average values) used as input to the PVPP model are derived from actual satellite data [74]. The measurements refer to the area of Cabauw, the Netherlands. Winter measurements refer to the period 28/02/2005 – 06/03/2005, while summer measurements refer to the period 11/07/2005 – 17/07/2005. In order for the energy production to be maximised, according to [75], solar panels should be facing towards

the south and be tilted at an angle of 40 degrees; the incident solar irradiance data is thus obtained for these exact installation settings. Furthermore, with a view to performing a realistic study, daily and seasonal variations are included. Irradiance data is provided by means of a lookup table and a graphical representation of it is shown in Figure 3.9. As expected, solar irradiance is higher during summer and lower during winter. There is, however, one winter day during which the irradiance levels are high. In addition, the corresponding active power production of a PVPP model with nominal power output of 0.7 MW is shown in Figure 3.10.

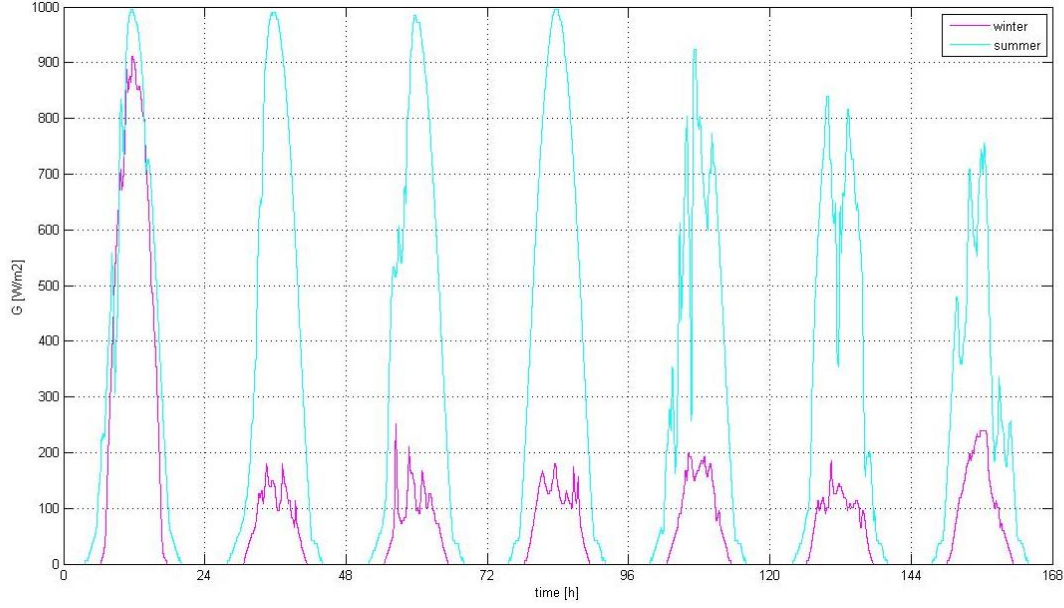


Figure 3.9: Solar irradiance weekly time series

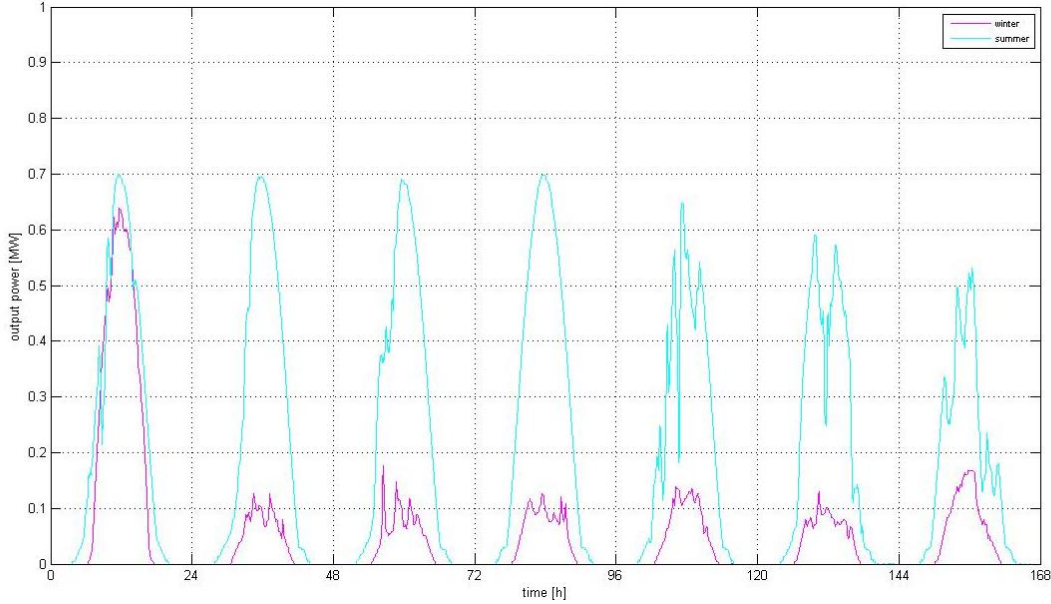


Figure 3.10: Active power output of a PVPP model with $P_{nom} = 0.7 \text{ MW}$

The second input of the 'PV Array' block is the terminal voltage magnitude u . Providing that the PWM-VSC operates within its design limits (current limits are not violated), the generated solar power equals the converter output active power:

$$P = P_{sol}, \quad 0 \leq P_{sol} \leq 0.95 \quad (3.27)$$

By combining (3.14) and (3.27), the converter d-axis output current preliminary set-point (in per unit) can be calculated as follows:

$$i_{d,set} = \frac{P_{sol}}{u} \quad (3.28)$$

3.5.1.4 ‘VOLTAGE CONTROLLER’ BLOCK

The PVPP is equipped with a PWM-VSC which is able to vary its reactive power output and thus to take part in voltage control at its terminals or at the PCC. As it can be concluded from equation (3.15), the reactive power exchanged with the grid can be controlled, provided that the current rating of the power electronic converter is sufficient to circulate reactive current even at nominal active current. The model of the voltage controller is depicted in Figure 3.11 [76]:

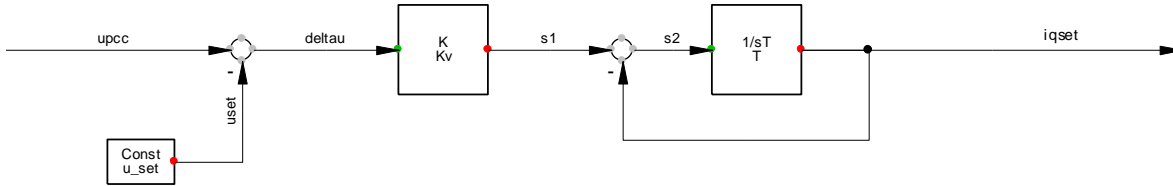


Figure 3.11: Block diagram of the Voltage Controller model

Here, the PCC voltage is controlled. First the actual per unit value of u_{PCC} is measured and is then compared to the reference value u_{set} (usually defined at 1 pu) so as to create an error signal. The error signal is multiplied with a gain constant K_V and then is driven through an integrator block with a time constant T (the integrator is part of a closed-loop under unity feedback system). The values of parameters used can be found in Table B.2 of APPENDIX B. Finally, the q-axis converter output current preliminary set point is calculated, based on the following equation in transfer function form:

$$i_{q, \text{set}} = \frac{K_V}{1 + sT} (u_{PCC} - u_{set}) \quad (3.29)$$

A PCC voltage higher than the reference one will result in reactive power absorption by the DRG converter (inductive behaviour). On the contrary, when the voltage at the PCC is lower than the reference one, reactive power injection occurs (capacitive behaviour).

3.5.1.5 ‘CURRENT LIMITER’ BLOCK

The converter current must be limited to protect the semiconductor switches in the power electronic converter. This block uses the preliminary set-point values of d and q-axis currents ($i_{d, \text{set}}$, $i_{q, \text{set}}$) as input and outputs their final set-point values ($i_{d, \text{ref}}$, $i_{q, \text{ref}}$). The limiter boundaries are specified by giving the maximum amount of reactive power the DRG plant can generate in per unit. From this value and the nominal active power, the nominal current is calculated for nominal terminal voltage. This way of specifying the current limits is more user friendly than specifying the current limits directly [62]. Therefore, the maximum converter apparent current is:

$$i_{\max} = \frac{\sqrt{P_{\text{nom}}^2 + Q_{\max}^2}}{u_{\text{nom}}} = 1 \text{ p.u.} \quad (3.30)$$

To reduce the possibility of active power curtailment, d-axis current is prioritised over q-axis current. Thus, the d-axis current limit is equal to the total current limit:

$$i_{d, \max} = i_{\max} \quad (3.31)$$

The active current final set-point is calculated using the following expression:

$$i_{d, \text{ref}} = \begin{cases} i_{d, \text{set}}, & i_{d, \text{set}} \leq i_{d, \max} \\ i_{d, \max}, & i_{d, \text{set}} > i_{d, \max} \end{cases} \quad (3.32)$$

As far as the reactive current is concerned, the limiting procedure is twofold. Not only must it be ensured that the total current limit is not exceeded, but also the operating power factor range is taken into account. Hence, the q-axis current limit is:

$$i_{q, \max} = \min \left\{ \sqrt{i_{\max}^2 - i_{d, \text{ref}}^2}, i_{d, \text{ref}} \cdot \tan(\cos^{-1}(PF_{\min})) \right\} \quad (3.33)$$

The reactive current final set point is calculated using the following expression:

$$i_{q,ref} = \begin{cases} i_{q,ref}, & |i_{q,ref}| \leq i_{q,max} \\ i_{q,max}, & |i_{q,ref}| > i_{q,max} \text{ and } i_{q,ref} > 0 \\ -i_{q,max}, & |i_{q,ref}| > i_{q,max} \text{ and } i_{q,ref} < 0 \end{cases} \quad (3.34)$$

3.5.2 WIND POWER PLANT MODEL

3.5.2.1 OVERVIEW

In this subsection the aggregated Wind Power Plant (WPP) model is described. With respect to the time scale that is of interest in this study (see Figure 3.1) and the time scales of phenomena related to the WPP operation, several simplifications that lead to the development of a long-term dynamic model can be allowed. In the following paragraphs an effort is made to provide detailed information regarding, not only the structure and the operation of the developed model, but also the simplifying assumptions made at each part.

Figure 3.12 illustrates the single-line diagram of a three-phase aggregated WPP with 400 V nominal AC output voltage, connected –through a 20/0.4 kV transformer and a 0.8 km line– to the Point of Common Coupling, located at the MV distribution grid. The line specifications can be found in Table A.4 and Table A.5 of APPENDIX A, depending on whether the WPP is connected to a node of Feeder 2 or Feeder 1, respectively. The wind turbine (WT) graphical symbol at the bottom of the diagram represents a number of N_{WT} variable speed wind turbines with direct drive synchronous generators, interfaced via fully rated converters. The nominal power of each WT is 2 MW. Despite the fact that each individual WT is connected to its own step-up transformer, only one transformer is modelled. The impedance of the aggregated step-up transformer is equal to the individual turbine transformer impedance divided by N_{WT} ; the specifications of the aggregated transformer can be found in Table C.1 of APPENDIX C. Finally, the connection lines within the WPP have been ignored.

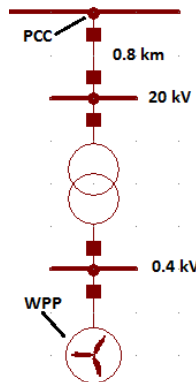


Figure 3.12: Single line diagram of a Wind Power Plant (WPP) connected to the MV distribution grid

The concept behind the aggregation is the following: the instantaneous power generated by a variable speed wind turbine is dependent on the actual value of the rotor speed, rather than on the wind speed. Therefore, in the aggregated model of a wind park with variable speed wind turbines, the rotor speed of the individual turbines is kept track of and the electrical power of the individual turbines is added [77]. Hence, instead of modelling the whole wind park, one has just to model one individual wind turbine. Since the wind turbines in the park are equipped with voltage controllers, one voltage controller is attached to the aggregated model. Furthermore, in a simplified scheme where an identical wind speed profile is applied to all the individual wind turbines of the park, the power output (in pu) of a single WT is simply multiplied with the nominal WPP power (real magnitude) in order to calculate the total output power of the WPP. Based on the above stated, the block diagram of the WPP model is depicted in Figure 3.13.

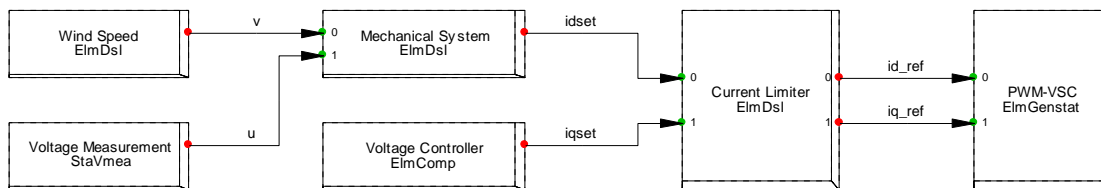


Figure 3.13: Block diagram of the Wind Power Plant (WPP) model

In general, control is performed in the DQ0 reference frame, meaning that equations (3.10) and (3.11) above, along with their accompanying assumptions, hold. Starting from the ‘Wind Speed’ block, where the wind speed time series is accessed

via a lookup table, we then reach the ‘Mechanical System’ block, where the mechanical input power is calculated. Subsequently, with the use of the rotor speed controller, mechanical power is transformed to electrical power and a preliminary calculation of the converter d-axis output current set-point $i_{d,set}$ is performed. In the ‘Voltage Controller’ block, the PCC voltage is regulated to a reference value, resulting in a preliminary calculation of the q-axis converter output current set-point $i_{q,set}$. The preliminary current set-points are then fed to the ‘Current Limiter’ block, where restrictions regarding the WPP operating power factor and the maximum apparent current limit of the PWM converter are applied. Finally, the output currents reference set-points are fed to the ‘PWM-VSC’ block, resulting in the grid current injection.

A first look at the system reveals many similarities with the PVPP model (see Figure 3.8). Indeed, some blocks are the same, except from the ‘Wind Speed’ and ‘Mechanical System’ blocks; the ‘Current Limiter’ block is also slightly different than the one described in paragraph 3.5.1.5. In the following paragraphs, a detailed description of from the ‘Wind Speed’ and ‘Mechanical System’ blocks is given, as well as a clarification regarding the ‘Current Limiter’ block. In order to avoid extensive text repetition, for a detailed description of the rest of the participating blocks (namely ‘PWM-VSC’, ‘Voltage Controller’ and ‘Current Limiter’ blocks) the reader is encouraged to refer to the corresponding paragraphs of subsection 3.5.1. It is important to clarify that specifications and values of parameters used in the WPP model can be found in APPENDIX C; only when it is absolutely necessary are such values given in the text.

3.5.2.2 ‘WIND SPEED’ BLOCK

The wind speed weekly time series (linearly interpolated 10 min. average values) used as input to the WPP model are derived from data collected by an actual measurement mast [78]. The measurement mast is installed in the area of Cabauw, the Netherlands. Winter measurements refer to the period 25/02/2007 – 03/03/2007, while summer measurements refer to the period 03/07/2007 – 09/07/2007. Measurements are taken at 80 meters height, which coincides with the hub height of a 2 MW onshore wind turbine [79]. Furthermore, with a view to performing a realistic study, daily and seasonal variations are included. Wind speed data is provided by means of a lookup table and a graphical representation of it is shown in Figure 3.14. As expected, wind speeds are higher during winter (average value 10.26 m/s) and lower during summer (average value 7.37 m/s). There is, however, one winter day, during which the prevailing wind speeds are high. In addition, the corresponding active power production of a WPP model with nominal power output of 4 MW (2x 2 MW) is shown in Figure 3.15.

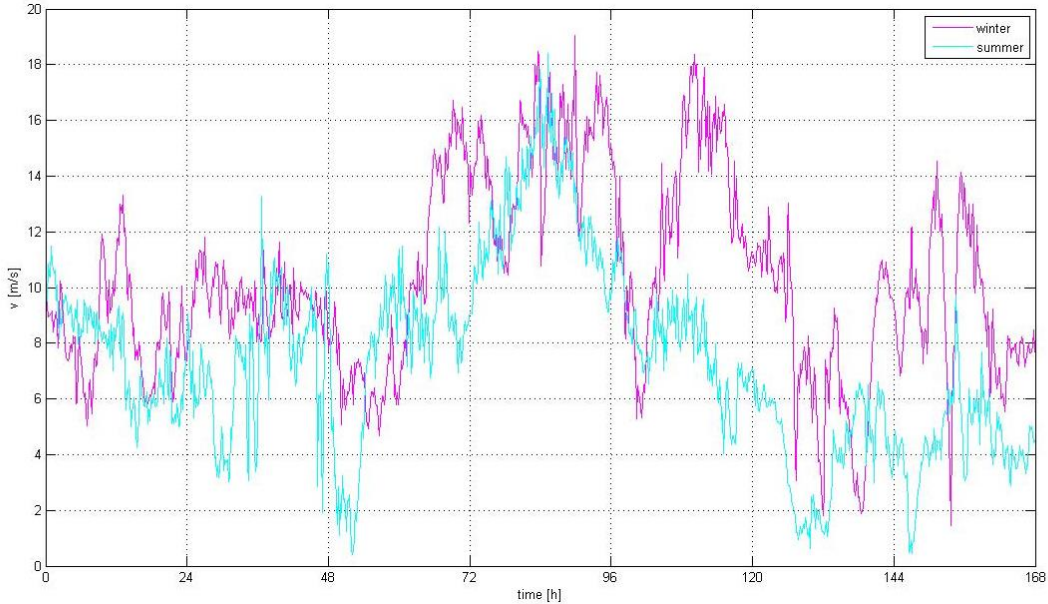
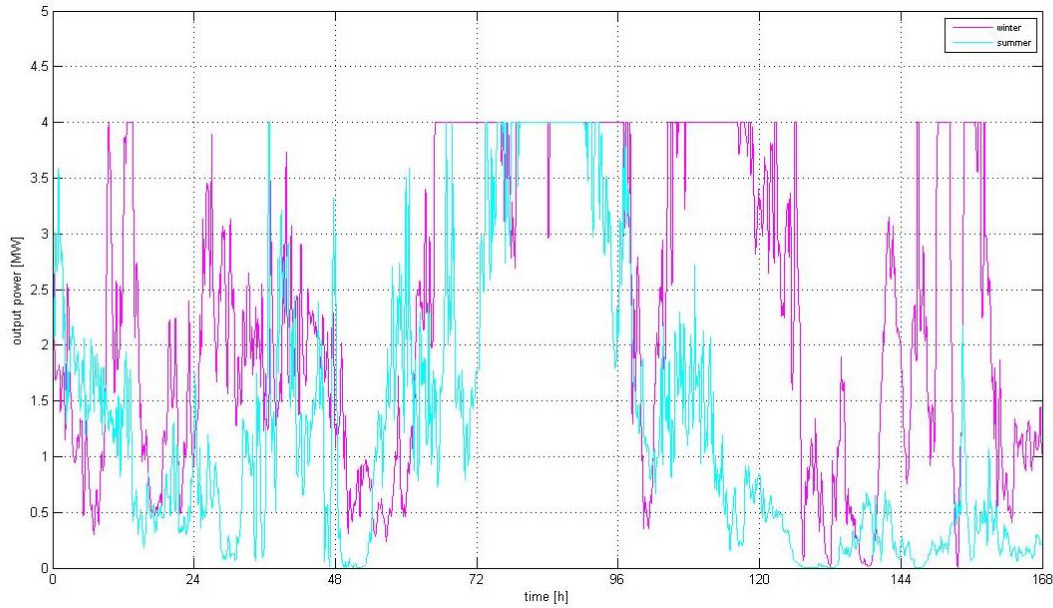


Figure 3.14: Wind speed weekly time series

Figure 3.15: Active power output of a WPP model with $P_{nom} = 4 \text{ MW}$

It should be stated that, due to the nature of the wind speed data, the turbulence term is neglected. Besides, in case of variable speed wind turbines, turbulence is hardly reflected in the output power due to the functioning of the rotor as an energy buffer [77]. Additionally, since no geographical layout of the WPP is defined, it is assumed that a single wind speed value acts on all the individual wind turbines of the aggregated wind park model; this further implies that wake effects are neglected.

3.5.2.3 ‘MECHANICAL SYSTEM’ BLOCK

This block is responsible for producing the converter active current preliminary set-point signal. The model of the mechanical system is depicted in Figure 3.16. At first, the wind speed is fed as an input to the sub-block of the rotor model, where the mechanical power extracted from wind (P_w) is calculated. Afterwards, via the rotor speed controller, the corresponding active power set-point is calculated (P_{set}). Finally, dividing P_{set} by the terminal voltage value results in the calculation of converter d-axis current preliminary set-point ($i_{d,set}$).

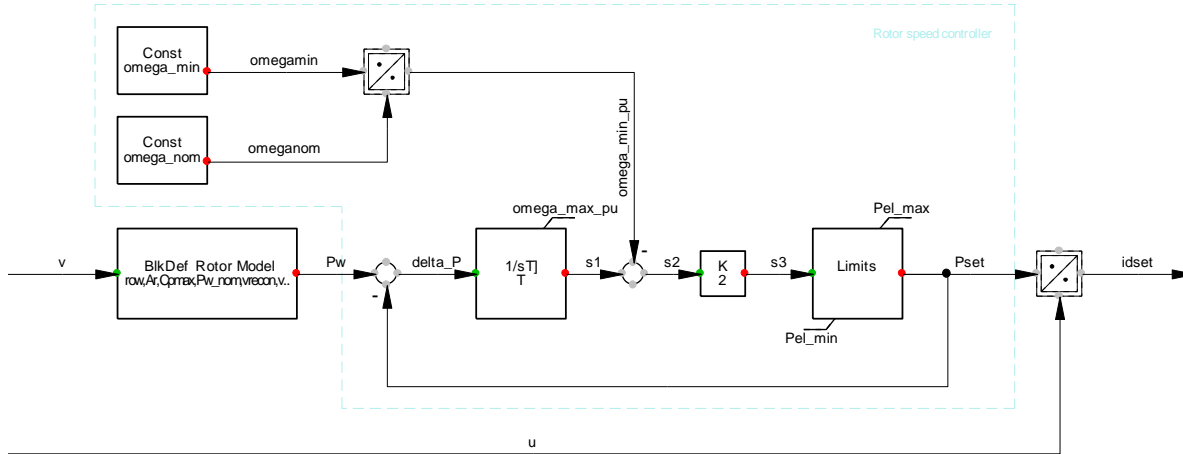


Figure 3.16: Block diagram of the Mechanical System model

In the following paragraphs, the operation of the two main parts of the ‘Mechanical System’ model, namely ‘Rotor model’ and ‘Rotor Speed Controller’, is analysed.

Rotor model

In the presented wind turbine model a quasi-static rotor model is used, which assumes an algebraic relationship between the wind speed and the mechanical power extracted from the wind. Any dynamic phenomena, such as blade and tower bending and tilt, are neglected. The rotor is modelled using the following equations [62]:

$$P_w = \frac{\rho}{2} \cdot A_r \cdot c_p(\lambda, \theta) \cdot v_w^3 \cdot \frac{1}{P_{nom}} \quad (3.35)$$

With

$$c_p(\lambda_i, \theta) = 0.22 \cdot \left(\frac{116}{\lambda_i} - 0.4 \cdot \theta - 5 \right) \cdot \exp \left(-\frac{12.5}{\lambda_i} \right) \quad (3.36)$$

And

$$\lambda_i = \frac{1}{\frac{1}{\lambda + 0.08 \cdot \theta} - \frac{0.035}{\theta^3 + 1}} \quad (3.37)$$

where P_w is the power extracted from the airflow [pu], ρ is the air density [kg/m^3], c_p is the performance coefficient or power coefficient, λ is the ratio of the blade tip speed v_t over the wind speed upstream the rotor v_w , A_r is the rotor swept area [m^2], θ is the blade pitch angle [deg] and P_{nom} is the nominal active power of the individual wind turbine [W]. Equations (3.35) - (3.37) are based on numerical approximations and are only valid for a 2 MW wind turbine with the characteristics given in Table C.2 of APPENDIX C.

In general, for wind speeds lower than the nominal, the rotor speed is controlled in such a way that optimal energy capture is achieved. In other words, the power coefficient must obtain its maximum value. The circumstances under which this can happen are defined by the following equation:

$$c_{p,max} = c_p(\lambda = \lambda_{design}, \theta = 0) \quad (3.38)$$

In [76] it is argued that the optimal pitch angle equals zero below the nominal wind speed and from the nominal wind speed on increases steadily with increasing wind speed. Moreover, the design tip speed ratio can be found by solving:

$$\left. \frac{\partial c_p(\lambda, \theta = 0)}{\partial \lambda} \right|_{\lambda=\lambda_{design}} = 0 \quad (3.39)$$

The calculations of λ_{design} and $c_{p,max}$ are performed in section C.3 of APPENDIX C. In this study, it is assumed that the performance coefficient c_p is always equal to its maximum value $c_{p,max}$. Then, the complicated $c_p(\lambda)$ characteristic of equations (3.36) and (3.37) can be omitted from the model and be replaced by (3.40). Only a minor error results from this simplification, because the rotor speed versus power control characteristic is such that c_p is kept at its maximum as much as possible. In other words, a perfect rotor speed controller is assumed [62]. The resulting equation for computing the power extracted from wind is:

$$P_w = \frac{\rho}{2} \cdot A_r \cdot c_{p,max} \cdot v_w^3 \cdot \frac{1}{P_{nom}} \quad (3.40)$$

Last but not least, a high wind speed shutdown mechanism has been implemented. Most wind turbines are designed to shut down when wind speed averages over 25 m/s and will typically remain disconnected until a restart criterion is satisfied [80]. The restart criterion used is the 10 min. average wind speed dropping to 22 m/s. This protection mechanism has been modelled using a Set / Reset Flip-Flop.

Rotor Speed Controller

The used 'Rotor Speed Controller' is shown inside the dashed coloured polyline of Figure 3.16. The next few text lines constitute an attempt to justify the creation and application of this controller. Normally, a more detailed and complicated variable speed wind turbine model would be equipped with a rotor speed controller which operates as follows [62]:

- Several times per second, the actual rotor speed is measured. From this value, a set-point for generator real power is derived using a control characteristic (a rotor speed versus generator power characteristic like the one in Figure 3.17 would be used)
- Taking into account the rotor speed, a torque set-point is calculated
- The power electronic converter is controlled in such a way that the generator torque follows the set-point.

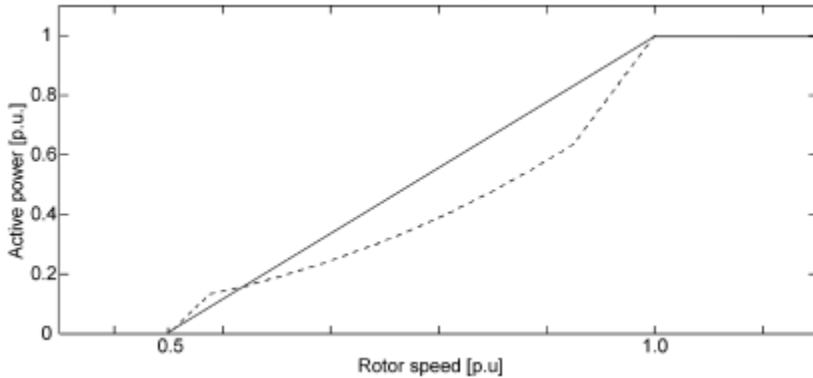


Figure 3.17: Normal rotor speed versus power control characteristic (dashed) and its first-order approximation (solid)

The generator stator current is controlled by a PWM-VSC and therefore the active and reactive power can be adjusted very quickly. Moreover, as in most power system studies where electromagnetic transients are of no interest, the flux derivative terms in the stator equations of the direct drive synchronous generator can be neglected. This means that generator torque set-points can be reached instantaneously by injecting the appropriate stator current. In this situation it is not necessary to include the equations describing the generator. Instead, the combination of the generator and the converter can be modelled as a torque source, which immediately generates an amount of torque equal to the set-point generated by the rotor speed controller [62].

The mechanical power and electrical power are used to calculate the rotor speed, which is the only remaining state variable in the simplified model presented in Figure 3.16. For the time constant T it stands that:

$$T = 2 \cdot H \quad (3.41)$$

where H is the per unit inertia constant of the rotor structure. More precisely, all rotating mass is represented by one element, the so called “lumped-mass” representation [76]. In the case of a variable speed wind turbine the shaft can be neglected, since the power electronic converter decouples the electrical and mechanical behaviour. Therefore, the shaft properties are hardly reflected in the WT response to wind speed changes [81]. The calculation of H is made according to equations [4]:

$$H = \frac{J \cdot \omega_{0,m}^2}{2 \cdot VA_{base,2}} \quad (3.42)$$

$$VA_{base,2} = P_{nom} \quad (3.43)$$

where J is the total moment of inertia of the rotating mass [$\text{kg}\cdot\text{m}^2$], $\omega_{0,m}$ is the nominal mechanical rotor speed of the synchronous generator [rad/s] and P_{nom} is the nominal active power of the individual wind turbine [W].

Additionally, the rotor speed versus power controller is represented by a gain constant K because a linear approximation of the control characteristic is used (see Figure 3.17). From the rotor speed, the electrical power set-point P_{set} is derived [pu]. Consequently, the converter d-axis output current preliminary set-point $i_{d,set}$ [pu] is also derived.

It is worth noting that the integrator, in which the rotor speed is stored, is limited to the maximum rotor speed of the WT, as defined by its technical specifications. This allows for the pitch angle controller to be omitted, as it is no longer needed for limiting the speed. Besides, the maximum rate of change of the pitch angle is in the order from 3 to 10 deg/s, depending on the size of the wind turbine [62]. Hence, a blade can be rotated at its maximum extent (about 20 deg) within very few seconds; this time period is shorter than the time scales that are of interest in this study. Finally, the different rotor speed versus power characteristic leads to small, but still acceptable, differences in generated active power [77].

3.5.2.4 ‘CURRENT LIMITER’ BLOCK

This block is the same as the one described in paragraph 3.5.1.5, except from one extra added manipulation which is hereby described. According to equations (3.40) and (3.43), all pu quantities within the ‘Mechanical System’ block are calculated with respect to the base quantity $VA_{base,2}$.

Nevertheless, this is not in accordance with equations (3.16) and (3.17), which describe the fact that the PWM-VSC is oversized and its nominal apparent power is set to be equal to the VA_{base} . Thus, in order to express the converter d-axis output current preliminary set-point $i_{d,set}$ with respect to $VA_{base,2}$, this must be multiplied with 0.95 before the calculations inside the ‘Current Limiter’ block can take place.

3.6 INTELLIGENT NODE MODEL

3.6.1 OVERVIEW

Based on the Intelligent Node (IN) description in the previous chapter (see subsection 2.5.4), for the needs of this study an IN model with two AC ports and an energy storage device at the DC side has been implemented. According to [43], in order to effectively control the voltage profiles in a MV network, the IN node should be connected to the end of each MV feeder. The benchmark network used in this study (see section 3.3) consists of two MV feeders; this indicates that a 2-port IN, consisting of two back-to-back connected PWM converters, should be used. Furthermore, the existence of a Battery Energy Storage System (BESS) at the DC side offers the capability of independent active power control at the converters AC sides.

Figure 3.7 illustrates the single-line diagram of a three-phase, 2-port, IN with BESS. Each one of the two converters operates at 400 V nominal AC output voltage and is connected through a 20/0.4 kV transformer to the MV distribution grid. The transformers not only make an isolated ground for IN, but also boost the PWM converters output voltage to the grid voltage level. The specifications of the transformer can be found in Table D.1 of APPENDIX D; the connection lines from the IN to the MV grid have been ignored.

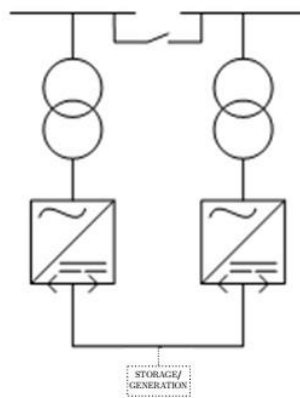


Figure 3.18: Single-line diagram of a 2-port Intelligent Node (IN) connected to the MV distribution grid

The block diagram of the IN model is depicted in Figure 3.19. Signal names with the subscript '1' refer to PWM-VSC number 1; equivalently, signal names with the subscript '2' refer to PWM-VSC number 2.

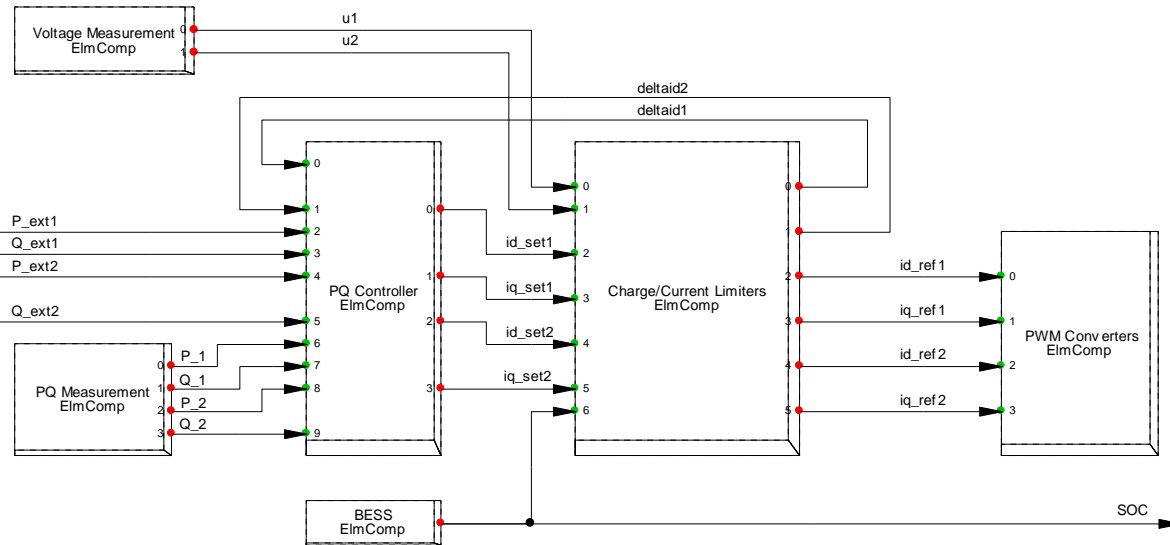


Figure 3.19: Block diagram of the Intelligent Node (IN) model

In general, control is performed in the DQ0 reference frame, meaning that equations (3.10) and (3.11), along with their accompanying assumptions, hold. In addition, it should be pointed out that the model receives the active and reactive power reference signals externally; these are generated by the coordinated voltage control algorithm and fed to the model so as to be eventually exchanged with the grid. Similarly, the signal carrying information regarding the current state of charge (SOC) of the battery is an output of the model, serving as an input to the voltage control algorithm. Inside the 'PQ Controller' block the power reference signals are compared to the actual measured values, resulting in the converter

currents preliminary set-points. Consequently, the preliminary current set-points are driven through the ‘Charge/Current Limiters’ block, where limitations regarding the BESS charge/discharge limits and the converters AC current limits may apply. Hence, the current reference set-points are produced. Any difference that may arise between the preliminary and the reference d-axis current set-points serves as a feedback for the ‘PQ Controller’ block. Finally, the output currents reference set-points are fed to the ‘PWM Converters’ block, resulting in the grid current injection or absorption.

In the following paragraphs, a detailed description of IN model blocks is given. It is important to clarify that specifications and values of parameters used in the IN model can be found in APPENDIX D; only when it is absolutely necessary are such values given in the text.

3.6.2 ‘BESS’ BLOCK

The model for the Battery Energy Storage System (BESS) is based on the simple battery model presented in [82]. A Lead-Acid battery is assumed, where the total capacity and the initial state of charge are user-defined parameters. The BESS is allowed to discharge down to a minimum SOC value (SOC_{min}) and charge up to a maximum SOC value (SOC_{max}); these operational SOC limits can theoretically extend the life time of the system [83]. In addition, the initial SOC value SOC_0 [%] and the maximum power handled by the BESS $P_{BESS,max}$ [MW] must be specified. However, since an IN is composed of appropriately matched BESS and PWM converters, the maximum active power handled by the converters ($P_{1,max}$ and $P_{2,max}$, in [MW]) will never be larger than the one handled by the BESS. More precisely, the IN specifications are chosen so that:

$$P_{1,max} + P_{2,max} \leq P_{BESS,max} \quad (3.44)$$

The model is capable of calculating the current value of SOC based on the power exchange between the battery and the converters. Since an economic evaluation of the system is out of the scope of this study, the above stated equipment is assumed to have 100 % efficiency. Hence, the power exchange between the battery and the converters is given by:

$$P_{BESS} = P_1 + P_2 \quad (3.45)$$

where P_{BESS} is the exchanged power [MW], and P_1 and P_2 are the measured active powers [MW] at the AC terminals of converters 1 and 2, respectively. A positive value of P_{BESS} indicates battery discharge, while a positive value of P_1, P_2 indicates active power injection to the grid. On the contrary, a positive value of P_{BESS} indicates battery charge, while a negative value of P_1, P_2 indicates active power absorption from the grid.

Normally, a DC/DC converter is used to interface the BESS with the DC side of the PWM converters, by appropriately regulating the voltage applied to the battery and thus facilitating the charging operation. In our case though, a DC/DC converter is not modelled. Instead, the DC bus voltage is assumed to always be appropriately high, so that charging operation is not hindered.

3.6.3 ‘PWM CONVERTERS’ BLOCK

The PWM converters are considered to be lossless, meaning that the electrical power at the DC side can be fully converted to AC power at the grid side. The converter is modelled as a current source that supplies a sinusoidal current at the fundamental grid frequency [62]. By controlling the d and q components of the current injected into (or drawn by) the power network, active and reactive powers can be independently controlled according to equations (3.14) and (3.15). Each converter is capable of providing or absorbing any combination of active and reactive power as long as its nominal rating is not exceeded. With (3.16) being valid, the following equation holds:

$$S_{nom} = P_{max} = Q_{max} = 1 \text{ p.u.} \quad (3.46)$$

where S_{nom} is the converter rating [pu] and P_{max}, Q_{max} are the maximum active and reactive power [pu], respectively, that can be handled by the converter. Of course, the sizing of the converters should not violate the restriction posed by (3.44).

Although it is left out of the scope of this study for simplification reasons, the issue of the converter maximum DC voltage limitation, as described in [84], is not expected to cause any problems. More specifically, the reactive power exchange is mainly dependent on the voltage difference between the AC voltage the VSC can generate from the DC voltage and the grid AC voltage. In the case of a VSC connected to the grid via a transformer reactance, the power injection capability increases with decreasing grid AC voltage. Similarly, in this study an Intelligent Node is expected to inject power to the grid only when the grid AC voltage at the connection point is below 1 pu, meaning that no capability limitation will occur.

3.6.4 ‘PQ CONTROLLER’ BLOCK

The ‘PQ Controller’ block is responsible for producing the converter d and q-axis current preliminary set-points, namely $i_{d,se1}$ and $i_{q,se1}$ [pu]. This requires that the active and reactive power reference signals P_{ext} and Q_{ext} [pu] are compared to the corresponding actual measured (at the converter terminals) values P and Q [pu]. The model of the PQ controller is depicted in Figure 3.20. The index ‘1’ shown in several signal names implies that the PQ controller of the PWM converter 1 is shown; PWM converter 2 is equipped with an identical controller.

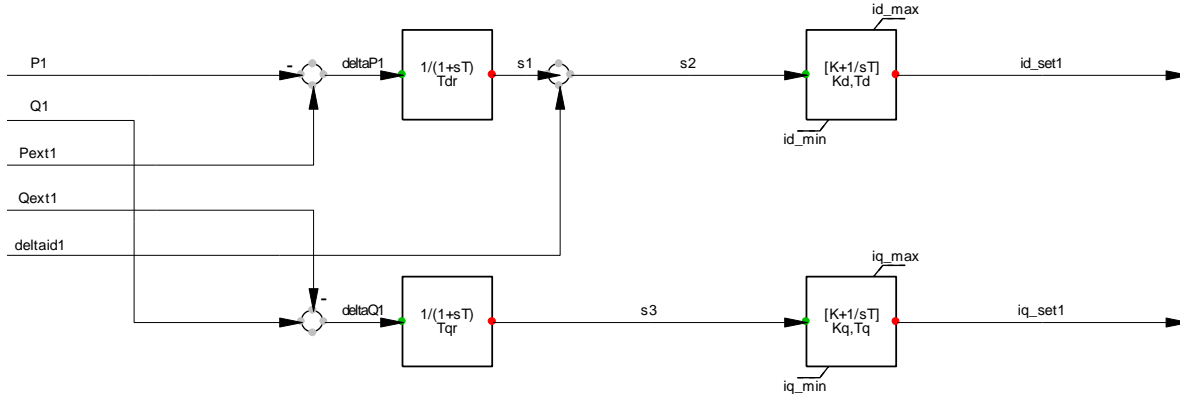


Figure 3.20: Block diagram of the PQ Controller model

The control deviations ΔP and ΔQ are filtered with a first-order delay element so as to avoid an oscillatory behaviour of the controller. After that, the signals are used as an input to a PI controller. In the active path, the signal Δi_d is added. This signal originates from the ‘Charge / Current Limiter’ and is the difference between the d-axis current preliminary set-point (as set by the PQ controller) and the d-axis current reference set-point (after limitations in the ‘Charge / Current Limiter’ have been applied). The feedback of this signal to the ‘PQ Controller’ block prevents a windup of the PI controller, which would otherwise cause excessive overshoot in case of a large change in the d-axis current set-point [82]. Regarding the tuning of the PI-controllers, as it can be seen in Table D.4 of APPENDIX D, small values have been chosen for the gain constants K_d and K_q in order to minimise the power steady-state error. Furthermore, the values of the time constants T_d , T_q allow the converter to quickly respond (within several tens of seconds) to large changes of the external power reference signals, while at the same time overshoot is kept at low levels.

3.6.5 ‘CHARGE / CURRENT LIMITER’ BLOCK

This block accommodates two protective functions. The ‘Charge / Discharge Limiter’ ensures that the BESS state of charge is within specified limits, while the ‘Current Limiter’ ensures that the current at the AC side of the converters is bounded to an upper safety limit. It is important to point out that the charge limiter is a local actuator and is included in the IN model for completeness reasons. Since the SOC value is exported to the Coordinated Voltage Controller (see Figure 3.19), not operating the BESS outside the SOC safety boundaries is something that is taken care of beforehand, at the coordination level.

Charge / Discharge Limiter

Once the BESS state of charge reaches the maximum allowed value, further charging is prevented until a (lower) SOC safety value is reached. Similarly, once the SOC reaches the minimum allowed value, further discharging is prevented until a (higher) SOC safety value is reached. The implemented protection control scheme is better understood by means of a flow chart (see Figure 3.21). The algorithm execution is repeated at every simulation step.

The controller is made aware of the BESS overall power exchange, by calculating the following expression:

$$P_{check} = u_1 \cdot i_{d,se1} + u_2 \cdot i_{d,se2} \quad (3.47)$$

During the time that the protection is active, the power exchange over the BESS is set to zero by applying the following restriction:

$$P_1 = -P_2 \quad (3.48)$$

The d-axis current set-point values are then corrected (for both PWM converters) according to:

$$i_{d,cor1} = \frac{u_1 \cdot i_{d,se1} - u_2 \cdot i_{d,se2}}{2 \cdot u_1} \quad (3.49)$$

$$i_{d,cor2} = \frac{u_2 \cdot i_{d,sel2} - u_1 \cdot i_{d,sel1}}{2 \cdot u_2} \quad (3.50)$$

where u_1 and u_2 are the voltage magnitudes at the converters terminals [pu]. Equations (3.49) and (3.50) ensure that the two converters are fairly influenced by the protective control command of equation (3.47).

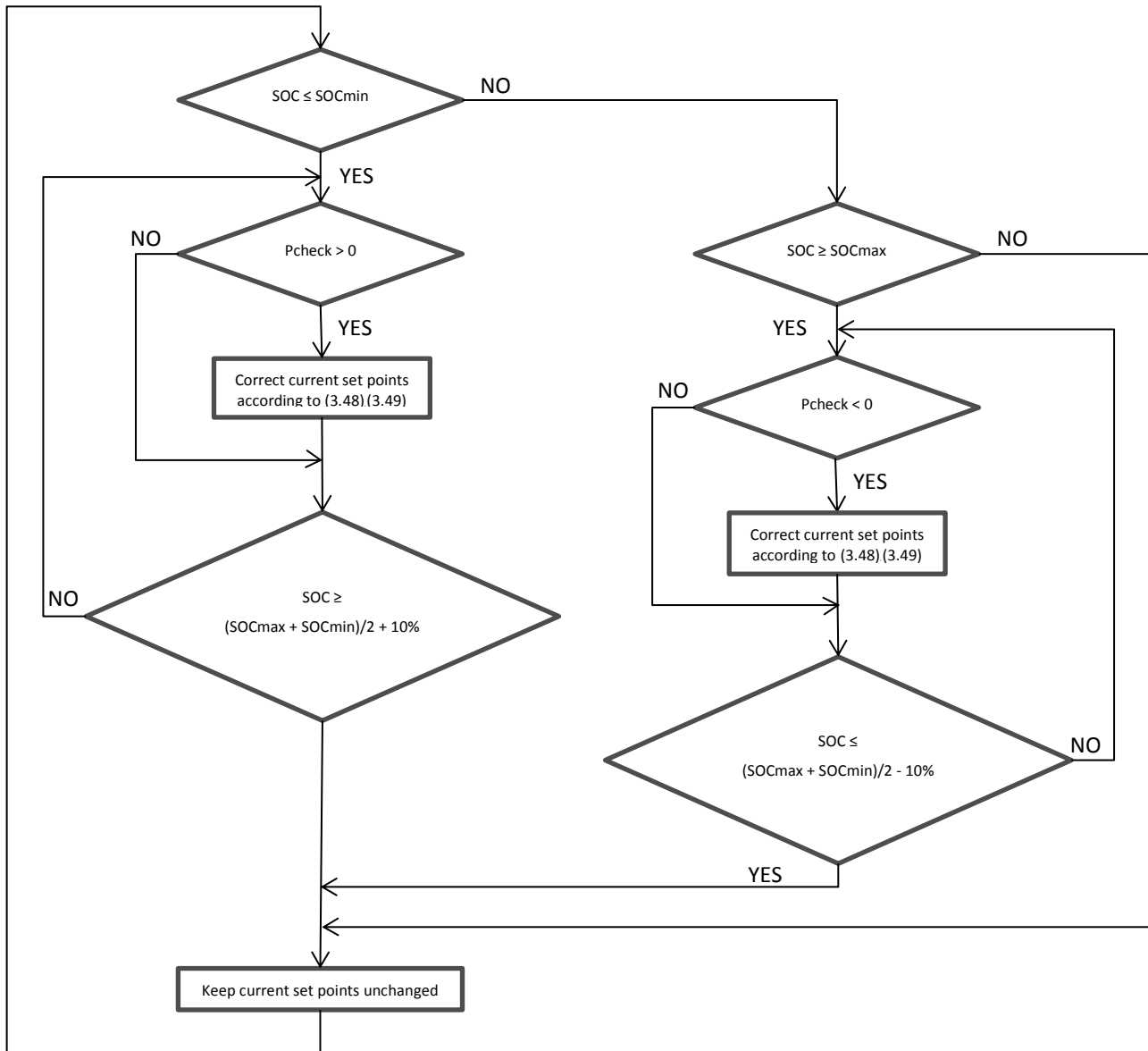


Figure 3.21: Flow chart of the Charge / Discharge Limiter control algorithm

Current Limiter

The limiter boundaries are specified by the converter nominal apparent power in per unit. From this value, the nominal current is calculated for nominal terminal voltage. Therefore, the maximum converter apparent current is:

$$i_{max} = \frac{S_{nom}}{u_{nom}} = 1 \text{ p.u.} \quad (3.51)$$

where u_{nom} is the converter nominal terminal voltage [pu]. With a view to a more effective operation of the IN, a choice of prioritising d or q-axis current is offered.

More specifically, a converter connected to a network with high R/X ratio would benefit from prioritising d-axis current; similarly, a converter connected to a network with low R/X ratio would benefit from prioritising q-axis current. When d-axis is prioritised, the d-axis current limit is equal to the total current limit, according to equation (3.31). Consequently, the active current final set-point is calculated using (3.32). On the other hand, when q-axis is prioritised, the q-axis current limit is equal to the total current limit and the active current final set-point is calculated according to:

$$i_{q,max} = i_{max} \quad (3.52)$$

$$i_{q,ref} = \begin{cases} i_{q,set}, & i_{q,set} \leq i_{q,max} \\ i_{q,max}, & i_{q,set} > i_{q,max} \end{cases} \quad (3.53)$$

3.7 CONCLUSIONS

Concluding the modelling chapter, an overview of the modelling approach was given and the developed models were described in detail. First, the most important aspects of the Cigré European MV distribution network benchmark model were discussed, along with a description of its main components; however, the detailed specifications are listed in APPENDIX A. Subsequently, the main load modelling representations were described. For the purposes of this study, a static load model was implemented, based on realistic parameters and consumption data. Furthermore, models for two types of DRG were created: a Photovoltaic Power Plant (PVPP) model and a Wind Power Plant (WPP) model. Both models were analysed, starting from the point where power is initially extracted from the renewable prime mover and until the point of injecting electric power to the grid. Aspects regarding voltage control and current limits were also discussed, while detailed specifications of the PVPP and WPP models are listed in APPENDIX B and APPENDIX C, respectively. Finally, the Intelligent Node model was presented. Topological and operational details were given, along with IN control functionalities that were included with a view to performing the simulations of Chapter 4. Again, specification data about the IN model can be found in APPENDIX D.

4 VOLTAGE CONTROL CONCEPT

4.1 INTRODUCTION

In this chapter the proposed coordinated voltage control algorithm is initially described and analysed. The main two parts of the Coordinated Voltage Controller, namely the Advanced OLTC Controller and the IN Controller, are separately treated. Before proceeding to the simulations part, the test system is presented. In order to prove the value and the usefulness of the proposed controller, the test system is simulated under various control schemes. The main simulation results are presented and analysed with respect to specific criteria, while the most important findings and phenomena arising from these results are discussed. At the end of the chapter, comparative results for all four tested voltage control schemes are presented.

4.2 COORDINATED VOLTAGE CONTROL CONCEPT

4.2.1 PREVIOUS WORK AND BASIC DESCRIPTION

As explained in subsection 2.3.1, network voltage deviations need to be limited within specific boundaries. This can in turn pose limits to the maximum DRG penetration in the MV distribution network. Hence, by controlling the network voltage one can increase the DRG hosted capacity. In general, a basic aspect of a voltage control methods is whether it is centralised or local. Centralised voltage control is based on an overall EMS that first estimates the power system state by collecting several data and then dispatches the DRG units, with a view to minimising an objective function via Optimal Power Flow (OPF). On the other hand, local voltage control is deployed by combining automatic voltage regulation on the transformers with active and reactive power control of the DRG units. Up to now, many studies have been carried out to evaluate suitable solutions that facilitate connecting more DRG units in distribution networks.

One possibility to control the network voltage is the sophisticated HV/MV transformer control. More specifically, in [33] and [85], centralised OLTC control schemes based on several node voltage measurements and a state estimation technique are proposed. The state estimation technique, although rather complicated as a method, offers the advantage of minimum communication needs. Moreover, the authors of [86] and [54] have managed to control the OLTC using only local voltage measurements along with load diversity information of the feeders. These methods, although computationally intensive, can be implemented without needing any communication links.

Regarding the voltage control methods using active and / or reactive power dispatch, a voltage sensitivity analysis method using local voltage measurements is presented in [87], while in [37] a coordination between the OLTC control and the reactive power dispatch of DRG units is made possible. In a similar approach, the authors of [29] use a state estimation technique to reduce the communication channels needed. Additionally, in [26] the reactive power support offered by appropriately controlled capacitor banks is also taken into account. It should be noted that methods based on reactive power control of DRG units can potentially suffer from a drawback. In case there is a need for DRG units to operate at relatively low power factor values, active power curtailment is necessary; to tackle this issue, the costly solution of heavily oversizing the converter units must be applied.

Finally, solutions combining distributed storage and controlled power flow offered by the Intelligent Node are investigated in [61] and [59]. More precisely, in [61] the IN controls the active power flow in order to improve the voltage profiles of MV distribution feeders. The Cauchy's gradient method is used, along with the assumption of available load and generation information. The authors of [59] do the same thing by using a simpler algorithm, which however necessitates the availability of node voltage measurements.

In this study a novel coordinated voltage control method, aiming at increasing the DRG capacity of MV distribution networks, is presented. The novelty of this method lies in the fact that it combines the control of the HV/MV transformer OLTC device along with active power control offered by the Intelligent Node. The coordination centre is physically located at the HV/MV substation. The control objective, as well as the applying boundary conditions, is described in subsection 4.2.2. Accordingly, coordination and communication aspects are treated in subsection 4.2.3.

4.2.2 CONTROL OBJECTIVE AND BOUNDARY CONDITIONS

Control objective

According to the control objective of the developed algorithm, the voltage magnitude at every node of the controlled MV network part must not deviate more than 3 % compared to the nominal value. In other words, voltage variations must be bound within the range of $U_{nom} + 3\% / - 3\%$.

Boundary conditions

The two applying boundary conditions are:

- i. The current loading of every line (cable or overhead line) of the controlled MV network part must never exceed its nominal value (100 %).
- ii. With respect to the voltage control algorithm objective, a voltage variation accounting to slightly more than 3 % compared to the nominal value is considered to be acceptable only if its duration is less than or equal to 1 minute.

Regarding boundary condition 2, the reasoning behind its application is twofold. First, as it will be described in the following paragraphs, in this study a time delay of 40 seconds is considered for the OLTC operation [26]. Second, an IN is triggered after the aforementioned time delay period and it also needs some time itself in order to act. With these in mind, it was decided that a maximum acceptable voltage limits violation time of 1 minute should be adopted.

4.2.3 COORDINATION AND COMMUNICATION ASPECTS

The proposed Coordinated Voltage Controller receives measurement data from the MV network, processes this data and makes the appropriate decisions regarding the corrective actions that should be taken (if necessary). It is important to point out that upon the detection of voltage limits violations, the responsible OLTC device will act first. If the problem cannot be solved by the OLTC device (see subsection 4.2.4), then the responsible Intelligent Node(s) will take corrective action (see subsection 4.2.5). The organisation scheme is illustrated in Figure 4.1.

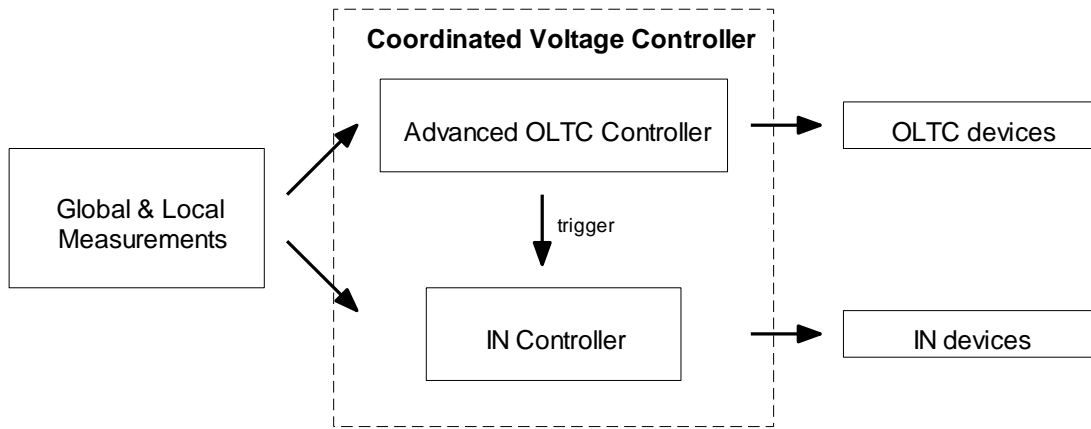


Figure 4.1: Organisation of the Coordinated Voltage Controller

The existence of communication links between the Coordinated Voltage Controller and the MV network nodes and devices is of crucial importance when it comes to the operation of the proposed control algorithm. More specifically, each node of the controlled network part accommodates a voltage sensor, which transmits the voltage magnitude signal to the coordination centre. Each Intelligent Node further accommodates a SOC level sensor and an actuator. The SOC level sensor transmits the SOC level signal to the coordination centre, while the actuator receives the active and reactive power set-point signals from the coordination centre. Last but not least, information concerning the tap position of the HV/MV transformer OLTC is exchanged between the OLTC devices of the HV/MV transformers and the coordination centre. The above communication links can be better understood with the help of Figure 4.6 (see subsection 4.3.1, on page 55), where the blue dashed lines correspond to local signals transmission and the cyan dashed lines correspond to remote signals transmission.

Overall, the Coordinated Voltage Controller makes use of the following sensors:

- Voltage magnitude measurement at each MV node,
- SOC level measurement at each Intelligent Node and
- tap position measurement at each HV/MV transformer.

In addition, the following actuators are used:

- active and reactive power actuator at each Intelligent Node and
- tap position actuator at each HV/MV transformer.

All the signals that serve as inputs to the Coordinated Voltage Controller are digitally sampled and transmitted every 20 seconds, with the exception of the tap position signals which are transmitted every 40 seconds. The choice of 0.05 Hz sampling frequency is not binding. However, the chosen sampling frequency not only adequately describes the phenomena which are of interest in this study, but also allows for acceptable simulation times and prevents the production of excessive output data. Moreover, the time period between two successive tap position signals has been selected with a view to exactly matching the OLTC time delay (see subsection 2.5.2). Therefore, there is no possibility for a tap change to occur and not be identified by the voltage controller.

To ensure that the digital sampling occurs simultaneously at all nodes, digital clocks are placed at every node. These clocks are synchronised with the grid frequency, which is the same for all the nodes of the controlled MV network part. It is important to note that the value of a signal remains constant until the next clock pulse. In reality, the required performance for transmitting digital signals from (to) remote sensors (actuators) could be achieved by utilisation of the IEC 61850 GOOSE and SV services and also by using wireless 4G technologies [32]. However, despite its usefulness, the need for establishing communication links between –geographically– remote locations within a distribution network is generally considered by the DNOs as an inhibiting factor for implementing modern voltage control schemes.

4.2.4 ADVANCED OLTC CONTROLLER

4.2.4.1 OVERVIEW

The Advanced OLTC Controller represents the first of the two main parts of the broader Coordinated Voltage Controller. In fact, two separate OLTC controllers have been created, each one managing the OLTC mechanism of one of the two HV/MV transformers shown in Figure 4.6 (see subsection 4.3.1 on page 55). The block diagram of the controller responsible for managing the OLTC mechanism of HV/MV transformer 0-1 is depicted in Figure 4.2. A similar controller for the OLTC mechanism of HV/MV transformer 0-12 has also been created, but is not shown so as to avoid the repetition of similar text and figures. The only difference between the two controllers lies in the voltage measurement samples that are used as inputs.

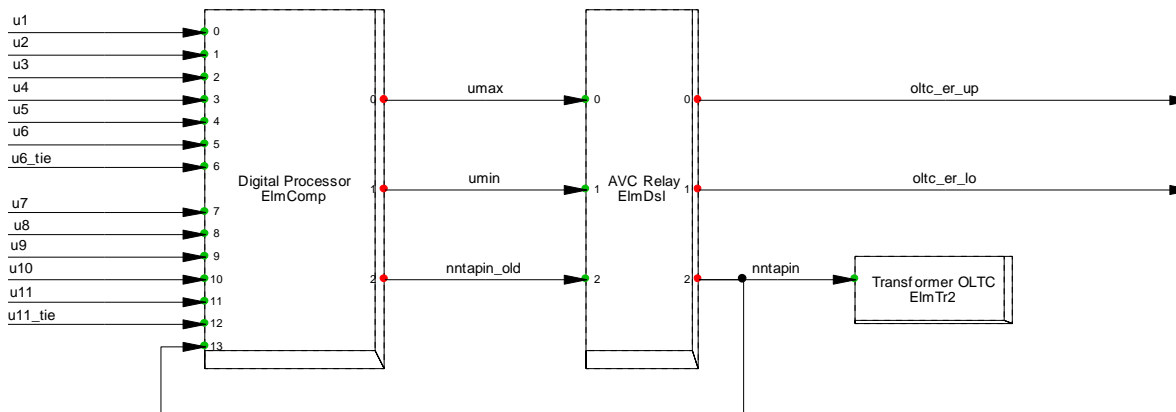


Figure 4.2: Block diagram of the Advanced OLTC Controller model (the shown model is for HV/MV transformer 0-1)

The controller accepts as inputs the voltage measurement samples of the nodes that belong to the MV feeder supplied by the relevant HV/MV transformer. The voltage measurement input signals are fed to the ‘Digital Processor’ block, where the maximum and minimum voltages are calculated. The maximum and minimum voltage values are necessary so that the decision for the appropriate tap position can be made by the ‘AVC Relay’ block later on. Of course, the signal carrying information about the current tap position of the OLTC must also be provided. Before that, the signal has to be processed inside the ‘Digital Processor’ block. Finally, an output signal carrying information about the new tap position is directed to the OLTC mechanism of the relevant HV/MV transformer, which then changes the tap position accordingly (if necessary). In addition, two error signals are produced by the ‘AVC Relay’ block as outputs. These signals have a non-zero value only when the upper or the lower voltage limit has been violated and the OLTC is incapable of performing a corrective action. A more detailed description regarding the operation of the ‘Digital Processor’ and the ‘AVC Relay’ blocks is given in the following paragraphs.

4.2.4.2 ‘DIGITAL PROCESSOR’ BLOCK

With reference to Figure 4.2, the following equations express the output signals as functions of the input signals of the ‘Digital Processor’ block:

$$u_{max} = \max\{u_1, u_2, u_3, u_4, u_5, u_6, u_{6_tie}, u_7, u_8, u_9, u_{10}, u_{11}, u_{11_tie}\} \quad (4.1)$$

$$u_{min} = \min\{u_1, u_2, u_3, u_4, u_5, u_6, u_{6_tie}, u_7, u_8, u_9, u_{10}, u_{11}, u_{11_tie}\} \quad (4.2)$$

where u_{max} is the maximum node voltage magnitude [pu] that appears at the nodes supplied by the aforementioned transformer, u_{min} is similarly the minimum node voltage magnitude [pu] and $u_1, u_2, \dots, u_{11_tie}$ are the voltage magnitudes [pu] at the respective nodes of the MV network.

Equations (4.1) - (4.2) need to be appropriately adjusted for the ‘Digital Processor’ block that is used in the Advanced OLTC Controller model for the HV/MV transformer 0-12. More specifically, the variables inside the brackets at the right side of equations (4.1) and (4.2) are substituted by $\{u_{12}, u_{13}, u_{14}, u_{8_tie}\}$.

Since all modelling and simulation tasks in this study have been carried out using PowerFactory software, it should be noted that the available programming language used for creating models (DSL – Digsilent Simulation Language) does not support algebraic loops. However, for the needs of the proposed control algorithm the new tap position that is calculated inside the ‘AVC Relay’ block must be available until the next clock pulse. Therefore, two separate variables are needed in order to express the current and the new tap position of the OLTC. To achieve this behaviour, a register block is used; the output of the register is the input delayed by one clock pulse. Regarding its operation, the following equations hold:

$$(nntapin_{old})|_N = (nntapin)|_{N-1}, \quad N \in \mathbb{N} \quad (4.3)$$

$$(nntapin)|_0 = 0 \quad (4.4)$$

where $nntapin_{old}$ is the current tap position, $nntapin$ is the new tap position and N is the pulse numbering of the digital clock.

4.2.4.3 ‘AVC RELAY’ BLOCK

The ‘Automatic Voltage Control Relay’ block can be seen as the most crucial part of the Advanced OLTC Controller. Here, the maximum and minimum node voltages are compared with the upper and lower voltage limits, respectively. The decision about the appropriate new tap position of the OLTC is then made, bearing in mind that the OLTC device is installed at the HV side of the HV/MV transformer. Three possible action cases can be distinguished:

- i. When the upper voltage limit is violated for a time period longer than 40 seconds, the new tap position is the current tap position increased by 1.
- ii. When the lower voltage limit is violated for a time period longer than 40 seconds, the new tap position is the current tap position decreased by 1.
- iii. When no voltage limit is violated, the new tap position is the current tap position.

The algorithm will not initiate a tap change action that would lead to a new voltage limit violation. For instance, one should consider the case when the maximum node voltage value exceeds the upper voltage boundary while, at the same time, the minimum node voltage value is close to the lower voltage boundary. Under these circumstances, a tap position increase would, on the one hand, solve the upper voltage boundary violation problem but, on the other hand, would result in an undesirable lower voltage boundary violation. In such cases, the controller refrains from changing the tap position. An appropriate error signal is transmitted instead, until the moment that a corrective action can be finally taken. Additionally, the algorithm ensures that the tap position stays within the maximum and minimum tap position range of the OLTC device.

The operation of control algorithm implemented in the ‘AVC Relay’ block can be better understood with the help of the flow chart of Figure 4.3. The algorithm execution is repeated at every clock pulse. For its implementation, relay and flip-flop units have been used.

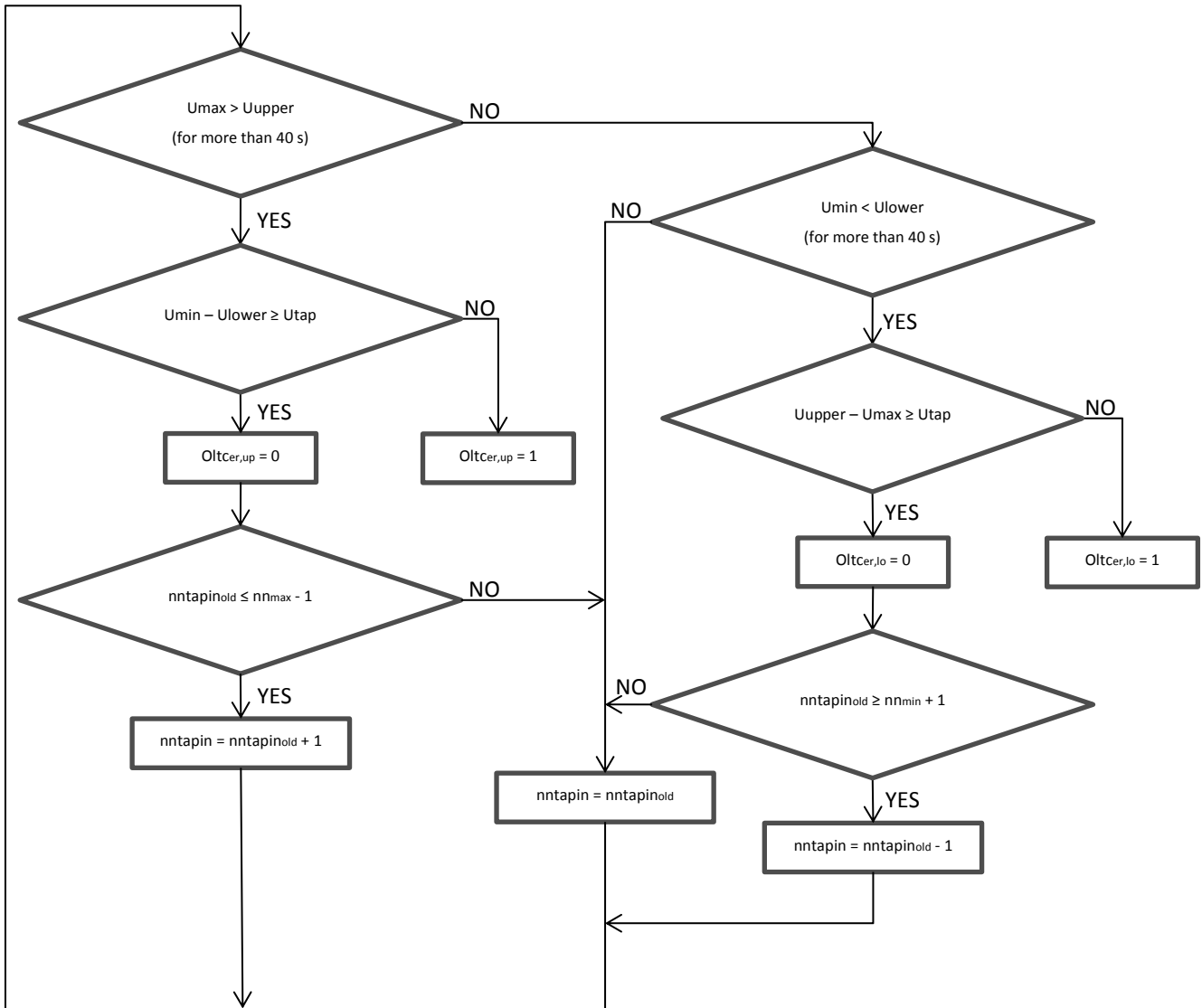


Figure 4.3: Flow chart of the AVC Relay control algorithm

So as to achieve a better understanding of Figure 4.3, Table 4.1 can be used as a legend listing the descriptions of the variables that appear in the flow chart. Parameter values for the 'AVC Relay' block can be found in Table E.1 of APPENDIX E.

Table 4.1: List of variables that appear in Figure 4.3

Variable symbol	Variable description
u_{max}	Maximum node voltage
u_{min}	Minimum node voltage
u_{upper}	Upper voltage boundary
u_{lower}	Lower voltage boundary
u_{tap}	Tap step size
$nntapin$	New tap position
$nntapin_{old}$	Current tap position
nn_{max}	Maximum tap position
nn_{min}	Minimum tap position
$oltcer,up$	Upper voltage boundary violation error signal
$oltcer,lo$	Lower voltage boundary violation error signal

4.2.5 PHILOSOPHY OF THE INTELLIGENT NODE CONTROLLER

4.2.5.1 OVERVIEW

The Intelligent Node Controller represents the second of the two main parts of the broader Coordinated Voltage Controller. In fact, two separate IN controllers have been created, each one managing one of the two INs shown in Figure 4.6. The block diagram of the controller responsible for managing Intelligent Node 8 is depicted in Figure 4.4. A similar controller for Intelligent Node 6 has also been created, but is not shown so as to avoid the repetition of similar text and figures. The difference between the two controllers lies in the input signals, namely the voltage measurement samples and the error signals. In particular, according to Table 4.2, the corresponding controller for Intelligent Node 6 accepts voltage measurement samples from a different group of supervised nodes, while the incoming error signals are only the ones produced by OLTC 0-1.

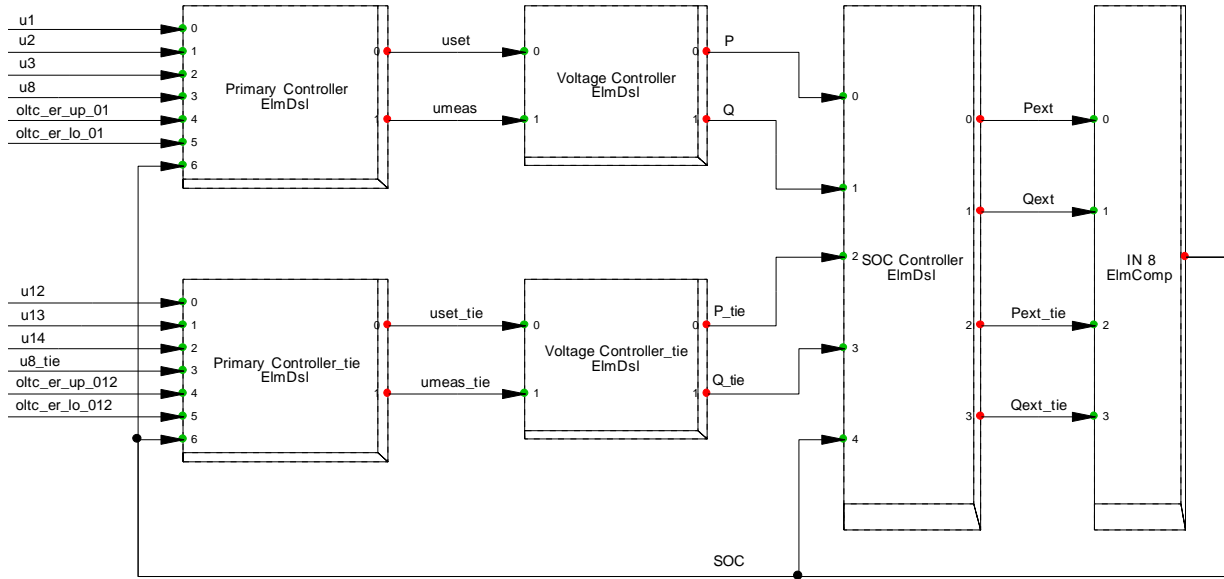


Figure 4.4: Block diagram of the Intelligent Node Controller model (the shown model is for Intelligent Node 8)

According to Figure 4.4, the ‘Primary Controller’ and the ‘Voltage Controller’ blocks exist twice; this is due to the fact that separate blocks are needed to control each one of the two sides of an IN separately. The ‘Primary Controller’ block accepts as inputs the voltage magnitudes of the supervised system nodes, the error signals from the relevant ‘Advanced OLTC Controller’, as well as the SOC level signal from the controlled IN. Each AC side of the IN is considered to supervise all these nodes that are between that IN and the substation secondary bus (following a radial path). With the help of Figure 4.6, Table 4.2 defines the responsibility sector of each device that participates in the coordinated voltage control scheme. It should be noted that all the supervised nodes, except from nodes 1 and 12 (located at the HV/MV substation secondary side), can be characterised as peripheral nodes.

Table 4.2: Responsibility share of each device participating in the coordinated voltage control scheme

Intelligent Node	Intelligent Node side	Supervised nodes	Relevant transformer OLTC
6	6	6, 5, 4, 3, 2, 1	0-1
	6_tie	6_tie, 7, 8, 3, 2, 1	0-1
8	8	8, 3, 2, 1	0-1
	8_tie	8_tie, 14, 13, 12	0-12

Based on the information received, the ‘Primary Controller’ chooses the appropriate operation mode. Each operation mode is characterised by a combination of a measured voltage signal and a voltage set-point signal. Subsequently, this pair of signals is fed to the ‘Voltage Controller’ block, where the IN preliminary active and reactive power set-points are calculated. Before reaching the IN device, the active and reactive power set-point signals are driven through the ‘SOC Controller’ block. There, in case of an imminent violation of SOC limits, the active power set-points are appropriately corrected; the reactive power set-point signals pass through this block without being processed. A detailed description regarding the operation of the ‘Primary Controller’, the ‘Voltage Controller’ and the ‘SOC Controller’ blocks is given in the following paragraphs.

4.2.5.2 ‘PRIMARY CONTROLLER’ BLOCK

This block supports six different IN operation modes, whilst each one of these modes necessitates the creation of different measured voltage and voltage set-point signals; each operation mode deals with a specific problem. Moreover, each one of the AC terminals (sides) of the IN can operate only at one mode at a given moment. Table 4.3 summarises the objective and the resulting function of each offered mode.

Table 4.3: Offered IN operation modes

Operation mode	Trigger by Advanced OLTC Controller	Objective	Resulting IN function
Action mode 1	Yes	Decrease the maximum supervised peripheral node voltage	Active power absorption (BESS charge)
Action mode 2	Yes	Increase the minimum supervised peripheral node voltage	Active power injection (BESS discharge)
Action mode 3	Yes	Enable the relevant OLTC to perform a tap position increase	Active power injection (BESS discharge)
Action mode 4	Yes	Enable the relevant OLTC to perform a tap position decrease	Active power absorption (BESS charge)
Charge mode	No	SOC level increase & voltage profile improvement	Active power absorption (BESS charge)
Discharge mode	No	SOC level decrease & voltage profile improvement	Active power injection (BESS discharge)

The four action modes can be seen as the primary operation modes, since these modes aim at correcting unacceptable voltage variations. On the other hand, the charge and discharge modes can be seen as secondary operation modes; they can even be completely deactivated, if necessary. The resulting active power exchange via the IN influences the voltage magnitudes of the adjacent nodes according to equation (2.4). Next, the conditions under which each operation mode is (de)activated are described:

- Action mode 1 is activated when the maximum peripheral node voltage exceeds the upper voltage boundary and the relevant OLTC is incapable of acting. This mode is deactivated only when the maximum peripheral node voltage falls below the upper voltage boundary minus a specified safety margin voltage.
- Action mode 2 is activated when the minimum peripheral node voltage exceeds the lower voltage boundary and the relevant OLTC is incapable of acting. This mode is deactivated only when the minimum peripheral node voltage rises above the lower voltage boundary plus a specified safety margin voltage.
- Action mode 3 is activated when the voltage at the secondary bus of the relevant HV/MV transformer exceeds the upper voltage boundary and the relevant OLTC is incapable of acting. This mode is deactivated only when the minimum peripheral node voltage becomes higher than lower voltage boundary by one tap step size, thus allowing for the relevant OLTC to act again. Then the tap position is increased by one step and the voltage problem is – indirectly–solved.
- Action mode 4 is activated when the voltage at the secondary bus of the relevant HV/MV transformer exceeds the lower voltage boundary and the relevant OLTC is incapable of acting. This mode is deactivated only when the maximum peripheral node voltage becomes lower than upper voltage boundary by one tap step size, thus allowing for the relevant OLTC to act again. Then the tap position is decreased by one step and the voltage problem is – indirectly–solved.
- Charge mode is activated only when none of the four action modes is active and the minimum peripheral node voltage rises above 1 pu; in all other cases it remains inactive. This ensures that all the other peripheral node voltages are also above 1 pu, meaning that the voltage profile will experience an overall improvement as node voltages decrease towards the nominal value. Since this mode is not automatically triggered, it can be completely deactivated during periods that action modes 1 or 4 need to engage. Charging the battery via action modes 1 or 4 is thus highly prioritised.
- Discharge mode is activated only when none of the four action modes is active and the maximum peripheral node voltage falls below 1 pu; in all other cases it remains inactive. This ensures that all the other peripheral node voltages are also below 1 pu, meaning that the voltage profile will experience an overall improvement, as node voltages increase towards the nominal value. Since this mode is not automatically triggered, it can be completely deactivated during periods that action modes 2 or 3 need to engage. Discharging the battery via action modes 2 or 3 is thus highly prioritised.

According to the analysis of action modes, the IN response heavily depends on whether the voltage violation occurs at a peripheral node or at the substation secondary bus. In the first case, the voltage problem is directly solved. In the second case though, the problem is indirectly solved. The reason for this distinction is the fact that the voltage at the substation secondary bus is solely influenced by the reactive power flow through the transformer. Hence, the control of active power flow via the IN has practically no influence on it. To quantify this influence, one can consider the case where IN 8 absorbs 850 kW from the side connected to Feeder 2 (side 8_tie). This results in a voltage drop of 0.08 pu at node 14, 0.0048 pu at node 13 and a voltage rise of 0.0001 pu at node 12. It is thus made clear that the operation of the IN has no direct influence on the voltage at the substation secondary bus.

Finally, the corresponding measured voltage and voltage set-point signals are given by the following equations :

$$u_{meas} = \begin{cases} relmax, & \text{for action mode 1, action mode 4 or charge mode} \\ relmin, & \text{for action mode 2, action mode 3 or discharge mode} \end{cases} \quad (4.5)$$

where $relmax$ and $relmin$ are the maximum and minimum voltage magnitudes [pu] of the supervised nodes, respectively (excluding the nodes at the HV/MV substations secondary bus). According to Table 4.2, different nodes participate in the calculations depending on which IN and which side of it are chosen.

$$u_{set} = \begin{cases} u_{upper} - u_{margin}, & \text{for action mode 1} \\ u_{lower} + u_{margin}, & \text{for action mode 2} \\ u_{lower} + u_{tap} + u_{margin}, & \text{for action mode 3} \\ u_{upper} - u_{tap} - u_{margin}, & \text{for action mode 4} \\ u_{nom}, & \text{for charge or discharge mode} \end{cases} \quad (4.6)$$

where u_{margin} is the safety margin voltage [pu] and u_{nom} is the nominal voltage magnitude of the MV distribution network [pu]. The values of the parameters in equation (4.6) are given in Table E.1 of APPENDIX E. However, for coherence reasons, the value of u_{margin} is given in Table E.2 and its choice is discussed in paragraph 4.2.5.3.

4.2.5.3 ‘VOLTAGE CONTROLLER’ BLOCK

This block accepts the difference between the measured voltage and the voltage set-point and, by using a filter and a PI controller, creates the active power set-point signal for the IN. For the needs of this study, the reactive power set-point has been deliberately set to zero. According to Table A.6, the lines of the studied MV distribution network have a R'_{LN}/X'_{LN} ratio larger than 1. This implies that regulating the reactive power flow is less efficient in terms of voltage control. Furthermore, system simulations show that when the system node voltages are generally high due to large amounts of reverse active power flow towards the HV/MV transformers, absorbing reactive power would indeed decrease the voltage but at the cost of line overloading; one of the boundary conditions of the control algorithm would thus be violated. The block diagram of the implemented voltage controller is depicted in Figure 4.5.

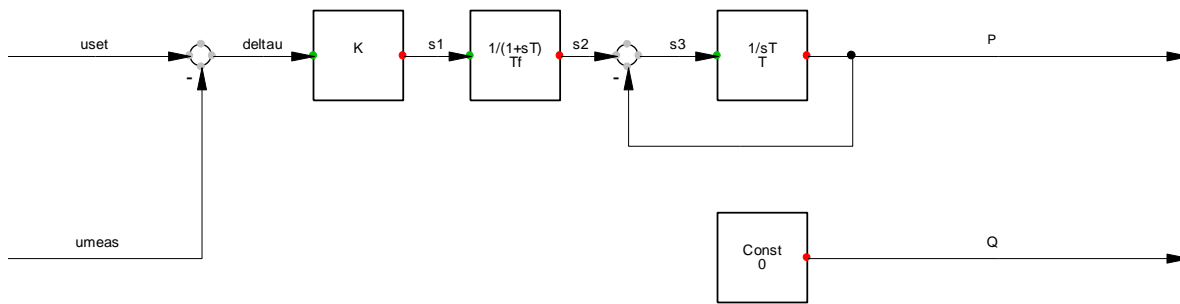


Figure 4.5: Block diagram of the Voltage Controller model

As already stated, each IN operation mode serves a different objective and, for this reason, different transfer functions need to be implemented. More specifically, equation (4.7) expresses in general form the implemented transfer function of the ‘Voltage Controller’ block:

$$P = -\frac{K}{(1 + sT)(1 + sT_f)}(u_{meas} - u_{set}) \quad (4.7)$$

where P is the active power set-point [pu], K is the overall gain, T is the PI controller time constant [s], T_f is the filter time constant [s], u_{meas} is the measured voltage magnitude [pu] and u_{set} is the voltage set-point [pu]. One important aspect is that the expression for the overall gain K is not constant, but depends on the operation mode according to equation (4.8).

$$K = \begin{cases} K_V & , \text{ for action modes } 1 - 4 \\ \frac{K_V}{K_{denom,d} \cdot (100 - SOC)} & , \text{ for discharge mode} \\ \frac{K_V \cdot (100 - SOC)}{K_{denom,c}} & , \text{ for charge mode} \end{cases} \quad (4.8)$$

Where K_V is the gain constant for action modes 1-4, $K_{denom,d}$ and $K_{denom,c}$ are the reciprocal gain constants for discharge and charge modes, respectively, and SOC is the BESS state of charge level [%]. By combining equations (4.5)-(4.8), the final expressions for the transfer function can be reached:

$$P = \begin{cases} -\frac{K_V}{(1 + sT)(1 + sT_f)} [relmax - (u_{upper} - u_{margin})], & \text{for action mode 1} \\ -\frac{K_V}{(1 + sT)(1 + sT_f)} [relmin - (u_{lower} + u_{margin})], & \text{for action mode 2} \\ -\frac{K_V}{(1 + sT)(1 + sT_f)} [relmin - (u_{lower} + u_{tap} + u_{margin})], & \text{for action mode 3} \\ -\frac{K_V}{(1 + sT)(1 + sT_f)} [relmax - (u_{upper} - u_{tap} - u_{margin})], & \text{for action mode 4} \\ -\frac{K_V}{(1 + sT)(1 + sT_f)} \frac{(100 - SOC)}{K_{denom,c}} (relmax - u_{nom}), & \text{for charge mode} \\ -\frac{K_V}{(1 + sT)(1 + sT_f)} \frac{1}{(100 - SOC)} (relmin - u_{nom}), & \text{for discharge mode} \end{cases} \quad (4.9)$$

The values of parameters in equation (4.9) have been chosen after performing extensive simulations of the whole system (see section 4.4) and are given in Table E.2 of APPENDIX E. In an attempt to analyse equation (4.9) and justify the chosen parameter values, the following important aspects are pointed out:

- The reader will notice that for action modes 1 and 2, the voltage difference expressions inside the brackets correspond to the deactivation conditions of the these modes, as described earlier. Hence, during the switch-off, stepwise changes in the active power exchange of the IN ports are prevented. Otherwise, once the IN operation is terminated there is a large possibility that the corrected voltage will exceed the limit again. The ‘Primary Controller’ block would then exhibit an oscillatory behaviour.
- A large value of the safety margin voltage u_{margin} can be beneficial for the IN time response against voltage variations but demands for a larger BESS sizing.
- Regarding the gain constant K_V , a large value enables the IN to quickly correct voltage variations, while also allowing for a better converter utilisation (in terms of power). On the contrary, a small value minimises the risk of controller oscillatory behaviour.
- As far as the applied filter time constant T_f is concerned, a high value can reduce the effect of K_V in oscillatory behaviour. However, the overall IN response to changes in the active power set-point can be considerably slowed down.
- Concerning only the charge and discharge operation modes, the (dis)charge rate of the BESS is a function of the SOC level. When the SOC level is high, the BESS is more eager to discharge and more reluctant to charge. When the SOC level is low, the exact opposite behaviour takes place. Such a choice improves the flexibility of the controller and is the necessary means of performing a full battery cycle within the period of one week. In other words, this extra degree of freedom results in better utilisation of the available battery capacity.
- Again, solely concerning the charge and discharge operation modes, the application of the reciprocal gain factors $K_{denom,c}$ and $K_{denom,d}$ is necessary so as to achieve lower values of the overall gain K ; low gain values are desirable only in these two operation modes.

The choice of the right values for the majority of the above parameters involves a trade-off between potentially positive and negative consequences. In general, the criteria that played a major role in choosing the values of Table E.2 are:

- i. Stable and quick response of the IN Controller (unacceptable voltage variations need to be corrected within 20 seconds, given that the triggering error signal is produced after the OLTC time delay has passed),
- ii. high converter utilisation (in terms of power),
- iii. small BESS capacity and
- iv. high BESS utilisation (in terms of capacity)

4.2.5.4 ‘SOC CONTROLLER’ BLOCK

This block ensures that the SOC level of the BESS remains within specified limits. In order to extend the battery life, once the BESS state of charge reaches the maximum allowed value minus a specified safety margin ($SOC_{max} - SOC_{margin}$) further charging is prevented. Similarly, once the SOC reaches the minimum allowed value plus the safety margin ($SOC_{min} + SOC_{margin}$) further discharging is prevented. The use of the SOC safety margin guarantees that this –globally acting– algorithm will be the first to engage, practically making the –locally acting– algorithm of subsection 3.6.5 a last resort measure (in fact, it shall never be executed). More specifically, the controller is made aware of the BESS overall power exchange by calculating the following expression:

$$P_{check,global} = P + P_{tie} \quad (4.10)$$

where P and P_{tie} are the preliminary active power set-points [pu]. The protection is active when the following logical expressions is true:

$$\left\{ \{P_{check,global} < 0\} \wedge \{SOC \geq SOC_{max} - SOC_{margin}\} \right\} \vee \left\{ \{P_{check,global} > 0\} \wedge \{SOC \leq SOC_{min} + SOC_{margin}\} \right\} \quad (4.11)$$

During the time that the protection is active, the power exchange over the BESS must equal zero. In order to fulfil this condition, the active power set-point values need to be corrected (for both PWM converters) according to (4.12) and (4.13).

$$P_{ext} = \begin{cases} \frac{P - P_{tie}}{2}, & P \cdot P_{tie} < 0 \\ 0, & P \cdot P_{tie} \geq 0 \end{cases} \quad (4.12)$$

$$P_{ext,tie} = \begin{cases} \frac{P_{tie} - P}{2}, & P \cdot P_{tie} < 0 \\ 0, & P \cdot P_{tie} \geq 0 \end{cases} \quad (4.13)$$

where P_{ext} and $P_{ext,tie}$ are the final (corrected) active power set-points [pu]. According to (4.12) and (4.13), if the preliminary active power set-points had different signs, then the corrected set-points keep the same signs but obtain new –fairly contributed– magnitudes. If, on the other hand, the preliminary active power set-points had the same sign or at least one of them was equal to zero, then the corrected set-points become both equal to zero.

4.3 SYSTEM CONDITIONS

4.3.1 OVERVIEW OF THE TEST SYSTEM

The Cigré medium voltage (MV) distribution network benchmark, described in section 3.3, is used as a basis for the test system. Since this network is derived from a physical MV network in southern Germany, its use is expected to provide realistic results, applicable to the majority of the countries situated in the North-European region. Furthermore, details for the MV loads used can be found in section 3.4.

As far as the DRG units are concerned, a number of Photovoltaic Power Plants (PVPPs) and Wind Power Plants (WPPs) have been used. The used model for the PVPP is presented in subsection 3.5.1, while the used WPP model is presented in 3.5.2. The placement of DRG units can be seen in Figure 4.6. More specifically, in the urban part of Feeder 1 (nodes 1-6) no DRG units are connected; this is a rational choice, since in reality no large PVPPs or WPPs are ever expected to be positioned at the city centre. On the contrary, 5 PVPPs and 1 WPP have been placed at the remaining suburban part of Feeder 1 (nodes 7-11). Regarding the rural part of the network, Feeder 2 additionally hosts 2 PVVPs and 1 WPP (nodes 12-14). Although the nominal output power of the DRG units varies depending on the simulated scenario, efforts have been made to constantly keep a balance between the penetration levels of PVPPs and WPPs.

For the needs of the developed voltage control strategy, Intelligent Nodes must also be connected to the system. According to [41], an Intelligent Node should be located at a strategically chosen normally open point (NOP) between two MV feeders. In particular, since the control of active power flow necessitates the use of storage devices, instead of equipping each feeder with its own storage device, it can be advantageous to apply a different solution; namely, to transform the NOP between these feeders into an Intelligent Node. The magenta coloured circles in Figure 4.6 indicate the positions of three NOPs in the test system. Given that the influence of the Intelligent Node is larger nearby, all these three NOPs were initially examined as potential positions for INs. After performing several system simulations, it was observed that the Intelligent Node at node 11 would never operate in one of the primary action modes and therefore it is not needed. Eventually, INs are only placed at nodes 6 and 8. Their sizing, which was also a product of simulations, is as follows:

- Intelligent Node 6 accommodates two PWM converters, each one with a nominal power of 1.2 MVA. The accompanying BESS can handle a nominal active power of 2.4 MW and has a total energy capacity of 3.7 MWh.
- Intelligent Node 8 accommodates two PWM converters, each one with a nominal power of 0.5 MVA. The accompanying BESS can handle a nominal active power of 1.0 MW and has a total energy capacity of 1.4 MWh.

More details regarding the specifications of the batteries can be found in Table D.3 of APPENDIX D.

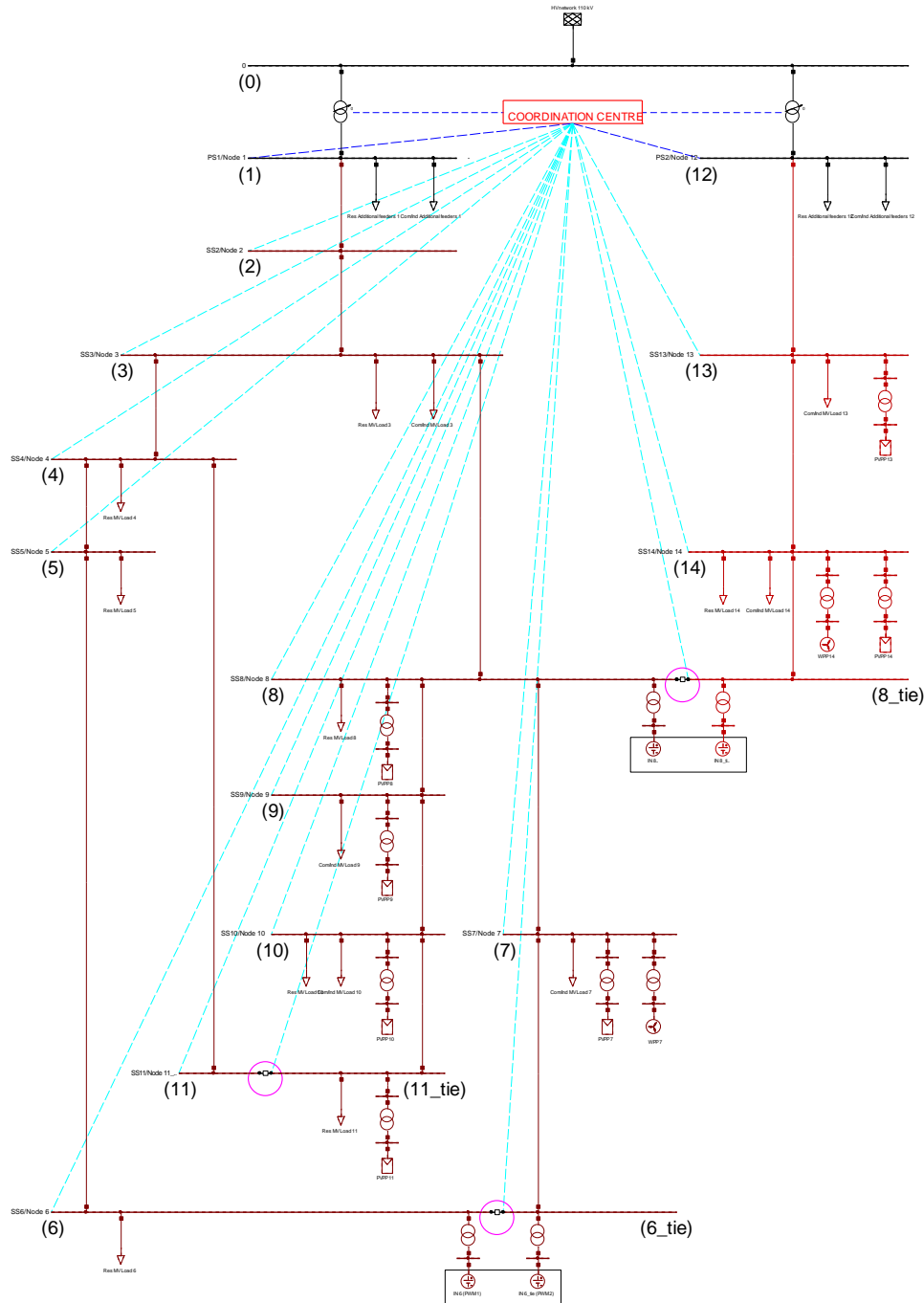


Figure 4.6: Single line diagram of the test system (communication links are denoted with dashed lines)

4.3.2 SIMULATION SCENARIOS

4.3.2.1 SEASONAL VARIATIONS

In order to draw realistic simulation results, this study features a summer / winter seasonal variation in terms of both load consumption and renewable generation. Information on the seasonal variation of MV loads can be found in subsection 3.4.1. The effects of summer / winter variation on the production of PVPPs and WPPs are presented in paragraphs 3.5.1.3 and 3.5.2.2, respectively. In all cases, weekly profiles have been used. Next, the most important aspects of the applied seasonal variation are pointed out.

1) Summer season

A summer week is characterised by relatively low load demand, high PVPP production and considerably reduced WPP production. At a specific summer day though, high production from both DRG types is observed; this creates the condition for studying a 'low load / high generation' extreme situation.

2) Winter season

During a winter week the load demand is higher. Here, a notably low PVPP production is combined with a significantly higher WPP production. At a specific winter day though, low production from both DRG types is observed; this creates the condition for studying a 'high load / low generation' extreme situation. Moreover, several interesting situations of 'low load / high generation' exist.

4.3.2.2 CONTROL STRATEGY VARIATIONS

In order to acquire a better understanding of the underlying phenomena, the simulated scenarios need to vary in terms of the applied voltage control strategy. This is anticipated to give a clearer perception of both the positive and the negative accompanying aspects of each control method, thus facilitating a straightforward comparison among them. The core principle of control strategy variations is the fact that each strategy is tested with the corresponding maximum permissible DRG penetration. In other words, the DRG penetration is not constant throughout the scenario variations but changes as a function of the applied voltage control scheme. This is a direct consequence of the third research question formulated in the current study. In the lines that follow, the three studied voltage control schemes, along with their main attributes, are presented.

1) Base case control scheme

This scheme represents the traditional voltage control method in MV distribution networks that is currently implemented by most DNOs. It is designed for unidirectional power flow and low DRG penetration. Most importantly, as mentioned in section 3.3, the OLTC of the HV/MV transformer offers 32 tap positions, symmetric around zero position; the tap step size is 0.00625 pu. The Basic OLTC Controller, described in subsection 2.5.2, is used. The controller objective is to keep the substation secondary bus voltage constant and equal to a specified set-point voltage, only allowing it to vary within a deadband range. The overall time delay for a tap movement is set to the typical value of 40 seconds [26].

2) Advanced OLTC control scheme

For the needs of this control scheme only the first part of the developed Coordinated Voltage Control concept is used, namely the Advanced OLTC Controller (see subsection 4.2.4). The corresponding operation of the OLTC can be better conceptualised with the help of Figure 4.3. Also here, the OLTC of the HV/MV transformer offers 32 tap positions (symmetric around zero position) and the tap step size is 0.00625 pu. However, one fundamental difference with respect to the Basic OLTC Controller of the previous scheme is the need for communication links between remote locations.

3) Coordinated voltage control scheme

As already indicated by its name, this scheme takes full advantage of the developed Coordinated Voltage Control concept of section 4.2. In addition to the previous scheme, the Intelligent Node Controller is also exploited here (see subsection 4.2.5), given that the newly connected Intelligent Nodes need to be appropriately controlled. The Intelligent Nodes offer additional flexibility in voltage control, by facilitating control of the active power flow. Again, the existence of communication links between remote locations is of fundamental importance.

Last but not least, all the above described control strategies premise the voltage support function provided by the DRG units. In this case, the voltage controller of paragraph 3.5.1.4 is considered. The reactive power that is generated or consumed by the DRG unit converter depends on the value of the PCC voltage; only local voltage measurements are needed. The operating power factor of a power plant is variable and limited to the range:

$$0.95(\text{cap.}) \leq PF \leq 0.95(\text{ind.}) \quad (4.14)$$

Equation (4.14) fully complies with the German standards presented in [39] and is expected to provide realistic results, applicable to the majority of the countries situated in the North-European region.

4.3.2.3 RESULTING SCENARIOS

By combining the 2 seasonal variations of paragraph 4.3.2.1 with the 3 control strategy variations of paragraph 4.3.2.2, one could assume that 6 different simulation scenarios already exist. Nevertheless, as it seemed proper to directly compare control strategies 1 and 2, control strategy 2 is tested twice; once by keeping the same amount of installed DRG as in control strategy 1 and once by increasing the installed DRG capacity to the maximum permissible value. Taking into account the seasonal variations, the Advanced OLTC control scheme practically creates 4 simulation scenarios. In a similar approach, control strategy 3 is also tested twice; once by only considering Intelligent Node 6 and once by considering both Intelligent Nodes 6 and 8. As a result, 10 distinct simulation scenarios are going to be presented and analysed in section 4.4.

4.4 PROOF OF CONCEPT

4.4.1 FOLLOWED APPROACH

According to section 4.2, it is clear that the proposed Coordinated Voltage Controller was not developed at once. Similarly, prior to performing the final system simulation so as to evaluate the performance of the proposed controller, the test system is first simulated under simpler voltage control schemes. Each time, the system is tested with the maximum permissible DRG capacity and the controller performance is evaluated with regard to the evaluation criteria established in subsection 4.4.2. In addition, not only any possible weaknesses that hinder the controller performance are identified –as the first research question suggests–, but also the most interesting observed phenomena are discussed. With reference to the second research question, this has allowed for the development of the proposed final algorithm to be more targeted towards dealing with specific issues. As a result, the performance level of the proposed controller is increased. Finally, with respect to their performance, a direct comparison of all the tested voltage control schemes is made.

At this point, the followed methodology for adjusting the DRG installed capacity needs to be clarified. More precisely, the nominal output power of a PVPP can only be adjusted in steps of 0.1 MW, while in each feeder all the PVPPs must have the same size. As far as a WPP is concerned, the structure of the implemented WPP model provides limited flexibility in adjusting the size of the park (see paragraph 3.5.2.1). Hence, the nominal output power of a WPP can only be adjusted in steps of 2 MW.

4.4.2 EVALUATION CRITERIA

The applied evaluation criteria directly stem from the research questions formulated in subsection 1.4.2. Of course, in order to objectively measure the performance of the proposed coordinated voltage control algorithm all three control schemes of paragraph 4.3.2.2 will be tested against the same criteria. In particular, one primary criterion and three secondary criteria can be distinguished.

Primary evaluation criterion

The primary evaluation criterion is the amount of maximum DRG capacity that can be hosted by the studied MV distribution network, as permitted by the different voltage control schemes. This primary criterion specifically serves the control objective; the larger the installed capacity, the better the performance of the applied control scheme.

Secondary evaluation criteria

In order to examine a variety of aspects related to the behaviour of a control algorithm, three evaluation criteria are considered:

- Voltage Quality Index (*VQI*). The proposed evaluation method quantifies voltage quality, by calculating the deviation of each MV node voltage from the nominal voltage. A small *VQI* value is desirable, since it implies that node voltages are closer to the nominal value. On the other hand, a large *VQI* value implies large and / or long voltage variations. This method was originally developed in [41] for evaluating voltage profiles at a specific moment in time. Here, it is extended by using linearly interpolated 10 min. average values of voltage measurements taken throughout the whole simulation week. The applied index can be mathematically expressed as follows:

$$VQI = \frac{1}{j_{max}} \cdot \sum_{j=0}^{j_{max}} \left\{ \sqrt{\sum_k (u_k(t_j) - 1)^2} \right\} \quad (4.15)$$

where *j* represents the numbering of 10 min. average voltage measurements, *j_{max}* is the total number of 10 min. average measurements in one week (and is equal to 1080), *k* represents the number of MV node and *u_k(t_j)* is the voltage magnitude of node *k* at the time instant that corresponds to the measurement *j*.

- b. Number of tap changes performed in one week (N_{tap}). This criterion refers to the wear and tear that the OLTC mechanisms are subject to. A small value is desirable, since it results in increased lifetime of the relevant mechanical parts, as well as less inspection and maintenance works.
- c. Communication infrastructure requirements. The need for communication infrastructure greatly influences the applicability of a control algorithm in the real world. Establishing communication links between remote locations is already a rather discouraging factor, while a large number of installed sensors and actuators can complicate things even more.

4.4.3 BASE CASE CONTROL SCENARIO

Controller configuration and basic results

Before proceeding to the graphical presentation of produced results and their detailed analysis, it is deemed appropriate first to present several basic results which are directly related to the satisfaction of the applying evaluation criteria. More specifically, information on the maximum installed DRG capacity under the base case control scenario is given in Table 4.4. The number of tap changes performed by the HV/MV transformers OLTCs within the period of one week, as well as the resulting Voltage Quality Index are given in Table 4.5.

Table 4.5 further contains the parameters used for configuring the Basic OLTC Controller. In particular, it is important for the reader to know the values used for the OLTC set-point voltage beforehand, since their influence on the resulting system behaviour is quite large.

Table 4.4: Base case control scenario – maximum hosted DRG capacity

Network section	Nominal output power [MW]		
	PVPPs	WPP	Total DRG
Feeder 1	3.5	4.0	7.5
Feeder 2	4.6	4.0	8.6
Feeders 1 & 2	8.1	8.0	16.1

Table 4.5: Base case control scenario – Basic OLTC Controller parameters and simulation results

Season	HV/MV transformer	OLTC parameter			Simulation results	
		U_{SET}	$U_{DB,L}$	$U_{DB,U}$	N_{tap}	VQI
		[pu]	[pu]	[pu]	[-]	[-]
Summer	0-1	0.99375	0.9875	1.0000	27	0.0346
	0-12	0.98125	0.9750	0.9875	32	
Winter	0-1	1.00625	1.0000	1.0125	37	0.0374
	0-12	0.98125	0.9750	0.9875	30	

According to Table 4.4, the total installed DRG capacity, permitted by the basic voltage control scheme, accounts for up to 16.1 MW. It should be noted that the maximum load demand of the MV distribution system is 40.3 MVA. The maximum permissible DRG capacity is thus 40 % of the peak system load demand. More importantly, this amount is equally split between PVPPs and WPPs, something that is pursued throughout the whole course of this study; constantly keeping an equal mixture of DRG types is expected to create a solid basis for drawing conclusions, later on.

With respect to Table 4.5, one can observe that the OLTC set-point voltage (U_{SET}) is higher for transformer 0-1 than for transformer 0-12. Bearing in mind that Feeder 1 is far more loaded than Feeder 2 (see Table 3.1), a comparatively higher setting for U_{SET} is necessary in order to compensate for the larger voltage drops that would otherwise occur. This value is even higher in winter, since the voltage drop caused by the ‘high load / low generation’ extreme situation must be dealt with. The fact that Feeder 2 is lightly loaded reduces the influence of load demand on voltage drops. Therefore, the corresponding setting for transformer 0-12 is the same both for summer and winter seasons.

Regarding the satisfaction of the secondary evaluation criteria, the following points are valid:

- a. As far as the number of tap changes is concerned, the OLTC of transformer 0-1 operates more frequently in winter, while the one of transformer 0-12 is slightly affected by the seasonal variation. In addition, in summer tap changer 0-1 performs fewer operations than tap changer 0-12; however, this behaviour is reversed during winter. The tap changing behaviour is analysed and explained later on, in the text section that deals with transformer-related aspects.

- b. The VQI is a bit lower in summer than in winter. The larger voltage set-point value for OLTC 0-1 in winter is mainly the reason for this, since the node voltages in Feeder 1 obtain higher values and thus diverge more from the nominal value. This behaviour is further analysed and can be better understood by means of a graphical representation in the text section that deals with voltage-related aspects.
- c. The communication infrastructure needed by the base case control scheme is minimum. All the controllers operate using local control signals, hence eliminating the need for advanced communication infrastructure.

Voltage-related aspects

In this text section a better understanding of the occurring voltage variations can be achieved, since pages from 61 to 63 contain graphical simulation results. More precisely, Figure 4.7 shows the voltage graphs of critical nodes during a summer and a winter week, respectively. The green dashed line indicates the nominal voltage value, while the red dashed lines indicate the upper and lower voltage boundaries. Nodes 1, 6, 7, 11, 12 and 14 are characterised as critical because these are the nodes where the largest voltage variations can occur; in a radial configuration (all NOPs are open), these nodes correspond to the outermost nodes of the system. Furthermore, Figures 4.8 and 4.9 show the voltage profiles as a function of time and distance from substation for a summer and a winter week, respectively. Here, the deep red colour indicates that the voltage approaches the upper boundary, while the deep blue colour indicates that the voltage approaches the lower boundary. Detailed simulation results can be found in Table F.1 of APPENDIX F.

Figure 4.7 indicates that, although voltages at Feeder 1 nodes do not violate the upper voltage boundary during summer, the DRG capacity is limited by the winter season. Since Feeder 1 has a significant load demand, the resulting large voltage drop at node 11 in the evening of day 7 demands for a high voltage set-point setting. This is actually the reason for the limited DRG penetration. Similarly, voltages at Feeder 2 nodes do not reach the upper voltage boundary during winter. Here, the DRG penetration is limited by the large voltage rises occurring during the summer season (see the highlighted area in Figure 4.7 (b)).

Figure 4.8 provides the “big picture” of the system during a summer week. Regarding Feeder 1 (graphs (a), (b) and (c)), during evenings and nights the voltage at all shown nodes is lower than at the substation secondary bus. Days 3 and 4 are exceptions due to the large production from the WPP. During these specific days a voltage rise is observed even at the network branch where no DRG units are connected (see graph (a)). More precisely, nodes 2 and 3 (distance ≤ 7.2 km) indeed experience a voltage rise owing to the reverse active power flow through lines 1-2 and 2-3. On the contrary, nodes 4, 5 and 6 sense a slight voltage drop (distance >7.2 km). In addition, at noon, during high production from PVPPs the voltage at all shown nodes of Feeder 1 is higher than at node 1.

As far as Feeder 2 is concerned (graph (d)), the blue colour at 0.0 km indicates a lower voltage set-point for OLTC 0-12. In addition, since Feeder 2 is lightly loaded, the voltage at nodes 13 and 14 is almost always higher than the one at node 12. The DRG penetration in this feeder is limited by the extreme ‘low load / high generation’ situation occurs at noon of day 3. Strangely enough, this extreme situation does not take place at night, as one would normally expect. Indeed, the load served by both feeders at night is about 2 MW less than at noon. However, the loss of PVPP production at that time accounts for 8.1 MW, thus making a night situation not challenging enough.

Figure 4.9 gives an overview of system node voltages during a winter week. Concerning Feeder 1 (graphs (a), (b) and (c)), voltage drops generally occur due to the large load demand during winter. There are however several exceptions, when large WPP and / or PVPPs production is combined with moderate load demand. The highest voltage values take place at node 7 (see graph (c)), which is not only the most distant node, but also has a WPP installed.

During winter, the extreme ‘high load / low generation’ situation occurs in the afternoon of day 6; similar –less extreme– situations occur almost each afternoon. Under these circumstances, the load peaks are 30 % – 50 % larger when compared to the summer season. Hence, the resulting voltage drops along the feeder branches demand for a very high voltage set-point value of OLTC 0-1.

As already mentioned, several interesting situations of ‘low load / high generation’ also exist. For instance, in the early hours of days 2, 4, 5 and 6, maximum WPP production coincides with minimum load demand in the system (see the highlighted areas in Figure 4.7 (c)). Similarly, at noon of day 1, large production from the PVPPs and the WPP is combined with moderate load demand. Under these circumstances, moderate voltage rises along the feeder branches are observed; but when combined with high the voltage set-point value of OLTC 0-1, the upper voltage boundary is reached. In addition, although the voltage rise along Feeder 2 is larger than the one along the longest branch of Feeder 1 (see graph (c)), the voltage at node 14 is lower than the voltage at node 7. This peculiarity is due to the lower voltage set-point value of OLTC 0-12.

At this point it is important to observe that graphs a, b and c of Figure 4.9 present a large part of orange / red-coloured surface, implying that at many nodes –and during relatively long time periods– the voltage is considerably higher than 1 pu. The choice of a high OLTC voltage set-point is the reason for that. The above remark leads to a VQI value that is 8% higher in winter than in summer.

Last but not least, the above observations reveal two intrinsic weaknesses of the Basic OLTC controller, namely the fixed setting of the OLTC voltage set-point and the ignorance regarding the actual values of the feeder node voltages. Given that the OLTC controller must deal with both voltage rises and drops within the period of one week, a fixed U_{SET} value forces the controller to consider these two opposite voltage issues as one single issue. Since a voltage violation at one of the feeders nodes cannot actually be sensed by the controller, the system operation must be simulated beforehand and choose –by trial and error approach– a U_{SET} value which sufficiently deals with both upper and lower voltage limit violations occurring within a week. The resulting controller performance is poor, something that is confirmed by the presented simulation results. For instance, in Figure 4.7 (c), when the upper voltage limit is reached at node 7 (in the early hours of day 6), the minimum feeder voltage (at node 1) is only 0.02 pu less. This value is considerably lower than 0.06 pu, which is the difference between the upper and the lower voltage boundaries. As a consequence, although the voltage rise along the feeder is still quite small, the DRG capacity cannot be increased because the upper voltage limit would be violated.

The next thing that comes to mind is what would happen if the controller could obtain (or estimate) the magnitudes of node voltages and then appropriately vary the value of U_{SET} . With a view to answering this question, a more sophisticated OLTC control algorithm was implemented and tested. This algorithm, which was originally proposed in [85], has the same objective as the Basic OLTC controller, meaning to keep the transformer secondary bus voltage within the range defined by equation (2.5). The basic difference is that the values of the voltage set-point and the corresponding deadband range are able to vary depending on whether the upper or the lower voltage boundary is violated. It should be noted that the maximum and minimum node voltages were obtained using remote measurements, while in [85] a state estimation technique is used.

Simulation results showed that an increase of the hosted DRG capacity was indeed possible, although it was accompanied by a large increase of the performed tap changes. Nevertheless, the increase of the DRG penetration was not as large as possible, owing to the fact that the third intrinsic weakness of the Basic OLTC controller had not yet been dealt with. This weakness is analysed in the text section that discusses the transformer-related aspects.

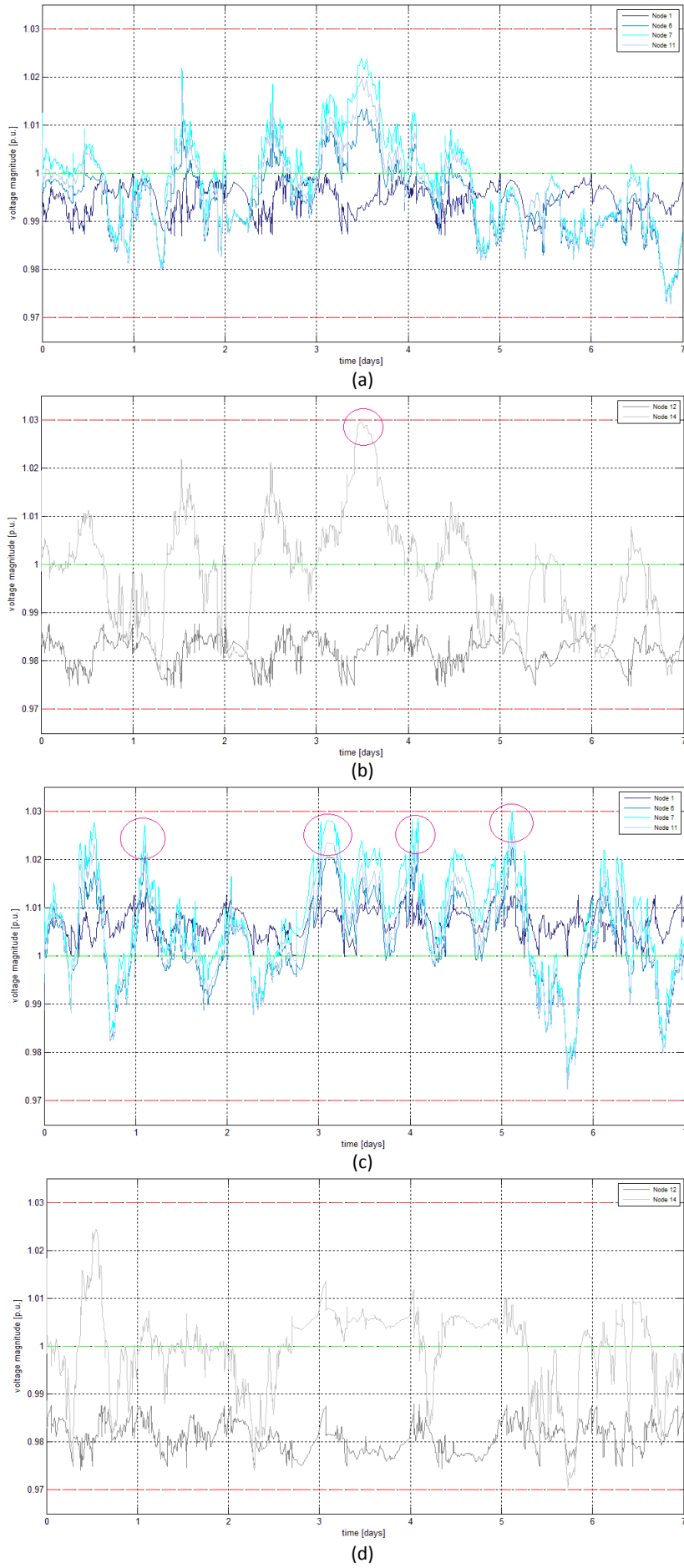


Figure 4.7: Critical nodes voltage for base case control scenario: (a) F1 - summer, (b) F2 – summer, (c) F1 – winter, (d) F2 - winter

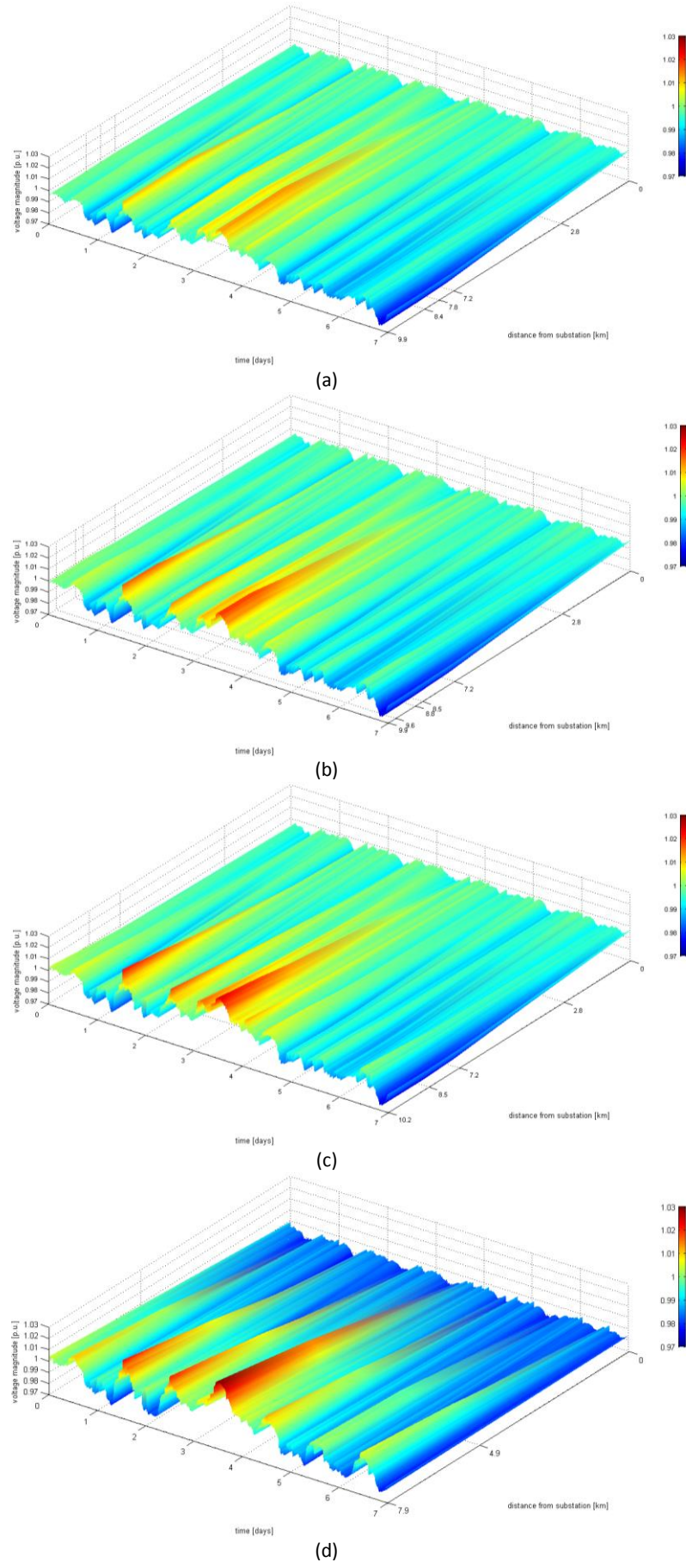


Figure 4.8: Voltage as a function of time and distance from substation, for base case control scenario during summer:
 (a) branch '1-2-3-4-5-6', (b) branch '1-2-3-8-9-10-11', (c) branch '1-2-3-8-7', (d) branch '12-13-14'

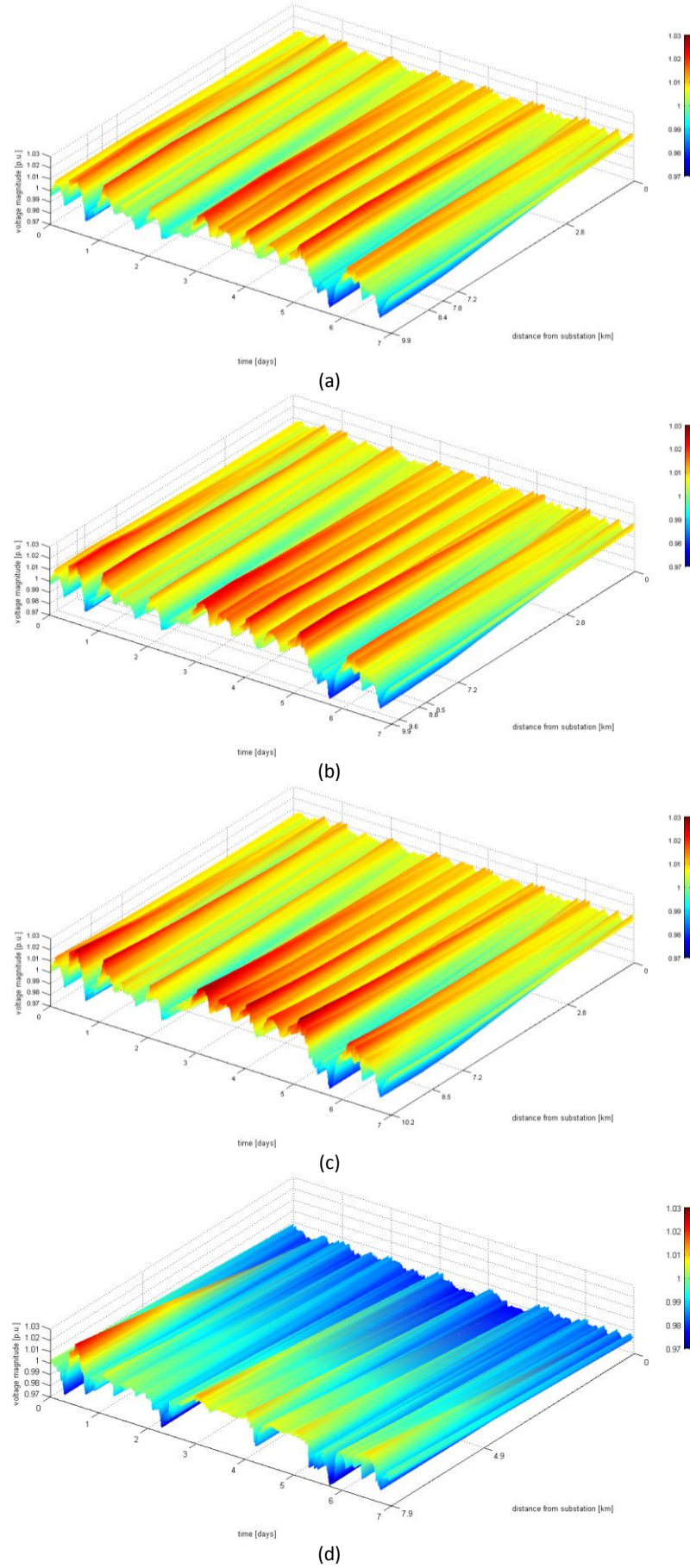


Figure 4.9: Voltage as a function of time and distance from substation, for base case control scenario during winter:
 (a) branch '1-2-3-4-5-6', (b) branch '1-2-3-8-9-10-11', (c) branch '1-2-3-8-7', (d) branch '12-13-14'

Transformer-related aspects

In this text section a better understanding of the Basic OLTC Controller operation can be achieved. Pages from 66 to 69 contain graphical simulation results for transformers 0-1 and 0-12, both for a summer and a winter week. The provided graphs show the transformer secondary bus voltage, the tap position and the power flow (active, reactive and apparent) as functions of time. Regarding the transformer secondary bus voltage graphs, the red dashed lines define the deadband range, while the green dashed line denotes the OLTC voltage set-point. For a better understanding of the analysis that follows, the reader should have in mind that the active and reactive power flows through the HV/MV transformer are not equal to the power flows at the beginning of the served feeder; a large portion of power is consumed by the MV loads at nodes 1 and 12. As already pointed out in subsection 3.4.1, these loads represent a number of other MV feeders that are not modelled in detail. More specifically, during both summer and winter periods the load served by Feeders 1 and 2 is roughly 9 times less than the whole MV network load.

Initially, Figure 4.10 describes the operation of transformer 0-1 during a summer week. The most important thing one must notice here is the obvious pattern between the tap changes (graph (b)) and the reactive power flow through transformer 0-1 (graph (c)); the tap position decreases before noon and increases after midnight. This can be explained by the fact that, in an effort to maintain the transformer secondary bus voltage within the deadband range, the tap changer must compensate for the voltage drop across the transformer reactance. The voltage drop is a direct result of the reactive power demand of nodes 1 – 11, whose main component originates from the load demand; according to Figure 3.5, this is higher at noon and in the afternoon. Especially at noon though, the reactive power consumption of DRG units also increases, owing to high active power production and thus higher PCC voltages. This extra reactive power component accounts for 30 -50 % of the total reactive power flow through transformer 0-1. In particular, at noon of days 2, 3 and 4, when the production of the PVPPs and the WPP is large, the tap position obtains its minimum value ($n_{ntapin} = -3$). This behaviour is clearly undesirable, since the tap changer should not increase the voltages at periods of high DRG production. After midnight, load demand is lower and the tap position returns back to zero. Furthermore, during periods of high renewable generation, the reactive power flow is comparable to the active power flow. This is because part of the loads active power demand is covered by locally produced power, allowing for less active power to be imported from the HV network.

Regarding Figure 4.11 and transformer 0-12, the same remarks as for transformer 0-1 are also valid here. Several differences exist, though. First, the resulting tap positions are generally higher due to the choice of a lower voltage set point. In addition, the performed tap changes are more in this case (32 instead of 27). The reason for this is the higher reactive power flow through transformer 0-12, which means that greater voltage drops at the transformer secondary bus have to be dealt with. As a confirmation, one can look at Figure 4.8 (d) and observe the deep red colouring of nodes 13 and 14. The existence of such high voltages forces the converters of the DRG units to ask for more reactive power. Furthermore, during the extreme ‘low load / high generation’ situation, the drawn reactive power from the HV network even surpasses the active one (see the highlighted areas in Figure 4.11 (c)). This could potentially cause large voltage drops along the HV transmission lines, since according to Table 2.1 a HV transmission line has predominantly inductive impedance.

The same pattern between the reactive power flow and the tap change can be also seen during winter. Figure 4.11 indicates a larger variability of reactive power, leading more to a more frequent operation of OLTC 0-1 with respect to the summer season ($N_{tap} = 37$). The increased reactive power variability comes as a result of the winter load demand curve. According to Figure 3.5, the load demand is generally higher during winter and therefore its impact on power flow is increased. Especially in the evenings, when the load demand peaks occur, the resulting voltage drops over the transformer reactance force the tap position towards more negative values. The exact opposite behaviour takes place at nights, with the tap position obtaining more positive values. In general, the tap position ranges from -2 down to -5, as a result of choosing a high voltage set-point value.

On the contrary, since Feeder 2 is less loaded, it is also less influenced by the large load variability during winter. Thus, as it can be seen in Table 4.5, the difference in the number of tap changes between summer and winter seasons is negligible. Finally, both Figure 4.12 and Figure 4.13 indicate that the active power flow is dominant during winter. This is a combined result of lower local active power production from DRG and higher load demand, in comparison with the summer season.

Last but not least, the above observations reveal another intrinsic weakness of the Basic OLTC Controller. This weakness is of fundamental importance, since it originates from the controller objective. More precisely, the Basic OLTC Controller acts so as to control the HV/MV transformer secondary bus voltage (by keeping it within a predefined deadband), although this voltage is not necessarily the problematic one. In addition, the controller action is solely determined by the reactive power flow through the transformer. These two aspects enable the controller to perform well in a system with no DRG units. In this case, a voltage drop across the transformer reactance due to the load reactive demand is indeed an indication of low voltages along the feeders. A tap position decrease would thus be the appropriate corrective action.

On the contrary, the controller behaviour is significantly deteriorated in a system with DRG units. Since a HV/MV substation serves a number of MV feeders, the voltage drop over the transformer reactance could be quite large. In the case that one of the feeders incorporates DRG units, a decrease of the tap position during periods of high renewable production would

boost the –already high– node voltages; this is demonstrated in Figure 4.7 (c). What is more, when DRG units are equipped with voltage control function, a significant part of reactive power demand may be due to the PWM converters of the DRG units. Hence, a voltage drop across the transformer reactance not only does not indicate low node voltages along the feeder, but could be combined with even higher voltages. Consequently, a tap position decrease would create even worse voltage problems. This valid for all voltage control methods presented in paragraph 2.5.3.2. However, the results for a $Q(U)$ method are expected to be worse. That is to say, a high reactive power demand causes the OLTC to decrease the tap position and thus increase the node voltages, while a $Q(U)$ control method further increases the reactive power demand in case of increased node voltages. This behaviour indicates the existence of a positive feedback loop.

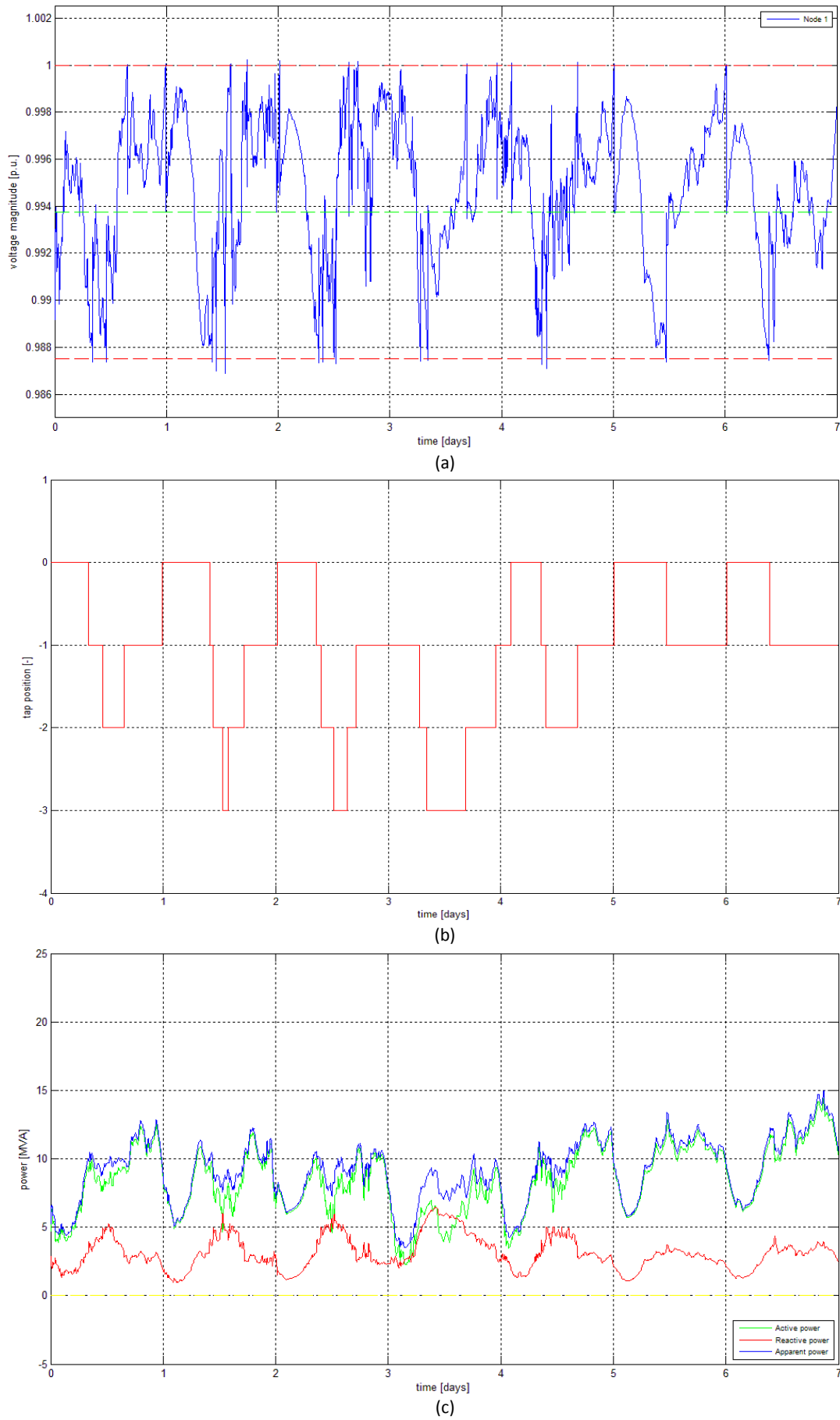


Figure 4.10: Transformer 0-1 results for base case control scenario during summer: (a) secondary bus voltage, (b) tap position, (c) power

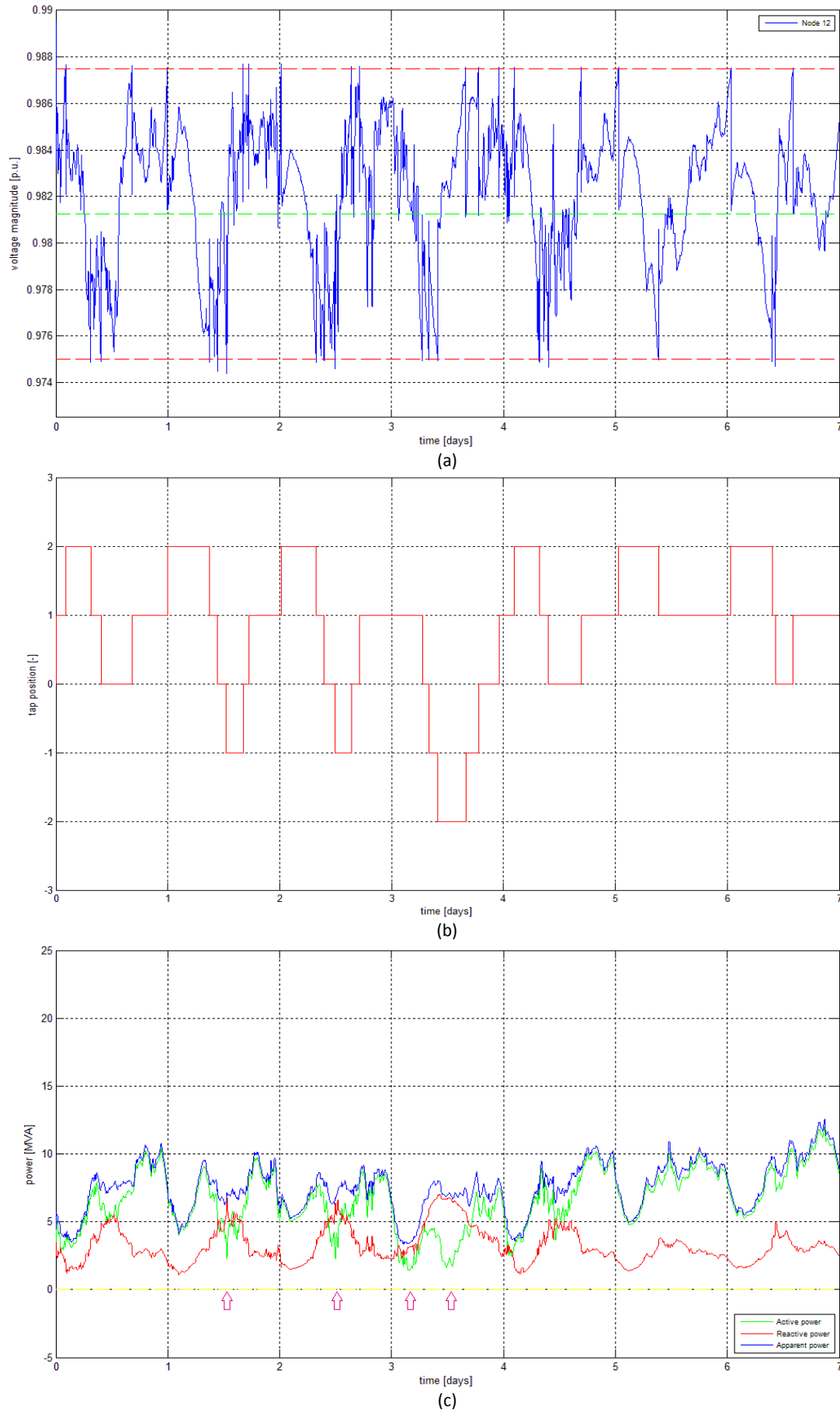


Figure 4.11: Transformer 0-12 results for base case control scenario during summer: (a) secondary bus voltage, (b) tap position, (c) power

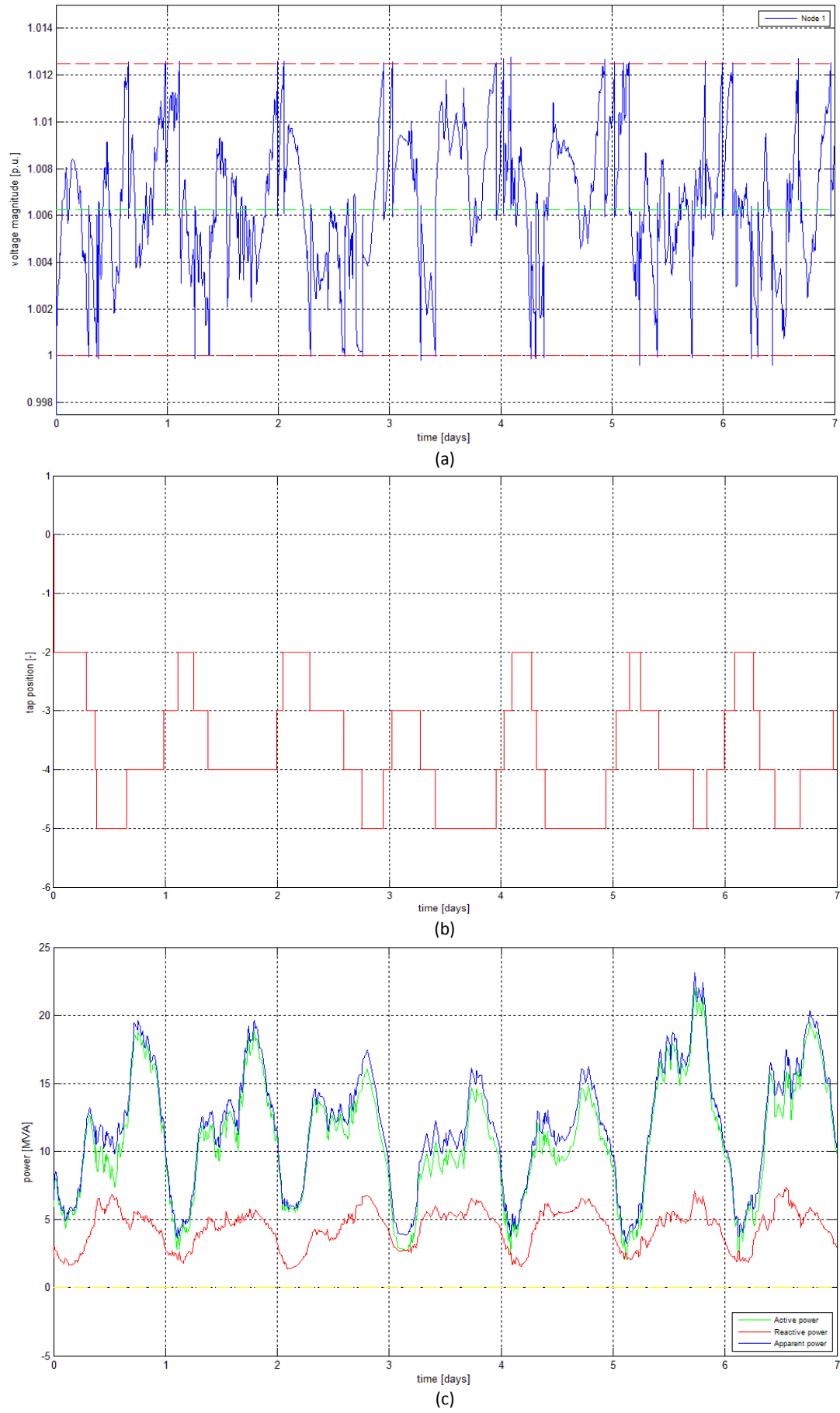


Figure 4.12: Transformer 0-1 results for base case control scenario during winter: (a) secondary bus voltage, (b) tap position, (c) power

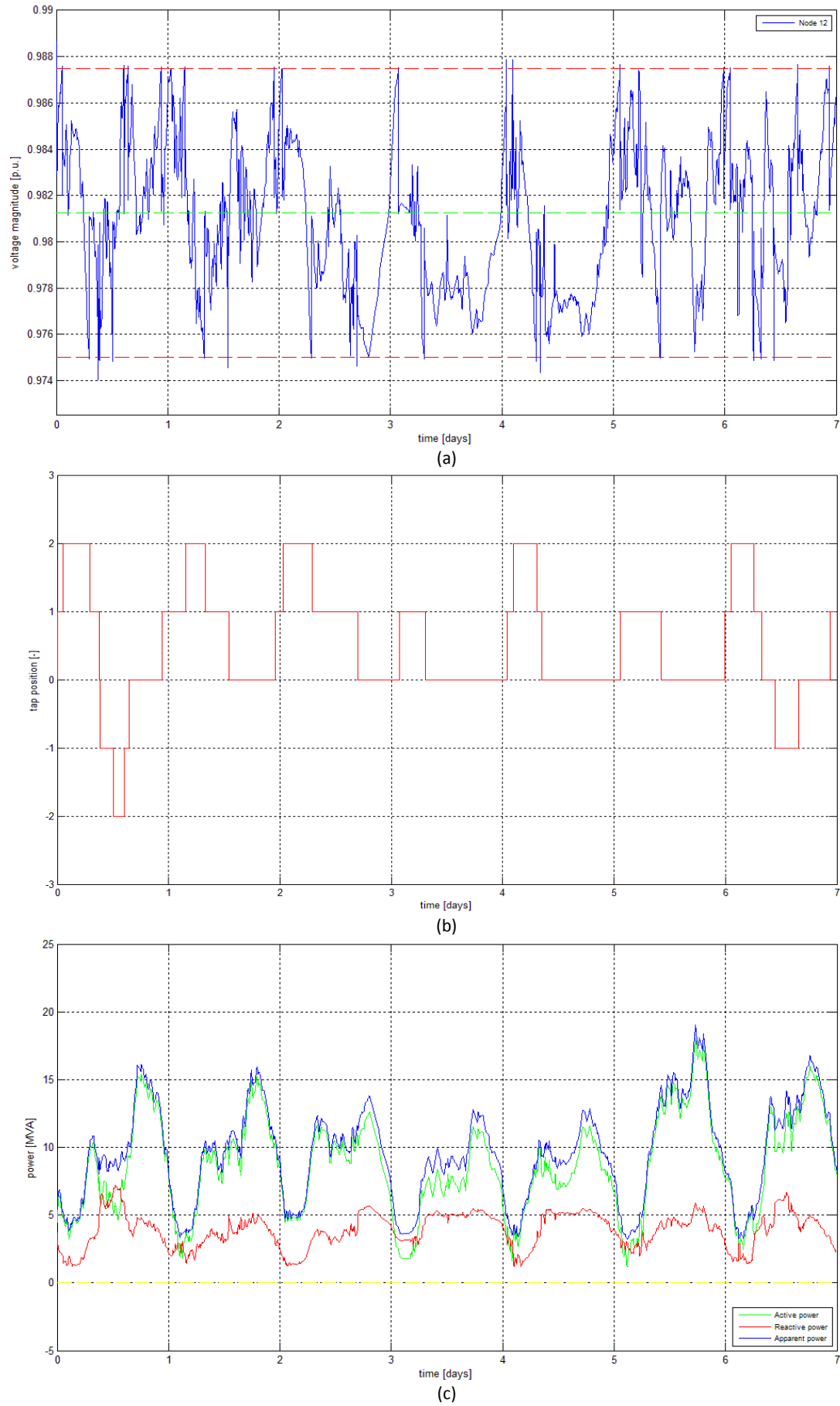


Figure 4.13: Transformer 0-12 results for base case control scenario during winter: (a) secondary bus voltage, (b) tap position, (c) power

4.4.4 ADVANCED OLTC CONTROL SCENARIO

4.4.4.1 SAME DRG CAPACITY

Before proceeding to the analysis of the advanced OLTC control scheme in paragraph 4.4.4.2, it is deemed useful to directly compare it with the base case control scheme. To accomplish this, the test system was simulated using the same amount of installed DRG capacity, according to Table 4.4. The number of tap changes performed by the HV/MV transformers OLTCs within the period of one week, as well as the resulting Voltage Quality Index are given in Table 4.6. The percentage differences between the two control schemes are given inside the brackets.

Table 4.6: Advanced OLTC control scenario (unchanged hosted DRG capacity) – simulation results

Season	HV/MV transformer	N_{tap}	VQI
		[\cdot]	[\cdot]
Summer	0-1	1 (-96%)	0.0361
	0-12	0 (-100%)	(+4%)
Winter	0-1	7 (-81%)	0.0334
	0-12	1 (-97%)	(-10%)

Regarding the frequency of performed tap movements, one can notice that in fact very few tap changes take place. This is because, according to the algorithm of the Advanced OLTC Controller (see Figure 4.3), a tap change is initiated only if the upper or lower voltage boundary is violated. The controller is thus insensitive to less significant voltage variations. Since the DRG penetration in the MV network is still low, during a summer week OLTC 0-1 operates only once and OLTC 0-12 does not operate at all. The slight increase of the resulting VQI seems reasonable enough, given that the tap changer barely intervenes. During winter, OLTC 0-1 performs a few tap changes, mainly caused by the larger load demand and the resulting voltage drops. In this case, the VQI is improved.

Based on the above, one can conclude that advanced OLTC control scheme indeed succeeds in decreasing the performed tap changes and thus the wear and tear of the tap changer. Nevertheless, when the network does not experience significant voltage variations that would cause the voltage limits to be violated, the resulting scarce operation of the tap changers leaves the voltages intact. The fact that corrective actions are seldom taken is something that does not favour voltage quality. In the next paragraph, the same control scheme will be tested under more severe conditions, allowing us to draw more conclusions. For consistency reasons, the controller communication aspects also discussed there.

4.4.4.2 MAXIMUM HOSTED DRG CAPACITY

Basic results

Prior to the graphical presentation of produced results and their detailed analysis, several basic results which are directly related to the satisfaction of the applying evaluation criteria are presented. More specifically, information on the maximum installed DRG capacity under the advanced OLTC control scenario is given in Table 4.7. The number of tap changes performed by the HV/MV transformers OLTCs within the period of one week, as well as the resulting Voltage Quality Index are given in Table 4.8.

Table 4.7: Advanced OLTC control scenario – maximum hosted DRG capacity

Network section	Nominal output power [MW]		
	PVPPs	WPP	Total DRG
Feeder 1	3.5	8.0	11.5
Feeder 2	6.2	4.0	10.2
Feeders 1 & 2	9.7	12.0	21.7

Table 4.8: Advanced OLTC control scenario – simulation results

Season	HV/MV transformer	N_{tap}	VQI
		[\cdot]	[\cdot]
Summer	0-1	5	0.0291
	0-12	3	
Winter	0-1	20	0.0353
	0-12	2	

According to Table 4.7, the total installed DRG capacity, permitted by the advanced OLTC control scheme, accounts for up to 21.7 MW. This equals to 54 % of the peak system load demand and can be translated to almost 35 % increase when compared to the maximum installed DRG capacity under the base case control scenario. The PVPPs account for almost 45 % of the total amount, while the WPPs for the rest 55 %. Feeder 1 holds 53 % of the total DRG capacity, mainly owing to the large wind park at node 7. On the other hand, the renewable capacity of Feeder 2 is mainly due to photovoltaics.

Regarding the satisfaction of the secondary evaluation criteria, the following hold:

- a. The number of tap changes is significantly smaller compared to the base case control scenario. The OLTC of transformer 0-1 operates more frequently in winter, while OLTC 0-12 is slightly affected by the seasonal variation. In general, tap changer 0-1 performs more operations than tap changer 0-12. The tap changing behaviour is analysed and explained later on, with the help of the relevant simulation graphs.
- b. When compared to the corresponding values for the base case control scenario, the *VQI* for the advanced OLTC control scenario is lower during summer and slightly lower winter. This aspect is further analysed and can be better understood by means of voltage graphs in the text section that deals with voltage-related aspects.
- c. The communication infrastructure needed by the controller is quite large. More specifically, in [33] it is proved that the maximum voltage can happen only at a DRG connecting bus or at the substation bus, provided that the R'_{LN}/X'_{LN} ratio is constant along the whole feeder. Additionally, minimum voltage points can occur only at the end of the feeder, as well as in between any DRG connecting buses. Based on the above, the controller does not necessitate the existence of voltage sensors at nodes 4 and 5 (and of course neither at nodes 6_tie, 8_tie and 11_tie). Overall, the Advanced OLTC Controller needs 10 communication links in order for the 10 voltage sensors to communicate with the coordination centre.

The basic simulation results for this control scenario indicate a significant increase of the DRG penetration, along with a reduction of tap changing operations and an improvement of the voltage quality in the network. This is due to the different philosophy of the OLTC controller. In particular, only the necessary tap changes are performed, since the controller no more tries to keep the substation secondary bus voltage within the deadband limits. Additionally, the reactive power flow through the HV/MV transformer no more negatively influences the OLTC operation.

Voltage-related aspects

In this text section a better understanding of the occurring voltage variations can be achieved, since the upper-positioned graphs of Figures 4.14 – 4.17 show the voltage of critical nodes as a function of time and the middle-positioned graphs show the tap changing sequence of the respective OLTCs. Each figure describes a different combination of MV feeder and season. Detailed simulation results can be found in Table F.2 of APPENDIX F.

Figure 4.14 refers to Feeder 1 during a summer week. A noticeable voltage rise occurs in the middle of the week, when the –large– WPP and the PVPPs reach their nominal output power; the extreme ‘low load / high generation’ situation actually takes place. At that instant, both the maximum and minimum node voltages seem to approach the upper and lower voltage boundaries, respectively (the moderate load demand forces the voltage at node 1 to go down). Hence, it is this exact situation that limits the DRG capacity of Feeder 1 under the advanced OLTC control scenario. The fact that two consecutive, yet opposite, tap changes take place within approximately 1 hour gives an idea of how severe this situation is. Furthermore, with the exception the extreme ‘low load / high generation’ situation, node voltages generally stay close to the nominal value. This results in an improved *VQI* of the system during summer.

Figure 4.15 also shows large voltage differences, mainly as a result of high active power production from PVPPs (Feeder 2 hosts a large capacity of photovoltaics). Moreover, the load demand is also quite large at noon; the total reactive power demand is what causes u_1 to drop. Also here, the DRG capacity of Feeder 2 is limited during the extreme ‘low load / high generation’ situation in day 4. During this extreme situation, two consecutive, yet opposite, tap changes take place within approximately 20 minutes.

Figure 4.16 gives an overview of Feeder 1 node voltages during a winter week. The high variability and peak values of load consumption, in combination with the high WPP production, indicate that the upper and lower voltage boundaries are reached more often. On the one hand, there are several moderate ‘low load / high generation’ situations which result in tap position increases. On the other hand, the extreme ‘high load / low generation’ situation results in consecutive tap position decreases. The fact that several large voltage drops must be dealt with is also indicated by the more negative tap positions of OLTC 0-1. The above described behaviour results in more tap changes than in summer. Although none of these voltage variations is limiting for the DRG capacity, the *VQI* of the system is higher during winter.

Regarding Feeder 2, Figure 4.17 suggests that several unremarkable voltage differences occur during high DRG production periods. Since this feeder has a larger share of PVPPs, the maximum voltage difference occurs at noon of day 1. This also when the only two, in total, tap changes are performed.

Last but not least, the above observations reveal one weaknesses of the Advanced OLTC Controller, namely the inability to deal with situations that involve large differences between the maximum and minimum node voltages. More precisely,

when one of the voltage boundaries is breached, while at the same moment the maximum and minimum node voltages of the controlled network part differ by more than 5.375 % of the nominal value, the operation of the OLTC is hindered. This limiting value is defined as the difference between the upper (1.03 pu) and lower (0.97 pu) voltage boundaries minus the tap step size (0.0625 pu). In situations like this, although a possible tap position increase (decrease) from the OLTC would momentarily fix the upper (lower) voltage boundary violation, it would simultaneously create a lower (upper) voltage boundary violation. It is needless to say that the tap position would start oscillating until the node voltages obtain less extreme values.

The solution to the previously described issue is to reduce the voltage difference down to manageable –by the OLTC– levels, by altering the power flow at the problematic network part. This what the Coordinated Voltage Controller does in subsection 4.4.5, where the ability to control the power flow using Intelligent Nodes is taken advantage of.

Transformer-related aspects

In this text part, several interesting aspects related to the power flow through the HV/MV transformers are discussed. For this reason, the lower-positioned graphs of Figures 4.14 – 4.17 are of interest.

First, an observation which is valid for all four presented graphs is the fact that the reactive power imports from the HV network are generally increased. This is due to the larger installed capacity of DRG (also participating in voltage control), which is made possible by the application of the Advanced OLTC Controller. Reasonably enough, the reactive power flow through the HV/MV transformers reaches its higher values during periods of increased DRG production. The occurring peak value (around 8 MVar) is the same for both transformers and is observed both in summer and winter.

Second, the ratio of the imported active power over the imported reactive power is generally lower when compared to the base case control scenario. There are even several interesting situations of moderate load demand and high renewable generation which result in a ratio lower than unity.

Another important observation is that the active power flow through transformer 0-1 can even be reversed at night. The reason is that the large WPP at node 7 is able to reach its nominal output, while at the same time the night load demand is minimal. According to the highlighted areas in Figure 4.14 (c) and Figure 4.16 (c), this phenomenon takes place not only in winter, but in summer as well.

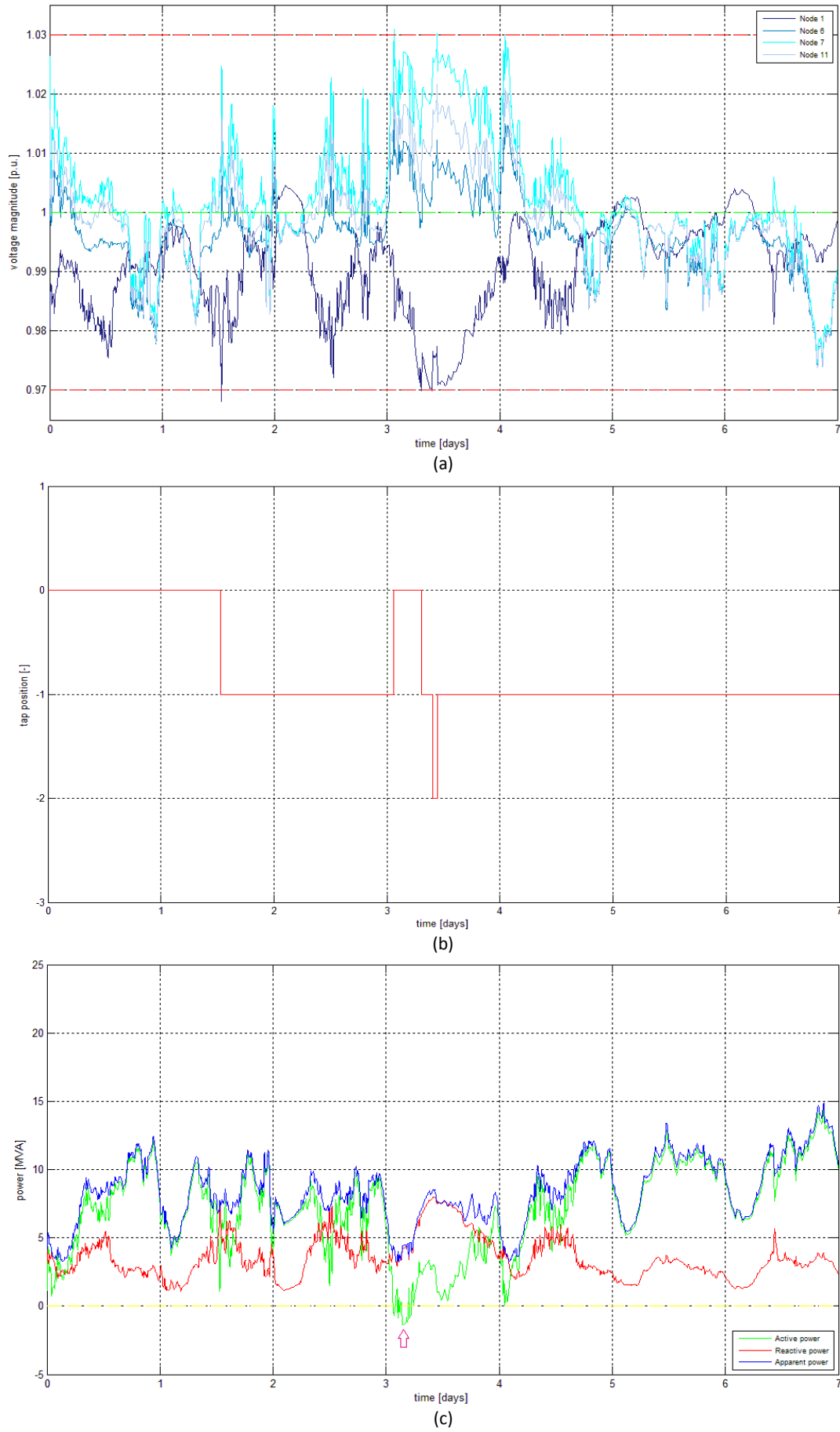


Figure 4.14: Transformer 0-1 results, for advanced OLTC control scenario during summer:
 (a) critical nodes voltage, (b) tap position, (c) power

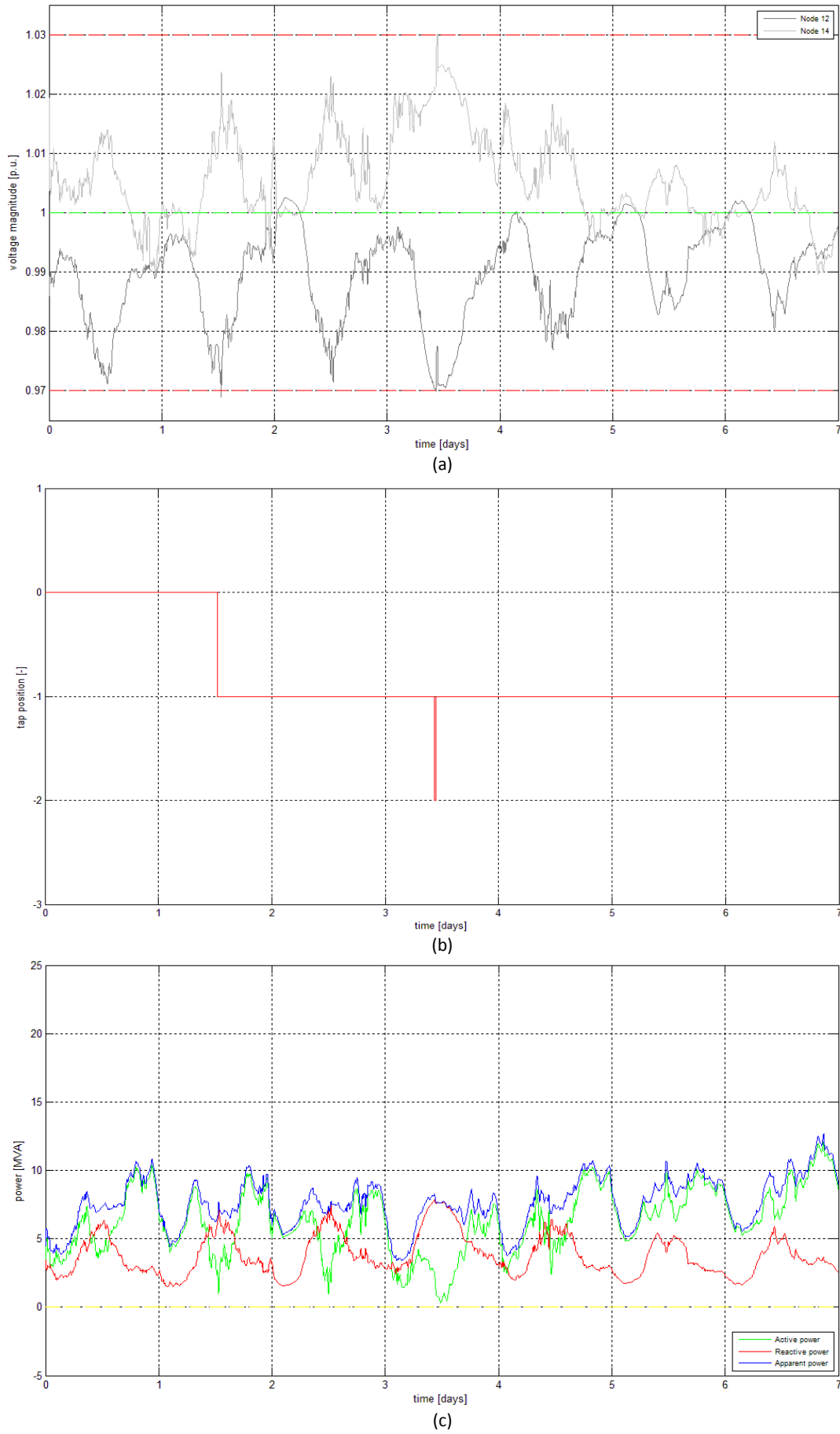


Figure 4.15: Transformer 0-12 results, for advanced OLTC control scenario during summer:
 (a) critical nodes voltage, (b) tap position, (c) power

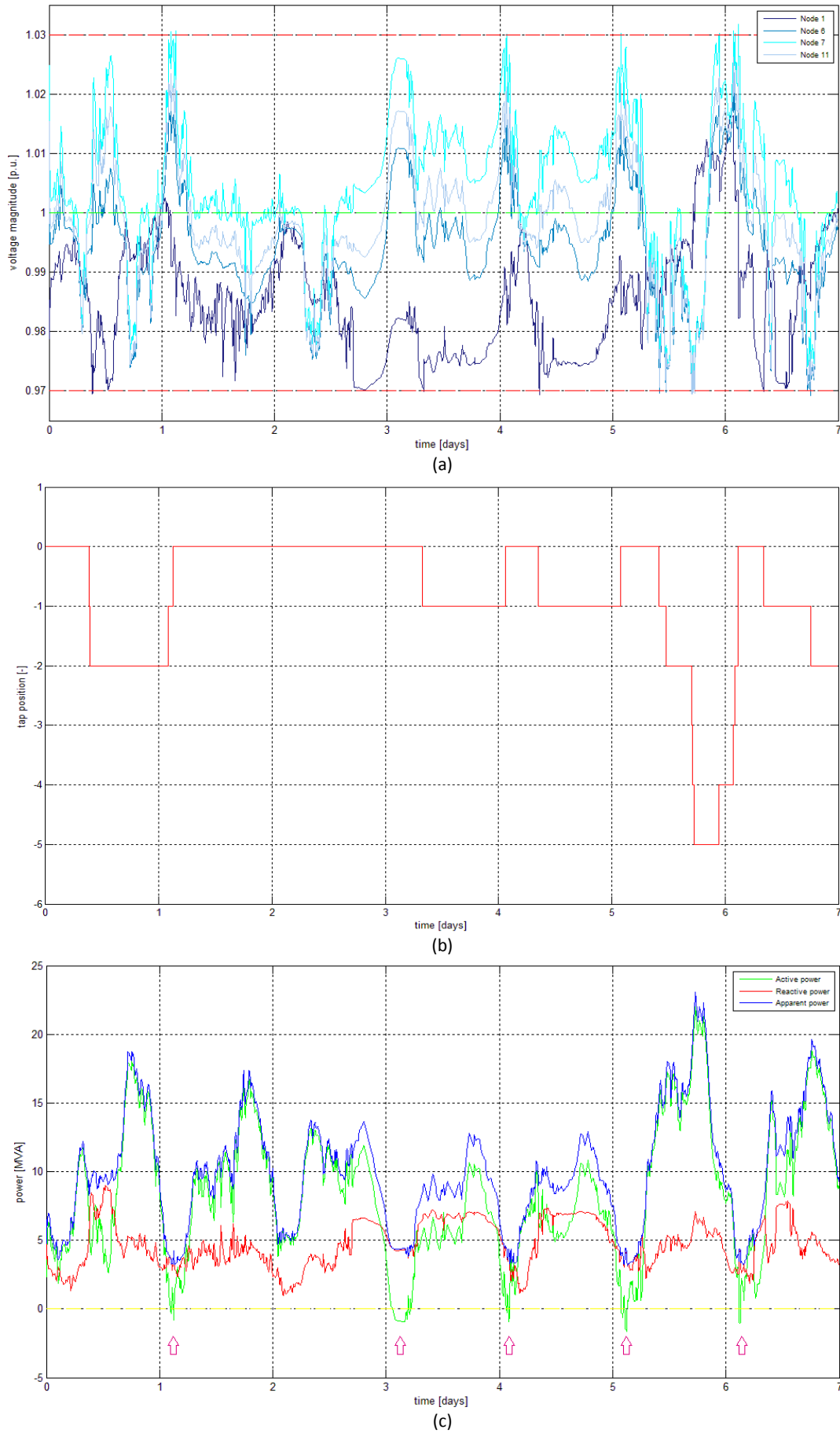


Figure 4.16: Transformer 0-1 results, for advanced OLTC control scenario during winter:
 (a) critical nodes voltage, (b) tap position, (c) power

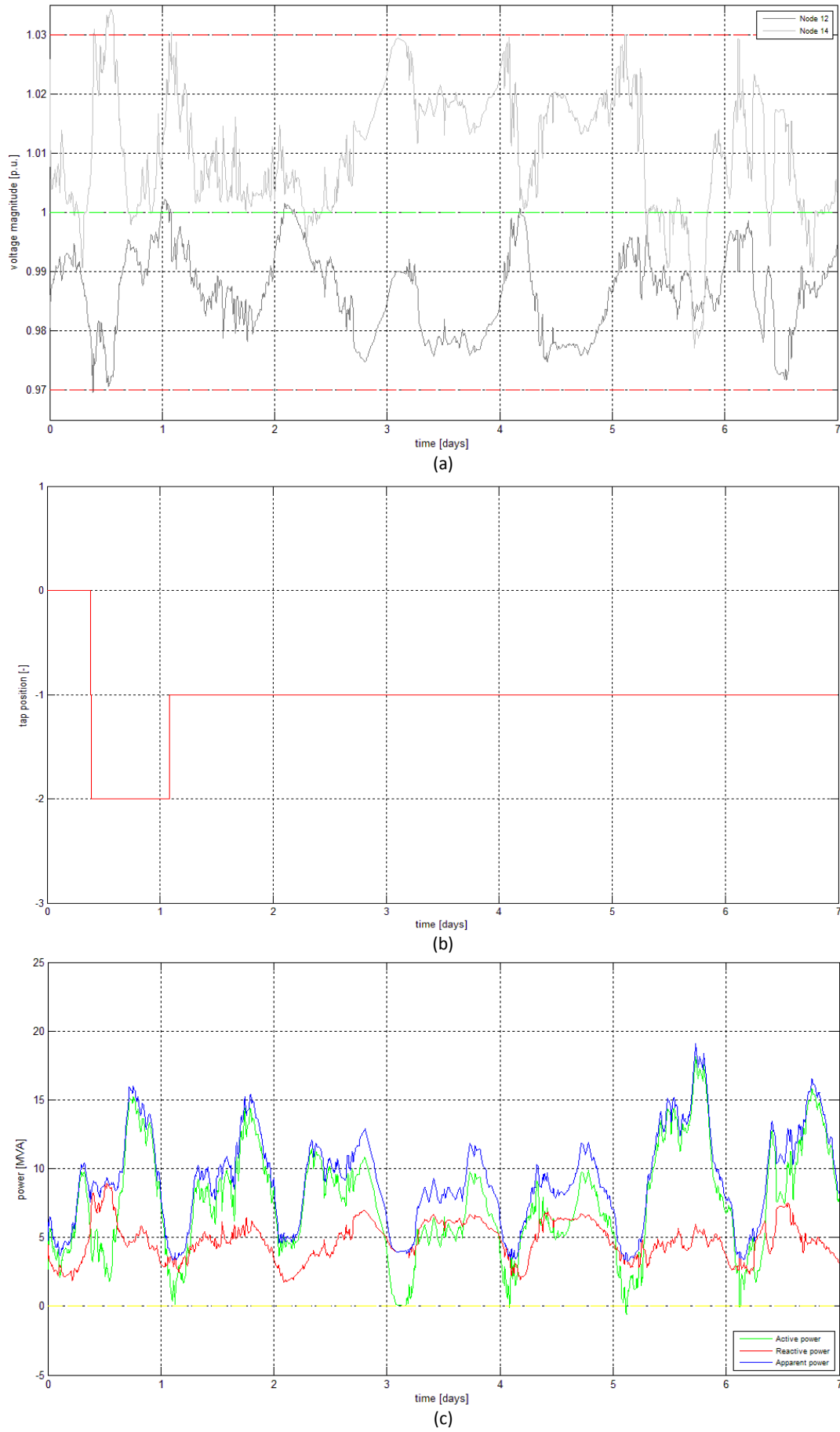


Figure 4.17: Transformer 0-12 results, for advanced OLTC control scenario during winter:
 (a) critical nodes voltage, (b) tap position, (c) power

4.4.5 COORDINATED VOLTAGE CONTROL SCENARIO

4.4.5.1 IN 6

Basic results

This paragraph describes the most important aspects of the coordinated voltage control scenario, considering only Intelligent Node 6. Information on the maximum installed DRG capacity under the coordinated voltage control scenario with IN 6 is given in Table 4.9. The number of tap changes performed by the HV/MV transformers OLTCs within the period of one week, as well as the resulting Voltage Quality Index are given in Table 4.10. Given that the installation of IN 6 does not influence the behaviour of Feeder 2 and OLTC 0-12, no changes are expected in the corresponding table cells.

Table 4.9: Coordinated voltage control scenario (IN 6) – maximum hosted DRG capacity

Network section	Nominal output power [MW]		
	PVPPs	WPP	Total DRG
Feeder 1	5.0	8.0	13.0
Feeder 2	6.2	4.0	10.2
Feeders 1 & 2	11.2	12.0	23.2

Table 4.10: Coordinated voltage control scenario (IN 6) – simulation results

Season	HV/MV transformer	N_{tap}	VQI
		[-]	[-]
Summer	0-1	9	0.0297
	0-12	3	
Winter	0-1	20	0.0388
	0-12	2	

According to Table 4.9, the total installed DRG capacity, permitted by the advanced OLTC control scheme, accounts for up to 23.2 MW (equals to 58 % of the peak system load demand). This is translated to 44 % increase when compared to the base case control scenario and 7 % increase when compared to the advanced OLTC control scenario. It should be noted that for larger DRG capacities, the loading of line 3-8 is exceeded before the node voltages experience values larger than the upper voltage boundary (1.03 pu). The PVPPs account for approximately 48 % of the total amount, while the WPPs for the rest 52 %. Feeder 1 holds 56 % of the total DRG capacity and its share has increased since the operation of IN 6 allowed for increasing the installed power of PVPPs (nodes 7 - 11) by 1.5 MW, in total. On the other hand, the renewable capacity of Feeder 2 remains the same.

Regarding the satisfaction of the secondary evaluation criteria, the following hold:

- An increase of the number of tap changes performed by OLTC 0-1 during a summer week is observed when compared to the advanced OLTC control scenario. This is normal, since Feeder 1 hosts an increased DRG capacity. Apart from that, one should bear in mind that it was during summer when the DRG capacity of Feeder 1 under the advanced OLTC control scenario was limited.
- When compared to the corresponding values for the advanced OLTC control scenario, the VQI for the coordinated voltage control scenario (with IN 6) is higher during winter, but only slightly higher during summer. This behaviour is explained later on in this paragraph.
- The communication infrastructure needed by the controller is considerably large. The presence of IN 6 can potentially result in a –controlled– meshed operation of Feeder 1. Based on the above, the controller necessitates the existence of voltage sensors at nodes 4, 5 and 6_tie. A SOC level measurement device, as well as active and reactive power actuators are accommodated by IN 6. Overall, the current implementation of the Coordinated Voltage Controller needs 13 communication links in order for the 13 voltage sensors, 1 SOC sensor and 2 actuators to communicate with the coordination centre.

Next, the operation of IN 6 is analysed with respect to the simulation results. The simulation results produced during a summer week are of the greatest interest, since action modes 1 and 4 (and of course the necessary discharge mode) are demonstrated (see paragraph 4.2.5.2). On the contrary, only the charge and discharge modes are featured in a winter week. What is interesting though, is that the operation of the ‘SOC Controller’ block, presented in paragraph 4.2.5.4, can be demonstrated. In the text sections that follow the most interesting results are presented and analysed.

Simulated cases

According to Figure 4.18 (a), there are four time periods during which an action mode is energised; actions cases are named with reference to the operation mode that is each time used (see Table 4.3). During the remaining summer week, IN 6 either operates in charge mode, or remains completely idle. Next, with a view to Figure 4.19, these four action cases are analysed. One should bear in mind that the dashed, magenta coloured lines in the graphs of Figure 4.19 show what the voltage of the problematic node would be if IN 6 had not been used.

- Action case 1 (# 1). According to Figure 4.19 (a), the voltage at node 7 crosses the upper voltage boundary. At the same time OLTC 0-1 is incapable of acting, since a potential increase of the tap position would cause the lower voltage limit to be violated at node 1. So, as indicated by the rightmost pink coloured error signal in Figure 4.18 (c), the OLTC notifies that the relevant IN must take action. As a consequence, active power is absorbed by the appropriate side of IN 6 (side 6_tie) until the maximum voltage is equal to the –specified by the Primary Controller– voltage set-point. The violation is fixed within 1 minute. If IN 6 had not acted, the upper limit voltage violation would have lasted for approximately 3 hours and 40 minutes.
- Action case 1 (# 2). This case occurs as a side-effect of action case 4 (# 2). Although this side-effect could not have been predicted by the Primary Controller, the problem is quickly identified and fixed. More specifically, the occurrence of action case 4 (# 2) results in a tap position decrease, which of course does not cause the maximum node voltage to violate the limit. However, at the same time the maximum node voltage in the controlled network part increases, while the minimum one decreases due to an increase of the DRG output. Finally, after 5 minutes the upper voltage limit is breached at node 7. Since the prevailing conditions do not allow OLTC 0-1 to act, the OLTC Controller instructs the Primary Controller of IN 6 to take action. This is indicated by the leftmost, pink coloured error signal in Figure 4.18 (c). Once the IN starts absorbing active power, the violation is fixed within 1 minute (see Figure 4.19 (b)).
- Action case 4 (# 1). This case describes the lower voltage limit violation at node 1. Given that this node is actually the substation secondary bus, the IN is obliged correct the voltage violation in an indirect way. Action mode 4 is thus energised and active power is drawn. As a result, the maximum node voltage drops and OLTC 0-1 is capable of decreasing the tap position without violating the upper voltage boundary. The violation of the lower voltage boundary in Figure 4.19 (c) lasts for approximately 1 minute. At this point, the following needs to be clarified. By looking at Figure 4.18 (b), one will notice a back and forth tap movement in day 3. Although the large time scale used in the graph creates the impression that this is an instantaneous phenomenon, these two consecutive tap changes occur within a period of 3 minutes. The first one is simply decided by the Advanced OLTC Controller, while the second one is the result of action case 4 (# 1).
- Action case 4 (# 2). The first lower voltage limit violation shown in Figure 4.19 (d) is corrected by OLTC 0-1 without engaging the IN. However, the prevailing conditions are such that another lower limit violation soon occurs. Under these circumstances, the OLTC controller can do nothing, except from transmitting an appropriate error signal to the IN Controller; this is the leftmost, yellow coloured signal in Figure 4.18 (c). As with the previous case, IN 6 intervenes and prevents an otherwise prolonged voltage boundary breach. Instead of 5 minutes, the violation lasts 1 minute. The two above described voltage regulating actions can be seen in Figure 4.18 (b) as two consecutive tap decreases.

Operational aspects

With regard to Figure 4.20, during a summer week the operation of one AC terminal of IN 6 (side 6_tie) results either in charging the BESS (action modes 1 and 4), or discharging it (discharge mode). The operation of the other AC terminal (side 6) always results in discharging the BESS (discharge mode). Of course, there are periods that the AC terminals do not operate at all. It should be noted that the discharge mode not only sustains the battery weekly cycle, but also improves the VQI of the system.

The battery size has been minimised to the extent that the operation of action modes 1 and 4 is never hindered. As it can be seen in Figure 4.20 (b), the battery capacity is such that all the energy input can be stored without violating the SOC limits. Moreover, the controller parameters choice (see Table E.2 of APPENDIX E) is such that the usable SOC range is fully exploited. Another important operational aspect is the sustainability of the system. More precisely, in order for the system to be able to sustain its operation, the SOC level at the end of the simulated week must equal the initial one.

As far as the gradient of active power in Figure 4.20 (a) is concerned, the observed maximum absolute value is about 3.5 % of the rated converter apparent power per second. This value is considered to be acceptable, given that the maximum active power output gradient of a wind farm, as defined by the Spanish TSO for frequency control, is 10 % of the rated apparent power per second [88].

Regarding the behaviour of the Coordinated Voltage Controller during a winter week, simulations showed that IN 6 never engaged in order to correct extreme voltage variations. Therefore, IN 6 does never operate in one of the primary action modes during winter and for this reason only a few selected simulation results are presented in Figure 4.21.

As previously stated, not only the battery capacity, but also almost all the Primary Controller parameters have been chosen with a view to increasing the performance of the action modes 1 and 4 during summer. During winter, only $K_{denom,d}$ and SOC_0 can be freely chosen. This degree of flexibility is not enough though to prevent the violation of SOC limits during a winter week, as illustrated in Figure 4.21 (c). One can notice the difference between the initial and the final active power set-points of IN 6 due to the engagement of the SOC Controller at times when the BESS cannot be further charged or uncharged. Adjusting the aforementioned two parameters can result in changing the type of violation (upper or lower SOC limit breach) and / or its duration, but the violation itself cannot be prevented. Finally, since the intervention of the SOC Controller practically impedes the operation of IN 6 with regard to improving the voltage profiles, the higher VQI value during winter is not surprising.

Utilisation aspects

During a summer week, PWM Converter 2 of IN 6 operates –at some point– in its nominal rated power. From this perspective, PWM Converter 2 is fully utilised. On the contrary, PWM Converter 1 utilisation is very low (around 5 %). Regarding the utilisation of IN 6 in terms of time, the device operates in one of the primary action modes approximately 4 hours per summer week. The periods, during which operation for voltage variation correction takes place, are indicated by the highlighted areas in Figure 4.20 (a). The operation time under the charge or discharge modes (operation for voltage profile improvement) is not taken into account.

In a similar approach, during a winter week the utilisation is 5 % for PWM Converter 1 and 20 % for PWM Converter 2. The utilisation of IN 6 in terms of time is considered to be 0 %. Assuming that 1 year consists of 26 identical summer weeks and 26 identical winter weeks, the utilisation of IN 6 in terms of time would be approximately as low as 1.2 %.

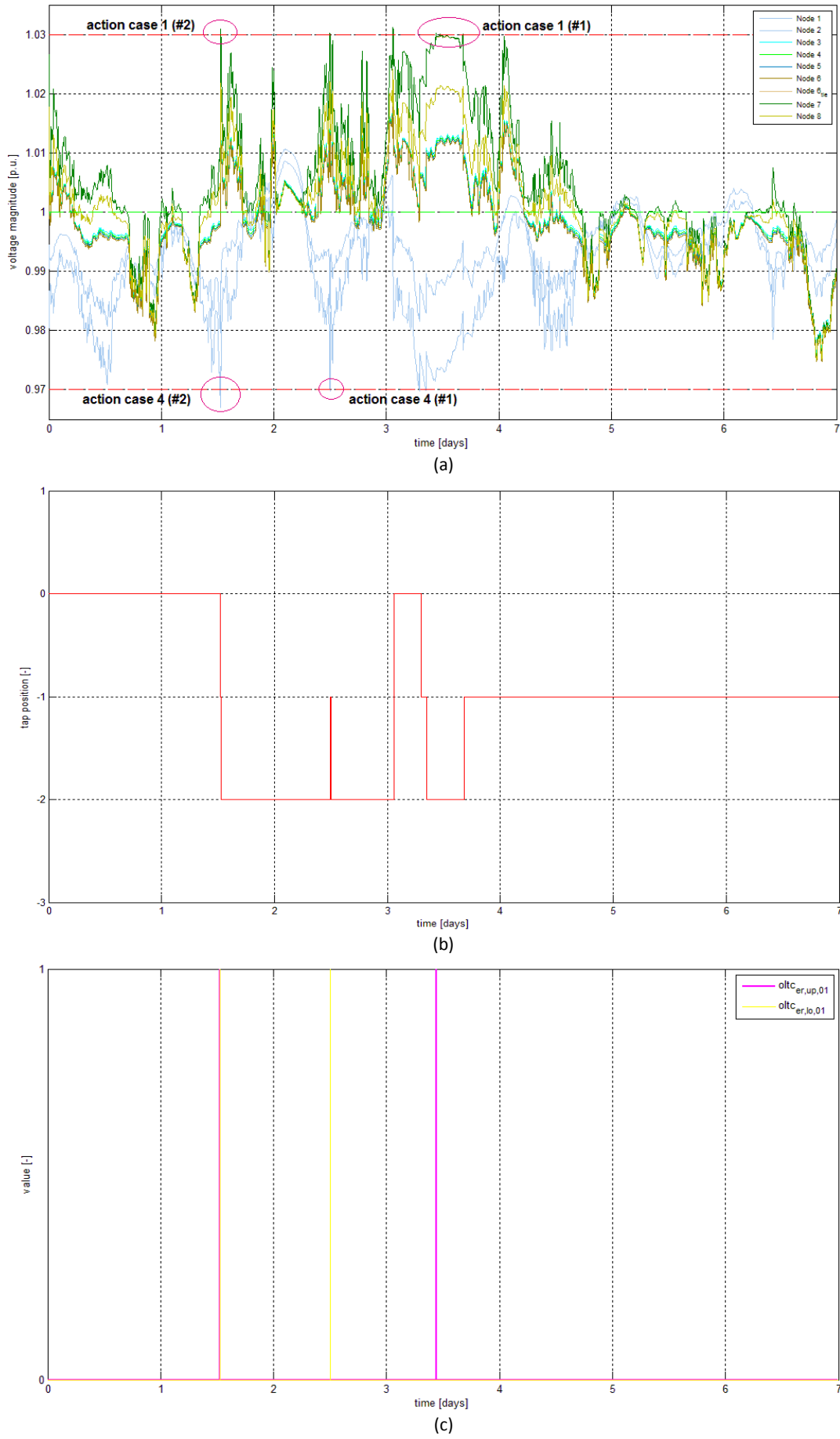


Figure 4.18: Results for coordinated voltage control scenario (IN 6 only) during summer:
(a) voltage at nodes controlled by IN 6, (b) tap position of OLTC 0-1, (c) OLTC 0-1 error signals

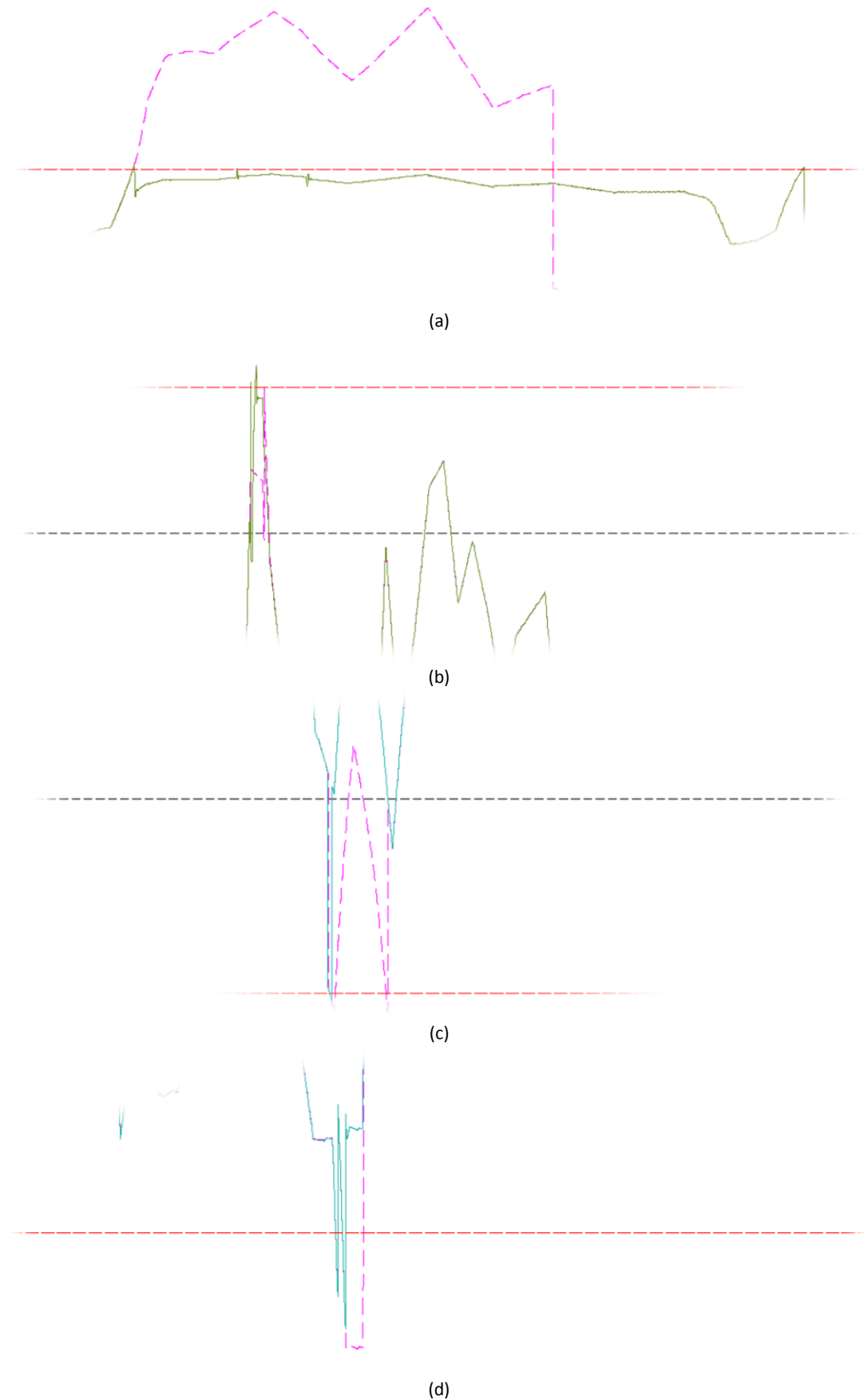


Figure 4.19: Detailed view of action cases for coordinated voltage control scenario (IN 6 only) during summer:
(a) action mode 1 (#1), (b) action mode 1 (#2), (c) action mode 4 (#1), (d) action mode 4 (#2)

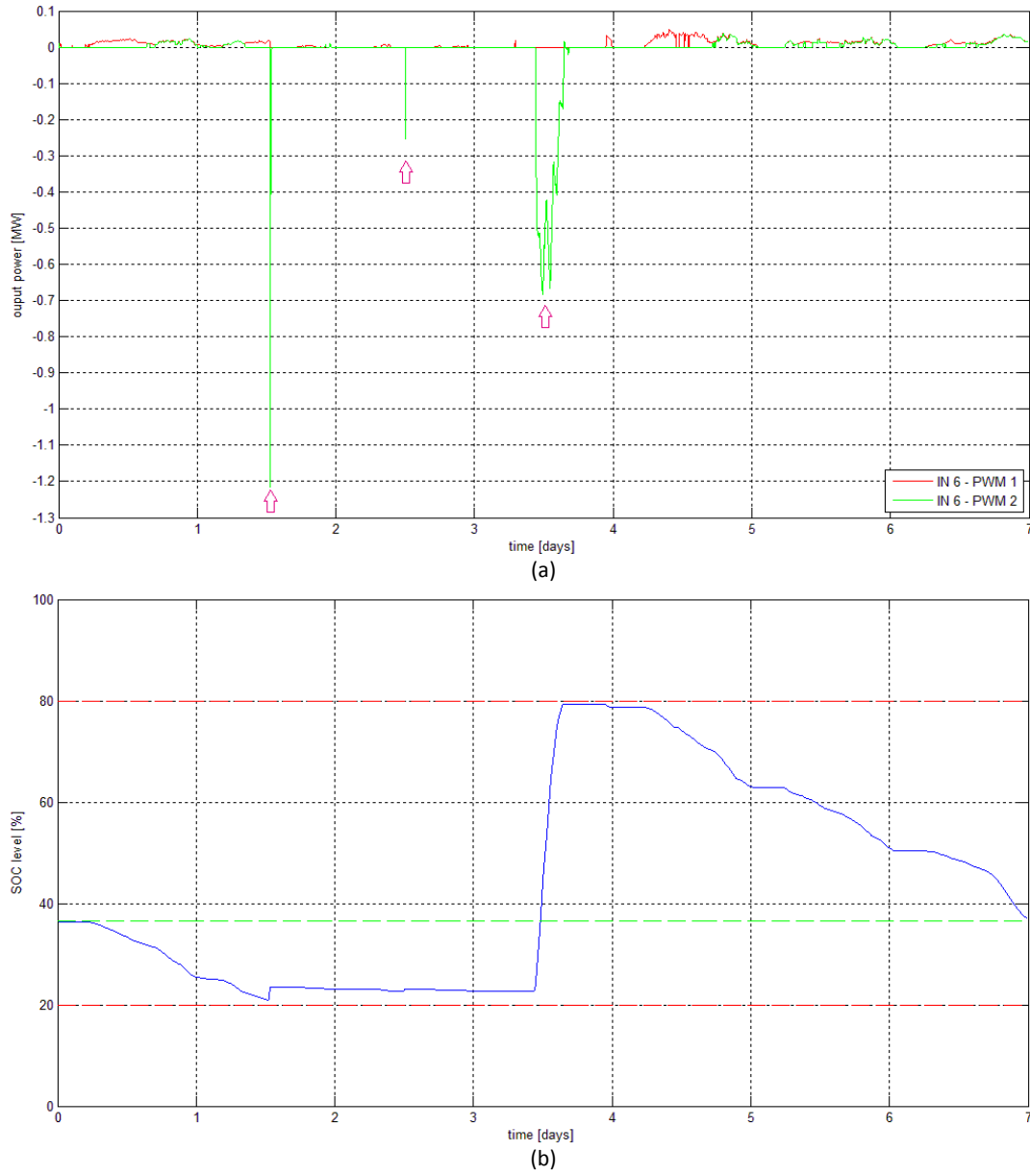


Figure 4.20: Results for coordinated voltage control scenario (IN 6 only) during summer:
 (a) active power exchange of IN 6, (b) SOC level of IN 6

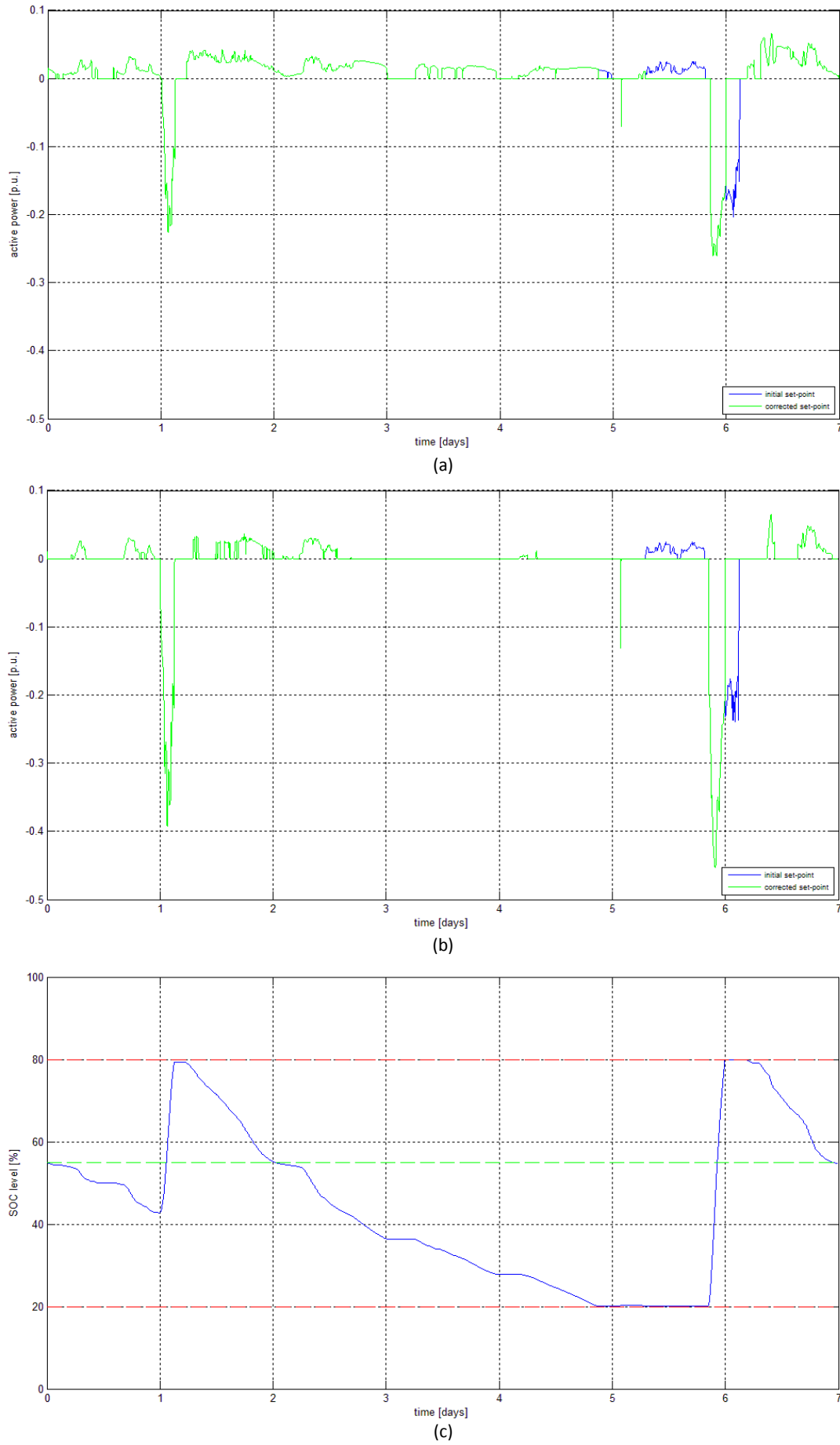


Figure 4.21: Results for coordinated voltage control scenario (IN 6 only) during winter:

(a) initial and corrected active power set-points for side 6, (b) initial and corrected active power set-points for side 6_tie, (c) SOC level of

4.4.5.2 INs 6 & 8

Basic results

This paragraph describes the most important aspects of the coordinated voltage control scenario, considering both Intelligent Node 6 and Intelligent Node 8. Information on the maximum installed DRG capacity under the coordinated voltage control scenario is given in Table 4.11. The number of tap changes performed by the HV/MV transformers OLTCs within the period of one week, as well as the resulting Voltage Quality Index are given in Table 4.12.

Table 4.11: Coordinated voltage control scenario (INs 6 & 8) – maximum hosted DRG capacity

Network section	Nominal output power [MW]		
	PVPPs	WPP	Total DRG
Feeder 1	5.0	8.0	13.0
Feeder 2	7.4	4.0	11.4
Feeders 1 & 2	12.4	12.0	24.4

Table 4.12: Coordinated voltage control scenario (IN 6 & 8) – simulation results

Season	HV/MV transformer	N_{tap}	VQI
		[\cdot]	[\cdot]
Summer	0-1	9	0.0314
	0-12	2	
Winter	0-1	20	0.0389
	0-12	2	

According to Table 4.11, the total installed DRG capacity, permitted by the coordinated voltage control scheme, accounts for up to 24.4 MW (equals to 61 % of the peak system load demand). This is translated to 52 % increase when compared to the base case control scenario and 5 % increase when compared to the coordinated voltage control scenario using only IN 6. It should be noted that for larger DRG capacities, the loading of lines 3-8 and 12-13 is exceeded before the node voltages experience values larger than the upper voltage boundary. The PVPPs account for approximately 52 % of the total amount, while the WPPs for the rest 48 %. Feeder 2 now holds 47 % of the total DRG capacity and its share has increased since the operation of IN 8 allowed for increasing the installed power of PVPPs (nodes 12 and 13) by 1.2 MW, in total. On the other hand, the renewable capacity of Feeder 1 remains the same.

Regarding the satisfaction of the secondary evaluation criteria, the following hold:

- A small decrease of the number of tap changes performed by OLTC 0-12 during a winter week is observed when compared to the coordinated voltage control scenario without IN 8. This has to do with the fact that the operation of IN 8 improves the voltage profile of Feeder 2 (operation in charge and discharge modes). Although voltages are generally not considerably improved, in this specific case a tap change is avoided.
- When compared to the corresponding values for the coordinated voltage control scenario without IN 8, the VQI for the coordinated voltage control scenario (with IN 8) is slightly higher during summer; the VQI is only marginally higher during winter. This is explained later on in this paragraph.
- The communication infrastructure needed by the controller is the largest of all the applied control schemes. The presence of IN 8 can potentially result in a –controlled– meshed operation of Feeders 1 and 2. Based on the above, the controller necessitates the existence of an additional voltage sensor at node 8_tie. An additional SOC level measurement device, as well as active and reactive power actuators are accommodated by IN 8. Overall, the Coordinated Voltage Controller needs 14 communication links in order for the 14 voltage sensors, 2 SOC sensors and 4 actuators to communicate with the coordination centre.

Next, the operation of IN 8 is analysed with respect to the simulation results. The simulation results produced during a summer week are of the greatest interest, since action mode 1 (and of course the necessary discharge mode) is demonstrated. On the contrary, only the charge and discharge modes are featured in a winter week. Nevertheless, the resulting operation of IN 8 during winter provides a useful example of controlled grid reconfiguration. In the text sections that follow, the most interesting cases are going to be presented and analysed; the operation of IN 6 is no different than the one described in paragraph 4.4.5.1 and thus will not be discussed here.

Simulated cases

According to Figure 4.22 (a), there are three time periods during which action mode 1 is energised. During the remaining summer week, IN 8 either operates in charge mode, or remains completely idle. Next, these three action cases are analysed with respect to Figure 4.23. Also here, the dashed magenta coloured lines in the graphs of Figure 4.23 show what the voltage of the problematic node would be if IN 8 had not been used.

- Action case 1 (# 1). According to Figure 4.23 (a), the voltage at node 7 crosses the upper voltage boundary. At the same time OLTC 0-1 is incapable of acting, since a potential increase of the tap position would cause the lower voltage limit to be violated. So, as indicated by the rightmost pink coloured error signal in Figure 4.22 (c), the OLTC notifies that the relevant IN must take action. As a consequence, active power is absorbed by the appropriate side of IN 8 (side 8_tie) until the maximum voltage is equal to the –specified by the Primary Controller– voltage set-point. The violation is fixed within 1 minute. If IN 8 had not acted, the upper limit voltage violation would have lasted for approximately 3 hours and 20 minutes.
- Action case 1 (# 2). This case, shown in Figure 4.23 (b), has exactly the same characteristics as with the previous one. Here, once the IN starts absorbing active power the violation is fixed within 1 minute. Nevertheless, if IN 8 had not acted the upper limit voltage violation would have lasted for approximately 10 minutes.
- Action case 1 (# 3). The case illustrated by Figure 4.23 (c) is the same as the previous two cases but this time the operation of IN 8 has only a minor impact on the system voltages. Here, a voltage violation that would have otherwise lasted 2 minutes, is now corrected within 1 minute. In order to get a clearer view, the presented graph has been zoomed compared to the other two.

Operational aspects

With regard to Figure 4.24, during a summer week the operation of one AC terminal of IN 8 (side 8_tie) results either in charging the BESS (action mode 1), or discharging it (discharge mode). The operation of the other AC terminal (side 8) always results in discharging the BESS (discharge mode). Of course, there are periods that the AC terminals do not exchange any power with the network. It should be noted that the discharge mode not only sustains the battery weekly cycle, but also help in improving the *VQI* of the system.

As with IN 6, the BESS size of IN 8 has been minimised to the extent that the operation of action mode 1 is never hindered. As it can be seen in Figure 4.24 (b), the battery capacity is such that all the energy input can be stored without violating the SOC limits. In addition, the controller parameters in Table E.2 allow for the usable SOC range to be fully exploited, while the initial and final SOC levels remain identical.

As far as the gradient of active power in Figure 4.24 (a) is concerned, the observed maximum absolute value is about 1 % of the rated converter apparent power per second. According to the reasoning presented in paragraph 4.4.5.1, this value is considered to be acceptable.

Regarding the behaviour of the Coordinated Voltage Controller during a winter week, simulations showed that IN 8 never engaged in order to correct extreme voltage variations. Therefore, IN 8 does never operate in one of the primary action modes during winter and for this reason only a few selected simulation results are presented in Figure 4.25.

Most importantly, Figure 4.25 (a) demonstrates a special feature of the Intelligent Node. During several time periods, active power absorption from Feeder 2 and active power injection to Feeder 1 take place simultaneously. This phenomenon resembles the closure of the NOP at node 8. In our case though, the amount of power entering from side 8_tie is not necessarily equal to the amount exiting from side 8. This procedure is regulated by the Coordinated Voltage Controller, instead.

As previously stated, not only the battery capacity, but also almost all the Primary Controller parameters have been chosen with a view to increasing the performance of the action mode 1 during summer. During winter, the limited flexibility in the parameters choice does not allow to take full advantage of the usable SOC range. The performed weekly cycle of the battery is shown in Figure 4.25 (c). Despite the use of a limited SOC range, the operation of IN 8 is not hindered by the SOC Controller (unlike the operation of IN 6 during winter). As a result, the improvement of the voltage profiles compensates for the increased installed capacity of PVPPs under this scenario. There is practically no difference between the winter *VQI* values shown in Tables 4.10 and 4.12.

Utilisation aspects

During a summer week, the utilisation –in terms of power– for PWM Converter 1 is only slightly more than 6 %, while for PWM Converter 1 is about 63 %. Regarding the utilisation of IN 8 in terms of time, the device operates in action mode 1 (operation for voltage variation correction according to the highlighted areas in Figure 4.24 (a)) approximately 4 hours and 30 minutes per summer week. In a similar approach, during a winter week the utilisation is 12 % for PWM Converter 1 and almost 10 % for PWM Converter 2. The utilisation of IN 8 in terms of time is considered to be 0 %. During a whole year, this number rises to approximately 1.3 %.

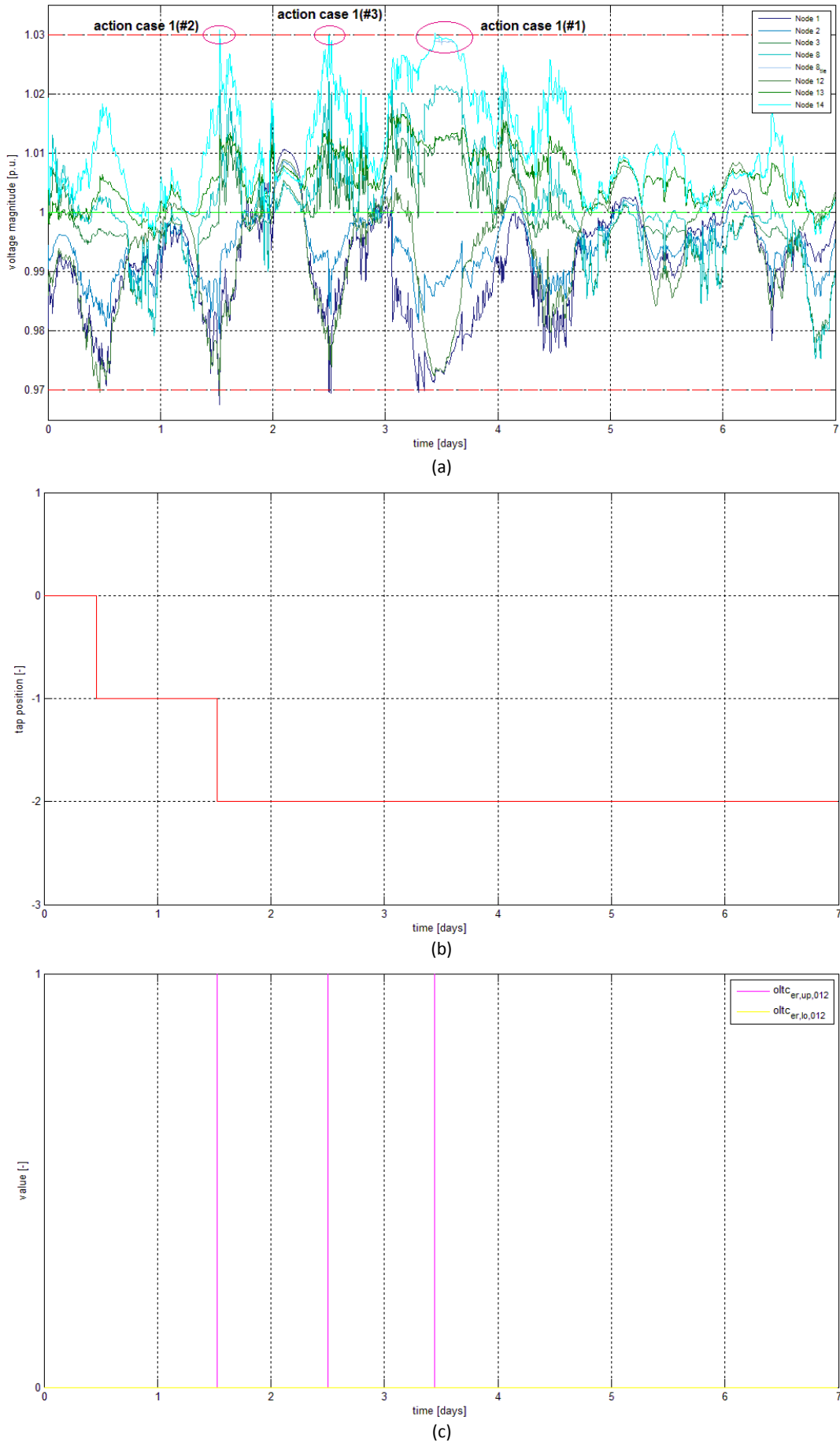


Figure 4.22: Results for coordinated voltage control scenario (INs 6 & 8) during summer:
(a) voltage at nodes of Feeder 2, (b) tap position of OLTC 0-12, (c) OLTC 0-12 error signals

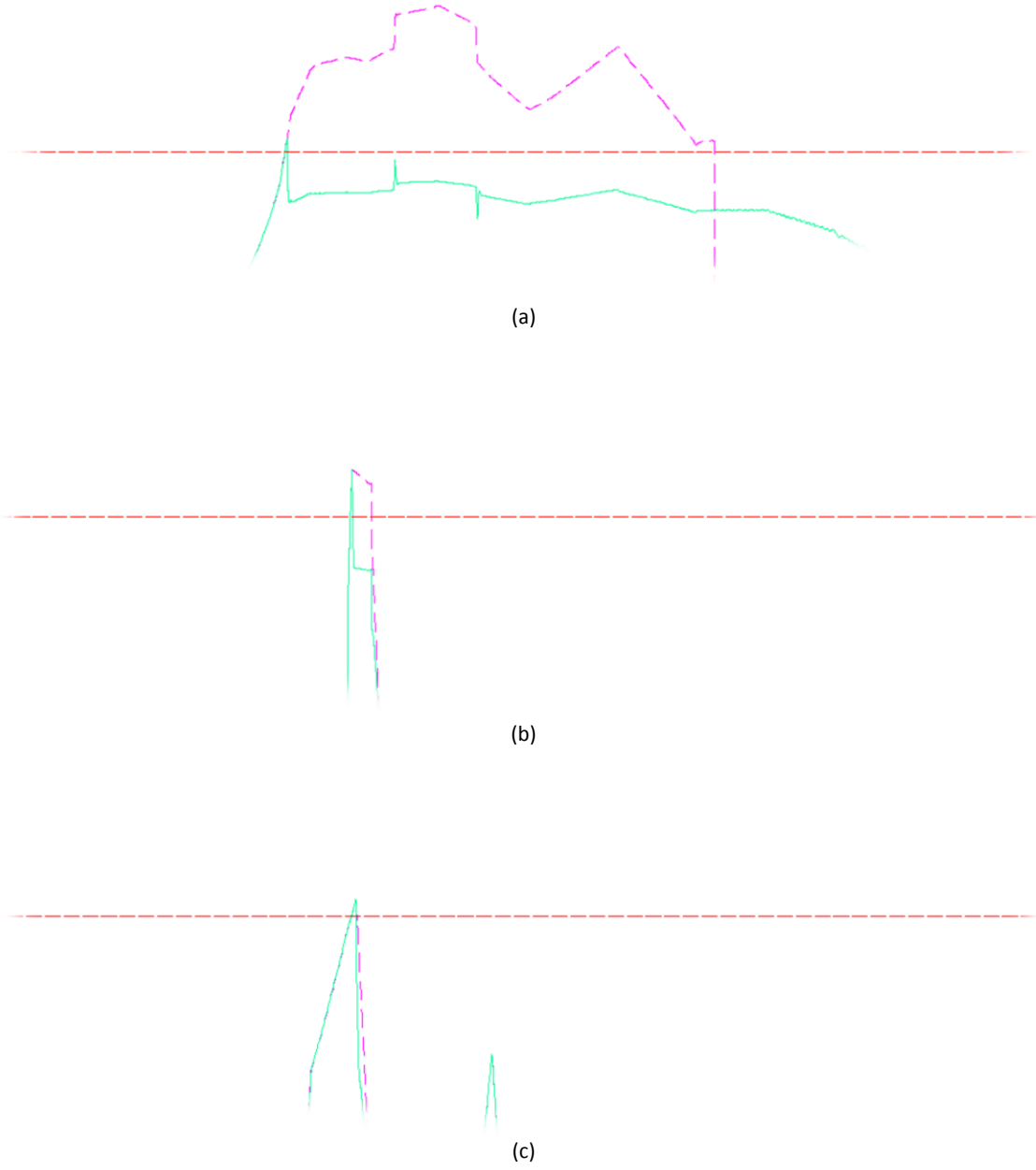


Figure 4.23: Detailed view of action cases for coordinated voltage control scenario (INs 6 & 8) during summer:
(a) action mode 1 (#1), (b) action mode 1 (#2), (c) action mode 1 (#3)

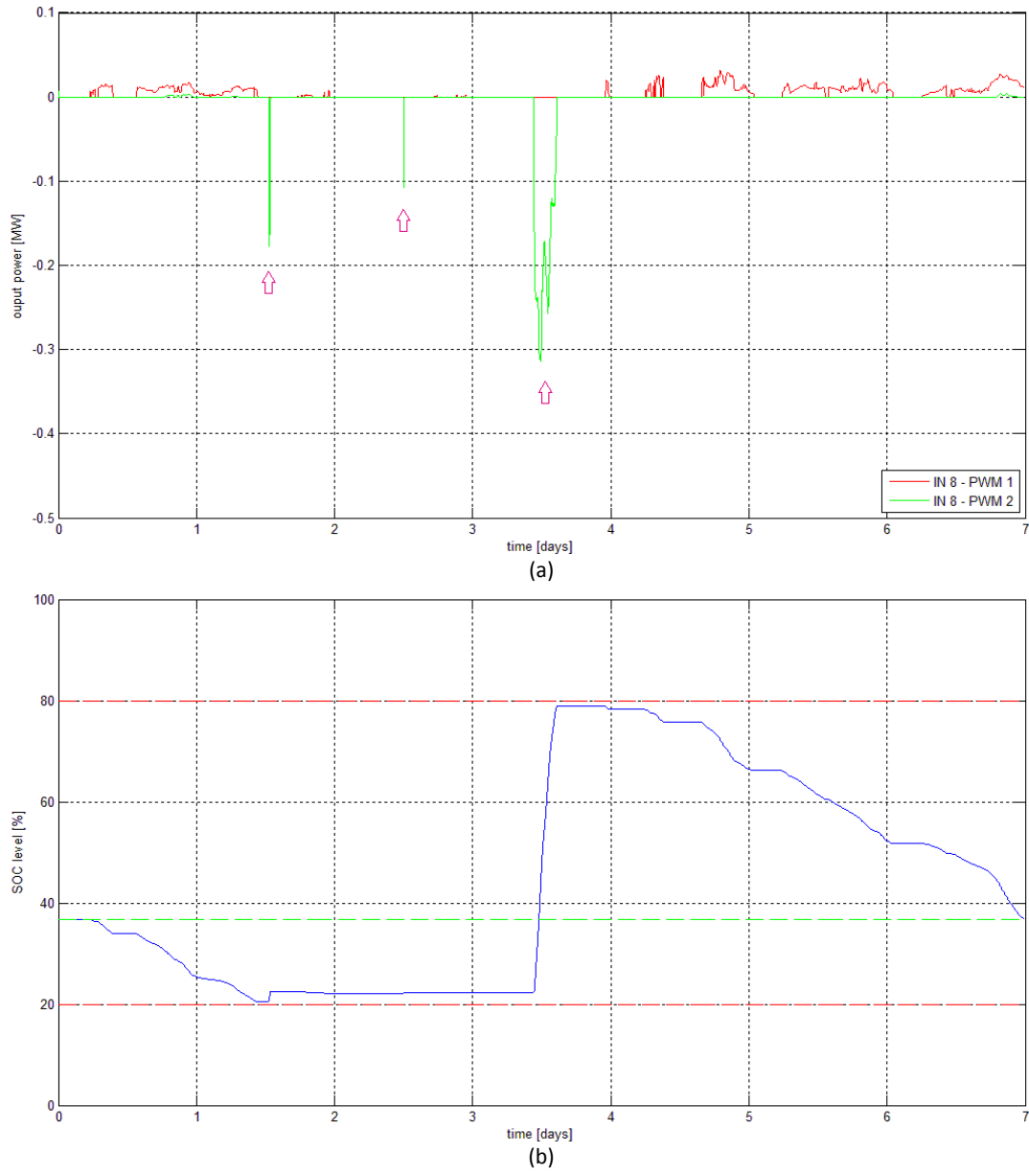


Figure 4.24: Results for coordinated voltage control scenario (INs 6 & 8) during summer:
 (a) active power exchange of IN 8, (b) SOC level of IN 8

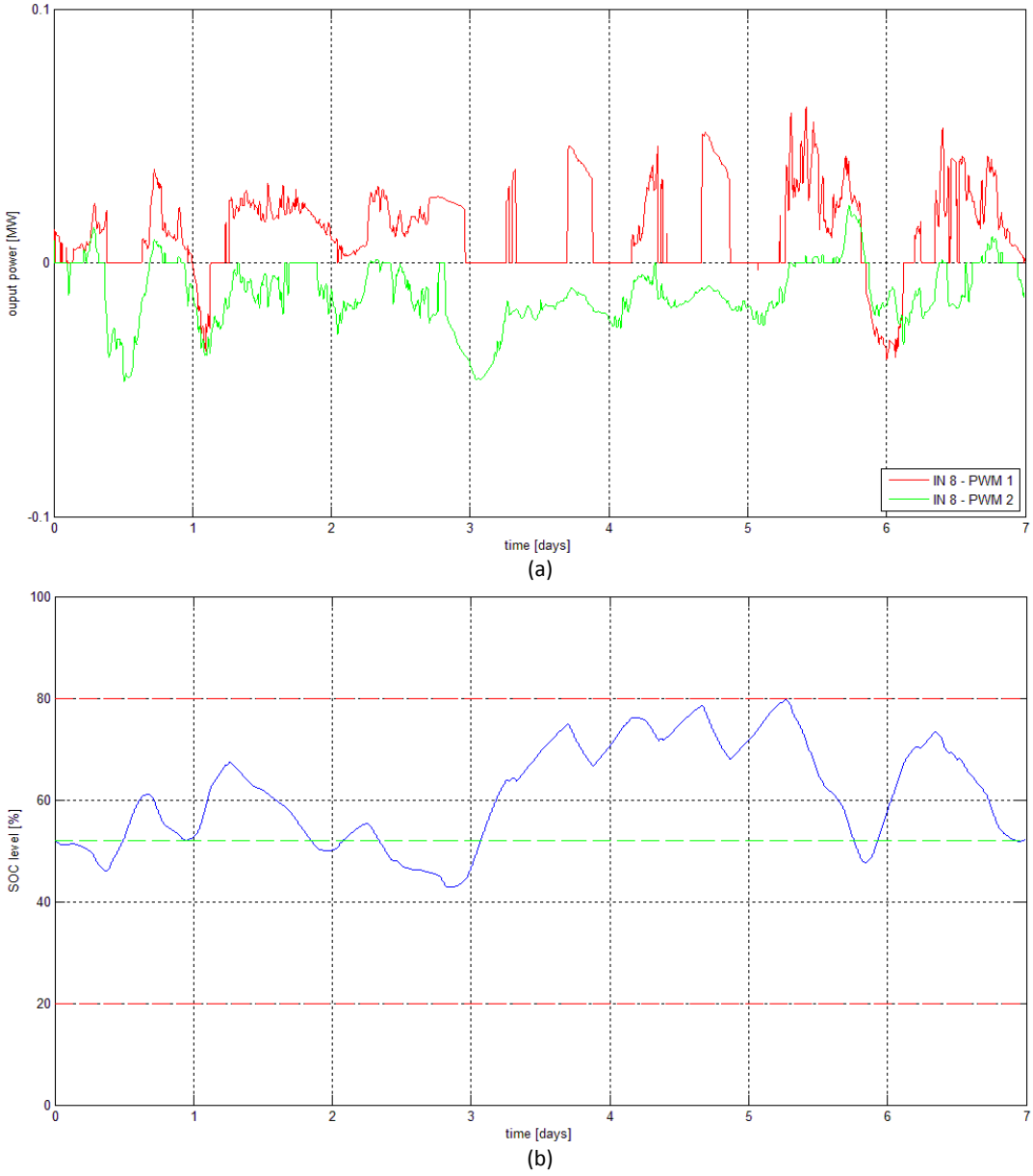


Figure 4.25: Results for coordinated voltage control scenario (INs 6 & 8) during winter:
 (a) active power exchange of IN 8, (b) SOC level of IN 8

4.4.6 COMPARISON OF CONTROL SCENARIOS

In this subsection a comparison among all the previously implemented and simulated control schemes is made. This comparison is based on the performance of each control scheme against the evaluation criteria established in subsection 4.4.2. In this context, the relevant results have been collected and are presented in the following tables. In particular, Table 4.13 gives the maximum possible installed DRG capacity, the number of tap changes performed in one week and Voltage Quality Index for all the different simulation scenarios. A better interpretation of the results is made possible with the help of Figures 4.26 - 4.28, later on. Furthermore, Table 4.14 describes the communication needs of each voltage control scheme. Here, the term refers to the infrastructure that is necessary for the transmission of signals between remote locations. Local transmission of signals is taken as granted and will not be of concern.

Table 4.13: Simulation results for different voltage control schemes

Voltage controller type	Season	OLTC	N_{tap}	VQI	P_{DRG}	
			[-]	[-]	[MW]	
Basic OLTC Controller	Summer	0-1	27	0.0346	16.1	
		0-12	32			
	Winter	0-1	37	0.0374		
		0-12	30			
Advanced OLTC Controller	Summer	0-1	5	0.0291	21.7	
		0-12	3			
	Winter	0-1	20	0.0353		
		0-12	2			
Coordinated Voltage Controller (IN 6)	Summer	0-1	9	0.0297	23.2	
		0-12	3			
	Winter	0-1	20	0.0388		
		0-12	2			
Coordinated Voltage Controller (INs 6 & 8)	Summer	0-1	9	0.0314	24.4	
		0-12	2			
	Winter	0-1	20	0.0389		
		0-12	2			

Table 4.14: Necessary remote communication infrastructure for different voltage control schemes

Voltage controller type	Communication links	Sensors			Actuators
		Voltage	SOC	Total	
Basic OLTC Controller	0	0	0	0	0
Advanced OLTC Controller	10	10	0	10	0
Coordinated Voltage Controller (IN 6)	13	13	1	14	2
Coordinated Voltage Controller (INs 6 & 8)	14	14	2	16	4

Before proceeding to the discussion of results presented in Table 4.13 and Figures 4.26 - 4.28, a word about communication aspects is in order. According to Table 4.14, the communication needs for the Basic OLTC Controller are zero. Such control schemes, whose operation depends solely on local control signals, are nowadays implemented by the majority of DNOs. The transition towards the proposed Coordinated Voltage Controller begins with the implementation of the Advanced OLTC Controller, where a great leap in the necessary communication infrastructure is observed. Thereafter, as the control algorithm becomes more complex by integrating a larger number of controlled devices, the need for communication infrastructure steadily increases.

The exact same trend is observed in Figure 4.26, where the maximum installed DRG capacity as a function of the applied control strategy is shown. The provided numbers and percentages correspond to the increase of installed renewable capacity with respect to the base case control scheme. In particular, the transition from the Basic OLTC Controller to the Advanced OLTC Controller is accompanied by the largest increase of renewable capacity that can be observed in the graph. From this point onwards, the penetration of DRG steadily increases as the applied control algorithm becomes more advanced. In an effort to relate the needed communication infrastructure to the maximum permitted DRG capacity for each controller type, an almost linear relation can be observed between the number of communication links (see Table 4.14) and the increase of installed renewable capacity (see Figure 4.26).

Finally, the upper limit for the installed DRG capacity under the Coordinated Voltage Control scheme is reached. As already stated in paragraph 4.4.5.2, the limiting factor is the line loading. A further increase of the DRG capacity would require a controller with a different orientation, namely towards power flow control of critical lines.

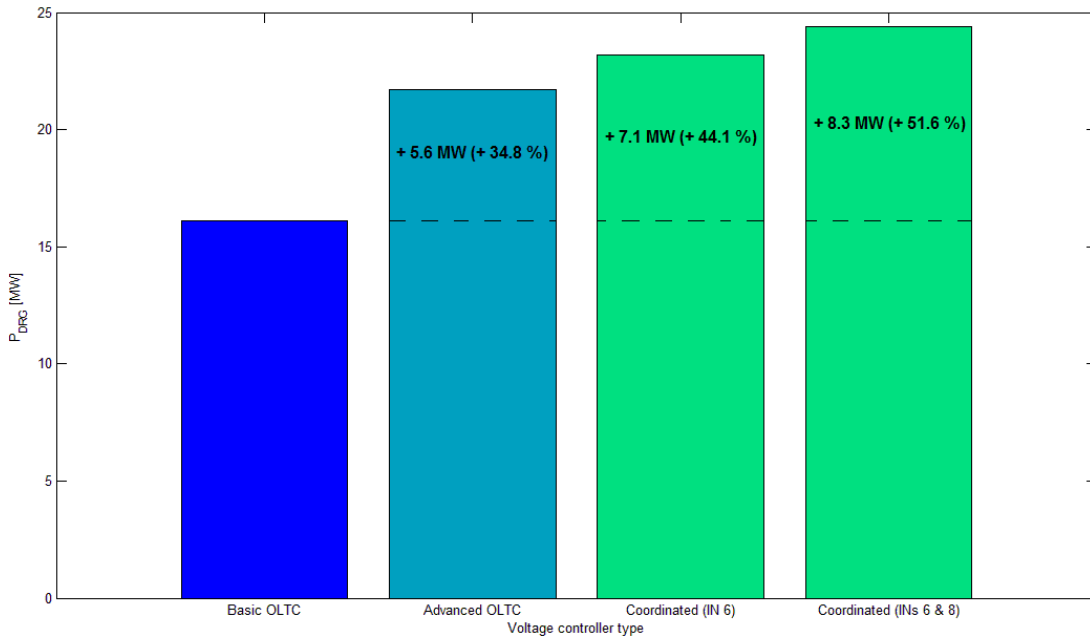


Figure 4.26: Maximum installed DRG capacity for different voltage controller types

Regarding the number of performed tap changes by the OLTCs, further manipulations of the data presented in Table 4.13 can offer a more general perspective shown in Figure 4.27. Regarding the behaviour of OLTC 0-1 shown in Figure 4.27 (a), first the influence of the voltage controller type on the number of performed tap changes is discussed. Initially, both during summer and winter, the application of the Advanced OLTC Controller manages to greatly reduce the performed tap movements. Furthermore, the application of the Coordinated Voltage Controller has no influence on the tap changing behaviour during winter and a negligible one during summer. By taking into account the seasonal variation, one can notice that less tap changes are performed during summer. The reasoning behind this is twofold. First, HV/MV transformer 0-1 serves a large load and the operation of OLTC 0-1 is more influenced by the load pattern (load peaks and variability). Second, the installed wind power capacity has a larger share in Feeder 1 and the power fluctuations are more intense during the windy winter week. Subsequently, the operation of OLTC 0-1 is more frequent in winter.

Regarding the behaviour of OLTC 0-12 shown in Figure 4.27 (b), the influence of the voltage controller type on the number of performed tap changes is the same as the one observed in Figure 4.27 (a). Nevertheless, the influence of the seasonal variation has the opposite effect. In particular, HV/MV transformer 0-1 serves a smaller load in comparison with transformer 0-1, meaning that it is less influenced by the load pattern. What is more, the installed photovoltaics capacity has a larger share in Feeder 2 and the power fluctuations are more intense during the sunny summer week. Subsequently, the operation of OLTC 0-12 is more frequent in summer.

Figure 4.27 (c) suggests that if the OLTCs of the two HV/MV transformers operate in the traditional way, the resulting tap changes are by far the most. The application of the Advanced OLTC Controller greatly reduces this number, while further advance towards the Coordinated Voltage Controller has only a negligible effect on the frequency of the tap changing operations. In general, the control schemes that use remote signals can significantly alleviate the operation of the OLTCs, since unnecessary tap changes no longer take place. By taking into account the seasonal variation, one can notice that during summer less tap changes are performed than during winter. The reasoning behind this behaviour is that a winter week is characterised by the extreme ‘high load / low generation’ situation and multiple moderate ‘low load / high generation’ situations. These situations are in general not limiting for the DRG capacity of the network and voltage variation issues are solved by the tap changers; thus more tap changes occur. By contrast, a summer week is characterised by the extreme ‘low load / high generation’ situation. This situation has proven to be limiting for the DRG capacity of the network and the occurring voltage variations cannot be solved by the tap changers; thus less tap changes occur.

As far the Voltage Quality Index of the system is concerned, Figure 4.28 suggests that, in general, no significant changes take place. Nevertheless, one can still observe that the application of the Advanced OLTC Controller improves the *VQI*, while further advance towards the Coordinated Voltage Controller has only a slight deteriorating effect on it. Overall, for all the different voltage controller types that were tested, the *VQI* is found to be worse during winter. It turns out that the more frequent, but less extreme, voltage variations that occur during a winter week have a large negative effect on the Voltage Quality Index. By contrast, the less frequent, but more extreme, voltage variations that occur during a summer week have a limited impact.

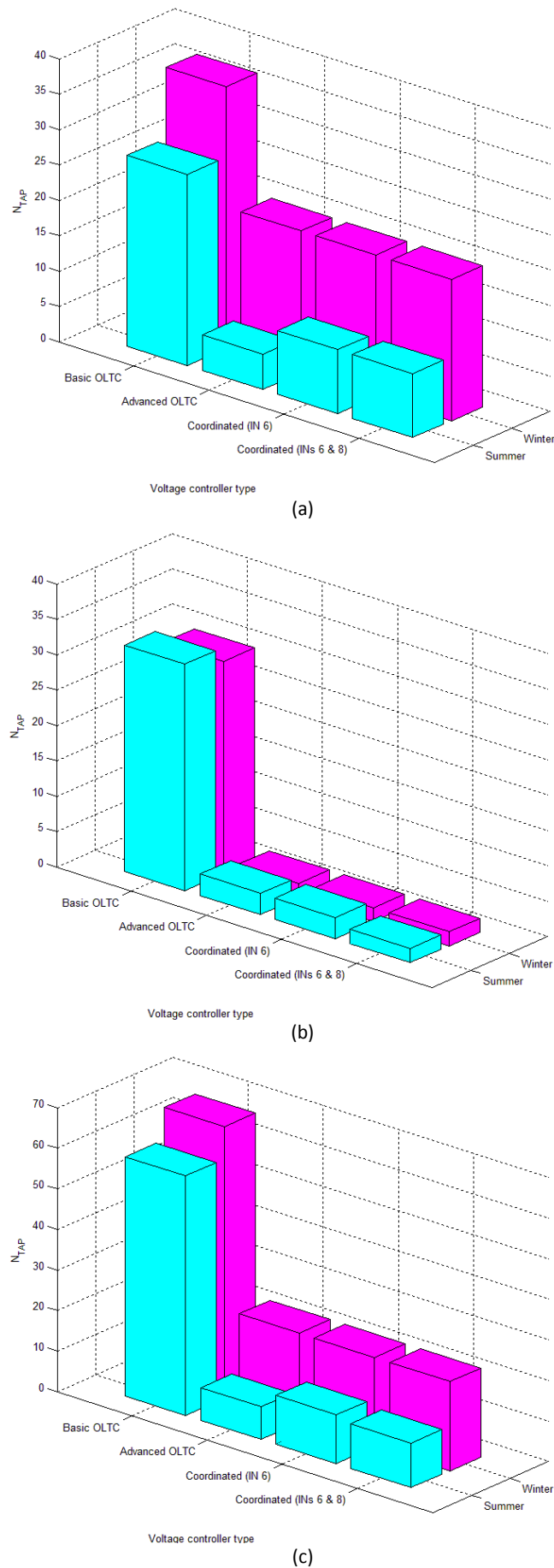


Figure 4.27: Number of tap changes performed in one week as a function of voltage controller type and season:
(a) OLTC 0-1, (b) OLTC 0-12, (c) OLTC 0-1 & OLTC 0-12

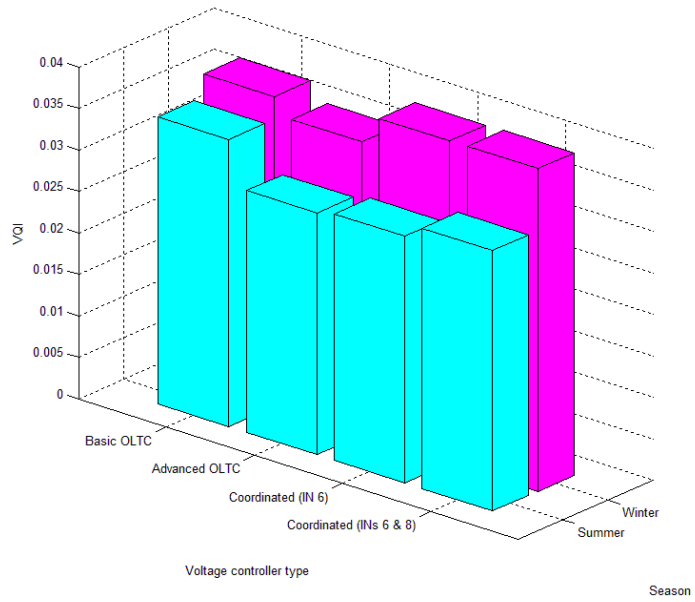


Figure 4.28: Voltage Quality Index as a function of voltage controller type and season

4.5 CONCLUSIONS

In this chapter, the main simulation results of this thesis were presented and analysed for a number of specific system conditions (i.e. summer and winter weeks) and voltage control schemes. Prior to this, an in-depth description of the implemented Coordinated Voltage controller took place, along with the presentation of the various simulation scenarios. Furthermore, several important phenomena that strongly influence the performance of the various control schemes were pointed out. At the end of this chapter, comparative results for all four tested voltage control schemes were provided. The conclusions arising of the simulation results analysis will be presented in the next chapter.

5 CONCLUSIONS AND FUTURE WORK

5.1 CONCLUSIONS

5.1.1 PROPOSED VOLTAGE CONTROL STRATEGY

This thesis worked from the fundamental principles of voltage control in electrical distribution grids to devise a coordinated control strategy that incorporates information exchange between the HV/MV substation transformer and the nodes of the MV network, also including Intelligent Nodes equipped with power electronics-interfaced battery systems. As a result, a new voltage control strategy has been developed, implemented and proved to be working.

When fully implemented (i.e. both INs 6 and 8 installed), the Coordinated Voltage Controller enables the MV distribution network to incorporate the maximum amount of DRG capacity. Any further increase of the installed DRG capacity is prohibited by line overloading. As an answer to the third research question from the viewpoint of voltage quality, the maximum permitted DRG capacity shows an increase of almost 52 % when compared to the basic voltage control scheme. Furthermore, regarding the evaluation criteria stated in the fourth research question, the number of tap changes performed by the two OLTCs shows a significant reduction of around 75 %, while an aggregation of the relevant results for a summer and a winter week reveals that the Voltage Quality Index remains at the same levels. Concerning voltage quality in general, it should be pointed out that the operation of the Coordinated Voltage Controller results in the correction of all extreme voltage variations within 1 minute. Moreover, the demonstrated controlled grid reconfiguration has a positive effect on voltage profiles.

As far as the communication needs of the Coordinated Voltage Controller are concerned, the fact that the controller results in a controlled meshed operation of Feeders 1 and 2 demands for extensive communication infrastructure. More precisely, 14 communication links are needed so that the voltages at 14 MV nodes can be controlled. In general, the number of communication links needed by the proposed method strongly depends on the number of controlled MV nodes, but also on the number of installed OLTCs and INs. It is further observed that the communication needs scale up almost linearly with the number of nodes, something that is confirmed by the studied test system. The required performance for transmitting digital signals from (to) remote sensors (actuators) can be achieved by utilisation of the IEC 61850 GOOSE and SV services, or by using wireless 4G technologies.

Regarding the general applicability of the proposed controlled method, although some features of the model are generally applicable, its design still has to be tailored to the specific network conditions. One thing that is generally applicable is that, irrespective of the applying MV distribution network topology, the INs must be placed at the NOPs located at the feeder ends (this is the suggested IN placement for voltage control purposes). Apart from that, the settings of the Coordinated Voltage Controller, as well as the size and number of the necessary INs are decided based on system simulations. These aspects strongly depend not only on the size and location of the MV loads, but also on the type, size and location of the connected DRG units.

When it comes to the utilisation of the Intelligent Nodes though, the proposed control scheme shows less satisfying results. In terms of power, the majority of the PWM converters accommodated by the INs never operate at their nominal output power. In particular, PWM Converter 1 of IN 6 is utilised only 5 %, while PWM Converter 2 is 100 % utilised (although only for several minutes). For IN 8, the corresponding percentages are 12 % and 63 %, respectively. In addition, assuming that 1 year consists of 26 identical summer weeks and 26 identical winter weeks, IN 6 operates in one of the primary action modes for 1.2 % of the time, while IN 8 for 1.3 %. Here, the operating time for voltage profile improvement is not taken into account; in that case, the overall operating time of the INs would be roughly 3/4 of the year.

To sum up, when both IN 6 and IN 8 participate in the control scheme, the proposed Coordinated Voltage Controller fully accomplishes its objective, while respecting the posed boundary conditions. In addition, the primary evaluation criterion is fully met and the secondary evaluation criteria are, in general, sufficiently satisfied. The modelled controller is particularly applicable to MV distribution networks across North Europe, since not only the benchmark network, but also the weather and consumption data used for the simulations are representative of this region. With these in mind, the proposed voltage control strategy is capable of facilitating the transition towards active MV distribution networks in Europe, by offering considerably higher DRG penetration levels and strictly bound network voltages. Therefore, from a technical point of view

alone, its implementation is strongly recommended. A cost-benefit analysis would of course be required before making important electrical and ICT investments in the distribution grid.

5.1.2 FACTORS LIMITING THE DRG PENETRATION

This section answers the first two research questions of this study, concerning the factors that limit the ability of a voltage controller to increase the installed DRG capacity in MV distribution networks and how can these limitations be overcome. Initially, the Basic OLTC controller shows a poor performance since it manages to keep the system node voltages within the limits only when the installed DRG capacity is low. The analysis of the relevant simulation results reveals three factors which are responsible for this performance.

- Fixed setting of the OLTC voltage set-point. Given that the OLTC controller must deal with both voltage rises and drops within the period of one week, a fixed U_{SET} value forces the controller to consider these two opposite voltage issues as one single issue.
- Lack of information regarding the actual values of the feeder node voltages. Since a voltage violation at one of the feeder nodes cannot actually be sensed by the controller, the system operation must be simulated beforehand and choose –by trial and error approach– a U_{SET} value which sufficiently deals with both upper and lower voltage limit violations occurring within a week.
- The controller action is solely determined by the reactive power flow through the transformer. While this aspect enables the controller to perform well in a system with no DRG units, the controller behaviour is significantly deteriorated in a system with DRG units. What is more, simulation results indicate that when DRG units are equipped with voltage control function, the operation of the Basic OLTC Controller can create even worse voltage problems. This valid for all voltage control methods presented in paragraph 2.5.3.2, with the $Q(U)$ method being the one that shows the most problematic behaviour.

As far as the Advanced OLTC Controller is concerned, the simulation results suggest that the above stated limiting factors no more apply. Here, the controller becomes aware of voltage limits violations throughout the network nodes and takes the appropriate corrective action. Nevertheless, a different factor now limits the maximum hosted DRG penetration, namely:

- Inability of the controller to deal with situations that involve large differences between the maximum and minimum node voltages. More precisely, when one of the voltage boundaries is breached while, at the same moment, the maximum and minimum node voltages of the controlled network part differ by more than 5.375 % of the nominal value, the operation of the OLTC is hindered.

The solution to the previously described limitation is to reduce the voltage differences within a feeder down to manageable –by the OLTC– levels. This exactly what the Coordinated Voltage Controller does, since the ability to control the power flow using Intelligent Nodes is taken advantage of. As a result, the DRG penetration in the MV distribution network increases. In this case, the upper limit of installed DRG capacity is posed by:

- Line overloading. In particular, for larger DRG capacities, the resulting higher amounts of reverse active power flow cause the loading limit of lines 3-8 and 12-13 to be exceeded ($> 100\%$) before the node voltages can experience values larger than the upper voltage boundary (1.03 pu). Any further increase of the DRG capacity would thus require a controller with a different orientation, namely towards controlling the active power flow through the critical lines.

5.1.3 TAP CHANGING FREQUENCY AND VOLTAGE QUALITY

The comparative analysis of the results in subsection 4.4.6 suggests that if the OLTCs of the two HV/MV transformers operate in the traditional way, the resulting tap changes are by far the most. The application of the Advanced OLTC Controller greatly reduces this number, while further advance towards the Coordinated Voltage Controller has only a negligible effect on the frequency of the tap changing operations. In general, the control schemes that make use of remote signalling can significantly alleviate the operation of the OLTCs, since only the absolutely necessary tap changes take place.

Furthermore, the existence of seasonal variation gives insight to the effects that the nature of voltage variations and the type of installed DRG have on the frequency of tap changes. First, one can notice that during summer less tap changes are performed than during winter. This is because a winter week is characterised by problematic situations which are in general not limiting for the DRG capacity of the network. The resulting voltage variations are less extreme and are solved by the tap changers; thus more tap changes occur. By contrast, in almost all the simulated scenarios, a summer week has been proven to be limiting for the DRG capacity of the network. The resulting extreme voltage variations cannot be solved by the tap changers; thus less tap changes occur. Next, the effect of the installed DRG type is made clear. The installed wind power capacity has a larger share in Feeder 1 and the power fluctuations are more intense during a windy winter week. Subsequently, the operation of OLTC 0-1 is more frequent in winter. Similarly, the installed photovoltaics capacity has a

larger share in Feeder 2 and the power fluctuations are more intense during a sunny summer week. Subsequently, the operation of OLTC 0-12 is more frequent in summer.

As far the Voltage Quality Index of the system is concerned, the application of the Advanced OLTC Controller improves the *VQI*, while further advance towards the Coordinated Voltage Controller has a slight deteriorating effect on it. Nevertheless, given that the observed differences are small, it can be argued that voltage quality is not hindered by the increased DRG capacity.

5.1.4 EFFECT OF REACTIVE POWER

Reactive power control is a widely used method for regulating voltage. Also in this study the interfacing converters of the DRG units are able to vary their reactive power exchange with the grid. In general, as the rating of a DRG unit is fixed, injecting or absorbing large amounts of reactive power necessitates a reduction in the active power injection and thus –if relying on a generation-based premium– a reduction in the net revenue of the DRG. To deal with this issue, in this study the converters of the DRG units are assumed to be reasonable oversized (+ 5.3 %) so that only small amounts of reactive power can be exchanged, without any active power curtailment.

Furthermore, an important aspect of reactive power control is the efficiency of the performed voltage regulation. The level of efficiency heavily depends on the impedance characteristics of network lines, namely the ratio of the line resistance over the line reactance. According to Table A.6, the lines of the studied MV distribution network have a R'_{LN}/X'_{LN} ratio larger than 1, being 1.31 for underground cable lines and 1.24 for overhead lines. Therefore, the flow of reactive power has a smaller impact on system voltages when compared to the active power flow. However, given that the R'_{LN}/X'_{LN} ratio of the used lines is not significantly larger than 1, regulating the voltage using reactive power remains undoubtfully an interesting option. Besides, unlike active power control, reactive power control does not necessitate any energy storage devices.

Finally, in spite of being a widely use method, the reactive power set-points of the proposed Coordinated voltage Controller have been deliberately set to zero. As a result, only active power is controlled by the installed Intelligent Nodes. In particular, system simulations showed that when the node voltages are generally high due to large amounts of reverse active power flow towards the HV/MV transformers, absorbing reactive power would indeed decrease the voltage but at the cost of line overloading; one of the boundary conditions of the control algorithm would thus be violated. In other words, from a point and onwards, controlling reactive power cannot help in further increasing the installed DRG capacity. Nevertheless, reactive power could be used for voltage profile improvement at times when the loading of lines is moderate. This issue is not treated in this study and forms a recommendation for future work.

5.1.5 CHOICE OF VOLTAGE LIMITS

In this study the voltage variation at any node of the MV network must be bound within the range of $U_{nom} + 3\% / -3\%$. With this in mind, one can observe a diversification from the power quality requirements currently implemented in most European countries. These requirements are based on the EN 50160 standard and suggest the use of less strict voltage limits, meaning that the supply voltage supplied by public distribution networks must be within the range of $U_{nom} + 10\% / -15\%$ [48]. However, in order for this statement to be true at the LV customer level, it makes sense that a more narrow voltage limit range should be used at the MV distribution level. The reasoning behind this approach is summarised below.

Given that the geographical span of a distribution network is not particularly large, the prevailing weather conditions are not expected to significantly vary throughout the network. This can lead to broad similarities in the demand time series of the served loads, meaning that voltage drops in different parts of the network coincide. Consequently, an already significant voltage drop at the MV distribution level can lead to an extreme voltage drop at the LV customer level. Thus, compliance with the voltage limits at the LV customer level presupposes the enforcement of a stricter lower voltage boundary at the MV distribution level. Similarly, the weather conditions uniformity can lead to broad similarities in the power production time series of the connected DRG units, meaning that voltage rises in different parts of the network coincide. In this case, an already significant voltage rise at the MV distribution level can lead to an extreme voltage rise at the LV customer level. Thus, compliance with the voltage limits at the LV customer level presupposes the enforcement of a stricter upper voltage boundary at the MV distribution level. The above conclusion suggests that a DNO will either fix the voltage within a narrow band, or demand from the connected customers to operate their equipment within wider voltage limits. It could be argued that this is actually a transfer of investment responsibility from the DNO to the customer.

Last but not least, the analysis of simulation results revealed another aspect of choosing broad voltage limits. More precisely, incorporating a large amount of DRG capacity in the studied MV network results in large amounts reverse power flow through the MV distribution lines. Especially when the installed DRG capacity reaches the maximum permissible value, line overloading issues start to arise. This implies that if less strict voltage limits were applied, the violation of the line loading limit would initially be the only factor preventing a further increase of DRG penetration; one would first have to

deal with this issue before voltage limits violations started appearing at higher penetration levels. Nonetheless the methods presented in this thesis are general and can be applied for any voltage tolerance band.

5.2 FUTURE WORK

Within the framework of this thesis an effort has been made to study all the involved aspects in depth. Nevertheless, bearing in mind that a thesis project is normally characterised by finite study and time limits, a number of aspects demand for further research. In this section several recommendations for future work are given.

In subsection 5.1.1 it was concluded that the implementation of the proposed Coordinated Voltage Controller is technically favourable for the operation of the tested MV distribution network. However, further study is needed in order to verify whether the implementation of the proposed control scheme is also economically advantageous. This will necessitate the economic valuation of all the participating system components (i.e. PWM converters, battery systems and communication infrastructure) with a view to calculating the additional cost per unit of renewable energy produced. Of course, in this case an efficiency factor must be considered for the PWM converters and the BESS devices. Furthermore, the comparison of control scenarios in subsection 4.4.6 showed some rather interesting results. More specifically, the transition from the Basic OLTC Controller to the Advanced OLTC Controller is accompanied by the largest observed increase of renewable capacity. As the applied control algorithm further advances, the penetration of DRG steadily increases. Exactly the opposite holds for the number of tap changes performed by the OLTCs, while no significant differences are observed in the value of the *VQI*. Additionally, the needed communication infrastructure shows a big leap the moment the Advanced OLTC Controller replaces the basic one. From this point and onwards, the need for communication infrastructure steadily increases depending on the version of the Coordinated Voltage Controller. In an effort to relate the needed communication infrastructure to the maximum permitted DRG capacity, an almost linear relation can be observed between the number of communication links and the increase of installed renewable capacity. This linearity, together with an appropriate choice of weighting factors, should also be taken into consideration by a potential economic evaluation of the system. In such a case, the economic evaluation may deduct for example, that the Advanced OLTC Controller or the Coordinated Voltage Controller (with IN 6 only) are –from an economic point of view– more advantageous solutions, despite the fact that Coordinated Voltage Controller (with INs 6 and 8) has been proven to be –from a technical point of view alone– the supreme solution.

At this point, the issue of low power utilisation of the INs needs to be addressed. As already explained in the description of the Coordinated Voltage Controller, the produced active power set-points cannot quickly obtain high values, since this can result in an overshoot of the IN d-axis output current; an oscillatory behaviour then takes place. With a view to solving this issue, a more advanced ‘PQ Controller’ block needs to be developed (see subsection 3.6.4). For instance, in order to calculate the IN output current, a more sophisticated IN model would require that the active and reactive power set-points (originating from the Coordinated Voltage Controller) are fed to a PI controller that features two control loops in cascade. Such a technique is used in [89], where it is shown that stepwise changes in active and reactive power set-points can be combined with quick converter response and minimum overshoots.

In this study the development of the proposed control algorithm was based on an incremental approach. The main advantage of this approach is the ability to identify and correct the applying limitations step by step, finally resulting in a well performing voltage controller. According to the author’s opinion, the following recommendations are of great importance when it comes to the development of an overall robust controller. First, the Coordinated Voltage Controller should be enhanced with reactive power control capability. This capability should be available only for operation under the charge or discharge modes, since any potential reactive power exchange during one of the four primary operation modes is prone to result in line overloading. This brings us to the second point of interest, namely the fact that an integral robust controller must be able to solve the arising line loading issues. Further research could possibly reveal that a different IN location is preferable when the controller must also deal with line overloading issues.

Last but not least, a future incorporation of the proposed voltage control algorithm into the Watt Connects project will allow for validating its performance under different system conditions. For instance, a simpler network topology can be used, consisting of two MV feeders supplied by the same HV/MV transformer. In spite of using a rudimentary topology, the presence of the unpredictable human behaviour will result in diverse load demand curves (unusually large load coincidence factors could be observed, e.g., when a user of the demonstration table varies the load demand of a large MV industrial customer) and various levels of DRG penetration (e.g., when a user varies at will the output of a DRG unit), thus creating a challenging environment for the proposed voltage control algorithm. In particular, this could force the INs to operate under action modes 2 and 3. This is of significant importance, since in this study the chosen benchmark network could not create the appropriate conditions for demonstrating these two operation modes.

APPENDIX A: CIGRÉ EUROPEAN MV DISTRIBUTION NETWORK

A.1 HV-MV subtransmission equivalent network

Table A.1: HV-MV subtransmission equivalent network parameters of European MV distribution network benchmark [42]

Nominal system voltage	Short circuit power	R/X ratio
[kV]	[MVA]	
110	5000	0.1

A.2 HV/MV transformers

The parameters for the HV/MV substation transformers are given in Table A.2. No magnetising impedance is considered and thus no-load losses are ignored (typically about 0.1 % or less of the transformer rating).

Table A.2: HV/MV transformer parameters of European MV distribution network benchmark [42]

Node from	Node to	Connection	V_p	V_s	Z_{TRF}	S_{rat}	I_m	P_{Fe}
			[kV]	[kV]	[pu]	[MVA]	[pu]	[kW]
0	1	3-ph Dyn1	110	20	0.001+j0.12	25	0	0
0	12	3-ph Dyn1	110	20	0.001+j0.12	25	0	0

A.3 Lines

Figure A.1 and Table A.3 give the geometries for the overhead lines and underground cables, from which line parameters can be derived [42]. The types of conductors used are designated by the Conductor ID. The associated conductor parameters are provided in Table A.4 for overhead lines and Table A.5 for underground cables [42]. The current rating for the chosen overhead lines has been calculated using the data of Table A.7. The current rating for the chosen underground cables was already available in DIgSILENT PowerFactory database.

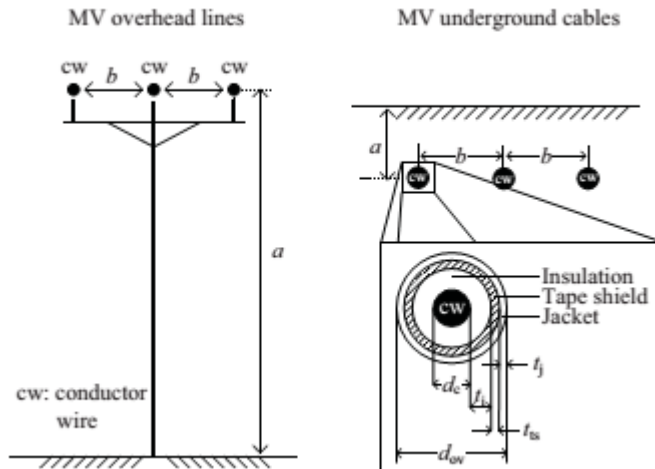


Figure A.1: Geometry of overhead and underground lines of European MV distribution network benchmark

Table A.3: Geometry of overhead and underground lines of European MV distribution network benchmark

Installation	<i>a</i>	<i>b</i>
	[m]	[m]
Overhead	9.5	1.0
Underground	0.7	0.3

Table A.4: Conductor parameters of overhead lines of European MV distribution network benchmark [42]
(coloured cells contain calculation results)

Conductor ID	Conductor type	Stranding	Cross-sectional area	<i>d</i> _c	GMR	<i>R'</i> _{DC} at 20°C	<i>R'</i> _{AC} at 50°C	<i>I</i> _{rat}
			[mm ²]	[cm]	[cm]	[\Omega/km]	[\Omega/km]	[A]
1	A1	7	63	1.02	0.370	0.4545	0.5100	320

Table A.5: Conductor parameters of underground lines of European MV distribution network benchmark [42]
(coloured cells contain calculation results)

Conductor ID	Conductor type	Stranding	Cross-sectional area	<i>d</i> _c	GMR	<i>R'</i> _{DC} at 20°C	<i>R'</i> _{AC} at 90°C	<i>t</i> _i	<i>t</i> _j	<i>t</i> _{ts}	<i>d</i> _{ov}	<i>I</i> _{rat}
			[mm ²]	[cm]	[cm]	[\Omega/km]	[\Omega/km]	[mm]	[mm]	[mm]	[mm]	[A]
2	NA2XS2Y	19	120	1.24	0.480	0.253	0.338	5.5	2.5	0.2	28.8	320

Table A.6 lists the network topology and the line lengths of the network of Figure 3.2 and provides the positive sequence resistance and inductance at 20 °C, as calculated with DIgSILENT PowerFactory using data from Table A.4 and Table A.5.

Table A.6: Connections and line parameters of European MV distribution network benchmark [42]
(coloured cells contain calculation results)

Line segment	Node from	Node to	Conductor ID	<i>l</i>	<i>R'</i>	<i>X'</i>	<i>R'/X' ratio</i>	Installation
				[km]	[\Omega]	[\Omega]	[-]	
1	1	2	2	2.82	0.7529	0.5732	1.31	underground
2	2	3	2	4.42	1.1801	0.8984	1.31	underground
3	3	4	2	0.61	0.1629	0.1240	1.31	underground
4	4	5	2	0.56	0.1495	0.1138	1.31	underground
5	5	6	2	1.54	0.4112	0.3130	1.31	underground
6	6	7	2	0.24	0.0641	0.0488	1.31	underground
7	7	8	2	1.67	0.4459	0.3395	1.31	underground
8	8	9	2	0.32	0.0854	0.0650	1.31	underground
9	9	10	2	0.77	0.2056	0.1565	1.31	underground
10	10	11	2	0.33	0.0881	0.0671	1.31	underground
11	11	4	2	0.49	0.1308	0.0996	1.31	underground
12	3	8	2	1.30	0.3471	0.2642	1.31	underground
13	12	13	1	4.89	2.2240	1.7914	1.24	overhead
14	13	14	1	2.99	1.3599	1.0953	1.24	overhead
15	14	8	1	2.00	0.9096	0.7327	1.24	overhead

A.4 Overhead line conductor rating

The current rating calculation for the overhead line conductor has been made according to IEC 61597 [63] and the resulting value is shown in Table A.4. The reader willing to reproduce this result should perform the relevant calculations, using the following parameter values.

Table A.7: Used parameters for overhead line conductor current rating calculation

Parameter	Unit	Value
Ambient temperature	[°C]	30
Final equilibrium temperature	[°C]	50
Prevailing wind speed	[m/s]	1
Intensity of solar radiation	[W/m ²]	800
Solar radiation absorption coefficient	[-]	0.5
Emissivity coefficient	[-]	0.6

A.5 Loads

Table A.8: Load parameters of European MV distribution network benchmark [42]

Node	Peak apparent power [kVA]		Power factor (inductive)	
	Residential	Commercial / Industrial	Residential	Commercial / Industrial
1	15300	5100	0.98	0.95
2	-	-	-	-
3	285	265	0.97	0.85
4	445	-	0.97	-
5	750	-	0.97	-
6	565	-	0.97	-
7	-	90	-	0.85
8	605	-	0.97	-
9	-	675	-	0.85
10	490	80	0.97	0.85
11	340	-	0.97	-
12	15300	5280	0.98	0.95
13	-	40	-	0.85
14	215	390	0.97	0.85

APPENDIX B: PHOTOVOLTAIC POWER PLANT MODEL

B.1 Step-up transformer

The specifications of the transformer used to interface each PVPP with the MV distribution network are taken from [90], where also a DRG unit equipped with a fully rated converter is connected to the MV level. It is important to note that the transformer rated power does not have a predefined value in Table B.1, since the rated power of each PVPP (S_{nom}) varies throughout the study, depending on the simulated scenario. Hence, in order to match S_{nom} , the rated power of the step-up transformer does not acquire a predefined value. Finally, no magnetising impedance is considered and thus no-load losses are ignored (typically about 0.1 % or less of the transformer rating).

Table B.1: Step-up transformer parameters of the PVPP model

Connection	V_p	V_s	Z_{TRF}	S_{rat}	I_m	P_{Fe}
	[kV]	[kV]	[pu]	[MVA]	[pu]	[kW]
3-ph Dyn5	20	0.4	0.001+j0.06	S_{nom}	0	0

B.2 ‘Voltage Controller’ block

Table B.2: Voltage controller parameters of the PVPP model

Parameter	Unit	Value
PCC voltage reference value, u_{set}	[pu]	1.00
Gain constant, K_V	[-]	50
Integrator time constant, T	[s]	1

APPENDIX C: WIND POWER PLANT MODEL

C.1 Step-up transformer

The specifications of the transformer used to interface each WPP with the MV distribution network are taken from [90], where also a WPP equipped with fully rated converter wind turbines is connected to the MV level. It is important to note that the transformer rated power does not have a predefined value in Table C.1, since the rated power of each WPP (S_{nom}) varies throughout the study depending on the simulated scenario. Hence, in order to match S_{nom} , the rated power of the step-up transformer does not acquire a predefined value. Finally, no magnetising impedance is considered and thus no-load losses are ignored (typically about 0.1 % or less of the transformer rating).

Table C.1: Step-up transformer parameters of the WPP model

Connection	V_p	V_s	Z_{TRF}	S_{rat}	I_m	P_{Fe}
	[kV]	[kV]	[pu]	[MVA]	[pu]	[kW]
3-ph Dyn5	20	0.4	$(0.001 + j0.06)/N_{WT}$	S_{nom}	0	0

C.2 ‘Mechanical System’ block

Table C.2: Mechanical system parameters of the WPP model [76]
(coloured cells contain calculation results)

Parameter	Unit	Value
Air density, ρ	[kg/m ³]	1.225
Area covered by rotor, A_r	[m ²]	4418
Maximum power coefficient, $c_{p,max}$	[-]	0.43821
Nominal output power (individual WT), P_{nom}	[MW]	2
Electrical power limiter - lower limit, $P_{el,min}$	[pu]	0
Electrical power limiter - upper limit, $P_{el,max}$	[pu]	1.00
Nominal rotor speed, Ω_{nom}	[RPM]	18
Minimum rotor speed, Ω_{min}	[RPM]	9
Maximum rotor speed, Ω_{max}	[pu]	1.16667
Total moment of inertia of the rotating mass, J	[kg·m ²]	5.9·10 ⁶
Inertia constant of the rotor structure, H	[pu]	5.24
Cut-out (disconnection) wind speed, u_{discon}	[m/s]	25
Reconnection wind speed, u_{recon}	[m/s]	22

C.3 Calculation of λ_{design} and $c_{p,max}$

$$\lambda_i = \frac{1}{\frac{1}{\lambda} + 0.08 \cdot \theta - \frac{0.035}{\theta^3 + 1}} \xrightarrow{\theta=0} \frac{1}{\lambda_i} = \frac{1}{\lambda} = 0.035 \quad (C.1)$$

$$c_p(\lambda_i, \theta) = 0.22 \cdot \left(\frac{116}{\lambda_i} - 0.4 \cdot \theta - 5 \right) \cdot e^{\left(-\frac{12.5}{\lambda_i} \right)} \xrightarrow{\theta=0} c_p(\lambda_i, \theta = 0) = 0.22 \cdot \left(\frac{116}{\lambda_i} - 5 \right) \cdot e^{\left(-\frac{12.5}{\lambda_i} \right)} \quad (C.2)$$

$$(C.2) \xrightarrow{(C.1)} c_p(\lambda, \theta = 0) = \left(\frac{25.52}{\lambda} - 1.9932 \right) \cdot e^{\left(-\frac{12.5}{\lambda} + 0.4375 \right)} \quad (C.3)$$

$$(C.3) \Rightarrow \frac{\partial}{\partial \lambda} \frac{\partial c_p(\lambda, \theta=0)}{\partial \lambda} = \left(-\frac{25.52}{\lambda^2} \right) \cdot e^{-\left(\frac{12.5}{\lambda} + 0.4375 \right)} + \left(\frac{25.52}{\lambda} - 1.9932 \right) \cdot \left(\frac{12.5}{\lambda^2} \right) \cdot e^{-\left(\frac{12.5}{\lambda} + 0.4375 \right)} \quad (C.4)$$

$$\frac{\partial c_p(\lambda_{design}, \theta=0)}{\partial \lambda} = 0 \stackrel{(C.4)}{\implies} \lambda_{design} = 6.325 \quad (C.5)$$

$$c_{p,max} = c_p(\lambda = \lambda_{design}, \theta = 0) \stackrel{(C.3), (C.5)}{\implies} c_{p,max} = 0.43821 \quad (C.6)$$

C.4 ‘Voltage Controller’ block

Table C.3: Voltage controller parameters of the WPP model

Parameter	Unit	Value
PCC voltage reference value, u_{set}	[pu]	1.00
Gain constant, K_V	[\cdot]	50
Integrator time constant, T	[s]	1

APPENDIX D: INTELLIGENT NODE MODEL

D.1 Step-up transformer

The specifications of the transformers used to interface an IN with the MV distribution network are taken from [90]. No magnetising impedance is considered and thus no-load losses are ignored (typically about 0.1 % or less of the transformer rating).

Table D.1: Step-up transformer parameters of the IN models

Connection node	Connection	V_p	V_s	Z_{TRF}	S_{rat}	I_m	P_{Fe}
		[kV]	[kV]	[pu]	[MVA]	[pu]	[kW]
6	3-ph Dyn5	20	0.4	0.001+j0.06	1.2	0	0
8	3-ph Dyn5	20	0.4	0.001+j0.06	0.5	0	0

D.2 ‘BESS’ and ‘PWM converters’ blocks

Table D.2: BESS and PWM converters parameters of the IN models

Connection node	BESS						PWM converters
	$P_{BESS,max}$	Total capacity	Useful capacity	SOC_0 (summer / winter)	SOC_{min}	SOC_{max}	
	[MW]	[MWh]	[MWh]	[%]	[%]	[%]	
6	2.4	3.7	2.22	35.7 / 55.0	20	80	1.2
8	1.0	1.4	0.84	36.8 / 52.0	20	80	0.5

Table D.3: Detailed battery specifications [82]

Parameter	Unit	Value
Cell type	[-]	Lead-Acid
Cell Capacity	[Ah]	80
Number of cells in row	[-]	50 (IN 6) / 27 (IN 8)
Number of cells in parallel	[-]	71
Cell internal resistance	[Ω]	0.001
Fully-charged cell voltage	[V]	13.85
Fully-discharged cell voltage	[V]	12.00
Nominal terminal voltage	[V]	650

D.3 ‘PQ Controller’ block

Table D.4: PQ Controller parameters of the IN models

Parameter	Unit	Value
Active power PI controller proportional gain, K_d	[pu]	$8 \cdot 10^{-4}$
Active power PI controller time constant, T_d	[s]	$1 \cdot 10^{-2}$
Active power filter time constant, T_{df}	[s]	$1 \cdot 10^{-1}$
Reactive power PI controller proportional gain, K_q	[pu]	$1 \cdot 10^{-3}$
Reactive power PI controller time constant, T_q	[s]	$1 \cdot 10^{-3}$
Reactive power filter time constant, T_{qf}	[s]	$1 \cdot 10^{-2}$
Minimum active current, $i_{d,min}$	[pu]	-1.00
Maximum active current, $i_{d,max}$	[pu]	1.00
Minimum reactive current, $i_{q,min}$	[pu]	-1.00
Maximum reactive current, $i_{q,max}$	[pu]	1.00

APPENDIX E: COORDINATED VOLTAGE CONTROLLER

E.1 ‘AVC Relay’ and ‘Primary Controller’ blocks

Table E.1: AVC Relay and Primary Controller parameters

Parameter	Unit	Value
Upper voltage boundary, u_{upper}	[pu]	1.03
Lower voltage boundary, u_{lower}	[pu]	0.97
Tap step size, u_{tap}	[pu]	0.00625
Nominal voltage magnitude, u_{nom}	[pu]	1.00
Maximum tap position, nn_max	[\cdot]	16
Minimum tap position, nn_min	[\cdot]	-16

E.2 ‘Voltage Controller’ block

Table E.2: Voltage Controller parameters

IN	u_{margin}	K_V	$K_{denom,c}$	$K_{denom,d}$	T	T_f
	[pu]	[\cdot]	[\cdot]	[\cdot]	[s]	[s]
6	0.00085	$8 \cdot 10^2$	$2 \cdot 10^3$	12	1	$1.1 \cdot 10^2$
8	0.00120	$8.2 \cdot 10^2$	$1.1 \cdot 10^4$	6.5	1	$1.1 \cdot 10^2$

APPENDIX F: DETAILED SIMULATION RESULTS

F.1 Base case control scenario

Table F.1: Base case control scenario – maximum & minimum voltage of selected nodes

Season	Network section	Maximum voltage			Minimum voltage		
		Magnitude	Node	Moment in time	Magnitude	Node	Moment in time
		[pu]	[‐]	[d / h:m]	[pu]	[‐]	[d / h:m]
Summer	Feeder 1	1.0238	7	4 / 11:50	0.9728	11	7 / 20:50
	Feeder 2	1.0296	14	4 / 11:50	0.9744	12	2 / 12:30
Winter	Feeder 1	1.0299	7	6 / 02:50	0.9722	11	6 / 17:30
	Feeder 2	1.0244	14	1 / 13:00	0.9705	14	6 / 17:30

F.2 Advanced OLTC control scenario

In Table F.2, the voltage values that are coloured in orange exceed either the upper, or the lower voltage limit. Nevertheless, since the relevant boundary condition of subsection 4.2.2 is not violated, they are still considered to be acceptable.

Table F.2: Advanced OLTC control scenario (maximum DRG penetration) – maximum & minimum voltage of selected nodes

Season	Network section	Maximum voltage			Minimum voltage		
		Magnitude	Node	Moment in time	Magnitude	Node	Moment in time
		[pu]	[‐]	[d / h:m]	[pu]	[‐]	[d / h:m]
Summer	Feeder 1	1.0309	7	4 / 01:30	0.9681	1	2 / 12:30
	Feeder 2	1.0301	14	4 / 10:40	0.9690	12	2 / 12:30
Winter	Feeder 1	1.0319	7	7 / 02:50	0.9692	6	7 / 20:00
	Feeder 2	1.0270	14	6 / 02:50	0.9698	12	1 / 09:20

NOMENCLATURE

Latin symbols

A	swept area
aP	ZIP model constant impedance fraction, PowerFactory load model fraction (active power)
aQ	ZIP model constant impedance fraction, PowerFactory load model fraction (reactive power)
bP	ZIP model constant current fraction, PowerFactory load model fraction (active power)
bQ	ZIP model constant current fraction, PowerFactory load model fraction (reactive power)
c	coefficient
cP	ZIP model constant power fraction, PowerFactory load model fraction (active power)
cQ	ZIP model constant power fraction, PowerFactory load model fraction (reactive power)
e_aP, e_bP, e_cP	PowerFactory load model exponents for active power
e_aQ, e_bQ, e_cQ	PowerFactory load model exponents for reactive power
G	solar irradiance
H	inertia constant
I, i	current
J	moment of inertia
j	discrete time instant
K	gain constant
l	line length
N	number, digital clock pulse numbering
n	exponential load model exponent, normalisation of transformer turn ratio
nn	outermost tap position
$nntapin$	tap position
$oltc$	trigger signal
P	active power
PF	power factor
Q	reactive power
R	resistance
S	apparent power
T	time constant
t	time
U, u, V	voltage
VQI	Voltage Quality Index
X	reactance
y	transformer admittance

Greek symbols

Δ	deviation of a quantity
δ	phase angle of voltage phasor
λ	blade tip speed ratio
ρ	air density
φ	phase shift between voltage and current, phase angle of impedance
Ω	rotor angular velocity

Subscripts

0	nominal value, initial value, regulated point
$base$	base quantity
$BESS$	Battery Energy Storage System
c	conductor, charge mode
$check$	check
cor	corrected value
cri	critical value
d	d-axis, discharge mode
DB	deadband
$denom$	denominator
$design$	design parameter
DG	Distributed Generation
$discon$	disconnection
DRG	Distributed Renewable Generation
el	electrical
er	error
ext	external
f	filter
Fe	transformer iron core
fix	fixed value
$global$	global
i	intentional, insulation
j	discrete time instant, jacket
k	MV node number
L	lower deadband boundary
LN	line
$lo, lower$	lower boundary
m	mechanical, magnetising
$margin$	safety margin
max	maximum value
$meas$	measured value
min	minimum value
nom	nominal value
old	value during the previous clock pulse
ov	overall
p	transformer primary side, active power, performance
$panel$	PV panel
PCC	Point of Common Coupling
q	q-axis, reactive power
$Q0$	minimum reactive power exchange
Q_{max}	maximum reactive power exchange
r	rotor
rat	rated
$recon$	reconnection
ref	final set-point
s	transformer primary side
sc	short circuit
SET	set-point of Basic OLTC Controller
set	set-point
sol	PV array
tap	transformer tap

<i>tie</i>	IN side connected to tie-switch
<i>TRF</i>	transformer
<i>ts</i>	tape shield
<i>U</i>	upper deadband boundary
<i>up, upper</i>	upper boundary
<i>V</i>	Voltage Controller
<i>w</i>	wind
<i>WT</i>	Wind Turbine

Superscripts

'	normalisation of line resistance and reactance
+	above nominal value
-	below nominal value

Complex quantities

\underline{x}	complex quantity: $\underline{x} = \operatorname{Re}(\underline{x}) + j \cdot \operatorname{Im}(\underline{x})$
$\operatorname{Re}(\underline{x})$	real part of \underline{x}
$\operatorname{Im}(\underline{x})$	imaginary part of \underline{x}
$ \underline{x} $	modulus of \underline{x}
\underline{x}^*	complex conjugate of \underline{x}

Acronyms

AC	Alternating Current
AM	Active Management
AVC	Automatic Voltage Control
BESS	Battery Energy Storage System
CHP	Combined Heat and Power
CIGRE	Conseil International des Grands Réseaux Électriques
CIRED	Congres International des Réseaux Electriques de Distribution
DAE	Differential-Algebraic Equation
DC	Direct Current
D-FACTS	Distribution-Flexible AC Transmission System
DG	Distributed Generation
DMS	Distribution Management System
DNO	Distribution Network Operator
DR	Demand Response
DRG	Distributed Renewable Generation
DSL	Digsilent Simulation Language
DSM	Demand Side Management
DSO	Distribution System Operator
EHV	Extra High Voltage
EMS	Energy Management System
EMT	Electro-Magnetic Transients
EMTP	Electro-Magnetic Transients Program
EN	European Norm
FACTS	Flexible AC Transmission System
GNE	Graphical Network Editor
GOOSE	Generic Object Oriented Substation Events
GUI	Graphical User Interface
HV	High Voltage
HVDC	High Voltage Direct Current

ICT	Information and Communication Technology
IEA	International Energy Agency
IEC	International Electrotechnical Commission
IEEE	Institute of Electrical and Electronics Engineers
IN	Intelligent Node
ISO	Independent System Operator
LDC	Line Drop Compensation
LV	Low Voltage
LVb	beginning of the LV network
LVe	end of the LV network
MPPT	Maximum Power Point Tracking
MV	Medium Voltage
MVb	beginning of the MV network
MVe	end of the MV network
NOP	Normally Open Point
ODE	Ordinary Differential Equation
OLTC	On-Load Tap Changer
OPF	Optimal Power Flow
PCC	Point of Common Coupling
pu	per unit
PV	Photovoltaic
PVPP	Photovoltaic Power Plant
PWM	Pulse Width Modulation
RES	Renewable Energy Sources
RMS	Route Mean Square
SCADA	Supervisory Control And Data Acquisition
SOC	State Of Charge
STATCOM	static synchronous compensator
STC	Standard Test Conditions
SV	Sampled Value
SVC	Static Var Compensator
SVR	Step Voltage Regulator
TNO	Transmission Network Operator
TRF	transformer
TSO	Transmission System Operator
VSC	Voltage Source Converter
WPP	Wind Power Plant
WT	Wind Turbine
XLPE	cross-linked polyethylene
ZIP	constant impedance (Z) constant current (I) constant power (P)

BIBLIOGRAPHY

- [1] A. R. Bergen and V. Vittal, Power System Analysis, New Jersey: Prentice Hall, 2000.
- [2] M. Reza, *Stability analysis of transmission systems with high penetration of distributed generation*, PhD dissertation, Delft University of Technology, 2006.
- [3] F. Milano, Power System Modelling and Scripting, London: Springer, 2010.
- [4] P. Kundur, Power System Stability and Control, New York: McGraw-Hill, Inc., 1994.
- [5] A. von Meier, Electric Power Systems: A Conceptual Introduction, New Jersey: John Wiley & Sons, Inc., 2006.
- [6] L. Grigsby, Electric Power Generation, Transmission, and Distribution,, Florida: CRC Press, 2012.
- [7] E. H. Allen and M. D. Ilic, "Interaction of Transmission Network and Load Phasor Dynamics in Electric Power Systems," *IEEE Transactions on Circuits and Systems—I. Fundamental Theory and Applications*, vol. 47, no. 11, pp. 1613-1620, Nov 2000.
- [8] T. H. Demiray, "Simulation of Power System Dynamics using Dynamic Phasor Models," Ph.D. dissertation, Swiss Federal Institute of Technology, Zurich, 2008.
- [9] V. Venkatasubramanian, H. Schattler and J. Zaborszky, "Fast time-varying phasor analysis in the balanced three-phase large electric power system," *IEEE Transactions on Automatic Control*, vol. 40, no. 11, pp. 1975-1982, Nov 1995.
- [10] P. W. Sauer and M. A. Pai, "Power system steady-state stability and the load-flow Jacobian," *IEEE Transactions on Power Systems*, vol. 5, no. 4, pp. 1374-1383, Nov 1990.
- [11] T. van Cutsem and C. Vournas, Voltage Stability of Electric Power Systems, London: Springer, 2008.
- [12] T. van Cutsem, J. Kabouris, G. Christoforidis and C. Vournas, "Application of real-time voltage security assessment to the Hellenic interconnected system," *Generation, Transmission and Distribution, IEE Proceedings*, vol. 152, no. 1, pp. 123-131, 10 Jan. 2005.
- [13] K. K. Kabere, K. A. Foley and A. I. Petroianu, "Assessment of commercially available software tools for transient stability: experience gained in an academic environment," in *AFRICON, 2004. 7th AFRICON Conference in Africa*, 15-17 Sept. 2004.
- [14] T. F. IEEE, "Load Representation for Dynamic Performance Analysis," *IEEE Transactions on Power Systems*, vol. 8, no. 8, pp. 472-482, May 1993.
- [15] E. S. Ibrahim, "A comparative study of PC based software packages for power engineering education and research," *Electrical Power and Energy Systems*, vol. 24, pp. 799-805, 2002.
- [16] *PSS®E Brochure*, Erlangen, Germany: Siemens AG, 2009.
- [17] A. B. M. Nasiruzzaman, "A Student Friendly Toolbox for Power System Analysis Using MATLAB," in *Matlab - Modelling, Programming and Simulations*, Scyo, 2010, pp. 67-86.
- [18] *DigSILENT PowerFactory 15 User Manual*, Gomaringen, Germany: DigSILENT GmbH, March 2013.
- [19] *PSCAD User Manual*, Winnipeg, Manitoba, Canada: Manitoba HVDC Research Centre Inc., 2005.
- [20] L. Gérin-Lajoie and J. Mahseredjan, "Simulation of an extra large network in EMTP: from electromagnetic to electromechanical transients," in *IPST '09*, Kyoto, Japan, June 2-6, 2009.
- [21] V. Jalili-Marandi, E. Robert, V. Lapointe and J. Bélanger, "A Real-time Transient Stability Simulation Tool for Large-scale Power Systems," in *IEEE Power and Energy Society General Meeting*, San Diego, CA, 22-26 July 2012.
- [22] F. Milano, "An Open Source Power System Analysis Toolbox," *IEEE Transactions on Power Systems*, vol. 20, no. 3, pp. 1199-1206, Aug 2005.
- [23] *SimPowerSystems User Guide (Second Generation)*, Hydro-Québec and The MathWorks, Inc., 2013.
- [24] R. D. Zimmerman, C. E. Murillo-Sánchez and R. J. Thomas, "Matpower: SteadyState Operations, Planning and Analysis Tools for Power Systems Research and Education," *IEEE Transactions on Power Systems*, vol. 26, no. 1, pp. 12-19, Feb. 2011.
- [25] G. Pepermans, J. Driesen, D. Haeseldonckx, R. Belmans and W. Dhaeseleer, "Distributed generation: definition, benefits and issues," *Energy Policy*, vol. 33, p. 787-798, 2005.
- [26] F. A. Viawan, *Voltage Control and Voltage Stability of Power Distribution Systems in the Presence of Distributed Generation*, PhD dissertation, Chalmers University of Technology, 2008.
- [27] IEA, "Distributed Generation in Liberalised Electricity Markets," International energy Agency, Paris, 2002.

- [28] C. L. Masters, "Voltage rise the big issue when connecting embedded generation to long 11 kV overhead lines," *Power Engineering Journal*, vol. 16, no. 1, pp. 5-12, Feb. 2002.
- [29] F. Bignucolo, R. Caldon and V. Prandoni, "Radial MV networks voltage regulation with distribution management system coordinated controller," *Electric Power Systems Research*, vol. 78, p. 634–645, 2008.
- [30] J. Lehner and T. Weißbach, "Global and local effects of decentralised electric power generation on the grid in the Western Balkan Countries (WBC)," *Energy*, vol. 34, pp. 555-563, 2009.
- [31] J. A. Pecas Lopes, N. Hatziargyriou, J. Mutale, P. Djapic and N. Jenkins, "Integrating distributed generation into electric power systems: A review of drivers, challenges and opportunities," *Electric Power Systems Research*, vol. 77, p. 1189–1203, 2007.
- [32] H. Laaksonen and F. Suomi, "New Functionalities and Features of IEDs to Realize Active Control and Protection of Smart Grids," in *22nd International Conference on Electricity Distribution*, Stockholm, 10-13 June 2013.
- [33] M. E. Elkhatib, R. El-Shatshat and M. M. A. Salama, "Novel Coordinated Voltage Control for Smart Distribution Networks With DG," *IEEE Transactions on Smart Grids*, vol. 2, no. 4, pp. 598-605, Dec. 2011.
- [34] A. Samadi, R. Eriksson, D. Jose, F. Mahmood, M. Ghandhari and L. Söder, "Comparison of a Three-Phase Single-Stage PV System in PSCAD and PowerFactory," in *2nd International Workshop on Integration of Solar Power into Power Systems*, Lisbon, 12-13 November 2012.
- [35] CIRED Working Group No 4, "Preliminary Report on Dispersed Generation," CIRED, Nice, 2 June 1999.
- [36] European Technology Platform SmartGrids, "Strategic Deployment Document for Europe's Electricity Networks of the Future," April 2010. [Online]. Available: http://www.smartgrids.eu/documents/SmartGrids_SDD_FINAL_APRL2010.pdf. [Accessed 19 September 2013].
- [37] N. H. Phuong, *Multi-Agent System based Active Distribution Networks*, PhD dissertation, Eindhoven University of Technology, 2010.
- [38] M. Kolenc, I. Papič and B. Blažič, "Coordinated reactive power control to ensure fairness in active distribution grids," in *IEEE 8th International Conference on Compatibility and Power Electronics*, Ljubljana, 5-7 June 2013.
- [39] W. Bartels, F. Ehlers, K. Heidenreich, R. Hüttner, H. Kühn, T. Meyer, T. Kumm, J.-M. Salzmann, J. M. Salzmann, H. D. Schäfer and K. H. Weck, "Technical Guideline: Generating plants connected to the medium-voltage network," BDEW - Bundesverband der Energie- und Wasserwirtschaft e.V., Berlin, June 2008.
- [40] P. M. van Oirsouw, Netten voor distributie van elektriciteit (in Dutch), Arnhem: Phase to Phase B.V., 2011.
- [41] F. Provoost, *Intelligent Distribution Network Design*, PhD dissertation, Eindhoven University of Technology, 2009.
- [42] CIGRE Task Force C6.04.02, "Benchmark Systems for Network Integration of Renewable and Distributed Energy Resources: Technical Brochure," May 2013.
- [43] R. de Graaff, *Flexible distribution systems through the application of multi back-to-back converters: Concept, implementation and experimental verification*, PhD dissertation, Eindhoven University of Technology, 2010.
- [44] G. Celli, F. Pilo, G. Pisano, V. Allegranza, R. Cicoria and A. Iaria, "Meshed vs. Radial MV Distribution Network in Presence of Large Amount of DG," in *IEEE Power Systems Conference and Exposition*, 10-13 Oct. 2004.
- [45] J. F. Baalbergen, *Coordinated Agent-Based Control for On-line Voltage Instability Prevention*, PhD dissertation, Delft University of Technology, 2013.
- [46] H. Laaksonen, "IED Functionalities Fulfilling Future Smart Grid Requirements," *International Journal of Distributed EnergyResources and Smart Grids*, vol. 9, no. 3, pp. 289-311, 2013.
- [47] CENELEC, *EN 50160: Voltage characteristics of electricity supplied by public distribution networks*, Brussels, 2007.
- [48] Netbeheer Nederland, "Netcode Elektriciteit (in Dutch)," December 2013.
- [49] K. Heuck, K. D. Dettmann and D. Schulz, *Elektrische Energieversorgung* (in German), Hamburg: Springer Vieweg, 2013.
- [50] A. Engler and A. Soultanis, "Droop control in LV-Grids," in *IEEE International Conference on Future Power Systems*, Amsterdam, 18 Nov. 2005.
- [51] M. Gascó and A. Ríos, "Control, Regulation and Storage Systems to Optimize the Integration of Solar Power," in *2nd International Workshop on Integration of Solar Power into Power Systems*, Lisbon, 12-13 November 2012.
- [52] M. Zarghami, M. Y. Vaziri, A. Rahimi and S. Vadhva, "Applications of Battery Storage to Improve Performance of Distribution Systems," in *IEEE Green Technologies Conference*, Denver, 4-5 April 2013.
- [53] L. M. Tolbert, T. J. King, B. Ozpineci, J. B. Campbell, G. Muralidharan, D. T. Rizy, A. S. Sabau, H. Zhang, W. Zhang, Y. XU, H. F. Huq and H. Liu, "Power Electronics for Distributed Energy Systems and Transmission and Distribution Applications," December 2005. [Online]. Available: [http://web.ornl.gov/sci/decc/Reports/PE%20For%20DE%20and%20T&D%20Applications%20\(ORNL-TM-2005-230\).pdf](http://web.ornl.gov/sci/decc/Reports/PE%20For%20DE%20and%20T&D%20Applications%20(ORNL-TM-2005-230).pdf). [Accessed 19 September 2013].
- [54] J. H. Choi and J. C. Kim, "The online voltage control of ULTC transformer for distribution voltage regulation," *Electrical Power and Energy Systems*, vol. 23, pp. 91-98, 2001.
- [55] J. H. Harlow, *Electric Power Transformer Engineering*, CRC Press: Florida, 2004.
- [56] D. Mende, T. Fawzy, D. Premm and S. Stevens, "Increasing the Hosting Capacity of Distribution Networks for Distributed Generation Using Reactive Power Control – Potentials and Limits," in *2nd International Workshop on Integration of Solar Power into Power Systems*, Lisbon, 12-13 Nov. 2012.

- [57] M. Jacksens, B. Meersman, T. L. Vandoorn, J. D. M. De Kooning and L. Vandevelde, "Overview of voltage control strategies in medium voltage networks with implementation of distributed generation," in *IET Conference on Renewable Power Generation*, Edinburgh, 6-8 Sep. 2011.
- [58] N. Okada, M. Takasaki, H. Sakai and S. Katoh, "Development of a 6.6kV - 1MVA transformerless loop balance controller," in *IEEE Power Electronics Specialists Conference*, Orlando, FL, 17-21 June 2007.
- [59] F. Provoost, J. Myrzik and W. Kling, "Optimized Voltage Control in Autonomously Controlled Networks," in *International Conference on Future Power Systems*, Amsterdam, 18 Nov. 2005.
- [60] R. de Graaff, J. Duarte, W. Kling and P. Vaessen, "Intelligent Nodes in Distribution Systems - Transition from Radial to Meshed Operation," in *20th International Conference on Electricity Distribution*, Prague, 8-11 June 2009.
- [61] R. de Graaff, J. Myrzik, W. Kling and J. Enslin, "Intelligent Nodes in Distribution Systems - Optimizing Steady State Settings," in *IEEE Power Tech 2007*, Lausanne, 1-5 July 2007.
- [62] J. G. Slootweg, *Wind Power Modelling and Impact on Power System Dynamics*, PhD dissertation, Delft University of Technology, 2003.
- [63] International Electrotechnical Commission, *IEC/TR 61597: Overhead electrical conductors – Calculation methods for stranded bare conductors*, Geneva, 1995.
- [64] A. J. Collin, I. Hernando-Gil, J. L. Acosta and S. Z. Djokic, "An 11 kV steady state residential aggregate load model. Part 1: Aggregation Methodology," in *IEEE PowerTech*, Trondheim, 19-23 June 2011.
- [65] S. Hesmondhalgh, "GB Electricity Demand – 2010 and 2025. Initial Brattle Electricity Demand-Side Model – Scope for Demand Reduction and Flexible Response," *Sustainability First*, February 2012.
- [66] P. Kadurek, W. L. Kling, P. F. Ribeiro and J. F. G. Cobben, "Electricity Demand Characterization for Analyzing Residential LV Distribution Networks," in *IEEE PowerTech*, Grenoble, 16-20 June 2013.
- [67] I. R. Navarro, *Dynamic Power System Load: Estimation of Parameters from Operational Data*, PhD dissertation, Lund University, 2005.
- [68] H. Bai, P. Zhang and V. Ajjarapu, "A Novel Parameter Identification Approach via Hybrid Learning for Aggregate Load Modeling," *IEEE Transactions on Power Systems*, vol. 24, no. 3, pp. 1145 - 1154, 2009.
- [69] D. Karlsson and D. J. Hill, "Modeling and Identification of Nonlinear Dynamic Loads in Power Systems," *IEEE Transactions on Power Systems*, vol. 9, no. 1, pp. 157-166, 1994.
- [70] A. Bokhari, A. Alkan, R. Dogan, M. Diaz-Aguiló, F. de León, D. Czarkowski, Z. Zabar, L. Birenbaum, A. Noel and R. E. Uosef, "Experimental Determination of the ZIP Coefficients for Modern Residential, Commercial, and Industrial Loads," *IEEE Transactions on Power Delivery*, vol. PP, no. 99, pp. 1-10, 2013.
- [71] DlgSILENT GmbH, *DlgSILENT Technical Documentation: General Load Model*, Gomaringen, 2008.
- [72] K. Prajapati and R. Roy, "A novel method for Distribution System Reconfiguration including Static Load Models and Daily Load Curve," in *2nd International Conference on Electric Power and Energy Conversion Systems*, Sharjah, 15-17 Nov. 2011.
- [73] F. Fernandez-Bernal, L. Rouco, M. Gonzalez and M. Alonso, "Modelling of photovoltaic plants for power system dynamic studies," in *Fifth International conference on Power System Management and Control*, 17-19 April 2002.
- [74] "SoDa: Solar Energy Services for Professionals," [Online]. Available: <http://www.soda-is.com/eng/index.html>. [Accessed 11 12 2013].
- [75] E. W. ter Horst and H. E. Smulders, "Horizontal PV Systems and Contamination of Modules, 1.5 Year Experience with Frameless Modules in 'PV NORD,'" PV NORD, 2005.
- [76] J. G. Slootweg, H. Polinder and W. L. Kling, "Reduced Order Models of Actual Wind Turbine Concepts," in *IEEE Young Researchers Symposium*, Leuven, Feb. 2002.
- [77] J. G. Slootweg and W. L. Kling, "Aggregated Modelling of Wind Parks in Power System Dynamics Simulations," in *IEEE Power Tech Conference*, Bologna, 23-26 June 2003.
- [78] "KNMI HYDRA PROJECT: Wind climate assessment of the Netherlands," KNMI, [Online]. Available: <http://www.knmi.nl/samenw/hydra/index.html>. [Accessed 26 01 2014].
- [79] C. L. Archer and M. Z. Jacobson, "Spatial and temporal distributions of U.S. winds and wind power at 80 m derived from measurements," *Journal of Geophysical Research*, vol. 108, no. D9, 2003.
- [80] M. Edgar, R. Jenkins, G. Stein, T. Johnson, S. Lam and A. Kensley, "High Wind Speed Shutdown Workgroup Report," National Grid, July 2013.
- [81] J. G. Slootweg, H. Polinder and W. L. Kling, "Initialization of Wind Turbine Models in Power System Dynamics Simulations," in *IEEE Power Tech Conference*, Porto, 10-13 September 2001.
- [82] DlgSILENT GmbH, "PowerFactory Application Manual: Battery Energy Storing Systems in PowerFactory," Gomaringen, 2010.
- [83] K. Le Dinh and Y. Hayashi, "Centralized BESS Control to Minimize Demand of PV-Supplied Micro-grid under Voltage Constraints," in *IEEE International Conference on Power and Energy*, Kota Kinabalu Sabah, 2-5 Dec. 2012.
- [84] S. G. Johansson, L. Carlsson and G. Russberg, "Explore the Power of HVDC Light® - a web based System Interaction Tutorial," in *IEEE Power Systems Conference and Exposition*, 10-13 Oct. 2004.
- [85] C. M. Hird, H. Leite, N. Jenkins and H. Li, "Network voltage controller for distributed generation," *IEE Proceedings - Generation, Transmission and*

- Distribution*, vol. 151, no. 2, pp. 150-156, 2004.
- [86] P. Kacejko, S. Adamek and M. Wydra, "Optimal voltage control in distribution networks with dispersed generation," in *IEEE Innovative Smart Grid Technologies Conference Europe*, Gothenburg, 11-13 Oct. 2010.
- [87] T. Sansawatt, *Adaptive Control for Active Distribution Networks*, PhD dissertation, The University of Edinburgh, 2012.
- [88] A. Gesino, Power reserve provision with wind farms: Grid integration of wind power, Kassel: kassel university press GmbH, 2011.
- [89] S. V. Giannoutsos and S. N. Manias, "A cascade control scheme for a grid connected Battery Energy Storage System (BESS)," in *2nd IEEE ENERGYCON Conference & Exhibition*, Florence, 9-12 Sept. 2012.
- [90] DIgSILENT GmbH, *DIgSILENT Template Description: Fully Rated WTG Template*, Gomaringen, 2011.

